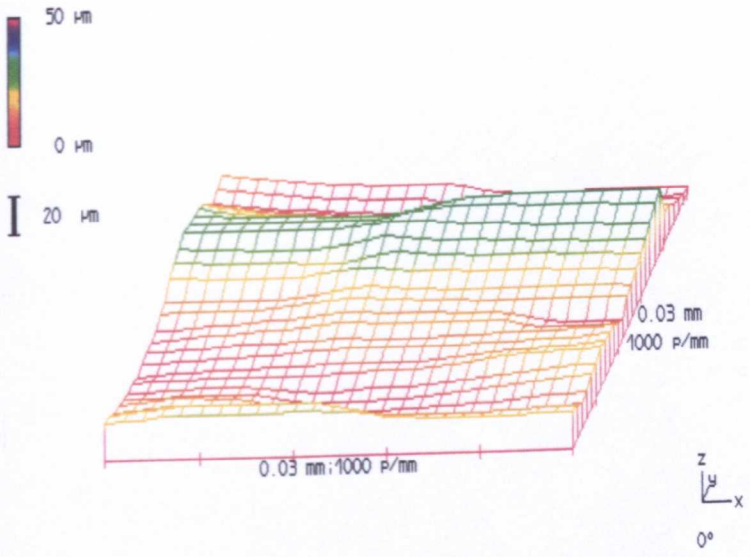

Figure 6.22: Laser profilometry image for trehalose recrystallised from 60:40 ethanol:water (34-18°C), S = 1.5

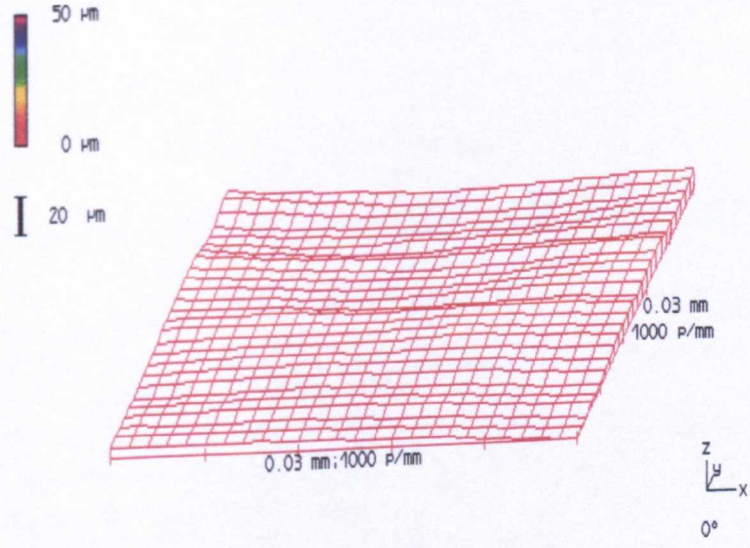

Figure 6.23: Laser profilometry image for trehalose surface washed with IPA following recrystallisation from 100% water

Manipulation of Carrier Particles for Inhalation

Claire Halina Pritchard, B.Sc. (Hons)

A thesis submitted in partial fulfillment of the requirements for the degree of Doctor of Philosophy.

De Montfort University, Leicester

September 2003.

The work presented in this thesis was carried out under an EPSRC CASE Award in collaboration with Quadrant Healthcare, Ruddington, Notts.

CONTENTS

CHAPTER TWO: MATERIALS AND EQUIPMENT

CHAPTER THREE: RECRYSTALLISATION AND INITIAL CHARACTERISATION OF MATERIALS

Note – Appendices

Appendices are numbered according to the chapter to which they refer. Not all chapters have an appendix, so the numbering is not continuous.

The only appendices that exist for and form part of this thesis are those listed below.

LIST OF FIGURES

Chapter One

Chapter Two

Chapter Three

Chapter Four

Chapter Five

Chapter Six

Chapter Seven

Chapter Eight

ACKNOWLEDGEMENTS

Firstly, I would like to express my sincere thanks to my supervisors Professor Mike Aulton, Dr Andy Twitchell and Dr Julian Blair for their continued support, advice and encouragement throughout the course of this research.

Special thanks are due to all the technical staff at De Montfort University, principally Richard, Colin, Lou, Norma and Jayshree. I would particularly like to thank Richard for all the support and encouragement he has, and continues to provide that I am sure is above the call of duty.

Sincere thanks are due to Quadrant Healthcare for their financial support and to their staff for help with use of technical facilities.

I would also like to take this opportunity to thank Dr Simon Connell, University of Nottingham for sharing his expertise with respect to Atomic Force Microscopy; Dr Fridrun Podczeck, University of London for kindly allowing use of their laser profilometry equipment and Dr Jan Skakle, University of Aberdeen for carrying out the X-ray crystallography experiments on a number of TOAc samples.

Last but by no means least, I would like to thank my parents for all the love and support they have provided, without which this thesis would not have been possible.

ABSTRACT

The work described in this thesis was performed to investigate the effect of altering the conditions of recrystallisation for selected sugars and sugar derivatives (lactose, trehalose dihydrate and trehalose octa-acetate (TOAc)) in order to assess the physical effect on the material surface. In addition to recrystallised materials, amorphous materials were also produced. The short-acting $beta_2$- agonist, salbutamol sulphate, was subsequently used to assess the relative performance of these materials as drug carriers in a dry powder inhaler (DPI). The main aim of the research was to establish whether a relationship exists between the surface characteristics of a material and the performance of the material as a drug carrier in a DPI.

A fundamental part of the research involved the physiochemical characterisation of the sugars, including solubility determinations for trehalose and TOAc in a range of ethanol:water solvents. Following recrystallisation, considerable time had to be spent in order to confirm the identity of the recrystallised TOAc material, as initial analysis was not conclusive in determining that the material had remained chemically unchanged following recrystallisation. Optimisation of drying of the TOAc material following recrystallisation was also performed, and X-ray crystallography of samples of the TOAc material suggested that it exists in at least three different crystalline forms.

Characterisation of the surface roughness using laser profilometry was performed before the materials (sieved to obtain a particle size range of 63 – 90 μm) were blended with salbutamol sulphate (micronised to a particle size of 5 μm). A multi-stage liquid impinger (MSLI) was used to quantify *in vitro* the performance of each material as a drug carrier from the DPI device - FlowCaps® (Hovione).

Overall, the results indicated that the surface roughness values (R_a) required to achieve the optimum performance as a drug carrier were in the range of 1.9 to 2.7 μm. In addition, when considering the hydrophilic or hydrophobic nature of the sugars assessed, a trend appeared to exist. The results indicated an optimum R_a in the range of 1.9 to 2.3 μm for materials that exhibited hydrophobic characteristics, and a range of 2.1 to 2.7 μm for materials that were considered hydrophilic.

In conclusion, the results obtained indicate that a relationship between the surface characteristics of a material and its performance as a drug carrier in a DPI does exist, but that the optimum relationship is determined by a number of factors. In addition to the surface characteristics, the physiochemical properties of the carrier material and the active drug together with the characteristics of the chosen DPI device itself, all contribute to the relationship that determines performance.

CHAPTER ONE

INTRODUCTION

1.1 OVERALL AIM OF THE INVESTIGATION

The work described in this thesis was performed to investigate the effect of altering the conditions of recrystallisation for selected sugars in order to assess the physical effect on the material surface. In addition to recrystallised materials, amorphous materials were produced. The relative performance of these materials as drug carriers in a dry powder inhaler (DPI) was subsequently assessed. The main aim of this research was to try to establish whether a relationship exists between the surface characteristics of a material and its performance as a drug carrier in a DPI.

1.2 GENERAL INTRODUCTION

Asthma is a condition that has been known of and described for more than 2000 years. The word itself derives from a Greek word meaning 'panting'. Asthma is a common condition affecting people of all ages and over the last few decades there has been a significant increase in the understanding of the condition and its causes. It is a chronic inflammatory disorder that occurs when the main air passages of the lungs (the bronchial tubes) become inflamed. The muscles of the bronchial walls tighten and extra mucus is produced, causing the airway to narrow. The inflammation that causes asthma makes airways overly sensitive to a wide range of environmental triggers, such as:

- Allergens (including pollen and moulds).
- Air pollutants and irritants.
- Respiratory infections, including the common cold.
- Physical exertion.
- Cold air.
- Certain medications, including beta-blockers (such as propranolol) or aspirin.
- Emotional stress.

Asthma symptoms can range from mild wheezing to severe difficulty breathing. In some cases breathing may be so laboured that an asthma attack becomes life-threatening. The incidence of asthma has risen dramatically in the past decade, especially among children living in inner city areas. The increasing prevalence of the disorder has lead to an increase in the development of products to treat the condition. Current treatment for asthma can be divided into two types, those that relieve the symptoms and those that modify the underlying disease.

Bronchodilators are medications that open constricted airways and provide temporary relief of asthma symptoms. Bronchodilators may be short acting or long acting and include $beta_2$- agonists such as salbutamol sulphate. Short-acting $beta_2$ agonists begin working within minutes and last 2 to 4 hours. Long-acting $beta_2$-agonists, such as salmeterol or formoterol last up to 12 hours. The short-acting medications are typically prescribed for relief or prevention of asthma symptoms or flare-ups. The most common drugs act quickly to relieve symptoms and can be used as a prevention measure before exercising.

Anti-inflammatory drugs are taken continually to prevent attacks. They reduce inflammation in the airways and prevent blood vessels from leaking fluid into airway tissues. The most widely used of these drugs include corticosteroids. Different corticosteroids used for the treatment of asthma include beclomethasone, fluticasone and budesonide. They help decrease the frequency of attacks and lower the dosage of other medications needed to calm symptoms.

Inhalation as a method of drug delivery has been well established in the treatment of asthma. The large surface area for absorption and the relatively low metabolic activity of

the lungs also make this organ system a potential route for the systemic delivery of drugs that cannot easily be delivery by other means. However, inhalation as a route of delivery is not easy. The function of an inhaler is to send the entire dose of pharmacologically active product into the wet mouth, past wet and sticky mucosa and sputum on the oropharynx and into the lung airways. The product then impacts the highly ramified network of bronchi and must battle a thick columnar epithelium covered by cilia and a continuously moving blanket of mucous. The function of the mucous is to sweep any dust particles, such as the pharmaceutical product, out of the lung and back into the throat from where it will be swallowed. When the route of administration is by inhalation, the active drug is delivered from either pressurised aerosols, from a nebuliser or as a dry powder.

With respect to pressurised inhalers, the propellant used originally was a mixture of chlorofluorocarbons (CFCs). Unfortunately, these compounds were identified as the cause of degradation of the earth's ozone layer.

Ozone (chemical formula 0_3) is very rare in the lower earth's atmosphere, averaging about 3 molecules of ozone for every 10 million air molecules. However, it is an important part of the upper atmosphere of the earth, which plays a significant role in the regulation of the temperature of the earth. It has been suggested that degradation of the ozone layer would lead to an overall increase in the temperature of the earth. This effect has been referred to as 'global warming' and the consequence of this if it occurs could be devastating for the balanced ecological systems that currently exist. Ozone plays a beneficial role by absorbing most of the biologically damaging ultraviolet sunlight (called UVB). The hole in the ozone layer means that a greater amount of UVB radiation is reaching the earth's

surface. The harmful effects of the excessive exposure of humans to UVB radiation include an increase in the incidence of skin carcinomas.

Repair of the hole involves the internationally agreed-upon "Montreal Protocol on substances that deplete the ozone layer" that came into effect in 1989. This agreement regulates the production of CFCs and other ozone-depleting substances. Production of the most damaging ozone-depleting substances was eliminated, except for a few critical uses, by 1996 in developed countries and will be eliminated by 2010 in developing countries. With adherence to the international agreement, it has been predicted that the ozone layer will recover over the next 50 years.

At the time of the Montreal Protocol, one of the small, but critical areas of CFC use was for medical inhalers used to treat lung diseases such as asthma. However, due to the eventual phasing out of CFC propellants for all applications, an alternative had to be found. This lead to the introduction of a hydrofluoroalkane (HFA) propellant system.

Unfortunately, the change from CFC to HFA propellants was not simply a case of replacing one propellant for another. Due to the different properties of the propellants, reformulation of the product was frequently required, including a redesign of the valve system used to meter each dose.

Partly because of the difficulties associated with the complete redevelopment of pressurised inhalers, there has been a significant increase in the development of non-propellant, dry powder systems over the last decade. Dry powder inhalers (DPIs) have several advantages over pressurised metered dose inhalers (pMDIs), including the

elimination of co-ordination issues frequently associated with pressurised inhalers. Another advantage of DPIs over pMDIs is that for degradable materials, such as proteins, storage in the solid state as a powder blend exhibits improved stability over the solutions or suspensions of the material that would be required with a pMDI.

With respect to DPIs, the most effective way to help drug delivery into the lungs is to make the drug particles of a suitable size. Studies[1] have indicated that it is desirable for all drug particles be 5 μm or less in diameter, and ideally between 2 and 3 μm (see below for further explanation). This particle size is typically achieved by micronisation, but the process itself causes agglomerates of powder by alteration of the powders adhesion and cohesion properties. These agglomerates then become an obstacle to the effective delivery to the lungs of the active product. Hence, in order to overcome the agglomeration, the active drug is usually blended with a larger inert 'carrier' particle. Currently, the industry standard carrier particle is lactose. As the material is entrained in a turbulent airflow, a proportion of the drug de-aggregates to create respirable particles. With a dry powder inhaler, the energy provided by the inhalation must therefore be directed not just at entraining the powder into the lungs but also at dispersing it as efficiently as possible back to a micronised particle size. The inhaled particles are deposited in the airway by one of three fundamental mechanisms; either by inertial impaction, sedimentation or diffusion.

1.2.1 INERTIAL IMPACTION

A particle in a stream of air is carried by its own momentum, which is the product of the particles mass (inertia) and velocity. When the airflow encounters an obstacle or bend, as

[1] Thorsson (1995), Olsson (1995), Scheuch *et al* (1992), Stuart (1984) and Rees *et al* (1982).

in the airways of the lung, the direction of the air flow changes. The inertial force of the particle in the airflow resists this change of direction, causing the particle to carry some distance along the original direction of motion. It therefore follows that a particle with a high momentum may impact on the surface in front of it, rather than follow the changed direction of the airflow.

In the case of inhalation through the mouth, the air stream encounters a sharp bend in the pharynx before it enters the trachea. In general, only particles with a diameter below 15 μm are able to reach beyond this point as the combination of larger particles and high airflow velocity in the upper airways makes impaction very likely. Therefore, with respect to dry powder inhalers, the drug carrier particles are frequently deposited by this mechanism at the back of the throat. As the surface that the particles impact upon is moist with mucous, the particles cannot 'bounce off' and do not continue travelling in the air flow. Invariably, the impacted particles are trapped by the mucous and cleared from the pharynx when they are swallowed. As the airways of the lung bifurcate and become narrower, the velocity of the airflow decreases and hence impaction ceases to be an important mechanism of drug deposition in the lower airways. In general, particles with a diameter greater than 5 μm will be deposited by inertial impaction.

1.2.2 SEDIMENTATION

Particles suspended in a gas are still subject to gravitational forces. This is also true of particles suspended in the air of respiratory tract. The particles settle on a surface within the airways depending on their size.

The term 'aerodynamic diameter' provides a simplified means of characterising the sizes of particles having different shapes and densities with a single dimension. The aerodynamic diameter is the diameter of a spherical particle having a density of 1 g/cm^3 that has the same inertial properties (i.e. settling velocity) in the gas as the particle of interest. The settling velocity relates to the velocity of a falling particle when the gravitational force downward is balanced by the air resistance force upward.

The aerodynamic diameter for all particles greater than 0.5 μm can be approximated using the following equation:

$$D_{ae} = D_{St}\sqrt{P_p}$$

where D_{ae} is the aerodynamic particle diameter (μm), D_{St} represents Stokes diameter (μm) and P_p represents the particle density (g/cm^3).

Particle density affects the motion of a particle through a fluid or gas (such as air) and is taken into account in the above equation. The Stokes diameter for a particle is the diameter of the sphere that has the same density and settling velocity as the particle. It is based on the aerodynamic drag force caused by the difference in velocity of the particle and the surrounding fluid or gas. For smooth, spherical particles, the Stokes diameter is identical to the physical or actual diameter. Stokes' Law indicates that the settling velocity of a particle increases with the square of the aerodynamic diameter.

Sedimentation is an important mechanism of deposition in the lower regions of the lungs for particles that escape deposition by impaction. This method of deposition is effective for particles between 5 μm down to 0.5 μm in diameter.

1.2.3 DIFFUSION (BROWNIAN MOTION)

The English botanist R. Brown observed in 1827 that finely divided particles in suspension undergo ceaseless random movement. This is due to the collision of the surrounding medium with the particles. The resultant effect on the particles is their directional movement (diffusion) from regions of high to low particle concentration. Consequently, inhaled drug particles diffuse to the walls of the respiratory tract. The rate of this process is inversely proportional to the size of the particle and therefore diffusion is the dominant mechanism of deposition in the lungs for particles smaller than 0.5 μm. It should be mentioned however that during inhalation, the length of time that air is suspended within the lungs is probably insufficient for all drug particles of this size to be deposited. It is therefore reasonable to assume that a significant proportion of particles smaller than 0.5 μm would be exhaled.

With respect to asthma, as the inhalation of drug particles is for local effect, the drug has to reach the lower regions of the lungs. For the inhalation of drugs for systemic effect, it is also desirable to reach the lower regions of the lungs as this is where there is a greater surface area available for drug absorption. As described above, sedimentation is the predominant mechanism by which particles are deposited in the lower lungs and for this method of deposition to be effective, the drug particles have to have a diameter of 5 μm or less. As discussed with diffusion, in order to prevent the exhalation of drug particles from

the lungs they have to have a diameter greater than 0.5 μm. As mentioned previously, studies have indicated that the ideal particle size range for effective deposition of drug to the lungs is 2 to 3 μm, which is in the middle of the size range possible for particles to be deposited in the lungs by sedimentation.

For this research, a model drug was chosen to assess the delivery performance of the carrier materials that were produced. The drug chosen was the short-acting $beta_2$- agonists salbutamol sulphate (also referred to in this thesis as salbutamol).

Salbutamol sulphate is a sympathomimetic agent, which has a selective action on $beta_2$-adrenergic receptors in bronchial smooth muscle. It is therefore indicated in the management of bronchial asthma, for the relief of wheezing and shortness of breath and is administered either as required or prophylactically. In addition to its use in respiratory medicine, salbutamol is used in obstetric practice to arrest premature labour, although this indication will not be discussed here.

Salbutamol may be administered by mouth, injection or inhalation, but if given by mouth it is subject to first-pass metabolism in the liver. About half is excreted in the urine as an inactive sulphate conjugate. By inhalation, the doses required are smaller and systemic absorption is low, which considerably reduces systemic effects such as headache or tachycardia. Systemic effects are more prominent when salbutamol is administered orally or by injection as the $beta_2$- selectivity is not absolute. The action of inhaled salbutamol depends on the direct stimulation of $beta_2$-adrenergic receptors in the lung. Salbutamol is a potent drug and when delivered by inhalation only a small quantity is required, typically 100 to 200 μg per inhalation, hence it was important to confirm the homogeneity of the blends produced prior to testing.

Historically, dry powder inhalers relied on a formulation process using simple drug carrier blends. The objective was primarily to allow for filling and metering of the product or device, to achieve adequate dilution and to ensure dose uniformity. Consequently. the ideal particle shape for use in dry powder inhalers was considered to be spherical, as the flow properties of such materials were favourable compared to other morphologies. However, the efficacy of a therapeutic aerosol is mainly determined by the amount of drug reaching the target site and the human lung has evolved to prevent the entry of atmospheric particulates. Therefore, unlike other routes of administration, delivering a known dose of drug to the lungs via inhalation required a multidisciplinary scientific approach. Previous work has focused on investigating both particle technology and drug delivery technology as means of increasing the proportion of drug that reaches the lung and it has been determined that drug distribution and deposition depends on several factors. These include the characteristics of the inhaled formulation, such as particle diameter, size distribution, shape, electrical charge, density and hygroscopicity in addition to the anatomy of the respiratory tract and breathing patterns such as frequency, tidal volume and flow. More recent work (Musante *et al*, 2002) indicates that the inhalation of relatively large and porous particles may be effective for the delivery of drugs to the lungs. This was reported to be due to improved aerosolisation properties of these particles compared to smaller, but more dense particles with comparable aerodynamic diameters.

In conclusion, complex and subtle interactions may occur between the drug substance, carrier(s), and the device components of a DPI that significantly affect the overall effectiveness of the drug product. For example, gravitational, fluid dynamic and other interactive forces, such as electrostatic, van der Waals and capillary forces are together responsible for different fluidisation behaviours exhibited by different powders in an

inhaler. Electrostatic charge interactions influence the overall efficiency of a DPI, since such forces are considered to be significant for attraction and adhesion between the drug substance particles, excipient particles, and device surfaces. Additionally, particle-size distribution, particle morphology, and moisture content can greatly influence the bulk properties of a formulation and thereby the product performance.

1.3 OUTLINE OF THIS THESIS

This research will investigate the effect of differences in the surface morphology of drug carrier particles on their overall performance from a selected DPI system.
Through the control and/or manipulation of variables connected to the solid-state material properties, it is possible to produce materials with altered characteristics. However, in order to manipulate a solid material it is essential to have an understanding of these properties.

1.4 INTRODUCTION INTO RECRYSTALLISATION

Crystallisation is a very complex operation. Mullin (1993) describes it as a process highly dependant on fluid and particle mechanics involving simultaneous heat and mass transfer in a multi-component system where the solution composition, particle size, particle shape and size distribution are changing continually.

The following sections will briefly review the main principles of the process.

1.4.1 EFFECT OF THE SOLVENT

An ideal solvent for the preparation of crystalline materials could be defined as one that demonstrated the following properties. It should not form solid solutions with the material being grown, it should be of low viscosity with a low volatility, be easily removed after crystal growth, be readily obtainable in a pure state, and also be cheap and non-toxic. Such a solvent does not exist, although there are a number that do possess at least some of these desirable attributes. Consequently, the use of mixtures is very common.

With respect to solvent mixtures, the possibility exists that due to a synergistic effect, greater solubilities than those predicted by the summation of the solubility parameters can be observed.

In polar protic solvents, such as water or methanol, the solvent molecules interact by forming strong hydrogen bonds. In order to dissolve, the solute has to break these bonds and replace them with bonds of similar strength.

The 'power' of a solvent and the temperature coefficient of solubility are important factors that should be considered when selecting a solvent for a cooling crystallisation process. The solvent power influences the volume of the crystalliser, and the temperature coefficient determines the crystal yield.

One proposed mechanism for the kinetic effect of a solvent is that the molecules of certain solvents have a stronger affinity for the fastest growing faces of a particular crystalline form. Consequently, they can adsorb on these faces and prevent the deposition of

oncoming solute molecules. This effect results in retardation of the growth of that modification to the advantage of another.

1.4.2 SUPERSATURATION OF A SOLUTION

In order for any solid matter to crystallise out of a solution, the solution has to be saturated. A saturated solution is in thermodynamic equilibrium with the solid phase at a specified temperature. If the temperature of a saturated solution is then lowered, the excess of solid material seeks to separate out.

By cooling a hot, concentrated solution slowly and without agitation, it is possible to prepare solutions that contain more dissolved solid than that designated by equilibrium saturation. Such solutions are said to be supersaturated. Crystals will only grow from a solution when the system is supersaturated, i.e. contain an amount of solute greater than the equilibrium (saturated) amount.

The supersaturation of a system may be expressed in a number of ways. In all cases however, it is essential that the temperature is specified since the equilibrium saturation concentration is temperature dependent.

The concentration driving force, Δc, the supersaturation ratio, S, and the relative supersaturation, σ, are among the most frequently referred to expressions of supersaturation. These functions can be defined as

$$\Delta c = c - c^* \qquad S = \frac{c}{c^*} \qquad \sigma = \frac{\Delta c}{c^*} = S - 1$$

where c is the solution concentration, and c^* is the equilibrium saturation at the given temperature. These equations may be used to calculate the supersaturation if the equilibrium saturation concentration is known, and the corresponding solution concentration at a given temperature can be measured.

The degree of initial supersaturation or the rate of cooling of a solution often exerts a considerable influence on the crystal habit, as can the state of agitation applied to the system. Rapid crystallisation, such as that produced by the seeding or the sudden cooling (supercooling) of a supersaturated solution may result in the formation of acicular crystals.

Impurities in the crystallising solution can stunt the growth of a crystal in certain directions, and crystallisation from solutions of a given substance in different solvents generally results in a change of habit.

Supersaturation and growth rate are the major features affecting crystal morphology. Crystals produced from solutions with low initial supersaturation ratios tend to be compact and small, with the low energy surfaces exposed. Increased concentrations produce larger crystals with dendritic growth characteristics. On increasing the supersaturation ratio, crystals that are much smaller, but compact and agglomerated are produced. These crystals tend to expose the high energy planes.

1.4.3 NUCLEATION OF A SOLUTION

In addition to supersaturation, there are two further steps required in order to achieve the formation of crystals from solution. Firstly the formation of crystalline nuclei, and finally the growth of these nuclei into crystals.

A crystal grows when atoms, ions or molecules are added to it. The way in which they are added to the solid determines the overall morphology of the solid as well as the number and distribution of imperfections within the crystal.

Nuclei may originate in the following ways, each of which has a potential for affecting the crystal habit of the material produced.

Primary nucleation describes homogeneous, or spontaneous nucleation that is due to cooling an unseeded solution into the labile region of the solubility curve - see later diagram.

Heterogeneous nucleation, describing nucleation induced by foreign particles is another form of primary nucleation. In practice, all primary nucleation is thought to occur as a result of this pathway as it is nearly impossible (under normal laboratory conditions) to prepare a saturated solution free from the influence of foreign particles such as airborne dust. The presence of impurities can be responsible for the initiation of crystallisation within a system, and sympathetic surfaces such as the wall of the crystallisation vessel could also act as a catalyst for nucleation.

As previously mentioned, supersaturation (although a pre-requisite) is in itself insufficient to cause crystals to form. The crystal nuclei must first form by collision of molecules of solute in the solution, or sometimes through the addition of seed crystals. Deliberate seeding with minute crystals is referred to as secondary nucleation. Fortuitous seeding by crystals left from a previous batch and also attrition of existing crystals gives rise to fragments that act as seeds. The degree of stirring will affect this factor.

Equations that define the rate of nucleation indicate that temperature, degree of supersaturation and interfacial tension are the main variables responsible for the determination of nucleation rate.

Within a fluid system there will be a statistical distribution of energy in the molecules constituting the system, and in areas where the energy level rises temporarily in a supersaturated region, nucleation will be favoured. If a foreign body that is crystallographically similar or the same as the material being crystallised is introduced into the supersaturated solution, the free energy barrier for nucleation is reduced and so crystal growth becomes more probable. Hence the best method for inducing crystallisation is to seed the supersaturated solution with small crystals of the material to be crystallised, typically of a particle size sub 45 μm.

The required size for the critical nucleus to stabilise and continue to grow increases with temperature. There is an optimum temperature for nucleation of a given system. Excessive supercooling does not aid nucleation, and if a system is sufficiently supercooled, it can set to an amorphous state and further cooling will not induce crystallisation.

As soon as stable nuclei form, they can begin to grow into visible crystals, if given sufficient time.

Rapid cooling increases the degree of supersaturation resulting in a large number of nuclei and a crop of small crystals. The production of very small crystals of a substance should be avoided. This is because small crystals tend to cohere into masses that are difficult to wash, and consequently the substance may be less pure than when crystals of a larger size are manufactured.

1.4.4 CRYSTAL GROWTH

Crystal growth could be considered as a reversal of the dissolution process, and as a consequence, the diffusion theories of Noyes and Whitney, and of Nernst could be applied to these systems. The resulting theory could be used to define the rate of matter deposited onto a crystal face at a rate proportional to the difference in concentration between the bulk solution and the crystal surface.

However, as crystals generally dissolve faster than they grow, growth is not simply the reversal of dissolution. The transport of the solute molecules to the surface, and their arrangement in an ordered fashion within the crystal lattice should also be considered as part of the process of crystal growth.

The following equation to represent crystallisation rate based on the theories of Noyes, Whitney and Nernst was proposed by Florence and Attwood (1988)

$$\frac{dm}{dt} = Ak_g(c_{ss} - c_s)^n$$

where m is the mass of solid deposited in time t, A is the surface area of the crystal, k_g is the overall crystal growth coefficient, c_{ss} is the solute concentration at supersaturation, c_s is the solute concentration at saturation and n represents the order of the crystal growth process. The crystal growth coefficient is derived from the diffusion coefficient of the solute, the diffusion layer thickness and the degree of agitation applied to the system.

It should be remembered that the growth of crystals causes the desaturation of the solution. If the solution becomes saturated rather than supersaturated, no further crystal growth will occur. Therefore, to ensure that the solution remains in a supersaturated state it must be continually cooled until a satisfactory end point is reached.

1.4.5 Crystal Morphology

Materials which naturally grow as needles or plates are often required in other shapes, which may not be easy to produce. Changes of habit can be altered through a modification of various growth parameters. These include the growth temperature, which is achieved through a change in the solute concentration, or alternatively through altering the pH of the solution or changing the solvent itself.

1.4.6 Crystal Habit

Crystals vary in size and in the development of different faces owing to the condition under which they are formed. Crystal habit describes the outer appearance of the crystal, although it is possible to alter the crystal habit without changing the internal crystal arrangement. For example, needle-shaped crystals are often termed acicular, but such a

term gives no indication as to the position of the crystals in the system of classification based on crystallographic axes.

1.4.7 MODIFICATION OF CRYSTAL HABIT

The crystal habit is influenced by the environment in which the crystal grows, and habit modification is determined by the influence of the solvent and foreign ions and molecules on the crystal surface. Hence, modification of crystal habit could be obtained by the addition of impurities or 'poisons' into the system. For example, surfactants in the solvent medium used for crystal growth can alter crystal form by adsorbing onto growing faces during crystal growth. Another example of the way in which crystal habit could be modified is with excessive supersaturation. Cooling rate and agitation can alter crystal habit since it changes the degree of supersaturation. By the addition of co-solvents or other solutes and ions, the habit may be changed by poisoning of the crystal growth in one or more directions.

1.4.8 SUPERSOLUBILITY CURVE

The work of Miers and Isaac (1906, 1907) postulates that a definite relationship exists between the concentration and the temperature at which crystals will spontaneously form in an initially unseeded solution. The form of that relationship is a supersolubility curve roughly parallel to and above the normal solubility curve.

The theory states that in the metastable zone (the region between the two curves) there will be no appreciable spontaneous nucleation, but above the supersaturation curve (in the

labile region) the degree of spontaneous nucleation is thought to be extensive. In the stable (unsaturated) region, crystallisation is impossible.

An example of a Miers solubility curve is given below.

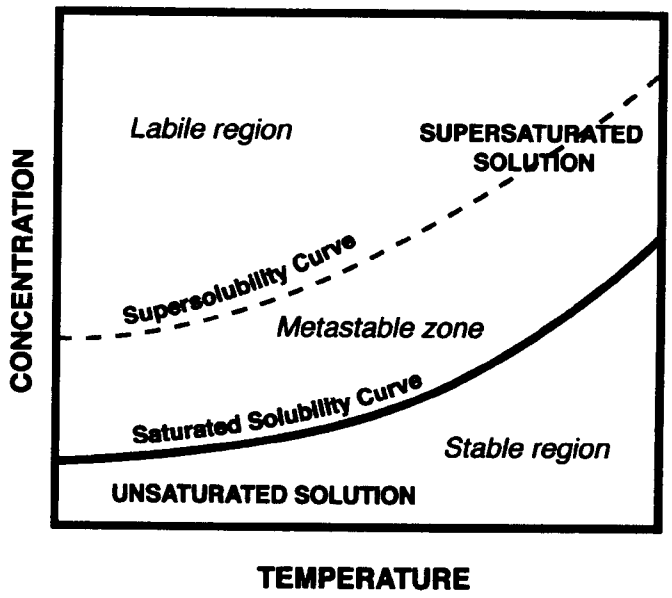

Figure 1.1: Miers Solubility Curve

It is possible to predict the general trend of a solubility curve using Le Chatelier's Principle, which refers to reversible reactions which can exist in equilibrium. It states that if there is any alteration to one of the factors maintaining the equilibrium of the system, such as temperature or pressure, then the equilibrium will alter in order to minimise the effect of the change.

1.4.9 RECRYSTALLISATION OF POLYMORPHS

It is known that many substances can exist in more than one crystalline form, the different forms being known as 'polymorphs'. The various modifications arise through packing of the molecules, atoms or ions in different arrays within the crystal or by differences in the orientation or conformation of molecules at lattice sites. The resulting crystalline materials usually possess different physical properties such as density, X-ray diffraction pattern, infra-red spectrum and melting points (although this is not always a useful diagnostic feature).

However, it is important to note that different crystal habits can appear without there being polymorphism. The habits acquired depend on the conditions of crystallisation such as solvent used, the temperature and the concentration and level of impurities present during recrystallisation.

With true polymorphs, the more soluble forms have less internal cohesion and are therefore generally less stable. These less stable forms are referred to as metastable polymorphs, as they will eventually convert to a more stable polymorphic form. Transformation of the modification into one that is more stable occurs by a process that may be rapid or slow depending on the material.

Solvates form when the solvent is incorporated into the crystal lattice, altering the crystal structure. This results in what is known as pseudopolymorphism and as the name suggests, solvates are not true polymorphs.

One theory regarding the crystallisation of polymorphs was suggested by Cardew *et al* (1985). They state that for a given supersaturation, the parameters being temperature and concentration, the form which crystallises out first is the one with the highest solubility with respect to the material with which the solution is saturated. This implies that it is possible to crystallise a desired form by controlling the supersaturation and harvesting the crystals at an appropriate time.

This theory can be explained by reference to Miers solubility curve. Material will be deposited out of solution earlier if the nuclei of the higher solubility form are produced. The deposition of this material at as great a rate as possible is thermodynamically preferable, as this reduces the time taken for the solution to re-establish its equilibrium with respect to the saturation of the solvent by the material.

The conclusions drawn by Khoshkhoo *et al* (1991) indicate that with respect to the suggestions of Cardew *et al* (1985), although supersaturation is an important factor in the crystallisation of polymorphs, its effect is dominated by the choice of solvent. The effect of the solvents may be simply related to the different order of solubility of the polymorphs in each solvent, i.e. the stable form in each solvent is different.

Different polymorphic modifications of a pharmaceutical substance can be prepared by crystallisation of the drug from different solvents under diverse conditions. If a metastable polymorphic modification is crystallised from a particular solvent solution, then it will follow Ostwald's rule of stages. This states that the crystals produced will subsequently be transformed into the stable polymorphic form. However, it is possible that conversion of a metastable form to the form considered stable under the conditions of temperature and

pressure to which it is exposed may occur in several stages. Ostwald's rule states that an unstable or metastable system may convert to other metastable forms before finally converting into the stable form. An unstable system will transform into one which most closely resembles it's own, i.e. into another transient state whose formation from the original is accompanied by the smallest loss of free energy. The rate of solid-state transformation will be dependent on the relative stability of the modification produced. The phase-transformation pathway is determined by the thermodynamic parameters, or chemical potentials of the solvent and the crystallised solid phase, based on the interaction between the chemical structure of the pharmaceutical and the solvent. The time over which transformation can occur may vary widely, and the conditions under which they may interconvert are complex. The process becomes more complicated to follow due to the additional possibility of the formation of pseudopolymorphs (hydrates or solvates) of the compound. Pseudopolymorphs have been observed to produce unwanted effects due to the presence of solvent.

1.4.10 WASHING OF HARVESTED CRYSTALS

Washing crystals on a filter helps to reduce the amount of mother liquor retained by a mass of crystals, but there is always the danger of reducing the final yield by dissolution during the washing operation. One method of minimising the material loss is to use a quantity of ice-cold solvent, as the solubility of the recrystallised material at this temperature should be significantly reduced compared to the same solvent at room temperature. If the crystals are readily soluble in the working solvent, another suitable liquid in which the substance is relatively insoluble may be used, but the efficiency of washing depends largely on the shape and size of the crystals.

1.5 INTRODUCTION INTO AMORPHOUS MATERIALS

In addition to crystalline materials, an assessment of amorphous materials as drug carriers in a DPI was also to be assessed.

The following sections are included to provide an insight into amorphous solids including their characteristics and preparation.

1.5.1 CHARACTERISTICS OF AMORPHOUS MATERIALS

Both crystals and amorphous materials share the attributes of the solid state. Their fundamental difference is in the basic nature of their atomic scale structure.

The term 'amorphous solid' is applicable to any solid having a non-periodic atomic array. The term 'glass' has conventionally been reserved for an amorphous solid actually prepared by quenching the melt. The term can also refer to an amorphous solid that exhibits a glass transition. The definition of a melt is a liquid that is close to its freezing point.

For an amorphous solid, the essential aspect with which the structure differs from that of a crystalline solid is the absence of long range order. The matrix of equilibrium atomic positions is strongly disordered, and there is no longer any translational periodicity. The identity of environment does not exist in such systems, but the atomic positions should not be thought of as randomly distributed in space. There is a high degree of local correlation. Thus, it can be claimed that amorphous solids, in common with crystals, have a high degree of short range order. This is as a consequence of the chemical bonding responsible for holding the solid together.

During a continuous cooling experiment, a change of phase can occur, e.g. a gas can become a liquid or a liquid can become a solid. On a plot of volume versus temperature the phase change in the case of crystalline materials is signified by a sharp break, if the cooling rate is sufficiently low. The liquid to crystal transition is marked by such a discontinuity to represent an abrupt contraction to the volume of the solid by the liquid. It is worth noting that there are exceptions to this observed behaviour, the notable exception being ice.

In the instances where an amorphous solid is produced, the change of phase is represented by a shallow bend in the observed plot. This occurs with higher cooling rates, and indicates that there is no volume discontinuity. This implies that the material acquires the characteristics of the low thermal expansion of a solid very rapidly, once the glass transition temperature (T_g) is reached, and subsequently passed.

The observed glass transition temperature depends upon the cooling rate at which the experiment is carried out. This is a characteristic kinetic dimension of the glass transition. It should be noted that glass transition temperatures for different materials span a wide range, indicating that certain materials are more easily produced as an amorphous form than others.

1.5.2 STABILITY OF AMORPHOUS MATERIALS.

Hancock *et al* (1995) stated that the packing arrangement of an amorphous solid is less thermodynamically stable than the packing arrangement in a crystalline form. There is

therefore a natural tendency for the physical transformation of an amorphous phase into a crystalline phase i.e. over time a glass will relax towards a more stable crystalline state with a lower free energy. The conversion from an amorphous to a more stable crystalline form is known as devitrification. The amount of energy lost during relaxation will be shown as an endotherm (termed the relaxation endotherm) on a DSC profile close to the glass transition temperature. The area under this peak corresponds to the amount of energy lost by the glass upon relaxation.

The degree of particle mobility determines the rate at which this transformation will take place. Sinko *et al* (1991) stated that when the temperature is below the glass transition temperature, restricted mobility hinders the rearrangement to a lower free energy. Large scale motion is frozen out, only limited rotational and vibrational motion is possible. There will be a physical aging of the material over time as more favourable packing arrangements are achieved. The length of time for complete conversion to a crystalline form will be dependent on the material itself and the conditions to which it is exposed. If the temperature is above the glass transition temperature, large scale translational and rotational motion are possible, hence the transformation to a crystalline form will take place more rapidly.

Amorphous solids are prone to absorb water, as a large number are hydrophilic. The absorbed water tends to plasticise the glass, reducing the T_g leading to an increase in particle mobility promoting a loss of amorphous structure.
The sugar derivative used in this work (trehalose octa-acetate (TOAc)) is hydrophobic in nature, which produces an amorphous material with a greater degree of stability compared to the other hydrophilic materials tested. With an eye to possible commercial applications

for the amorphous TOAc, increased stability is an obvious advantage. For further details on TOAc, refer to Chapter Three – Recrystallisation and Initial Characterisation of Materials.

1.5.3 PRODUCTION OF AMORPHOUS MATERIALS

As soon as the temperature of a liquid is lowered to its optimum crystallisation temperature, then it may begin to crystallise. It is important to remember that crystallisation takes time. Firstly, nucleation must occur and then the crystals grow by outward propagation of the crystal/liquid interfaces. If the temperature of a supercooled liquid is taken below the glass transition temperature of the material before crystallisation has had time to occur, then the supercooled liquid solidifies as the glass. Therefore, glass formation can be thought of as a matter of bypassing crystallisation.

According to Hancock *et al* (1997), formation of the amorphous state can be achieved by the following methods - quenching of the melt, vapour condensation, spray drying, lyophilisation, precipitation from solution or through milling or compaction of a crystalline material.

Amorphous materials for use in this research were produced by spray drying and by quenching of the melt in the case of TOAc.

For further details of the amorphous materials produced for this research, please refer to Chapter Five – Production and Preliminary Characterisation of Amorphous Materials.

CHAPTER TWO

MATERIALS AND EQUIPMENT

2.1 RAW MATERIALS

The raw materials used during the course of this research are itemised below.

α-Lactose monohydrate *	Pharmatose 325M. BN: 043813. Material supplied by DMV.
α-α-Trehalose dihydrate *	BN:24391. Material supplied by Quadrant Healthcare.
Trehalose octa-acetate (TOAc) *	BN: 033/164. Material supplied by Quadrant Healthcare.
Salbutamol sulphate	BN:46352. Material supplied by Norton Healthcare. The drug had been micronised and was supplied at a particle size of 5 μm.
Solvents	All solvents used were HPLC grade, purchased from Fisher Scientific.
Water	Millipore water was used in all experiments.

* For further details on these materials, refer to Chapter Three – Recrystallisation and Initial Characterisation of Materials.

2.2 EQUIPMENT

Equipment listed below was used during the course of this research.

2.2.1 CRYSTALLISATION VESSEL

Figure 2.1 illustrates the construction of the vessel used to carry out recrystallisation of materials. Two different capacity vessels were available, 400 ml and 2000 ml. Choice of vessel was dependent on the properties of the solution to be recrystallised and the amount of recrystallised material required.

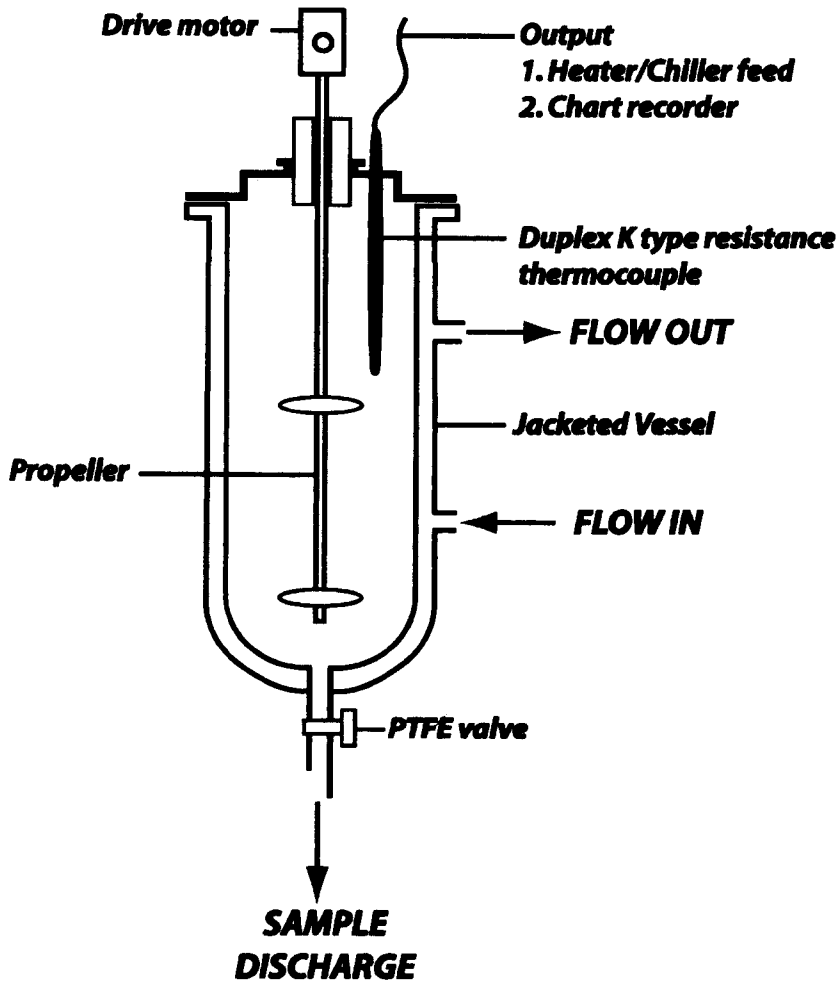

Figure 2.1: Crystallisation vessel

2.2.2 CHILLER-THERMO CIRCULATOR FITTED WITH DIGITAL CONTROLLER

Churchill Conair chiller-thermo circulator model 05/CTCV was used to pump the controlled temperature solution around the crystallisation vessel. The digital programmer/controller, model 818P, was manufactured by Eurotherm Controls and it accurately regulated the temperature of the solution being circulated to within 0.1 °C.

Calibration of the cooling equipment was carried out in order to ensure that the cooling rates required for recrystallisation were both accurate and linear. This calibration was monitored using a chart recorder attached to an independent thermocouple.

2.2.3 DIFFERENTIAL SCANNING CALORIMETRY (DSC)

Thermal Analysis Data Station 3600 connected to a Perkin Elmer DSC-4 differential scanning calorimeter was used for calorimetric measurements. Samples of approximately 5 to 10 mg were heated in pierced aluminium pans from 25 °C at a rate of 10 °C per minute. The DSC was calibrated daily prior to use by the heating of identical empty pierced aluminium pans at the same heating rate in order to obtain the baseline reading for the equipment.

2.2.4 FOURIER-TRANSFORM INFRA-RED SPECTROSCOPY (FT-IR)

A Nicolet 205 FT-IR spectrophotometer was used to analyse the majority of the samples. When this equipment was not available, a Shimadzu FT-IR-8300 spectrophotometer was used. Potassium bromide (KBr) used with the apparatus was purchased from the Sigma Chemical Company.

The Nicolet spectrophotometer was used to analyse samples by diffuse reflectance. Samples were ground together with KBr prior to analysis. In the Shimadzu equipment, KBr disks were analysed that were produced from the sample ground together with KBr being compressed into a disk by the application of approximately 10 tonnes of pressure. In all cases, the average sample size was approximately 10 mg.

2.2.5 Optical Microscopy

The equipment used was a Nikon SMZ-10 microscope with polarised light. An Olympus OM2-SPOT 35 mm camera was also attached.

2.2.6 Scanning Electron Microscopy (SEM)

Scanning Electron Microscope, Model LEICA S430 was used to produce images of selected materials. The equipment was operated at an accelerating voltage of 7.5 kV. Prior to analysis, all of the samples were lightly sputter coated in gold using an Edwards S150 Sputter coater, as SEM requires a conductive surface to enable image generation.

2.2.7 Thermal Gravimetric Analysis (TGA)

A Stanton Redcroft TG-750 was used to determine the water/solvent content of the samples analysed. A heating rate of 20 °C/minute to approximately 150 °C was used and the sample size for each experiment did not exceed 10 mg.

2.2.8 Nuclear Magnetic Resonance (NMR)

The equipment used to produce the NMR profiles of selected materials was a Bruker AC250. Both proton and carbon NMR analyses of the selected materials were carried out.

2.2.9 HOT STAGE MICROSCOPY

Hot stage microscopy was carried out on selected material samples using equipment at Quadrant Healthcare. The equipment used was a THMS 600 hot stage attached to a Nikon Labophot-2 light microscope. Images were captured with a JVC TK-1281EG camera and viewed using Lucia G software (version 2.3a).

2.2.10 DRYING OVEN

Either a standard Gallenkamp vacuum oven or a Gallenkamp HotBox size 1 oven were used to dry samples of the different batches of materials produced.

2.2.11 SPRAY DRYING EQUIPMENT

The Standard Niro Mobile Minor Spray Dryer was used at Quadrant Healthcare to manufacture spray dried samples of lactose, trehalose and TOAc. 63-90 μm was the target particle size range.

150ml of 20%$^{w}/_{v}$ load solutions were prepared for each material. Both the lactose and trehalose dihydrate materials were aqueous solutions. The TOAc solution was prepared using the solvent dichloromethane (DCM). The expected yield of material was approximately 50%. For further details, please refer to Chapter Five – Production and Preliminary Characterisation of Amorphous Materials.

2.2.12 SIEVING EQUIPMENT

Endecott certified sieves were used. A $\sqrt{2}$ progression was adopted – 710 μm, 500 μm, 355 μm, 250 μm, 180 μm, 125 μm, 90 μm, 63 μm and 45 μm were the sieve sizes used.

Sieve shaker used was an Endecott EVP1. The sieve shaker was operated for 15 minutes and the amplitude was set according to the manufacturers instructions.

Salbutamol sulphate was pre-screened with a 500 μm sieve before blending.

2.2.13 TURBULA® MIXER UNIT

Turbula® mixer unit type T2C was used to blend the materials at a speed setting of 62 r.p.m. For further details relating to the preparation of powder blends, please refer to Chapter Seven – Assessment of Inhalation Performance.

2.2.14 ULTRA-VIOLET SPECTROPHOTOMETER

Pye Unicam UV/VIS spectrophotometer model SP8-400 with 10 mm x 10 mm cuvettes.

2.2.15 HIGH PERFORMANCE LIQUID CHROMATOGRAPHY (HPLC)

Philips PU4100 liquid chromatograph and Philips PU4110 UV/VIS detector was used for the analysis of samples. Samples were injected using a Philips Autojector, model PU4700.

The HPLC was connected to a computer, and the results were processed using JCL6000 chromatography data system software version 5.07. For further details, please refer to Chapter Seven – Assessment of Inhalation Performance.

2.2.16 Dynamic Vapour Sorption (DVS)

A Surface Measurement Systems DVS 2000 automated vapour sorption analyser was used to investigate the vapour sorption of water on selected samples. The DVS instrument was run under the control of a dedicated PC. *DVSWin* software (version 2.16) was used to set up and subsequently run the experiments. The data analysis program runs within Microsoft Excel. The DVS equipment was set to 25 °C for all experiments. For further details, please refer to Chapter Six – Further Characterisation of Materials.

2.2.17 X-Ray Crystallography

The equipment used was a Bruker SMART 1000 CCD diffractometer using MoK (alpha) 1 radiation (0.71073 Å). Dr Jan Skakle at the University of Aberdeen carried out the analysis. A 2-theta range of 6 ° to 40 ° was used in the analysis of all samples. For further details, please refer to Chapter Six – Further Characterisation of Materials.

2.2.18 Atomic Force Microscopy (AFM)

A Digital Instruments Multi-Mode with Nanoscope IIIa controller atomic force microscope was used to analyse two of the TOAc samples. The instrument has a maximum scan range of 13 μm.

A different AFM instrument was subsequently used in order to analyse the TOAc over a greater scan area. The AFM used for this analysis was Digital Instruments Dimensions 3000 AFM with Nanoscope IIIa controller. This instrument has a maximum scan range of 100 μm. This equipment had a motorised stage which made it easier to move the sample underneath the AFM probe.

Both AFM instruments were located at the University of Nottingham and used under the direction of Dr Simon Connell. For further details, please refer to Chapter Six – Further Characterisation of Materials.

2.2.19 Laser Profilometer

UBM laser and microfocus measurement system supported by UBSoft computer software version 2.8. A Monacor video monitor was attached to visualise the surface for analysis. A surface area of 30 μm square was analysed, with 1 point per μm measured. A depth of field of ± 500 μm was set. Dr Fridrun Podczeck kindly provided the equipment for use at the University of London. For further details, please refer to Chapter Six – Further Characterisation of Materials.

2.2.20 Multi-Stage Liquid Impinger (MSLI)

A five stage Astra-Draco multi-stage liquid impinger (MSLI), supplied by Copely Instruments, was used to assess the performance of materials from the chosen DPI device. Assessment of performance was made through the determination and subsequent comparison of the average percent fine particle fraction achieved by each material. Further details for this equipment can be found in Chapter Seven – Assessment of Inhalation Performance.

2.2.21 Dry Powder Inhalation System

The DPI system used was a **FlowCaps®** inhaler, supplied by Hovione.

The inhaler utilised size 4 hard gelatin capsules for drug delivery. 20 mg was the target fill weight for each capsule, and 200 μg of salbutamol base was contained in each 20 mg of

blend. Further details of the device and blend production are included in Chapter Seven – Assessment of Inhalation Performance.

CHAPTER THREE

RECRYSTALLISATION AND INITIAL CHARACTERISATION OF MATERIALS

3.1 PRELIMINARY CHARACTERISATION OF THE CRYSTALLINE RAW MATERIALS

3.1.1 α-Lactose Monohydrate – Pharmatose 325M

α-Lactose (α-D-galactopyranosyl-D-glucose) (Fig. 3.1) monohydrate is a reducing heterodisaccharide. It is constituted of two different monosaccharides that are linked by an oxygen atom. The resultant dimer has an unsubstituted anomeric centre and consequently the properties of a free, reducing sugar.

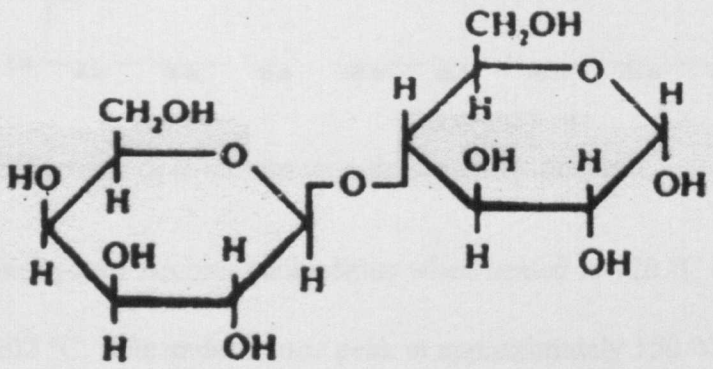

Figure 3.1: α-Lactose structure.

The opaque crystals of the raw material are the characteristic tomahawk shape associated with lactose. Figure 3.2 is a SEM image of the raw material.

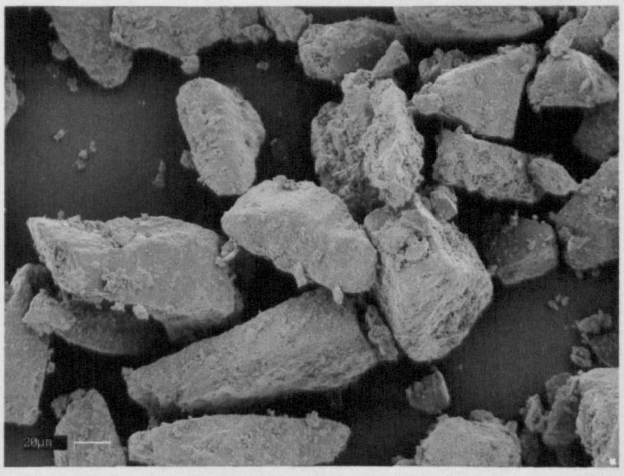

Figure 3.2: SEM image of the α-lactose monohydrate raw material.

A DSC profile of the raw material is given below.

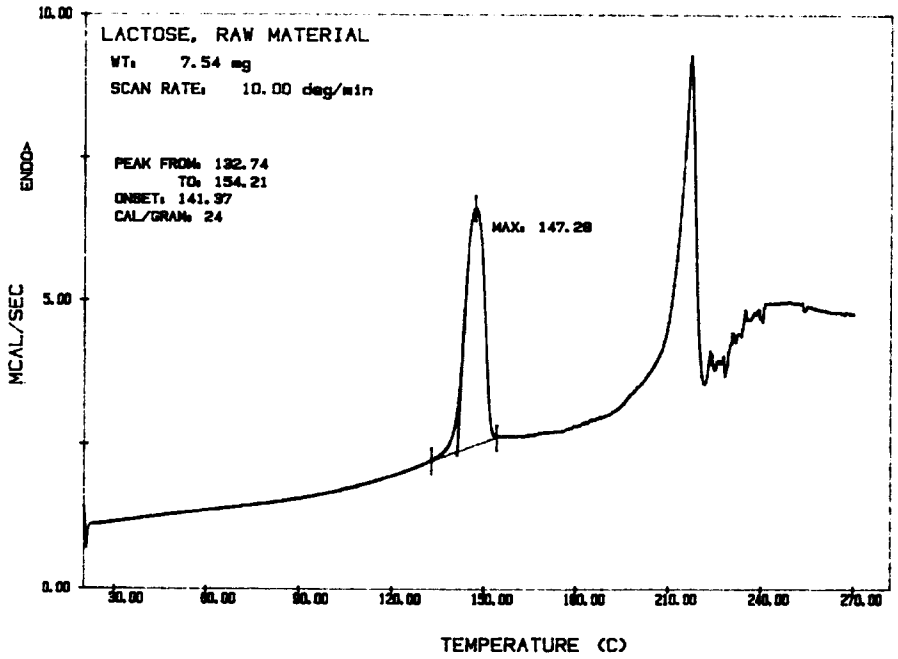

Figure 3.3: DSC profile of α-lactose monohydrate raw material.

α-Lactose monohydrate becomes anhydrous when heated to 120 °C and has a melting point of 201-202 °C. The endothermic peak at approximately 150 °C represents dehydration of the α-lactose monohydrate.

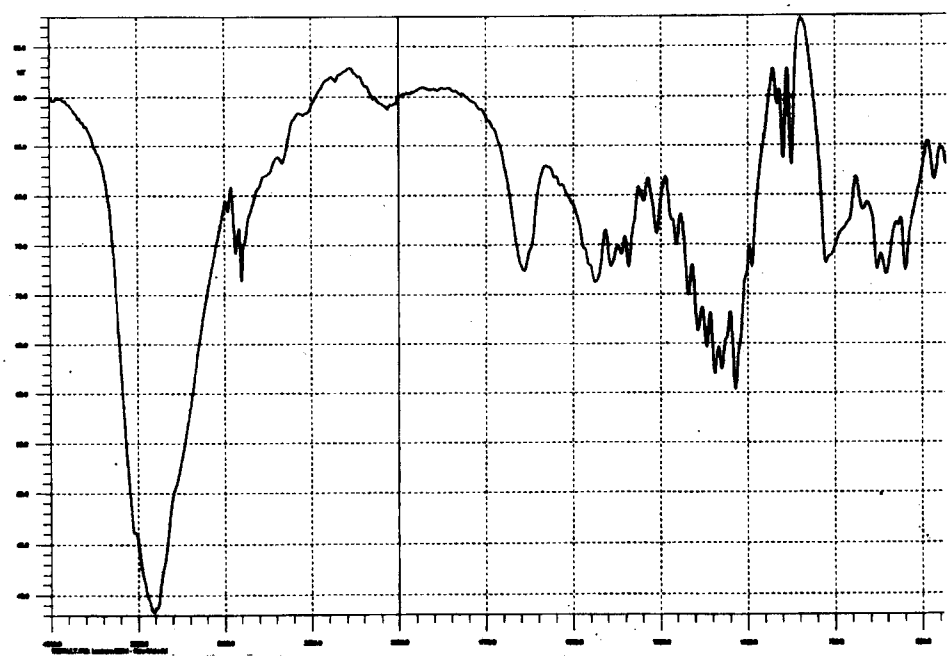

Figure 3.4: FT-IR spectrum of α-lactose monohydrate raw material.

The spectrum can be seen to contain well-resolved, sharply defined peaks as expected for a crystalline material. The O-H stretch region can be observed at approximately 3400 cm^{-1}.

3.1.2 α-α-Trehalose Dihydrate

α-α-Trehalose (α-D-glucopyranosyl-α-D-glucopyranoside) (Fig. 3.5) dihydrate is a non-reducing disaccharide, where two monosaccharide units are linked glycosidically through the oxygen atom of the reducing centre. Trehalose is abundant in nature, can be found in certain plants, algae, fungi and yeast and is the main carbohydrate component of the blood of a variety of insects. It performs a protective role allowing them to survive extreme conditions such as complete dehydration or freezing weather conditions.

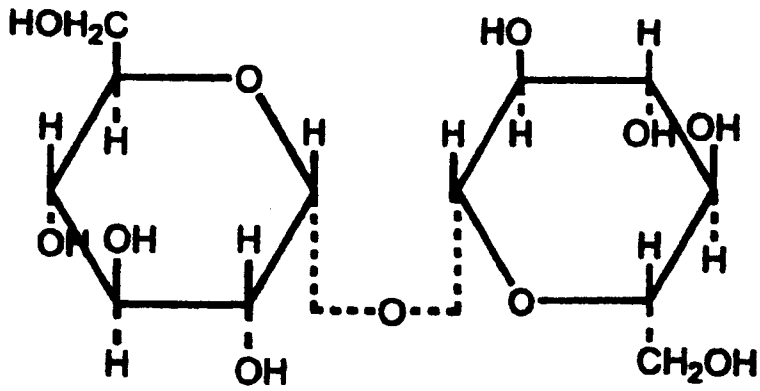

Figure 3.5: α-α-Trehalose structure

The molecule has hydrogen bond acceptor and donor groups that are thought to play a role in allowing trehalose to replace water in biological membranes, thereby imparting a form of cryogenic protection.

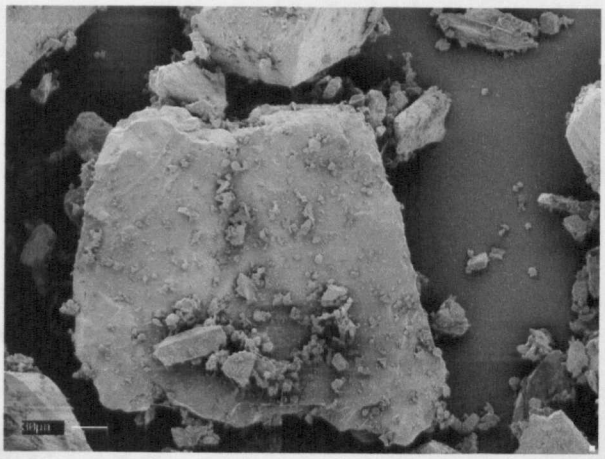

Figure 3.6: SEM image of α-α-trehalose dihydrate crystals (raw material)

The dihydrate is characterised by orthorhombic, bisphenoidal crystals (Fig. 3.6) and appears to have an irregular surface appearance.

Figure 3.7 below is a typical DSC plot of the raw material.

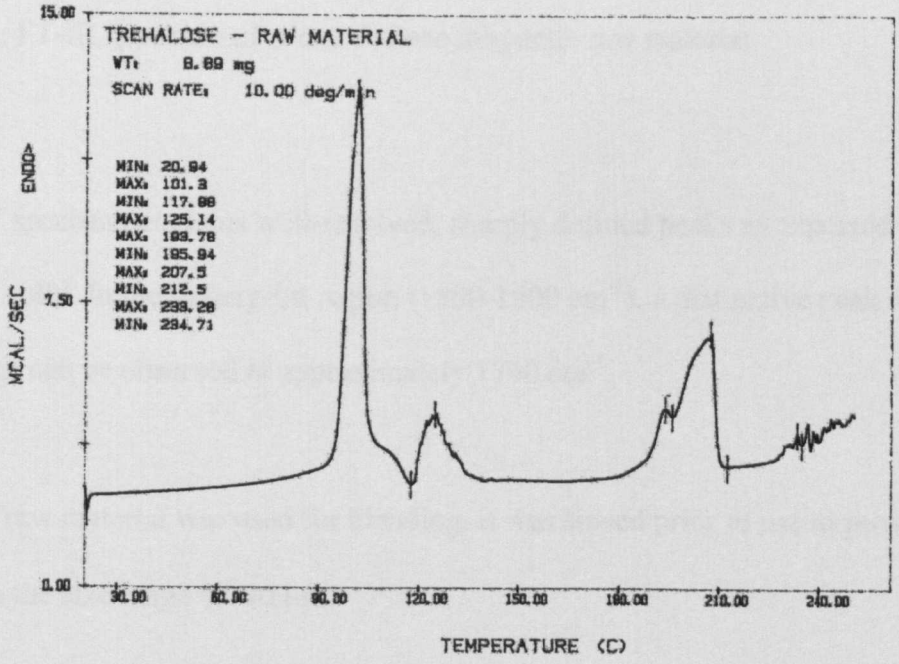

Figure 3.7: DSC profile of α-α-trehalose dihydrate raw material.

The endothermic peak at approximately 100 °C indicates a melt that is subsequently followed by an exothermic peak. This indicates rearrangement of the molecular structure of the sample prior to the loss of the water of crystallisation at approximately 130 °C.

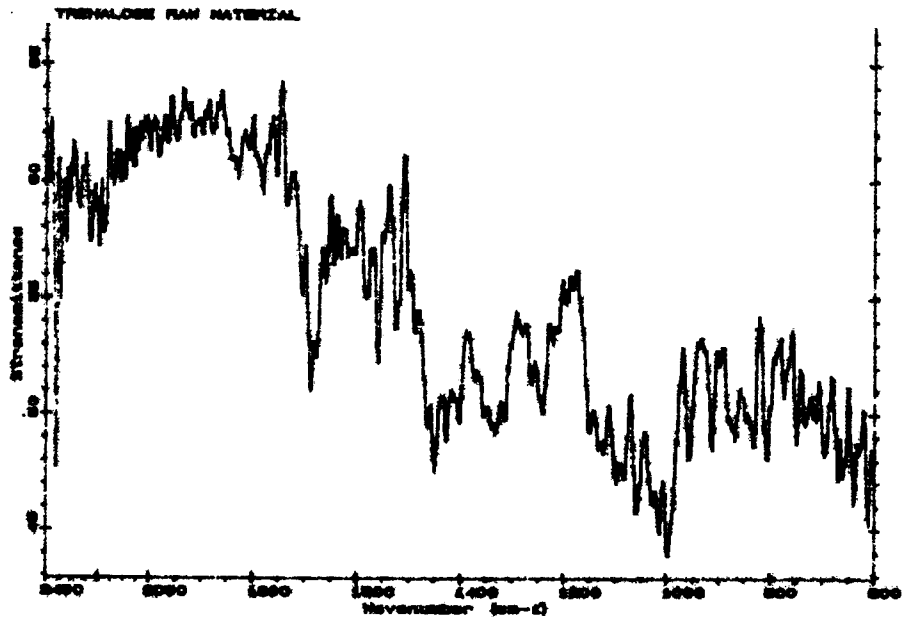

Figure 3.8: FT-IR spectrum of α-α-trehalose dihydrate raw material.

The FT-IR spectrum contains well-resolved, sharply defined peaks as expected with a crystalline solid. In the fingerprint region (1800-1500 cm^{-1}), a distinctive peak relating to C=O stretch can be observed at approximately 1700 cm^{-1}.

Where the raw material was used for blending, it was sieved prior to use to provide particles in the size range 63-90 μm.

3.1.3 Trehalose Octa-acetate (TOAc)

Chemical adaptation of the trehalose molecule allows a less hydrophilic material to be produced. Trehalose dihydrate is converted via a reaction with acetic anhydride-sodium acetate. The –OH groups are replaced with acetate ($-O_2C_2H_3$) groups to produce the oligosaccharide ester derivative (OED) trehalose octa-acetate (TOAc) (Fig. 3.9). The TOAc raw material is subsequently recrystallised from ethanol.

The literature contains very little information relating to the trehalose derivative, especially with respect to the physio-chemical properties of the material. In addition, there is little structural information. One of the few papers on the subject is by Young and Shin (1993) who reported the structures of two polymorphic forms of TOAc monohydrate. Unfortunately, the paper does not give specific details of the method and conditions used to produce each of the two polymorphs. The bulk of the report is simply a listing of the refined single crystal data used to generate the theoretical powder pattern.

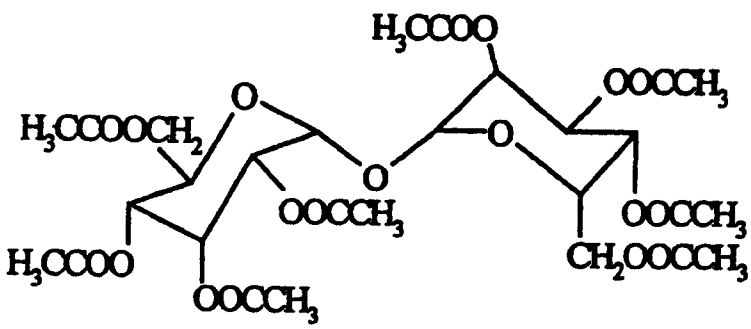

Figure 3.9: Trehalose octa-acetate structure

The TOAc raw material supplied was in a crystalline form consisting of opaque, acicular crystals typically around 0.5-2 mm in length by 0.3 mm.

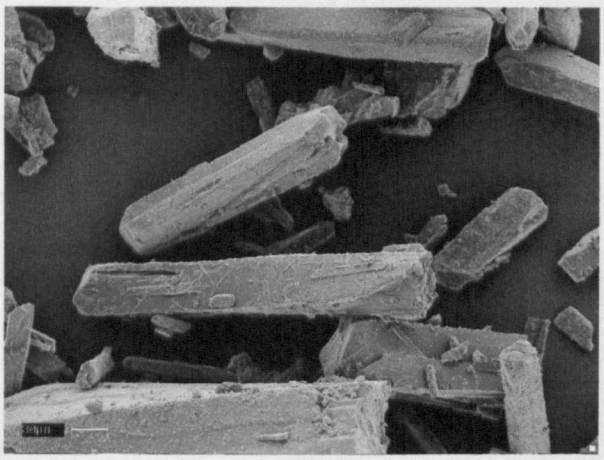

Figure 3.10: SEM image of TOAc raw material

The material shown above is an image of the TOAc raw material. The crystals are of an aciclic nature and are clearly extremely brittle, as fractures are easily observed.

A typical DSC trace obtained from the TOAc raw material is given below.

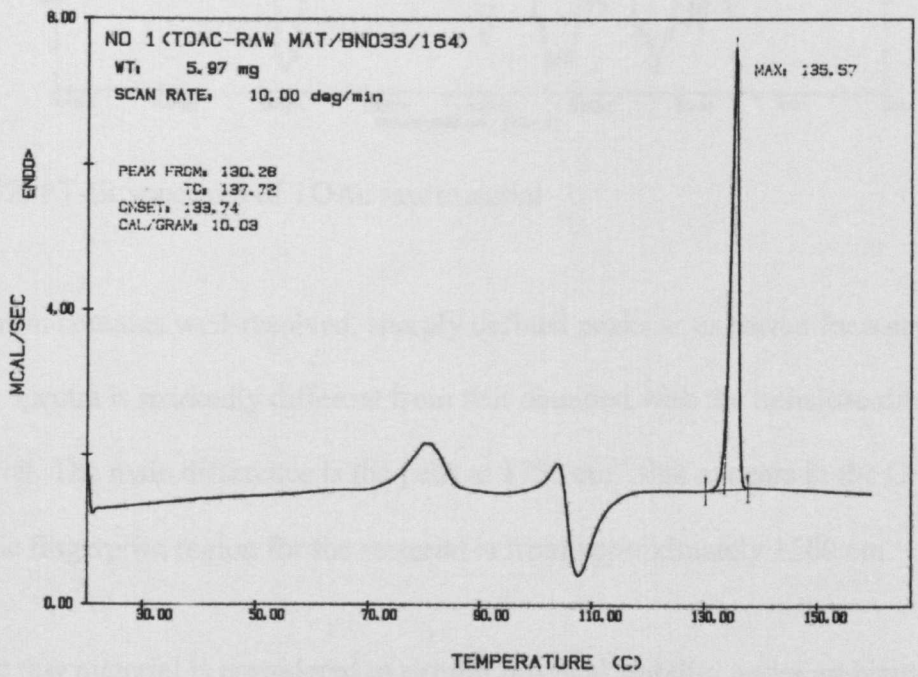

Figure 3.11: DSC profile of TOAc raw material.

In the DSC profile, four principle features are observed. There are three endothermic peaks at approximately 75 °C, 105 °C and 135 °C, and one exothermic peak around 108 °C.

The first peak is probably due to residual solvent in the material, and the second corresponds to a partial melt. The exothermic peak indicates a recrystallisation of the material, probably to a different polymorphic form, which subsequently melts at 135 °C.

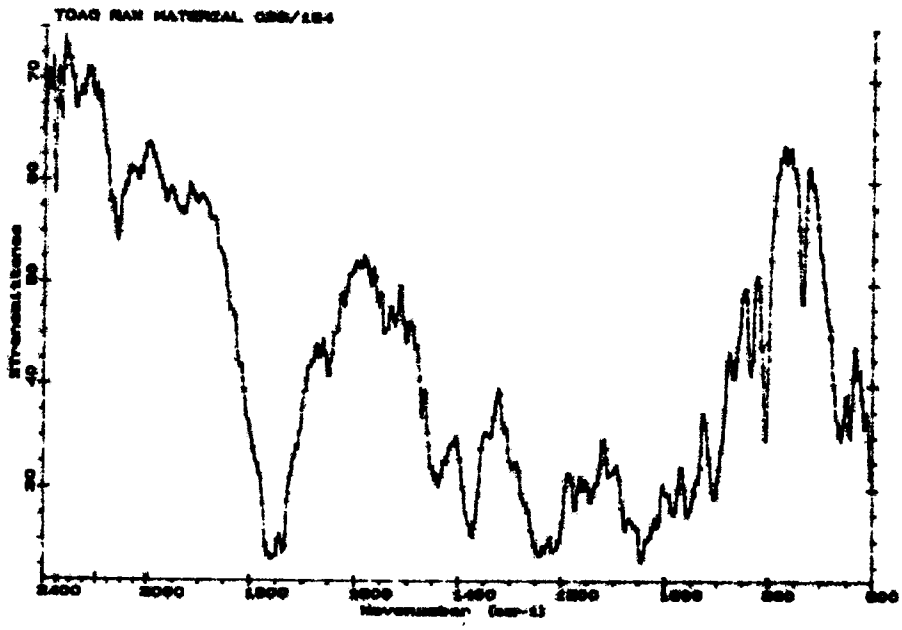

Figure 3.12: FT-IR spectrum of TOAc raw material

The spectrum contains well-resolved, sharply defined peaks as expected for a crystalline solid. The spectra is markedly different from that obtained with the trehalose dihydrate raw material. The main difference is the peak at 1750 cm^{-1} that appears in the C=O stretch region. The fingerprint region for the material is from approximately 1500 cm^{-1}.

The TOAc raw material is considered to exhibit physical stability under ambient storage conditions (Quadrant Healthcare).

Where the raw material was used to manufacture a blend, it was sieved prior to use to provide particles in the size range 63-90 μm. However, it should be mentioned that considering the morphology of the raw material there is a definite possibility that particles of a larger longitudinal length than 90 μm may have been present in the batch of material sieved.

3.2 SOLUBILITY PROFILES

In order to control the crystallisation of a material from solution, it is important to know the solubility of the material in the desired solvent. Only the solubility of trehalose and TOAc in solutions containing ethanol were to be determined, as information relating to the solubility of lactose in water was widely available.

3.2.1 SOLUBILITY OF LACTOSE MONOHYDRATE IN WATER

The solubility of lactose monohydrate in water is available from many published works. The graph overleaf represents the solubility of lactose in pure water. The figures used were taken from the Handbook of Pharmaceutical Excipients, second edition.

Solubility in water at:				
25 °C	**40 °C**	**50 °C**	**60 °C**	**80 °C**
216.0 mg/ml (1 in 4.63)	318.5 mg/ml (1 in 3.14)	490.2 mg/ml (1 in 2.04)	595.2 mg/ml (1 in 1.68)	934.6 mg/ml (1 in 1.07)

Figure 3.13: Solubility values for lactose monohydrate in water

Lactose (as the control material) was only to be recrystallised from pure water so therefore no further solubility analyses were required for this material.

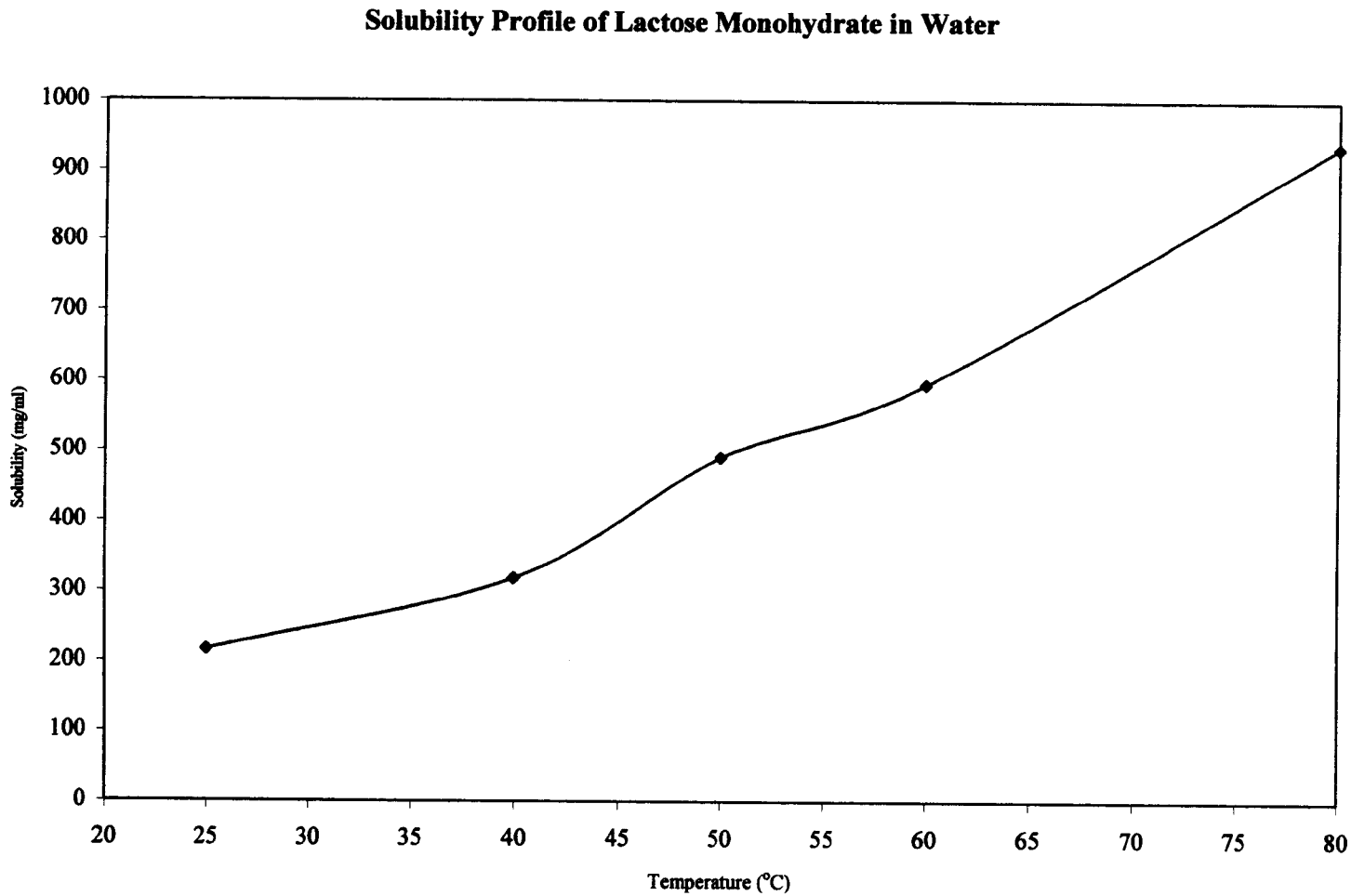

Figure 3.14: A graph of the solubility profile of lactose monohydrate in water (data from literature - Handbook of Pharmaceutical Excipients, second edition).

3.2.2 GRAVIMETRIC ANALYSIS OF TREHALOSE DIHYDRATE AND TOAC

Gravimetric analysis was the method used to determine the solubility of the trehalose and TOAc materials in a range of solvents containing ethanol:water. This method of analysis was chosen as it was the most effective method to accurately determine the solubility of the materials in selected solvents as equipment was readily available and was easy to set up. UV analysis of the solutions to determine concentration was not possible as the carbohydrate materials are not detectable in the UV range.

A multiple 10-station magnetic stirrer (Janke & Kunkel IKA Labortechnik Type RO 10) was used in conjunction with a customised water bath. The temperature of the water was controlled using a separate Grant W14 Type ZD-P water bath, heater and pump that circulated water through a copper element in the customised water bath. The temperature of the water inside the customised bath was also periodically checked independently with a thermometer.

3.2.2.1 METHOD FOR GRAVIMETRIC ANALYSIS OF TREHALOSE DIHYDRATE AND TOAC

20 ml of solvent was added to a scintillation vial into which approximately 1 g of either trehalose or TOAc raw material had been added. Each of the vials used also contained a magnetic flea. The vials were then sealed, and were placed appropriately into the water bath situated on top of the 10-station magnetic stirrer. The solutions were left to equilibrate with respect to temperature for one hour, with continual stirring. If an excess of material was not clearly visible in a vial, additional raw material was added.

For the next hour, the temperature of the water bath was fluctuated over approximately 0.5 °C from the required temperature in a cyclic manner. This was carried out because the solubility of a material in a solvent is dynamic when an excess of material is present. The solutions were then left at the required temperature for a minimum of two hours, with constant stirring and an excess of material clearly visible.

After this time, the saturated solutions were filtered quickly through a Whatman No. 50 filter with a vacuum applied. The filtrate was then returned to the water bath in a clean scintillation vial. A calibrated micropipette was used to dispense 5 ml of the saturated solution into a labelled, pre-weighed test tube. For each solution, three tubes were filled with 5 ml each.

The tubes were then stored in an oven at 60 °C to facilitate the evaporation of the solvent for approximately one month, until no solvent was visible. The tubes were then re-weighed twice weekly until they achieved a constant weight. The original weight of the tube was then deducted from the final weight to obtain the weight of material contained within the tube. As 5 ml of solution was added to each tube, the value obtained was divided by five in order to give the solubility in weight per ml. The average value from the three tubes for each solvent was then calculated, and this value was used to construct the solubility curve for each material.

3.2.3 SOLUBILITY OF TREHALOSE DIHYDRATE

There is currently very little published information relating to the solubility of trehalose dihydrate. What data there is relates to the solubility of the material in water only. It was

therefore necessary to conduct gravimetric experiments to determine the solubility of trehalose dihydrate in other selected solvents that could possibly be used to manipulate the morphology of recrystallised material. Two ethanol:water solutions were used to create additional solubility profiles for trehalose dihydrate. The solutions were 40:60 ethanol:water and 60:40 ethanol:water. Pure ethanol (HPLC grade) was used to produce each solution. A molecular sieve was used to ensure that the solvent remained completely free from water and as an extra precaution, the solvent was also stored in a desiccator when not in use.

Figure 3.16 is a solubility curve for α-α-trehalose dihydrate in water, generated from data published by Miller *et al* (1997).

Figure 3.17 is a graph showing the results of the gravimetric analysis conducted with α-α-trehalose dihydrate as described above. Two solvents were used, namely 40:60 ethanol:water and 60:40 ethanol:water.

Ratio of Ethanol:Water	**Solubility (mg/ml) at:**					
	15 °C	**25 °C**	**35 °C**	**45 °C**	**55 °C**	**65 °C**
40:60	164.9	254.9	357.4	508.2	715.1	923.1
60:40	66.5	100.0	161.9	258.1	443.5	677.1

Figure 3.15: Gravimetrically determined solubility values for α-α-trehalose dihydrate.

Figure 3.18 is a summary graph, showing the solubility curves for α-α-trehalose dihydrate from 10 °C to 65 °C for the three solvents mentioned above.

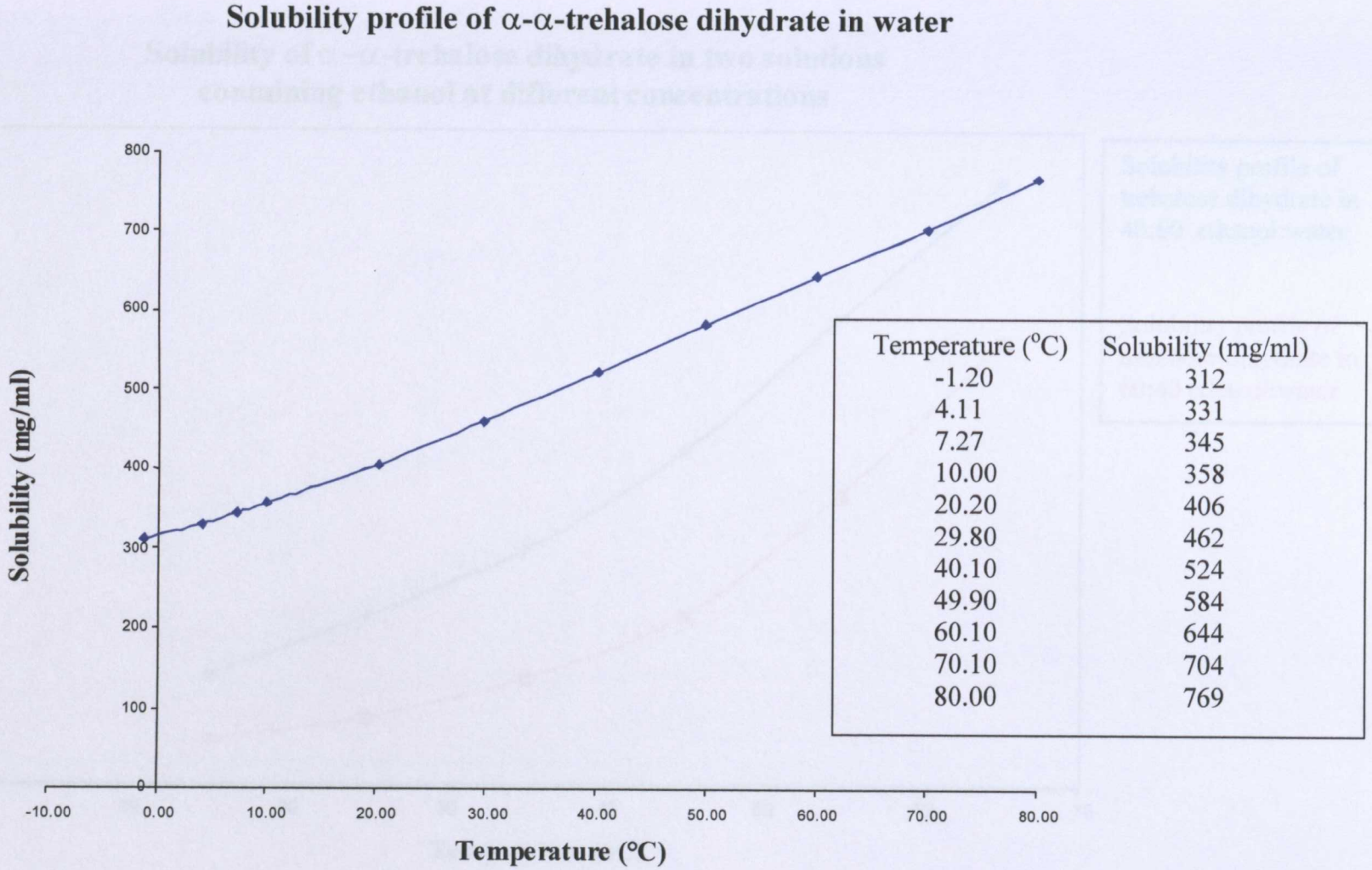

Figure 3.16: Solubility profile of α-α-trehalose dihydrate in water (from published data – Miller *et al* (1997)).

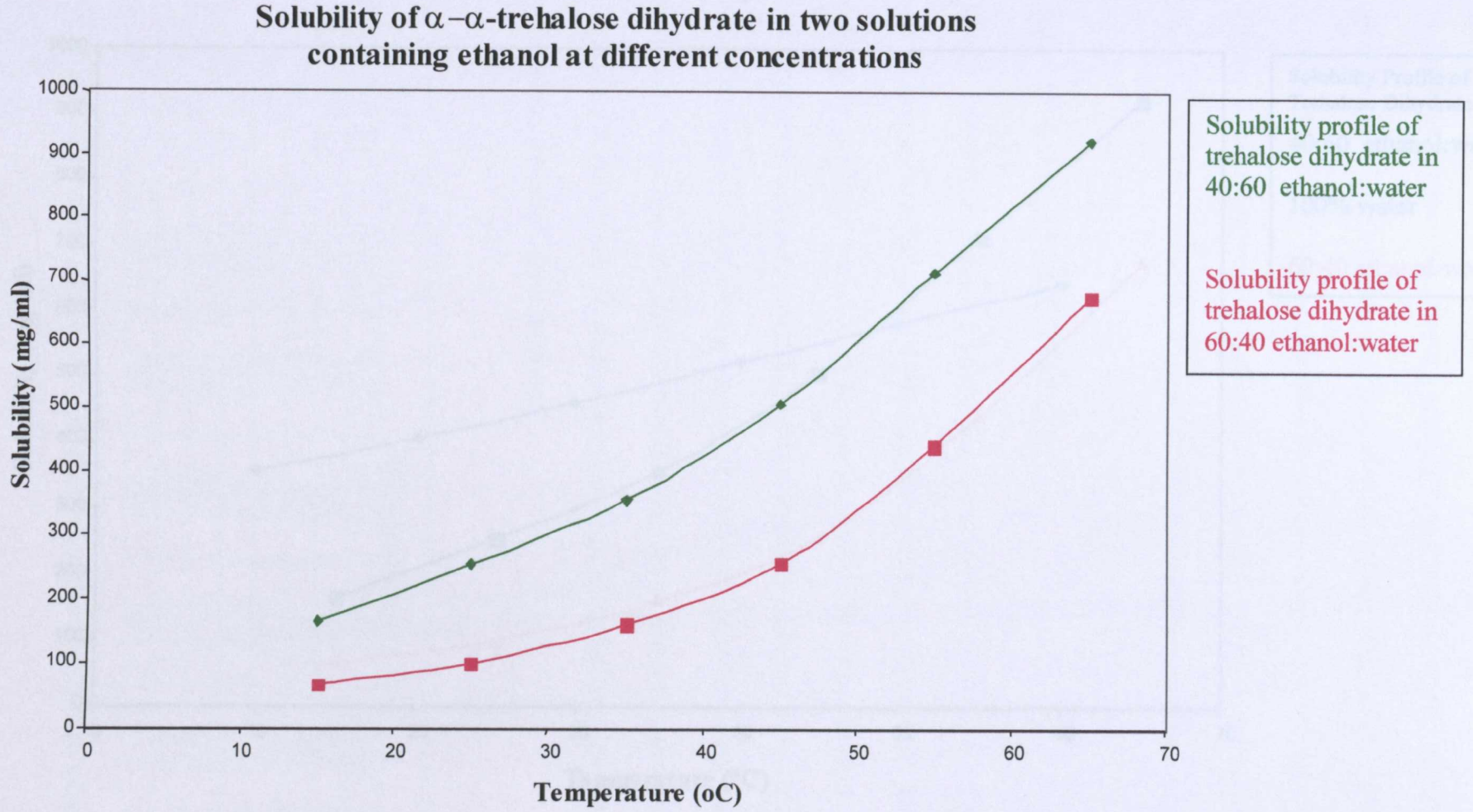

Figure 3.17: Solubility profile of α-α-trehalose dihydrate in 40:60 ethanol:water and 60:40 ethanol:water obtained from gravimetric analysis.

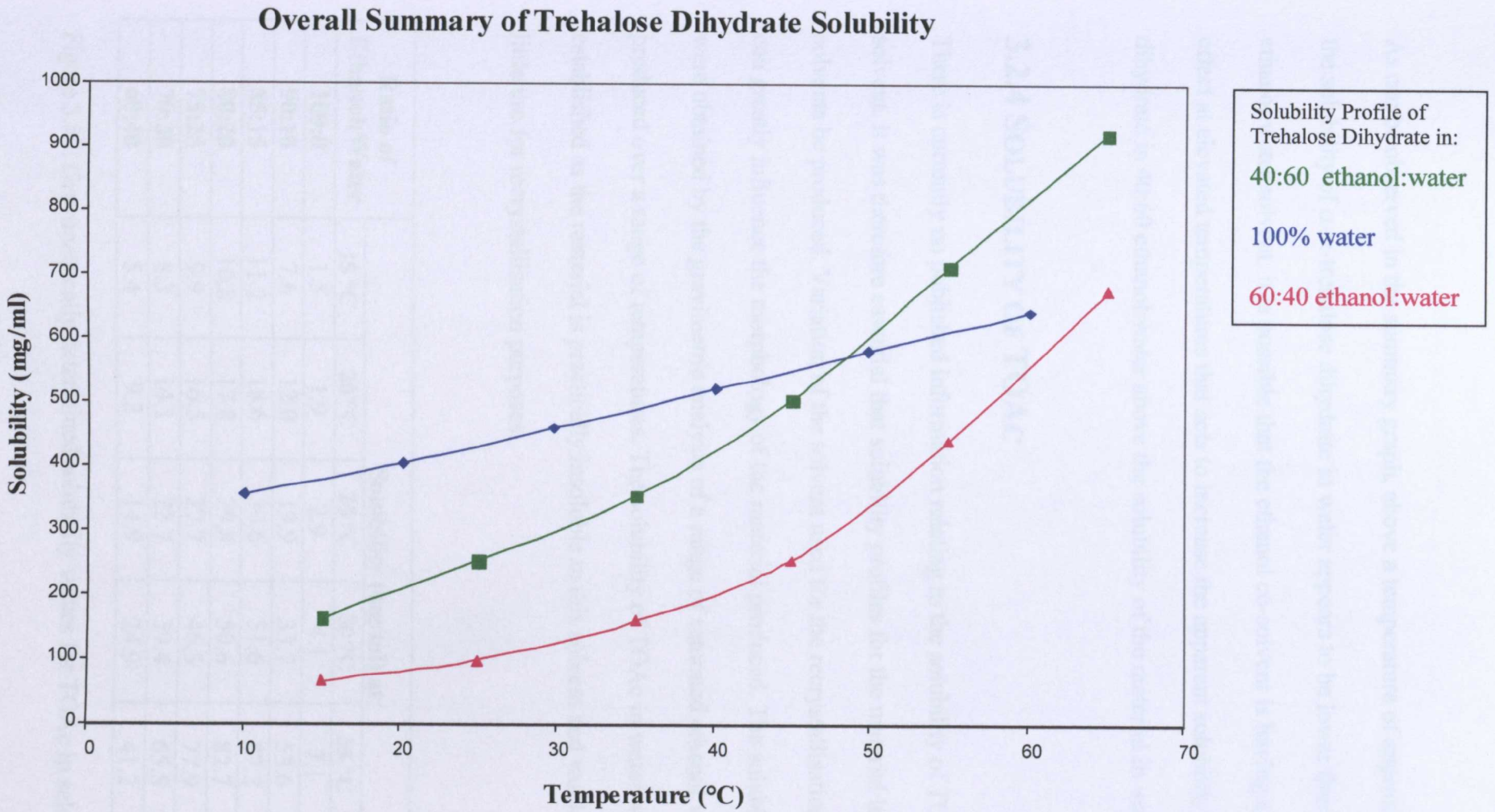

Figure 3.18: Summary graph of the solubility profile of α-α-trehalose dihydrate.

As can be observed in the summary graph, above a temperature of approximately 45 °C, the solubility of α-α-trehalose dihydrate in water appears to be lower than in a 40:60 ethanol:water solvent. It is possible that the ethanol co-solvent is having a synergistic effect at elevated temperatures that acts to increase the apparent solubility of α-α-trehalose dihydrate in 40:60 ethanol:water above the solubility of the material in water alone.

3.2.4 SOLUBILITY OF TOAC

There is currently no published information relating to the solubility of TOAc in any solvent. It was therefore essential that solubility profiles for the material in a variety of solvents be produced. Variation of the solvent used for the recrystallisation of a material can greatly influence the morphology of the material produced. The solubility profiles were obtained by the gravimetric analysis of a range of saturated ethanol:water solutions produced over a range of temperatures. The solubility of TOAc in water was not established as the material is practically insoluble in this solvent and would therefore be of little use for recrystallisation purposes.

Ratio of Ethanol:Water	Solubility (mg/ml) at:					
	15 °C	20 °C	25 °C	30 °C	35 °C	40 °C
100:0	1.5	1.9	2.9	4.1	7.1	12.7
90:10	7.6	12.0	19.9	33.7	53.6	97.9
85:15	11.2	18.6	30.6	51.6	87.2	161.8
80:20	10.8	17.8	29.8	50.6	82.7	156.8
75:25	9.9	16.5	27.7	46.3	77.9	142.4
70:30	8.3	14.1	23.7	39.4	65.8	118.3
60:40	5.4	9.2	14.9	24.9	41.2	74.6

Figure 3.19: Gravimetrically determined solubility values for TOAc in selected solvents.

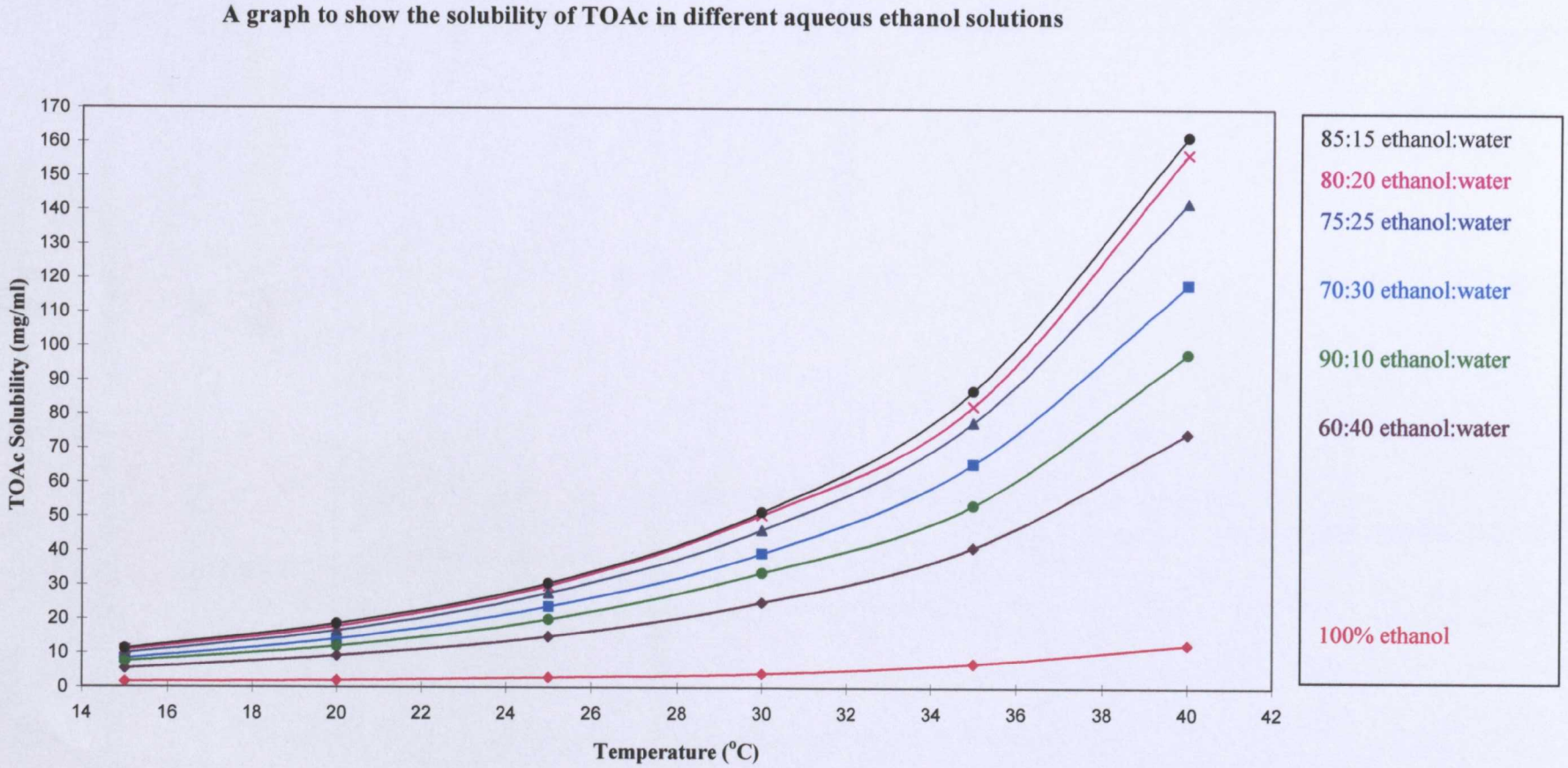

Figure 3.20: Summary graph of the solubility of TOAc in solvents containing ethanol.

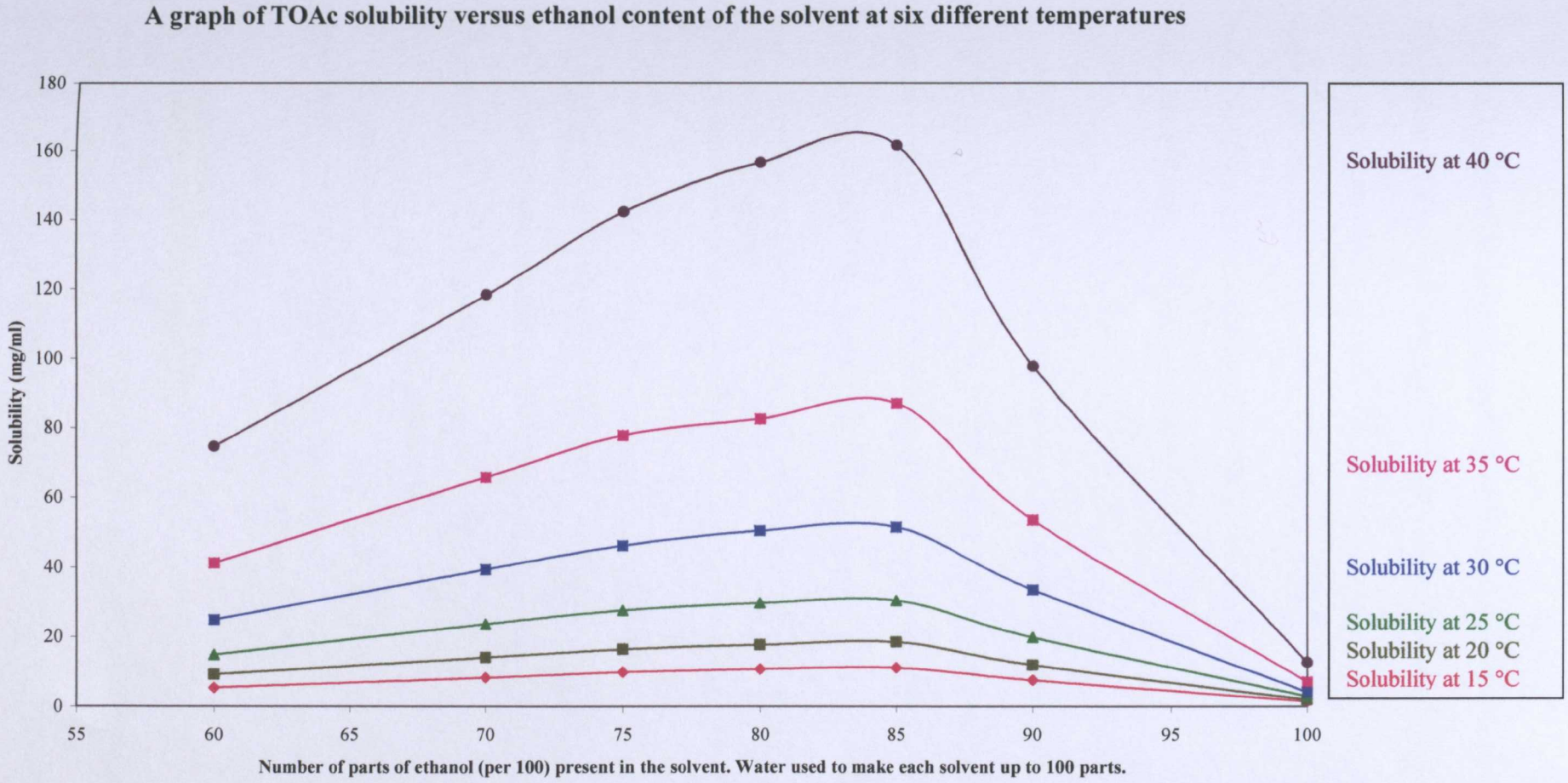

Figure 3.21: Summary graph of TOAc solubility versus ethanol content of the solvent at different temperatures.

Figure 3.20 shows the solubility profiles of TOAc in various solvents containing ethanol. The highest solubility was obtained with the solvent containing 15 percent water. The results of the gravimetric analysis indicate that in combination with ethanol, water has a synergistic co-solvent effect on the solubility of TOAc, with 15 percent as the optimum level. This finding was surprising considering the extremely hydrophobic nature of TOAc when water alone is used as the solvent.

Figure 3.21 presents the TOAc solubilities determined by gravimetric analysis versus the ethanol content of the solvent at different temperatures. The graph appears to show an area of slight irregularity in the curves between 75 and 85 parts of ethanol (per 100) that is particularly evident in the curve for the TOAc solubility at 35 °C. Such an irregularity could be indicative of a modification in the form of TOAc that is being recrystallised that corresponds with an alteration in the ethanol content of the solvent.

The following small-scale recrystallisation experiments were carried out in conjunction with the solubility determinations in order to further investigate the effect of the solvent on both the TOAc and trehalose material recrystallised from the solvents studied.

3.3 SMALL-SCALE RECRYSTALLISATION EXPERIMENTS TO DETERMINE THE EFFECT OF SOLVENT ON THE MORPHOLOGY OF α-α-TREHALOSE DIHYDRATE AND TOAc

Small-scale experiments into the effect of solvent on the morphology of recrystallised trehalose dihydrate and TOAc were carried out in conjunction with the determination of material solubility. The small remaining volumes of saturated solution not used in the gravimetric determination of solubility were used.

Approximately 2.0 ml of each solution was dropped using a pipette onto a labelled glass microscope slide. The solution was then left to allow recrystallisation of the material via solvent evaporation. As the volume of the solution was much smaller and the surface area larger, recrystallisation of the material on the glass slide would be observed more quickly than with the solutions in the test tubes. The use of a microscope slide would also facilitate the examination of the crystals under a microscope following their recrystallisation.

Following recrystallisation of the materials, it was hoped that examination of the samples would allow for an early indication of whether the morphology of the materials were significantly affected by modification of the solvent used for recrystallisation. In addition, it was also hoped that the results would indicate whether a change in the form of TOAc being recrystallised was possible as had been indicated by the solubility data generated for the material.

3.3.1 TREHALOSE DIHYDRATE

The trehalose samples that were recrystallised from both 40:60 and 60:40 ethanol:water solutions respectively appeared to have retained the morphology of the raw material.

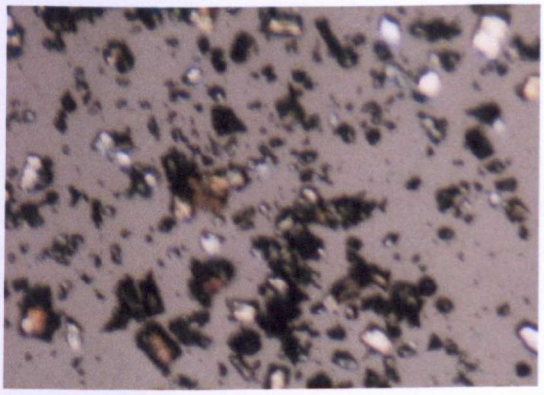

Figure 3.22: Trehalose recrystallised from 40:60 ethanol:water. (x20 magnification).

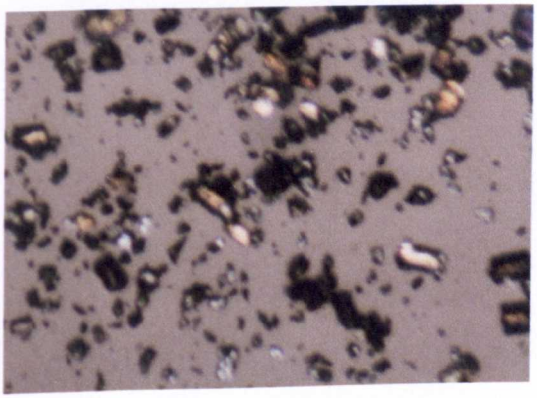

Figure 3.23: Trehalose recrystallised from 60:40 ethanol:water. (x20 magnification).

These results indicate that ethanol:water solvents studied in this research with trehalose dihydrate do not have a significant impact on the morphology of the material recrystallised.

3.3.2 TOAC

The small-scale recrystallisation experiments with TOAc resulted in the morphologies described in figure 3.24.

Ratio of Ethanol:Water	Morphology of material produced
100:0	Acicular crystals
90:10	Acicular crystals
85:15	Mix of acicular and orthorhombic, mainly acicular
80:20	Mix of acicular and orthorhombic
75:25	Mix of acicular and orthorhombic, mainly orthorhombic
70:30	Orthorhombic crystals
60:40	Orthorhombic crystals

Figure 3.24: Description of morphologies produced by recrystallisation of TOAc from different solvents containing ethanol.

Photographic images of the crystals obtained from each of the solvents mentioned in figure 3.24 are included below and overleaf.

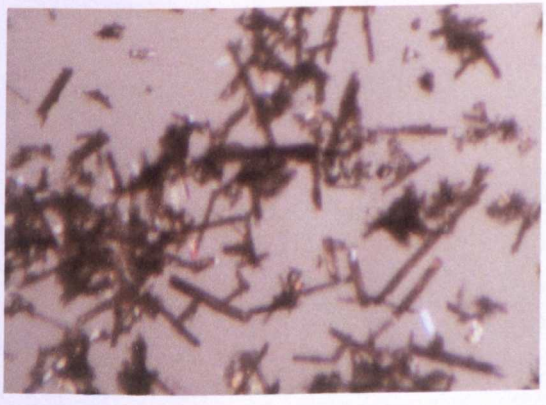

Figure 3.25: TOAc recrystallised from 100% ethanol (x20 magnification)

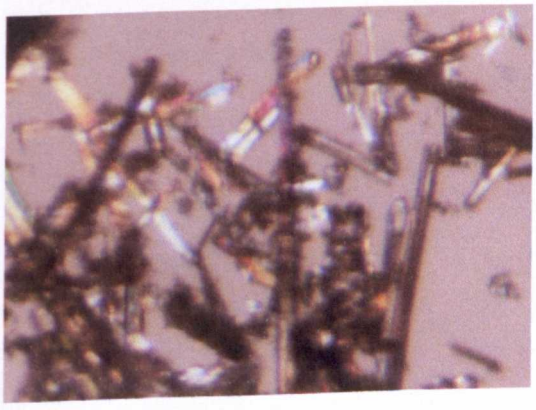

Figure 3.26: TOAc recrystallised from 90:10 ethanol:water (x40 magnification)

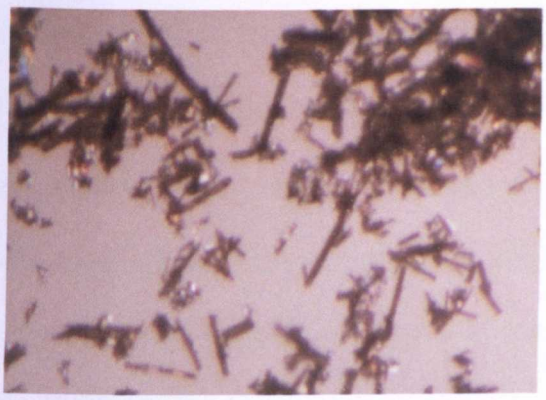

Figure 3.27: TOAc recrystallised from 85:15 ethanol:water (x20 magnification)

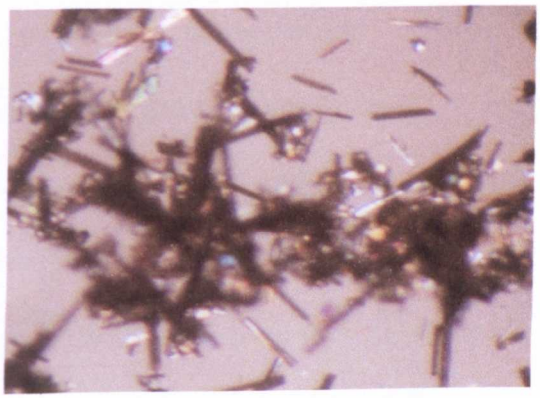

Figure 3.28: TOAc recrystallised from 80:20 ethanol:water (x20 magnification)

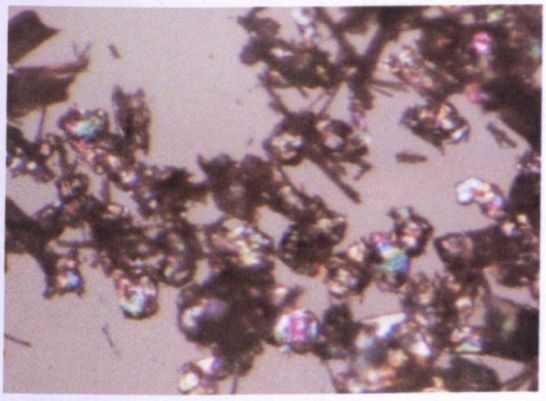

Figure 3.29: TOAc recrystallised from 75:25 ethanol:water (x20 magnification)

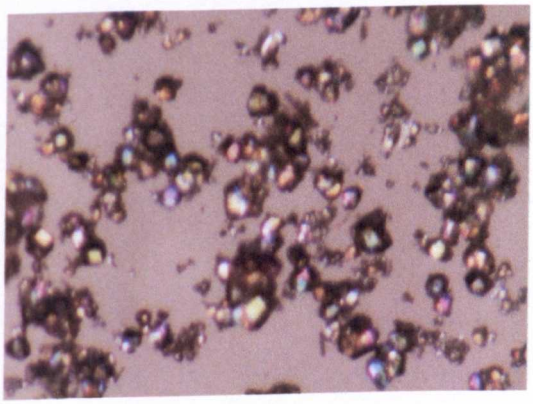

Figure 3.30: TOAc recrystallised from 70:30 ethanol:water (x20 magnification)

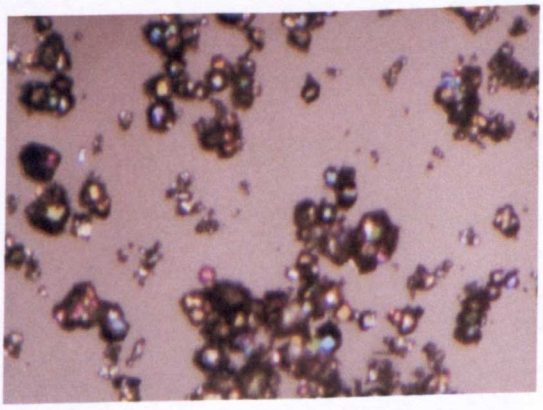

Figure 3.31: TOAc recrystallised from 60:40 ethanol:water (x20 magnification)

The rate of cooling directly relates to the rate of crystal growth, and agitation affects the kinetics of crystal growth and can therefore have an effect on the final product. The use of an agitator generally results in smaller, more uniform crystals that tend to have a higher purity compared to when one is not used. Mullin (1993) stated that this increased purity was due to the crystals retaining less of the mother liquor after filtration, making more efficient washing possible.

Certain of these variables had to be kept constant for all batches of material recrystallised. This was in order to facilitate assessment of the effect of changes to the recrystallisation conditions on the physical appearance of the material surfaces produced. Without this restriction, the number of possible permutations for assessment would be too great. In summary, the rate of cooling and the degree of agitation applied to the system were kept constant for all materials recrystallised.

3.5 PRODUCTION OF CRYSTALLISED MATERIALS

In the production of different batches of recrystallised materials, it was important to minimise the number of variables in order to make comparison of the results more viable. Consequently, for the research carried out the following basic method was adopted to recrystallise materials from solutions. A summary of the exact conditions used for each batch of material produced for assessment is also given below.

3.5.1 CALIBRATION OF EQUIPMENT

Prior to all recrystallisation experiments, the equipment used was calibrated with respect to temperature. This was carried out in order to ensure that the temperature and cooling

rates required for recrystallisation were both accurate and linear. The calibration was achieved using a chart recorder attached to an independent thermocouple.

Both crystallisation vessels were calibrated. Each was filled with an appropriate quantity of water, and the stirrer and both thermocouples were put in place. One thermocouple was attached to the chart recorder, the other was used as the controlling thermocouple of the digital Eurotherm programmer/controller (model 818P).

At appropriate intervals, the temperature of the water inside the vessel was checked with a third independent calibrated digital thermometer. This was used to ensure that the temperature displayed by the programmer/controller was accurate.

The programmer/controller was set to generate a range of temperatures and cooling rates. The range of cooling rates tested was from 0.5 °C per hour up to 30 °C per hour, and a range of starting temperatures were monitored up to a maximum of 40 °C.

It was determined that the Eurotherm programmer/controller was capable of achieving/maintaining the temperature required in the crystallisation vessel to within ± 0.2 °C and for the cooling rates tested the chart recorder showed the rates to be linear. However, it was only possible to determine the linearity of the cooling rates over a range of 16 °C, as that was the greatest range possible within the capacity of the chart recorder used. For this reason, it was decided that a cooling range of no greater than 16 °C should be used. For practical and safety considerations, it was decided that the finishing temperature of a recrystallisation run should be around room temperature. Hence for the

majority of recrystallisations it was decided to use a temperature range of 34 °C to 18 °C. Cooling rates of up to 30 °C per hour had been calibrated but it was decided to use a maximum cooling rate of 20 °C per hour.

3.5.2 METHOD OF RECRYSTALLISATION

For most batches, the starting temperature was to be 34 °C for the reasons stated above. The following method applies to a recrystallisation run from 34 °C to 18 °C. For any other temperature ranges the values should be substituted accordingly.

Using the solubility curve appropriate to the material and solvent required it was possible to determine the solubility of the material at 34 °C. From this information it was then possible to determine what solubility was required in order to give a solution with the required supersaturation ratio at 34 °C (either 1.2 or 1.5). The solubility curve was then used to determine what temperature should be used to obtain this saturated solution.

Appropriate quantities of solvent and raw material were placed into a sealed screw capped glass HPLC bottle and were left to equilibrate in a water bath set to the appropriate temperature. In order to ensure that the solution was saturated, it was ensured that an excess of material was always visible. The bottle was kept sealed while the solution reached equilibrium in order to minimise any evaporation of volatile components of the solvents. Each solution was left for a minimum of four hours at the required temperature to ensure that the equilibrium of a saturated solution had been achieved.

Once a saturated solution was obtained, it was quickly filtered using a Whatman number 50 filter. The filter was placed into a ceramic funnel that had a filter support incorporated. A vacuum was applied to speed the rate of filtration. The solution was filtered in order to ensure that it did not contain any undissolved material.

The filtrate was then transferred into the appropriately sized recrystallisation vessel. The recrystallisation equipment was set up to allow the solution inside the vessel to be held for a minimum of five minutes with gentle stirring at a temperature 0.5 °C above the temperature used to create the saturated solution. This was carried out in order to again ensure that the solution was free of undissolved material.

After this time, the solution was cooled at a rate of 3 °C per hour without agitation until the starting temperature of 34 °C was obtained. The system was cooled without agitation as stirring could have induced premature recrystallisation of material from the solvent. At 34 °C, the solution inside the vessel was a supersaturated solution with a known supersaturation ratio.

At this time, the stirrer was set to a speed of 500 r.p.m. and seed crystals were added to the solution. All seed crystals were sub 45 μm in size and approximately 250 mg was added to each run. The solution was then cooled at a rate of 20 °C per hour to 18 °C (the finishing temperature of the run).

Once the recrystallisation run was complete, the recrystallised material was harvested using a Whatman number 50 filter (as described previously).

The harvested crystals were subsequently washed with a solution of the original solvent that had been cooled on ice. The washing was required to remove any residual traces of mother liquor from the crystal surfaces and the solutions were used chilled in order to minimise the loss of material resulting from washing of the crystals. The vacuum was used in order to minimise the contact time of the solvent with the recrystallised material.

If a sample of the recrystallised material was to be treated with a surface wash of isopropyl alcohol (cooled on ice), this was carried out next.

The material was then dried prior to surface characterisation. Ambient drying of the material was preferable as oven drying could potentially have an affect on the surface characteristics of the material produced.

Once dried, each batch of material was sieved in order to obtain the particle size fraction of 63-90 μm required for production of the blends.

3.6 CONDITIONS USED FOR RECRYSTALLISATION OF MATERIALS AND INITIAL CHARACTERISATION

3.6.1 LACTOSE MONOHYDRATE

Only one batch of recrystallised lactose was to be produced for assessment from the DPI. The specific conditions of the recrystallisation are given below.

Solvent:	100% water
Supersaturation ratio:	1.5
Temperature range:	34-18 °C at a cooling rate of 20 °C per hour

3.6.2 Initial Characterisation of Recrystallised Lactose Material – Confirmation of Material Identity

The following image is of the recrystallised material obtained. As can be seen, the morphology of the recrystallised material is the same as for the raw material.

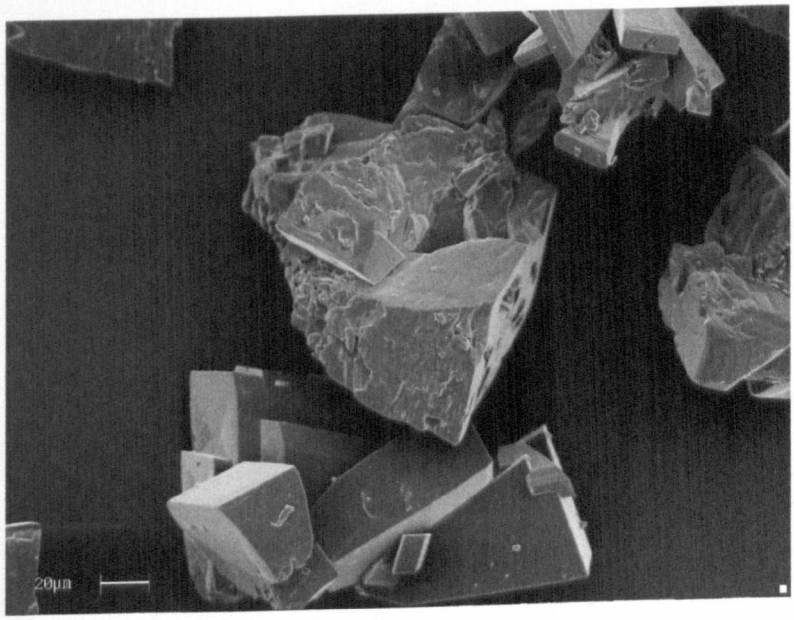

Figure 3.32: SEM photomicrograph of lactose material recrystallised from 100% water.

The recrystallised material has DSC and FT-IR plots very similar to that of the raw material. The DSC plot shows an improved peak resolution and a slightly increased melting point compared to the raw material that indicates a refined material with less impurities. The dehydration of the α-lactose monohydrate can still be observed at approximately 150 °C, but the small exotherm at approximately 180 °C represents a conversion of some of the material to the β form. The subsequent endotherms at approximately 200 °C and 220 °C represent the melting of the anhydrous α and β forms

respectively. TGA[2] of the recrystallised material showed it to have a similar moisture content to the raw material (5.2%).

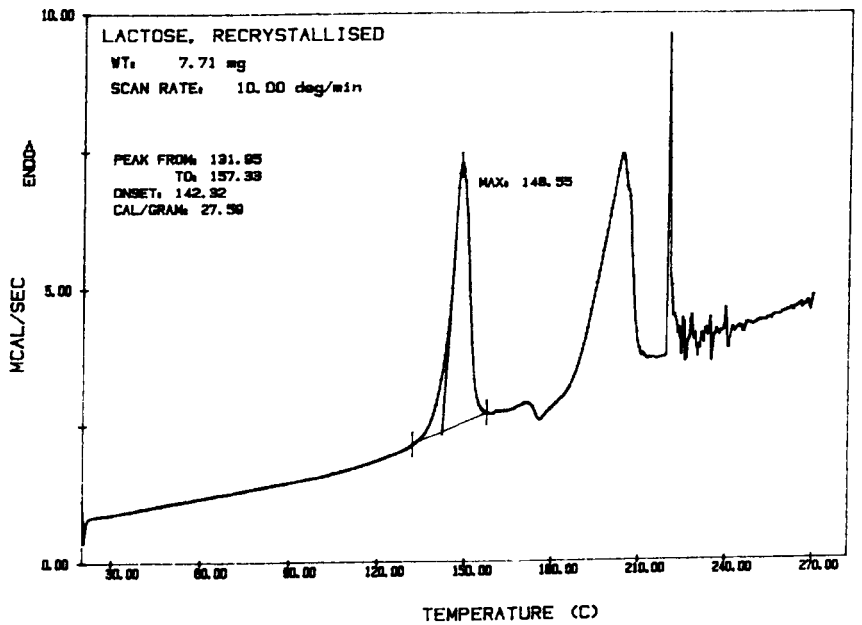

Figure 3.33: DSC of lactose material recrystallised from 100% water.

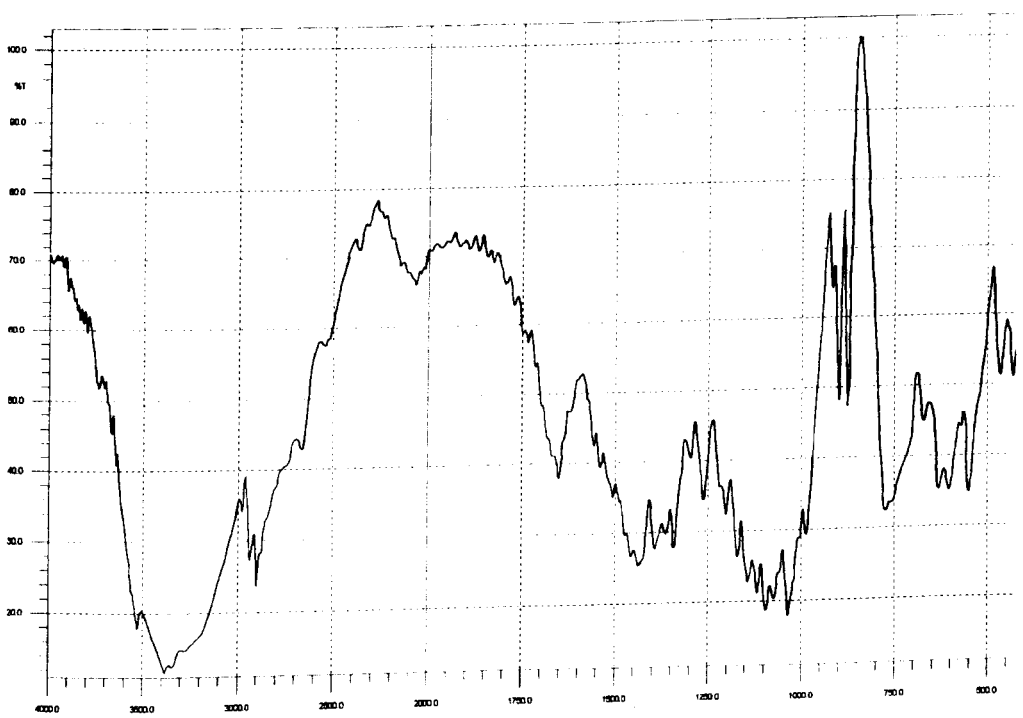

Figure 3.34: FT-IR spectrum of lactose material recrystallised from 100% water.

[2] Data not shown.

The O-H stretch region can still be clearly observed at approximately 3400 cm^{-1}.

3.6.3 TREHALOSE DIHYDRATE

Four batches of trehalose were to be recrystallised, and a sample of one of the batches was to be treated with a surface wash of isopropyl alcohol (IPA) following harvest. The specific conditions of recrystallisation for each batch of material to be tested from the DPI are given below.

Solvent:	100% water*
Supersaturation ratio:	1.5
Temperature range:	34-18 °C at a cooling rate of 20 °C per hour

*A proportion of this batch of material also received a surface wash with IPA following harvest.

Solvent:	40:60 ethanol:water
Supersaturation ratio:	1.5
Temperature range:	34-18 °C at a cooling rate of 20 °C per hour

Solvent:	60:40 ethanol:water
Supersaturation ratio:	1.5
Temperature range:	34-18 °C at a cooling rate of 20 °C per hour

Solvent:	60:40 ethanol:water
Supersaturation ratio:	1.5
Temperature range:	23-7 °C at a cooling rate of 20 °C per hour

3.6.4 Initial Characterisation of Recrystallised Trehalose Dihydrate Material – Confirmation of Material Identity

After production of one batch of trehalose, preliminary characterisation of the material was carried out after ambient drying in order to confirm the identity of the material recrystallised.

The morphology of the recrystallised material remained the same as observed with the raw material, as can be seen from the following SEM photomicrograph.

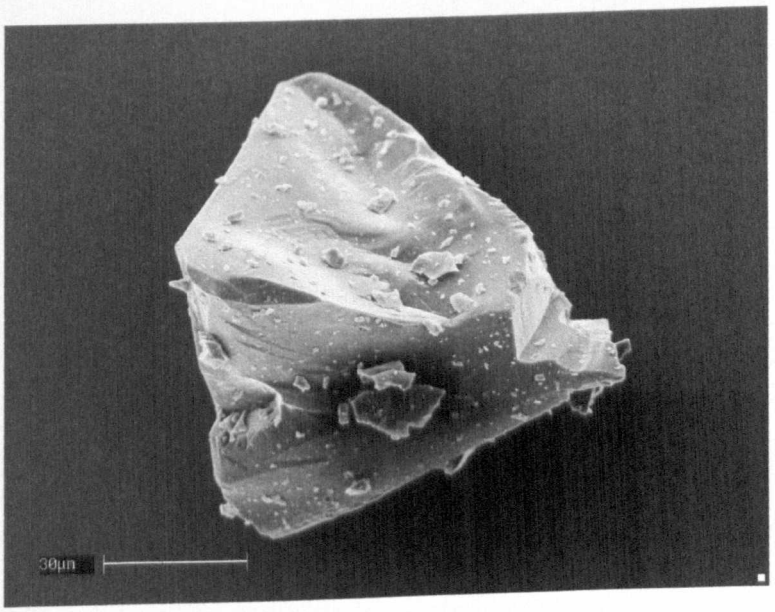

Figure 3.35: SEM image of trehalose recrystallised from water

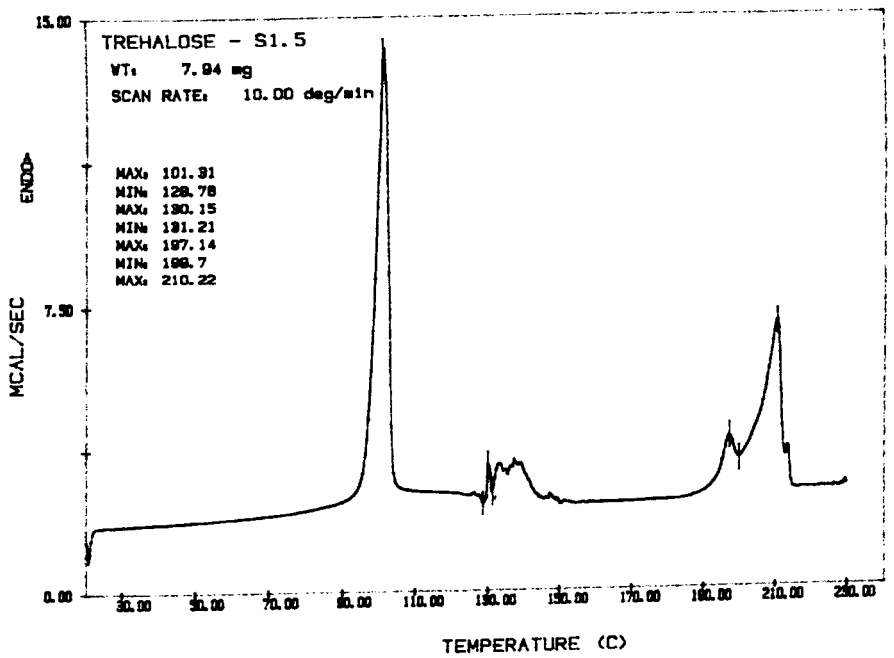

Figure 3.36: DSC of trehalose material recrystallised from water

The material recrystallised had a DSC profile very similar to the raw material, and no significant differences were observed in the FT-IR spectrum. The DSC plot shows an improved peak resolution and a slightly increased melting point compared to the raw material which both indicate a refined material with less impurities. In the FT-IR spectrum (figure 3.37), the peak corresponding to the C=O stretch at 1700 cm can still clearly be seen. In addition, TGA[3] of the recrystallised material showed it to have a similar moisture content to the raw material (8.75 %).

[3] Data not shown.

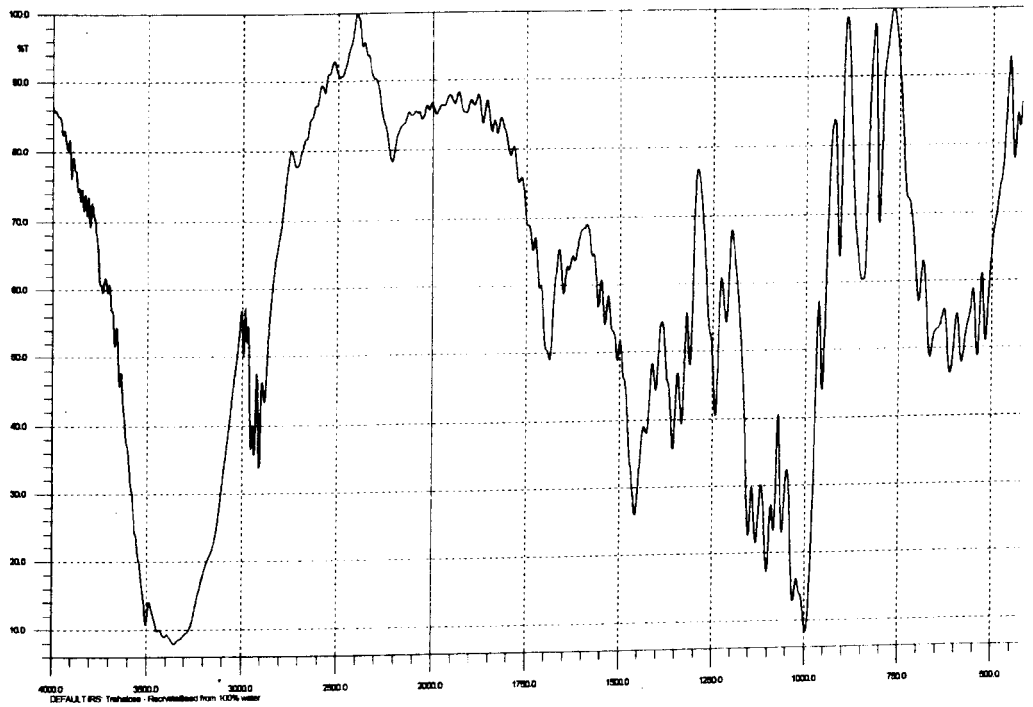

Figure 3.37: FT-IR of trehalose material recrystallised from water

3.6.5 TOAc

Four batches of TOAc were to be recrystallised, and a portion of one batch was to be treated with a surface wash of IPA. The specific conditions of recrystallisation for each material are given below.

Solvent:	70:30 ethanol:water
Supersaturation ratio:	1.2
Temperature range:	34-18 °C at a cooling rate of 20 °C per hour

Solvent:	70:30 ethanol:water*
Supersaturation ratio:	1.5
Temperature range:	34-18 °C at a cooling rate of 20 °C per hour

*A proportion of this batch of material also received a surface wash with IPA following harvest.

Solvent:	75:25 ethanol:water
Supersaturation ratio:	1.2
Temperature range:	34-18 °C at a cooling rate of 20 °C per hour

Solvent:	85:25 ethanol:water
Supersaturation ratio:	1.2
Temperature range:	34-18 °C at a cooling rate of 20 °C per hour

As a consequence of the morphologies observed in the small scale recrystallisation experiments, it was decided to recrystallise TOAc under controlled conditions with the above solvents. This decision was made in order to assess the effect of changing the recrystallisation solvent on the surface characteristics of TOAc in addition to the effect of a possible mixture of morphologies on the performance of the material as a drug carrier.

3.6.6 Initial Characterisation of Recrystallised TOAc Material – Confirmation of Material Identity

Following recrystallisation of the first batch of TOAc from 70:30 ethanol:water, initial characterisation of the material was carried out after ambient drying. This was carried out in order that the material identity could be confirmed.

One significant difference between the recrystallised material compared to the raw material was the morphology. Rather than the acicular needles, the recrystallised material was more orthorhombic in habit, and was therefore much closer in appearance to both the lactose and trehalose crystals.

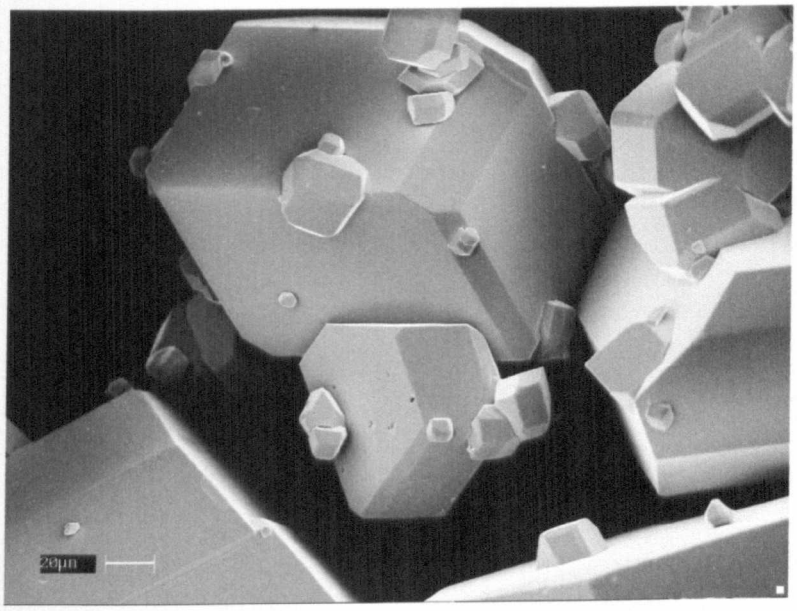

Figure 3.38: SEM image of material recrystallised from TOAc in 70:30 ethanol:water

Strong differences were observed in the DSC profile obtained for the recrystallised material (figure 3.39) compared to the raw material. It was therefore essential to use another method of analysis to identify whether the material produced as a result of the recrystallisation was still TOAc.

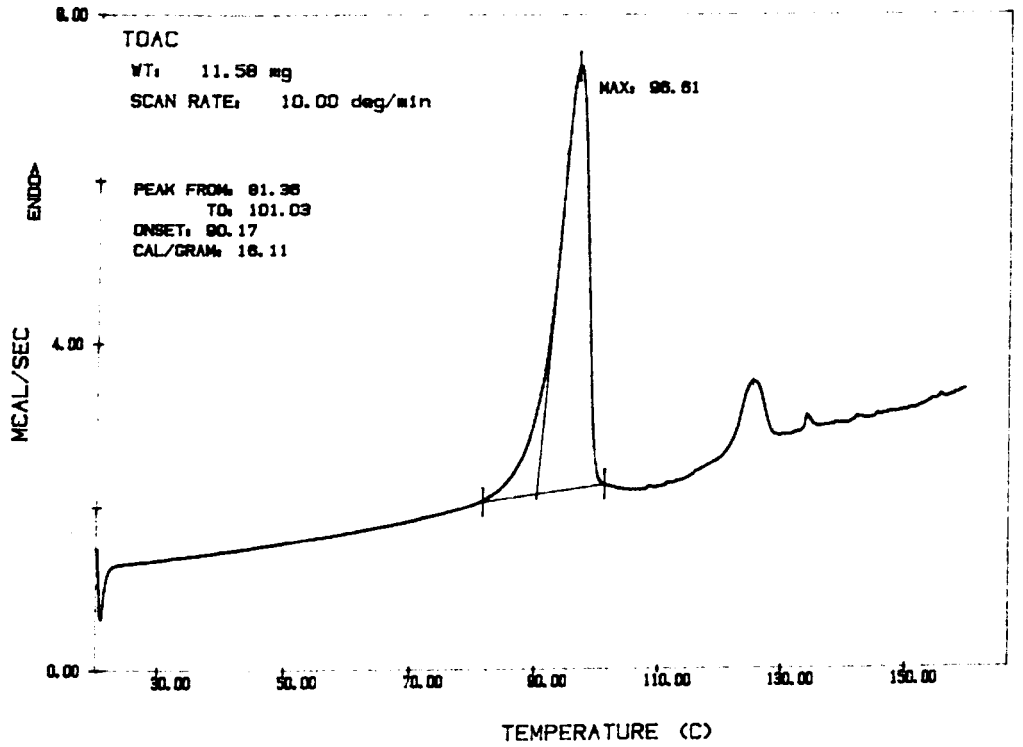

Figure 3.39: DSC profile of material recrystallised from TOAc in 70:30 ethanol:water

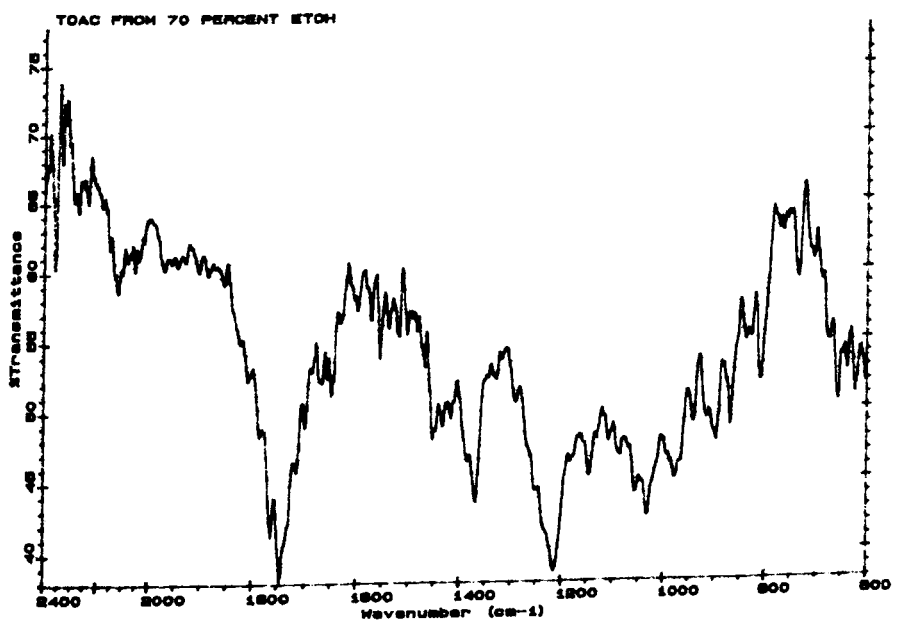

Figure 3.40: FT-IR profile of material recrystallised from TOAc in 70:30 ethanol:water

FT-IR of the material showed strong correlations with the raw material, although some slight variations were observed. These could be indicative of differences in the crystal structure or packing of the materials, and hence may indicate the presence of a polymorphic form. Alternatively, the differences observed could be due to the formation of a material containing less than the eight acetate groups associated with TOAc. In conclusion, due to the variations observed in the spectra it was decided that FT-IR was not in itself a conclusive method to assess whether the recrystallised material was still TOAc. The following chapter describes the work carried out in order to establish the identity of the material recrystallised from TOAc.

CHAPTER FOUR

FURTHER CHARACTERISATION OF RECRYSTALLISED TOAc – ESTABLISHING MATERIAL IDENTITY

4.1 INTRODUCTION

As it was not possible to confirm the identity of the recrystallised TOAc material using standard analytical techniques, it became necessary to identify the composition of the material using a different method of analysis. The following section of this chapter describes the technique used to confirm that the material recrystallised was still TOAc, rather than a modification containing less than eight acetyl groups.

4.2 NUCLEAR MAGNETIC RESONANCE (NMR)

The equipment used to produce the NMR profiles of selected materials was a Bruker AC250. Both proton and carbon NMR analyses of selected TOAc materials were carried out. Materials were selected on the basis that they gave different phase profiles on DSC analysis compared to the TOAc raw material.

The technique uses radiation in the radio-frequency region to excite atoms (either protons or carbon-13 atoms) so that their spins switch from being aligned to being aligned against an applied magnetic field. The range of frequencies required for excitation and the complex splitting patterns produced are very characteristic of the chemical structure of the molecule being analysed. It is therefore a good technique to identify whether the recrystallised material has retained the molecular structure of the raw material.

The NMR spectra obtained for TOAc can be found in appendix 4.

The results show that in solution, the molecules that make up each of the different batches of recrystallised TOAc materials are the same. There was water shown to be present in the

samples in the proton NMR plots, but this could be from the solvent used in the analysis. The peak (at approximately 1.8 ppm) was confirmed to represent water, as it disappeared when the sample was shaken with heavy water (deuterium oxide) and subsequently re-analysed.

All of the peaks for the recrystallised material were observed in the locations (as specified in the relevant NMR literature) that corresponded to TOAc. It could therefore be stated with confidence that the recrystallised TOAc was the same molecule as the TOAc raw material, but strong differences were observed in the crystal morphology and the DSC profiles obtained from the recrystallised batches of TOAc. The NMR technique could not be used to provide any structural information on the materials, as the technique analyses materials in solution rather than in the solid-state.

The following section describes optimisation of the technique for drying TOAc following recrystallisation.

4.3 OPTIMISATION OF TOAC DRYING

Following the unexpected identity and stability issues that arose following preliminary analysis of recrystallised TOAc, a detailed drying profile of the TOAc material was undertaken. This was carried out with a view to optimise the drying of the recrystallised material in order to obtain reproducible batches of TOAc, exhibiting the same DSC and stability characteristics prior to assessment of the TOAc material as a drug carrier.

4.3.1 PROFILE OF THE PHASE CHANGES OF RECRYSTALLISED TOAC RESULTING FROM DRYING

The drying of TOAc material under ambient conditions produced materials exhibiting different DSC profiles compared to the raw material. It was noted that there appeared to be a relationship between the DSC profile obtained and time, which indicated that the material was not in a stable form immediately after recrystallisation.

The following DSC profiles are of recrystallised TOAc dried under ambient conditions over a three-month period and demonstrate the unstable changing profile of the material.

4.3.1.1 AMBIENT DRYING

The first profile is that of TOAc recrystallised from 70:30 ethanol:water the day after manufacture following ambient drying overnight.

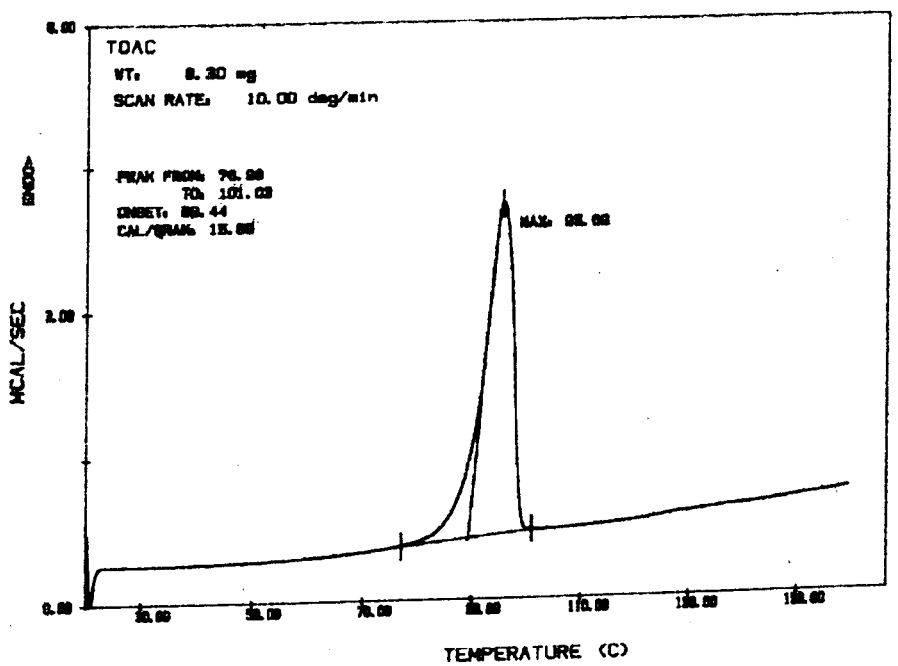

Figure 4.1: DSC profile of TOAc dried under ambient conditions for 24 hours

The profile contains a single peak at approximately 95 °C. It is possible that the endothermic peak observed at 95 °C correlates to the release of residual solvent from the material, as the ethanol-water solvent would boil at around this temperature.

The next profile is of the same material analysed one week after production.

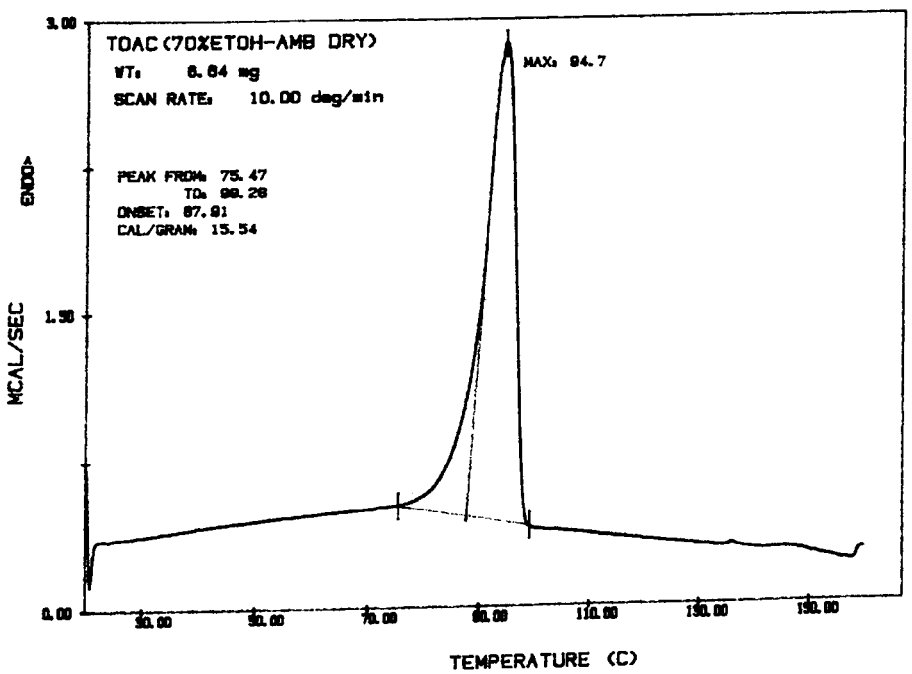

Figure 4.2: DSC profile of TOAc dried under ambient conditions for one week

The profile still contains a large peak at 95 °C but there is now slight evidence of a peak emerging at 135 °C.

The following profile is after one month of ambient drying.

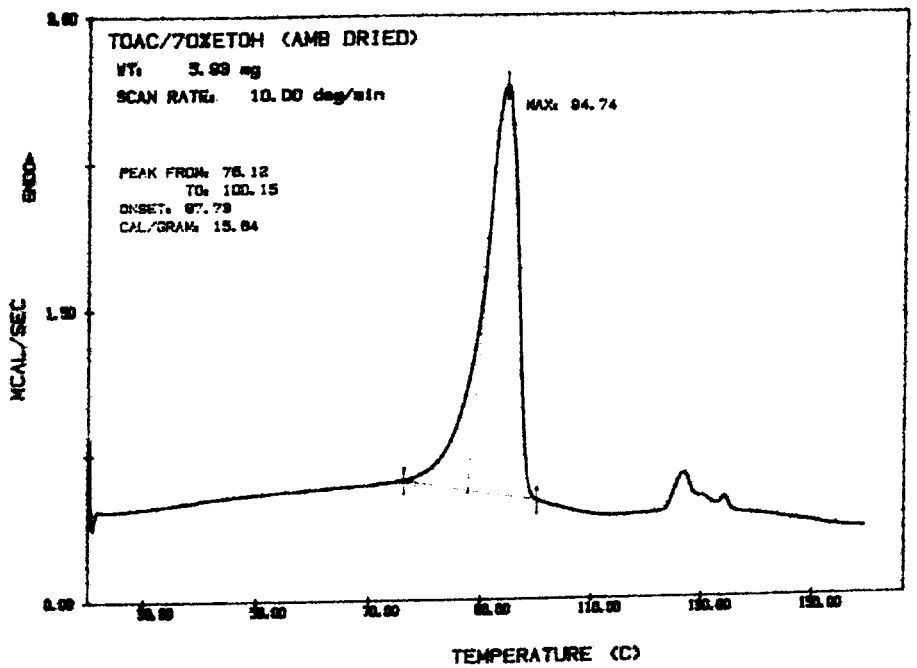

Figure 4.3: DSC profile of TOAc dried under ambient conditions for one month

In this profile, the peak at 95 °C is still dominating, but the peak at 135 °C is now more visible. In addition to this peak, there is the emergence of a peak at approximately 128 °C that has a larger intensity than the 135 °C peak.

Following three months storage under ambient conditions, the DSC profile below was obtained.

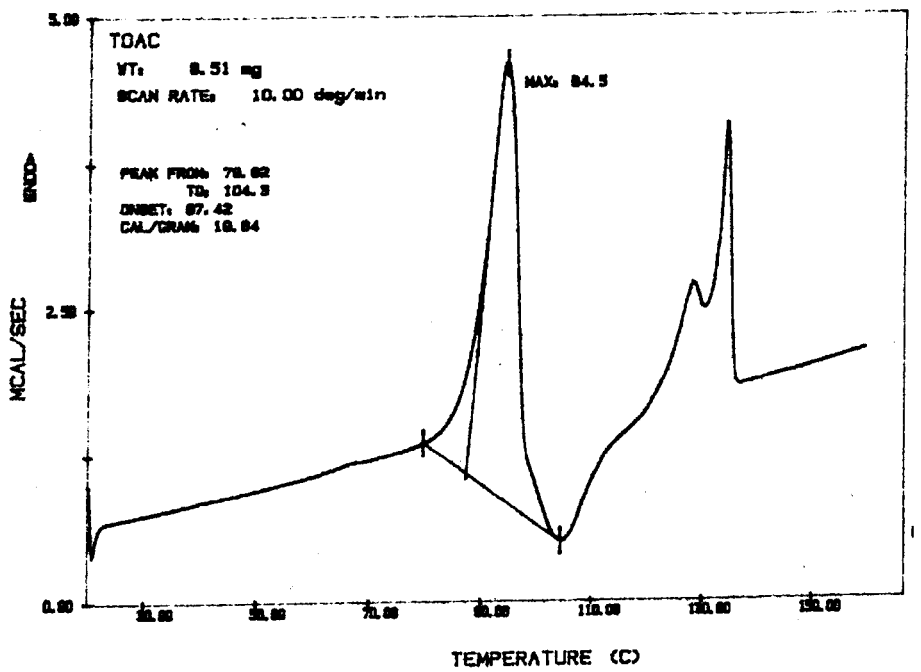

Figure 4.4: DSC profile of TOAc dried under ambient conditions for three months.

This profile still has a peak at 95 °C, but an exothermic peak immediately after indicates recrystallisation of the material. There is still clear evidence of a peak at 128 °C, although there is now a significant increase in the intensity of the peak at 135 °C.

These data indicated that a transformation of the material was occurring and it therefore seemed prudent to monitor changes in the DSC profile of the material over time until a stable material profile was obtained. A stable DSC profile would make it easier to confirm the identity of the TOAc following recrystallisation of future batches.

In order to speed up the drying process, samples of recrystallised material were dried in an oven at either 70 °C or 90 °C for varying lengths of time. It was hoped that by using an oven to dry the TOAc materials it would facilitate the production of batches of material exhibiting similar stability and DSC profiles in a much quicker time than ambient drying alone.

The preliminary batch of TOAc recrystallised from 70:30 ethanol:water was separated into a number of smaller batches. Each batch was subjected to drying under different conditions of temperature as described previously. This was carried out in an attempt to discover the dynamics of the DSC phase changes and allow for identification of a stable material profile.

4.3.1.2 Samples dried at 70 °C

Following exposure of recrystallised TOAc material to a temperature of 70 °C for one hour the DSC profile obtained showed peaks at both 95 °C and approximately 135 °C.

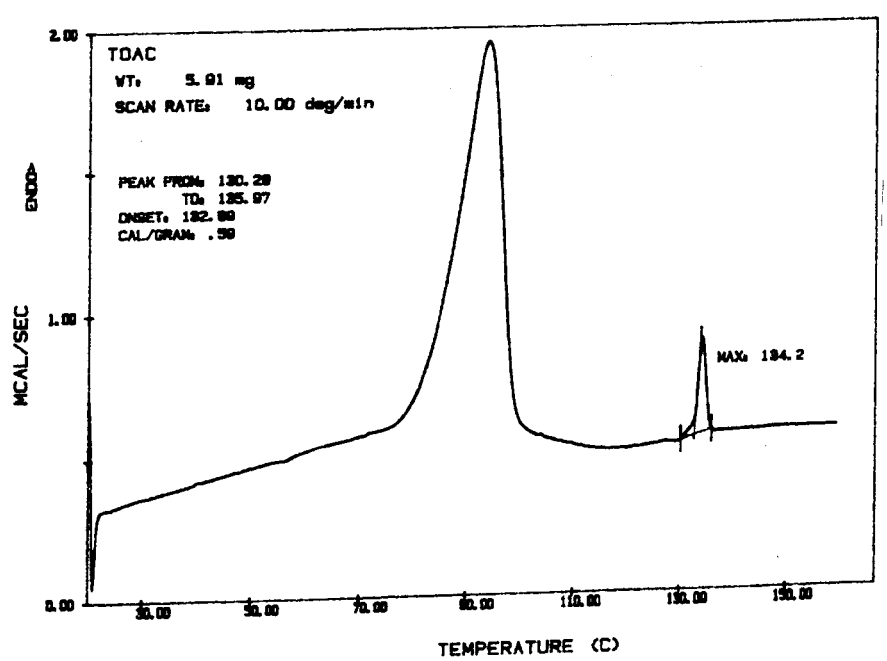

Figure 4.5: DSC profile of TOAc dried at 70 °C for one hour

After 24 hours at this temperature, the profile of the material still shows peaks at 95 °C and 135 °C, although now the peak at 135 °C is dominant.

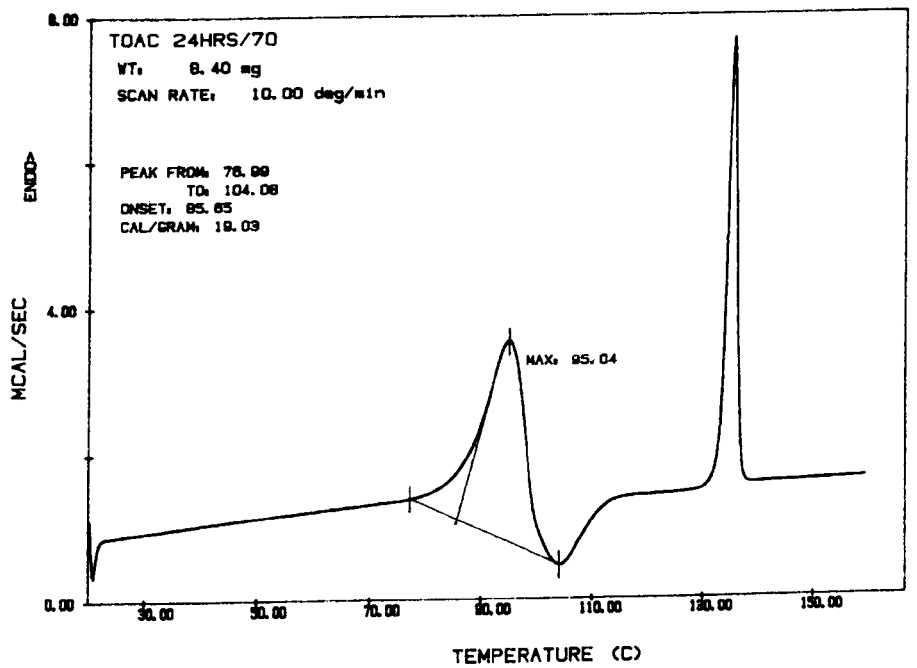

Figure 4.6: DSC profile of TOAc dried at 70 °C for 24 hours

The profile now clearly shows an exothermic peak following the partial melt at 95 °C, which indicates that recrystallisation of the material has taken place.

The profile of the material after 115 hours at 70 °C is very similar to that obtained from 24 hours exposure. The only difference is that the intensity of the peak at 95 °C appears to be diminishing.

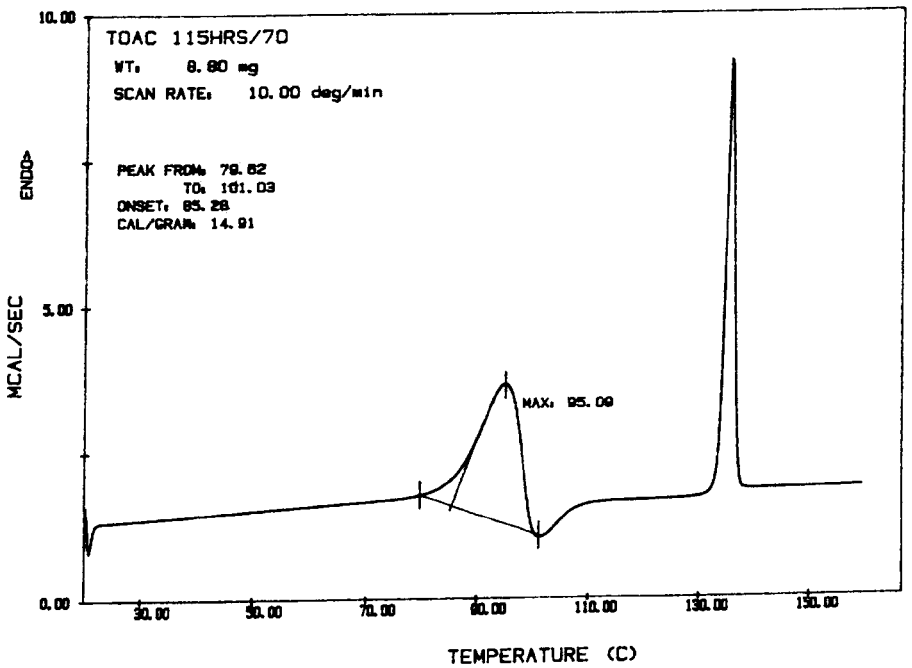

Figure 4.7: DSC profile of TOAc dried at 70 °C for 115 hours

The following profile was obtained from material dried at 70 °C for 336 hours.

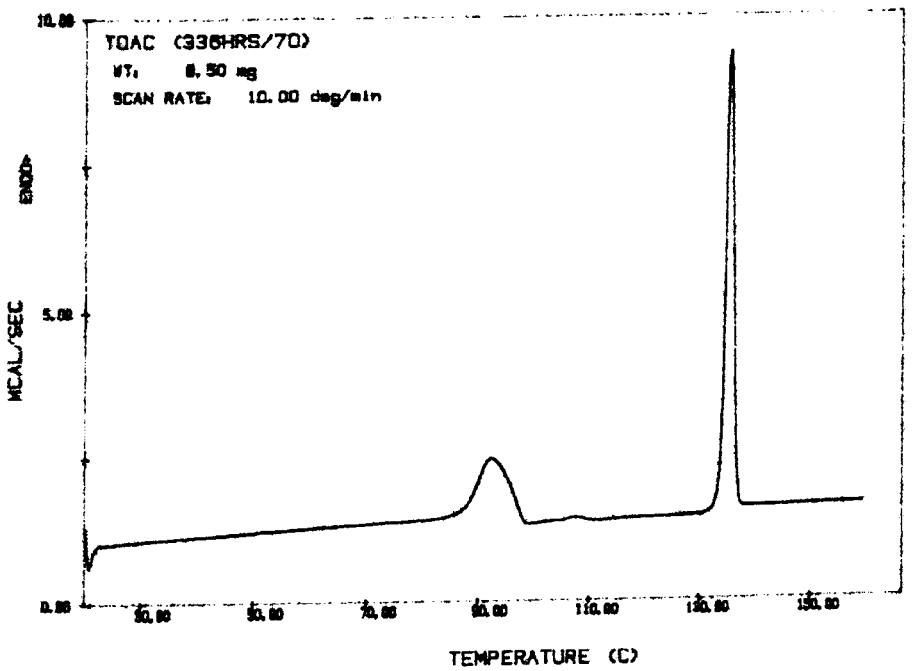

Figure 4.8: DSC profile of TOAc dried at 70 °C for 336 hours

This material still retains a peak at 95 °C, although it can be seen to be of a significantly reduced intensity compared to the earlier profiles. The peak at 135 °C is still clearly visible, but there also appears to be evidence of a peak emerging at approximately 108 °C.

4.3.1.3 SAMPLES DRIED AT 90 °C

The following profile is of the recrystallised TOAc following drying at 90 °C for one hour.

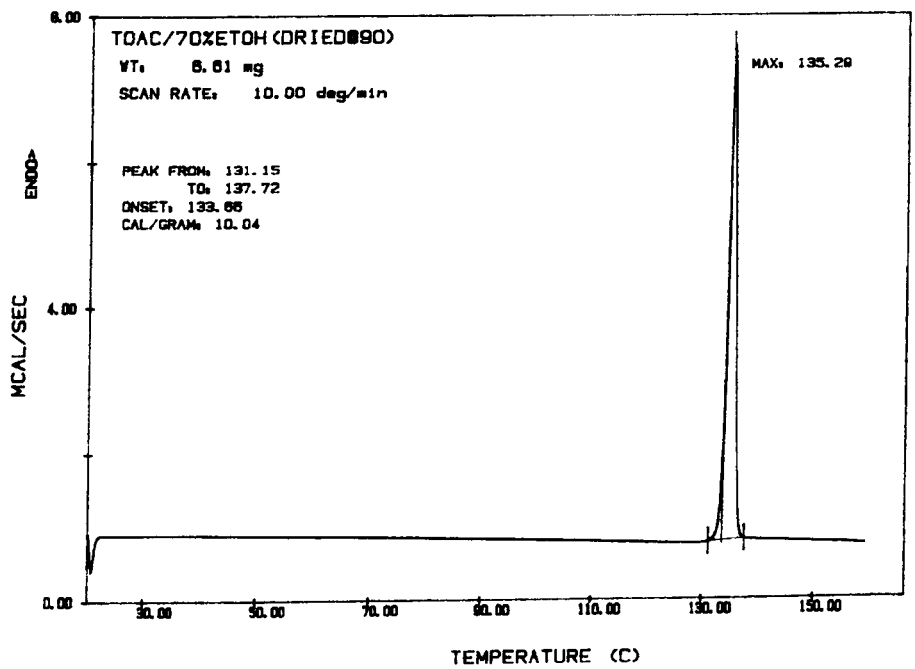

Figure 4.9: DSC profile of TOAc dried at 90 °C for one hour

After 1 hour at 90 °C, the DSC profile shows a single peak at 135 °C. No trace of the peak at 95 °C remains.

After 24 hours at this temperature, a second peak was observed to emerge at around 108 °C.

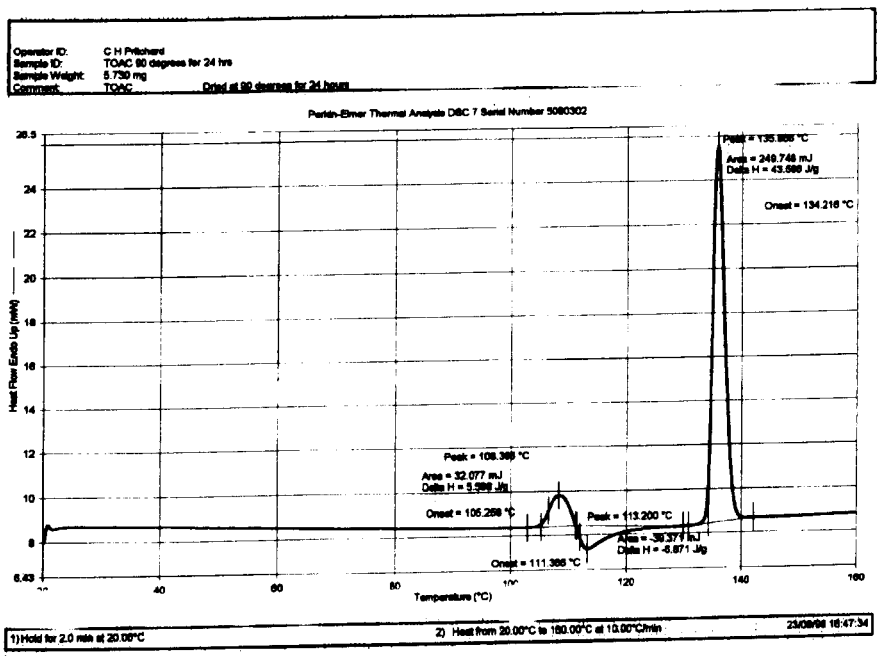

Figure 4.10: DSC profile of TOAc dried at 90 °C for 24 hours

Following this partial melt at 108 °C, an exothermic peak indicates that the material recrystallised before the main melt occurred at 135 °C.

After 144 hours, the peak at 108 °C is more pronounced.

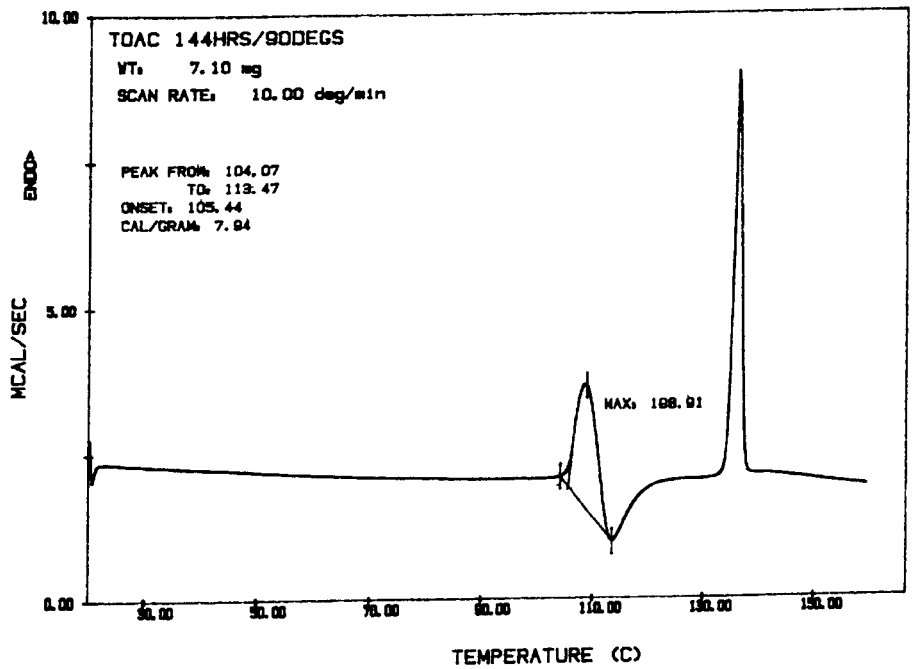

Figure 4.11: DSC profile of TOAc dried at 90 °C for 144 hours

The profile obtained corresponds well to the profile of peaks obtained when the raw material was analysed by DSC. The only difference is the absence of the small peak at around 75 °C, which was probably due to an impurity such as ethanol in the raw material. The moisture content of the samples dried at 90 °C for 24 and 144 hours were determined by TGA[4]. The materials were found to have a moisture content of <0.1%, the same value obtained for the raw material.

[4] Data not shown.

4.3.2 Morphology of Dried Materials

Following drying, the morphology of each material was observed under a microscope. In all cases, the materials remained orthorhombic. No reversion to an acicular form of TOAc was observed.

4.3.3 Short Term Stability of TOAc Material Dried at 90 °C

As the material dried at 90 °C exhibited a DSC profile similar to that of the raw material it was decided that this temperature should be used to dry all future batches of recrystallised TOAc. It also appears from the profiles of the samples dried at 70 °C that a conversion to a similar DSC profile was progressing. As conversions occur from metastable to stable forms, the results of the drying profile indicate that the DSC profile with peaks at 135 °C and 108 °C is of the most stable material. As the time taken to obtain this profile was significantly reduced with drying at 90 °C compared to 70 °C, this supported the decision to dry all future batches of TOAc at 90 °C.

The proviso on this was that an acceptable degree of stability for this material could be demonstrated.

Consequently, samples of the material dried at 90 °C were stored under ambient conditions in a sealed jar in the lab. More than one month later, the samples exposed to 90 °C for 1 hour, 24 hours and 144 hours were re-analysed in order to assess the stability of

the materials. The DSC profiles obtained after this time remained unchanged. It was therefore considered that materials dried under these conditions exhibited an acceptable thermodynamic stability to allow their performance as drug carriers to be assessed from the DPI.

4.4 SUMMARY OF TOAc DRYING

It was possible that the recrystallised material obtained was a solvate or hydrated modification of TOAc as the peak observed at 95 °C was likely to correlate to the ethanol:water solvent, as it is around this temperature that the solvent would boil. TGA[5] of the material left to dry under ambient conditions for 24 hours indicated a moisture content of 2.17% which supports this possibility.

NMR analysis of the recrystallised TOAc indicated that water was present in the TOAc samples dried under ambient conditions. It is possible that a portion of this water was present as a result of the solvent used in the NMR analysis as this possibility cannot be excluded. However, it appear more likely that the majority of the water detected was due to the recrystallised TOAc under analysis.

The recrystallised TOAc material was observed to be thermodynamically unstable when dried under ambient conditions. If the material was a pseudopolymorph, it did not demonstrate thermodynamic stability until the excess of moisture/solvent had been removed.

[5] Data not shown.

Drying of the material at 70 °C resulted in a different DSC profile compared to drying at 90 °C. Material dried at 70 °C resulted in a DSC profile containing a peak at 135 °C but still retaining a peak at 95 °C, although of a much diminished intensity. Drying at 90 °C, even for one hour produced a DSC profile that did not contain a peak at 95 °C.

It was interesting however that the sample dried at 70 °C retained a DSC endotherm at 95 °C even after drying at this temperature for over 300 hours. Therefore, the possibility still exists that the peak at 95 °C represents a true polymorphic modification of TOAc (rather than a pseudopolymorph) as well as any possible residual solvent present in the sample. However, to investigate this further, different analytical methods would be required.

The DSC profile of the material dried at 90 °C is closer to that of the raw material and as such, it is considered to be more stable. The thermodynamic stability of this material over an acceptable timeframe was also demonstrated. Consequently, all recrystallised batches of TOAc were dried at 90 °C for a minimum of 24 hours. The DSC profile of the recrystallised materials was monitored in order to confirm that the features of the DSC profiles obtained were consistent. This process was applied to all batches of TOAc recrystallised for assessment in the DPI.

CHAPTER FIVE

PRODUCTION AND PRELIMINARY CHARACTERISATION OF AMORPHOUS MATERIALS

5.1 INTRODUCTION

Solid materials can be divided into crystalline and amorphous solids. The crystalline form possesses an orderly array of aligned molecules, whereas an amorphous solid comprises disarrayed or disorderly arranged molecules. The crystalline form is tightly packed, therefore only radical or functional molecular groups on the external surface of the crystals can interact with external materials such as water. The molecules in an amorphous state are tangled, more open and porous; therefore, an individual molecule possesses more sites for external interactions, such as water absorption. An amorphous structure is in a thermodynamically unstable (metastable) state. The molecular structure of a glass is that of a liquid, but the diffusional motions of the molecule have been brought to a halt. Therefore an amorphous solid is sometimes referred to as a solid solution, a glass or also a vitrified solid.

An amorphous structure in a material can be obtained in various ways. Melting results in dispersion of molecules from crystalline to non-aligned state. If the melt is cooled very rapidly (quenched), the molecules do not have enough time to realign to crystallise. This results in an amorphous solid.
Spray drying, high shear grinding and extrusion are processes that can also result in the production of partial or complete amorphous structures.

Various materials also exist as semi-crystalline solids. A semi-crystalline form can be produced when crystallisation is stopped due to temperature or viscosity effects or alternatively due to the presence of long-strand or irregularly shaped molecules that can become tangled and disordered resulting in amorphous regions.

An amorphous solid can undergo structural change when the temperature of the material is increased. Above a critical value, known as the glass transition temperature (T_g), a glassy solid structure begins to change to a rubbery state.

The glass transition temperature is not itself a constant value for any material. Some variation can be observed according to the method of sample preparation, the analytical procedure used and sample history. For example, water is a plasticiser that can drastically reduce the glass transition temperature of a solid material following its addition. The variations in the T_g value are normally due to the extent of molecular relaxation and molecular arrangement in the amorphous structure.

When heat is applied to a crystalline solid, it simply melts. No other phase transition is exhibited. In contrast, when an amorphous material is heated above T_g the viscosity continually decreases. There are certain physical changes occurring at glass transition apart from viscosity change. These are increase in heat capacity, increase in thermal expansion coefficient, dielectric constant change and increase in free volume. DSC is a common method used to determine the T_g of a material. DSC is a thermal analysis technique used to measure changes in heat flows associated with transitions and works on the principle of increase in heat capacity of a material during transition. Other techniques used to determine T_g are nuclear magnetic resonance (NMR) and spin resonance spectroscopy (ESR). These techniques work on the principle of increased diffusivity or molecular mobility of material at the glass transition temperature, but were not used in the course of this research.

The T_g of the amorphous component of a semi-crystalline structure is often higher than that of the pure amorphous structure. The crystals act as physical cross links in the amorphous region thus limiting the subsequent mobility of the polymer chains in the amorphous region and hence increasing the T_g.

A semi-crystalline material however will exhibit both glass transition and melting. Glass transition is reversible while melting is irreversible. This means that upon cooling below the T_g value, the glass endotherm will reappear, while there will not be any endotherm (provided there is no recrystallisation during cooling). The molecules are disordered in a melt and possess normal liquid behaviour. Glass transition is a second order transition which is characterised by a change in specific heat whereas melting is a first order transition where a latent heat of melting is involved.

The following sections describe the methods used to manufacture and characterise the amorphous materials that were used for this research project.

The spray dried materials were manufactured at Quadrant Healthcare using established equipment and methodology.

5.2 LACTOSE MONOHYDRATE

5.2.1 SPRAY DRIED LACTOSE

The Standard Niro Mobile Minor Spray Dryer was used to manufacture spray dried lactose with a target particle size range of 63-90 μm. 150 ml of a 20% $^{w}/_{v}$ aqueous load solution was prepared.

Details of the operating conditions used are given below.

Feed Details			
Pump Settings/Tube Details	**Feed Times/Masses (Recorded over a 1 minute period)**		**Feed Rate (g/min)**
75 r.p.m. / 1.6 mm ID Tubing	from 392.00 g	to 386.66 g	5.34

Atomisation Type: Rotary
Atomisation Voltage: 10.0 V

Drying Conditions		
Inlet Temperature (°C)	**Outlet Temperature (°C)**	
	Start	**Finish**
180.0	94.4	94.0

Recovery		
Vessel Type	**Mass Recovered (g)**	**Percentage Recovered (%)**
Cyclone	17.91	59.7
Filter	Not Measured	

The material collected was sieved to obtain the desired particle size fraction of 63-90 μm.

The following SEM image is of the material obtained, and is typically characteristic of what one would expect for a spray dried particle.

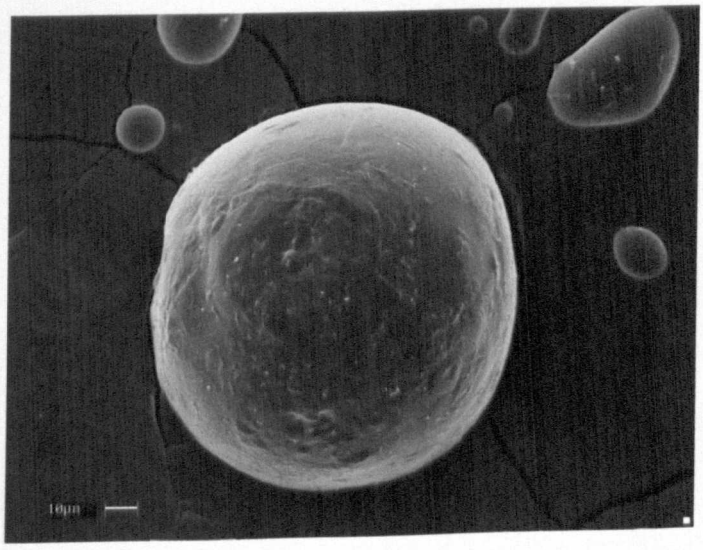

Figure 5.1: SEM image of spray dried lactose.

The following DSC plot of the material was obtained. The glass transition cannot easily be seen, but data published by Bhandari *et al* (2000) indicates that it occurs at approximately 101 °C.

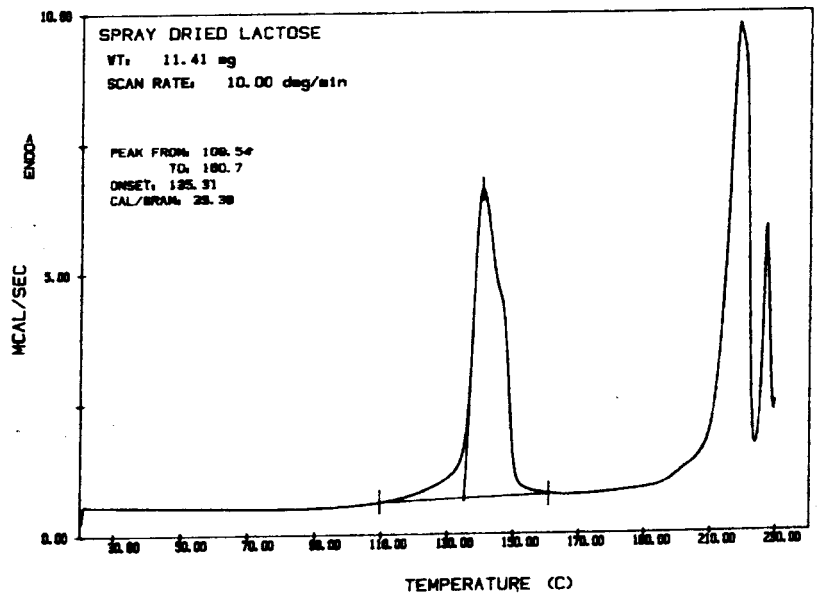

Figure 5.2: DSC of spray dried lactose

Spray dried lactose is known to be obtained as a semi crystalline solid, rather than as a purely amorphous solid and this is demonstrated by the DSC profile obtained for the material. Although the glass transition is not easily observed, the melting of the crystalline form can be clearly observed. Loss of the water of crystallisation can be observed at approximately 140 °C and then the subsequent melting of the two forms of crystalline lactose can clearly be seen at approximately 215 °C and 225 °C.

The following FT-IR spectrum of the material is different from that of the raw material in that there is less definition to the peaks. The lower resolution is what one would expect from a semi crystalline material, as the material's structure has amorphous regions that lack long range order.

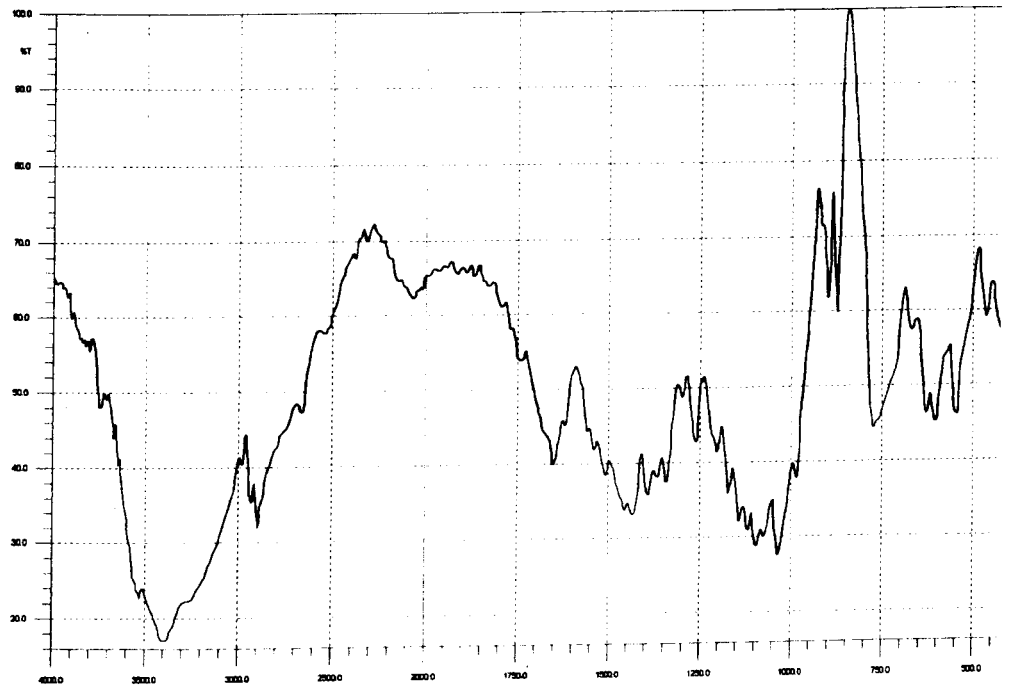

Figure 5.3: FT-IR spectrum of spray dried lactose.

5.3 TREHALOSE DIHYDRATE

In addition to forming crystalline materials, many oligosaccharides form amorphous glasses. Trehalose is frequently used to stabilise biological molecules such as proteins via production methods such as lyophilisation or spray drying. The material produced is invariably amorphous. It is also very hygroscopic and water soluble.

The T_g of trehalose has been reported as between 111 °C and 119 °C (Quadrant Healthcare).

5.3.1 SPRAY DRIED TREHALOSE DIHYDRATE

The Standard Niro Mobile Minor Spray Dryer was used to manufacture spray dried trehalose with a target particle size range of 63-90 μm. 150 ml of a 20% $^{w}/_{v}$ aqueous load solution was prepared.

Details of the operating conditions used are given below.

Feed Details			
Pump Settings/Tube Details	**Feed Times/Masses (Recorded over a 1 minute period)**		**Feed Rate (g/min)**
75 r.p.m. / 1.6 mm ID Tubing	from 380.00 g	to 374.80 g	5.20

Atomisation Type: Rotary
Atomisation Voltage: 10.0 V

Drying Conditions		
Inlet Temperature (°C)	**Outlet Temperature (°C)**	
	Start	**Finish**
170.0	90.0	98.0

Recovery		
Vessel Type	**Mass Recovered (g)**	**Percentage Recovered (%)**
Cyclone	15.07	50.2
Filter	Not Measured	

Figure 5.4 is an image of the material obtained.

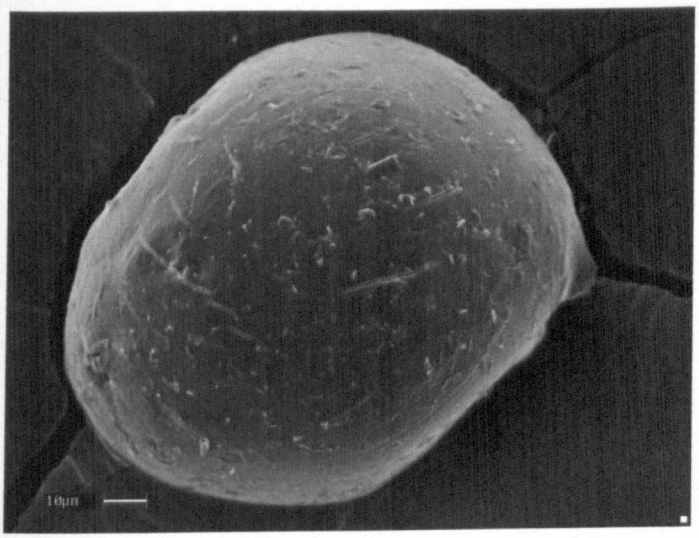

Figure 5.4: SEM image of spray dried trehalose.

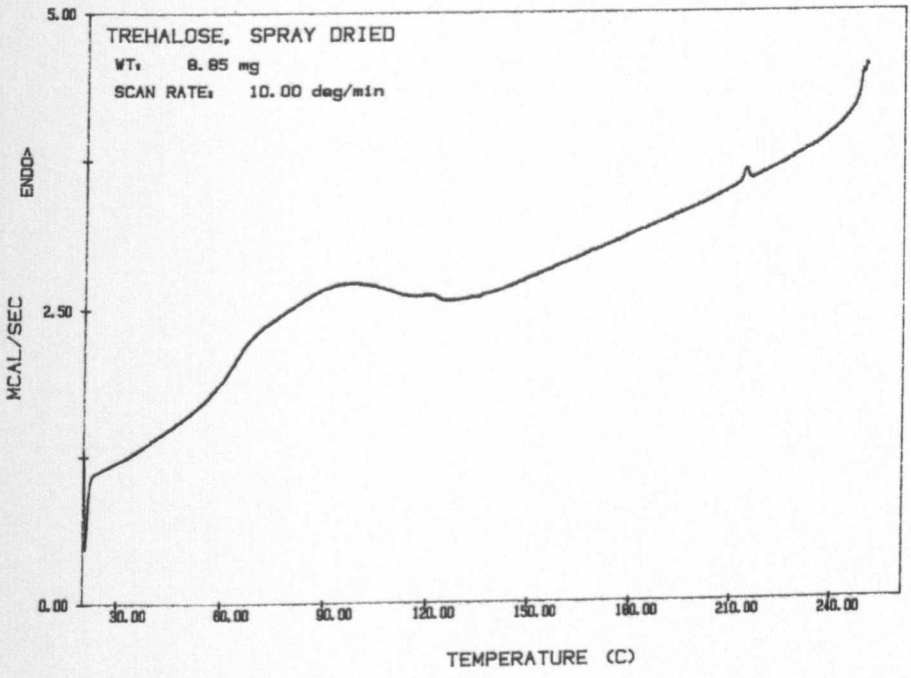

Figure 5.5: DSC profile of spray dried trehalose.

The DSC profile of the spray dried trehalose does not show a clear glass transition, although a small endotherm is evident at approximately 120 °C. The presence of water in the sample may be responsible for the lack of clarity of the glass transition, as water has

been known to reduce the T_g and water is likely to be responsible for the broad endotherm observed prior to the peak at 120 °C.

Figure 5.6 shows the FT-IR spectrum obtained for the spray dried trehalose. Compared to the spectrum obtained for the raw material, the spray dried sample has less well defined peaks, indicative of a material with a reduced long range order as would be expected with an amorphous material.

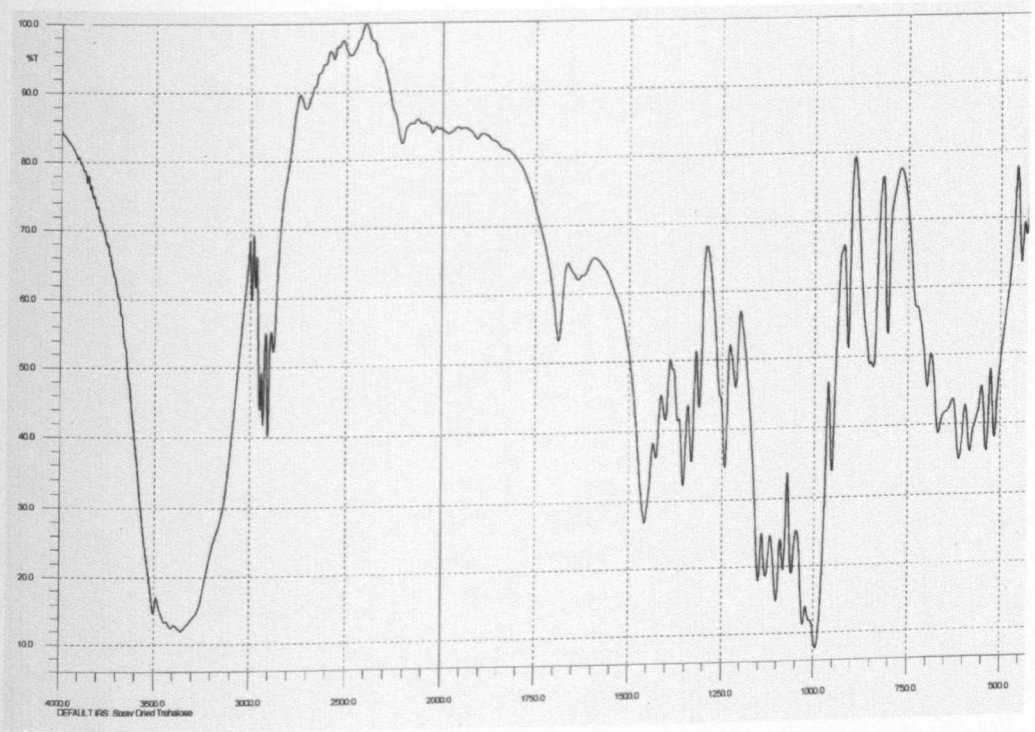

Figure 5.6: FT-IR spectrum of spray dried trehalose

5.4 TOAc

Chemical adaptation of the trehalose molecule allows a less hydrophilic material to be produced. This oligosaccharide ester derivative also forms an amorphous material, but with significantly different characteristics to the parent trehalose molecule.

The glass transition temperature (T_g) of TOAc is reported as 55 °C (Quadrant Healthcare plc, TM/99/053).

5.4.1 Spray Dried TOAc

The Standard Niro Mobile Minor Spray Dryer was used to manufacture spray dried TOAc with a target particle size range of 63-90 μm. 150 ml of a 20% $^{w}/_{v}$ dichloromethane (DCM) load solution was prepared.

Details of the operating conditions used are given below.

Feed Details			
Pump Settings/Tube Details	**Feed Times/Masses (Recorded over a 1 minute period)**		**Feed Rate (g/min)**
75 r.p.m. / 1.6 mm ID Tubing	from 938.00 g	to 930.60 g	7.4

Atomisation Type: Rotary
Atomisation Voltage: 10.0 V

Drying Conditions		
Inlet Temperature (°C)	**Outlet Temperature (°C)**	
	Start	**Finish**
80.0	53.8	51.1

Recovery		
Vessel Type	**Mass Recovered (g)**	**Percentage Recovered (%)**
Cyclone	10.34	34.5
Filter	Not Measured	

Figure 5.7 is a SEM image of the material obtained following sieving.

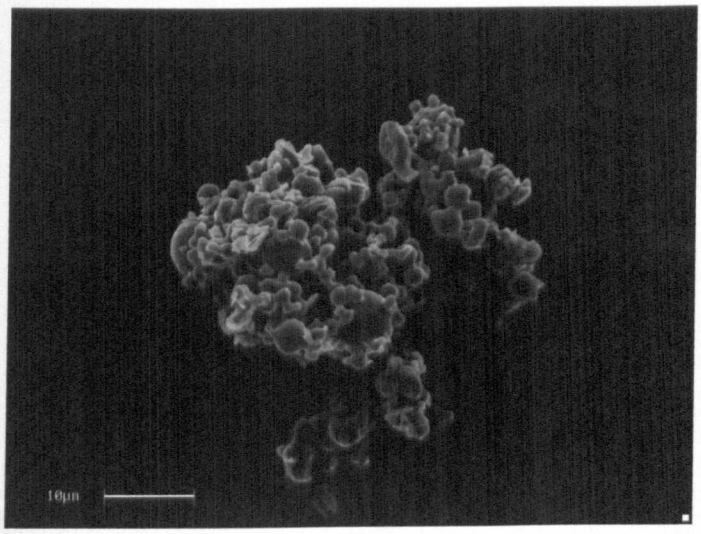

Figure 5.7: SEM image of spray dried TOAc

The spray dried TOAc material has a different appearance compared to the spray dried lactose and trehalose. The overall shape of the spray dried TOAc particles appears much more irregular, although the surface itself appears smooth. This could be due to partial collapse of the particles on drying or smaller particles fusing together during drying to produce larger particles in the required particle size range. The difference in the morphology could also be due to the different solvent used to create the load solution for TOAc, namely dichloromethane compared to the aqueous solutions used for both lactose and trehalose. Alteration of the solvent, concentration of the load solution, feed rate and/or drying temperatures could be investigated to determine the effect of modification of these parameters on the overall morphology of the spray dried TOAc particles produced. However, as spray dried TOAc particles in the required particle size range were produced such an investigation was beyond the scope of this research.

5.4.2 TOAc Quenched from the Melt

TOAc raw material was placed into a suitable volume Pyrex glass beaker. The beaker was then placed onto a hotplate, until the TOAc had become molten.

The molten material was then rapidly cooled (melt quenching). This was achieved by pouring the molten material onto a cold glass tile. Once the material had solidified, the amorphous glass was transferred to a mortar where it was ground to a fine powder using a pestle.

The powdered amorphous TOAc was then sieved to provide the required particle size range of 63-90 μm. Characterisation, blending and assessment of the material as a carrier was subsequently carried out.

The image below is of the amorphous material after it was powdered using a pestle and mortar and subsequently sieved.

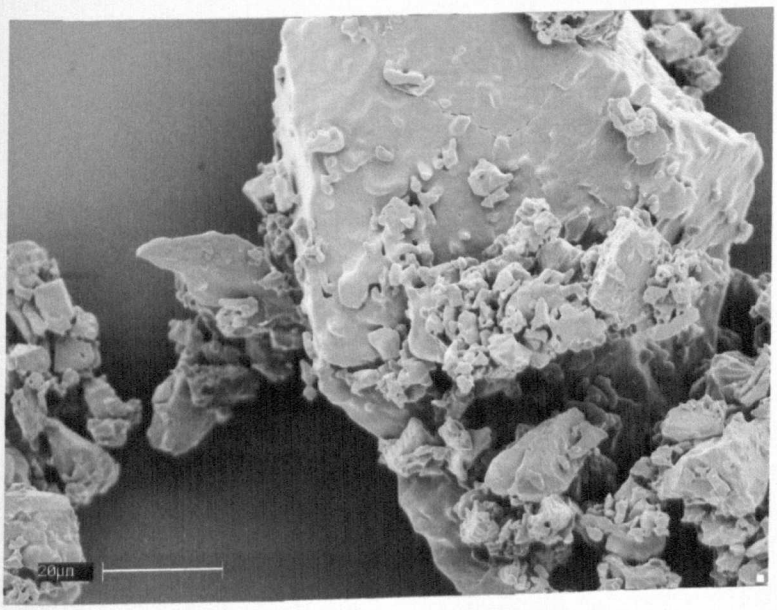

Figure 5.8: SEM image of powdered amorphous TOAc.

The material produced was of an irregular morphology, primarily due to the method of manufacture.

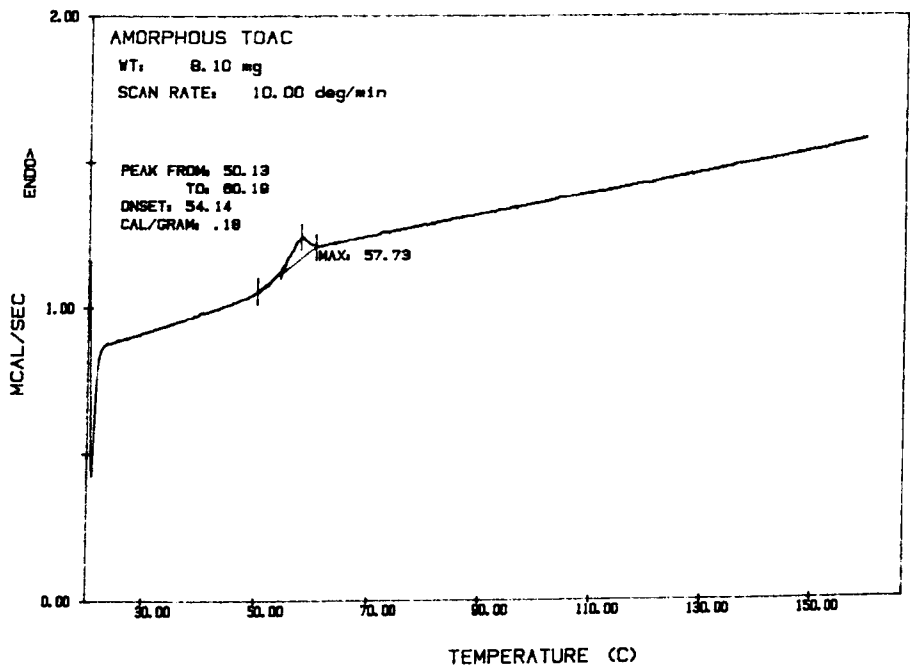

Figure 5.9: DSC profile of amorphous TOAc

The DSC profile obtained (figure 5.9) clearly shows the glass transition of the powdered material at approximately 55 °C.

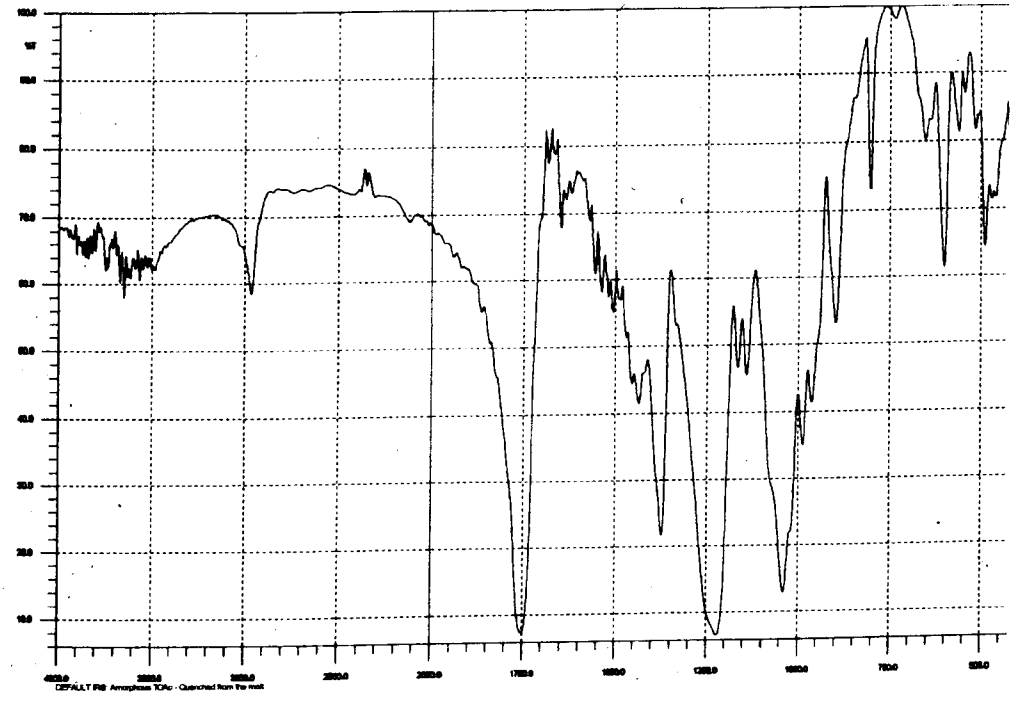

Figure 5.10: FT-IR spectrum of TOAc quenched from the melt

FT-IR analysis of the amorphous melt quenched material (figure 5.10) produced a spectrum with differences compared to the crystalline raw material. An example of the differences observed was that the profile for the melt-quenched material has a peak absent at around 2900 cm^{-1} and additional peaks appear at around 3500 cm^{-1} and 1175 cm^{-1}.

CHAPTER SIX

FURTHER CHARACTERISATION OF MATERIALS

6.1 HOT STAGE MICROSCOPY

Hot stage microscopy was carried out using a THMS 600 hot stage attached to a Nikon Labophot-2 light microscope. Images were captured with a JVC TK-1281EG camera and viewed using Lucia G software (version 2.3a).

Hot stage microscopy was carried out on selected material samples. This technique was used as an opportunity to observe the behaviour of the different materials when subjected to heat. It allowed observation of phase changes, such as when complete melt occurred, but also any partial melts and the subsequent recrystallisation that may occur with some of the samples before the final melt prior to degradation of the materials. However, this technique was primarily used as visual confirmation of the profiles obtained from DSC. It was also used to observe whether there was any discernable level of solvent/water in the materials that may indicate pseudopolymorphism or solvates. This would be observed when the material was heated under oil. Any gases of water or solvent vapour that were produced would be seen as bubbles in the silicon mounting oil. For the dried TOAc samples tested, no bubbling was observed. A sample of TOAc that had not been oven dried but had been stored under ambient conditions generated a small amount of bubbling in the mounting oil. This suggests that the TOAc material originally recrystallised was either a solvate, monohydrate or simply contained a discernable level of residual solvent prior to drying following the optimised method described in chapter four.

6.2 X-RAY CRYSTALLOGRAPHY

X-rays are electromagnetic radiation and have wavelengths in the order of a few angstroms (Å), which is equivalent to typical inter-atomic distances in crystalline solids.

They occur in the portion of the electromagnetic spectrum between gamma-rays and the ultraviolet and their discovery in 1895 enabled scientists to probe crystalline structure at an atomic level.

In 1912, Bragg recognised a predictable relationship among several factors. The distance between similar atomic planes in a mineral (the inter-atomic spacing) measured in Å; the angle of diffraction (called the theta angle) measured in degrees and the wavelength of the incident X-radiation, usually symbolised by the Greek letter lambda (λ). These factors were combined in Braggs Law:

$$n\lambda = 2d\sin\theta$$

where n is an integer; λ is the wavelength in angstroms; d represents the inter-atomic spacing in Å and θ is the diffraction angle in degrees.

Due to the regularly repeating atomic structure of crystalline solids, scattered X-rays were found to constructively interfere to produce a diffracted beam when the repeat distance was the same as the wavelength. A diffractometer is used to measure and record these diffracted beams and for practical reasons measure an angle twice that of the theta angle, which is called the 2-theta angle. Diffraction occurs in every possible orientation of 2-theta. The diffraction pattern produced records the X-ray intensity as a function of the 2-theta angle. A diffractogram is produced, where the vertical axis records the X-ray intensity and the horizontal axis records angles in degrees 2-theta. The diffracted beam is detected using a Geiger counter connected to a chart recorder, and in normal use the counter is set to scan over a range of 2-theta values at a constant angular velocity.

Routinely, a 2-theta range of 5 to 70 degrees is sufficient to cover the most useful part of a powder pattern.

X-ray diffraction has been in use in two main areas, for the fingerprint characterization of crystalline materials and the determination of their structure. Each crystalline solid has a unique characteristic X-ray powder pattern that may be used as a fingerprint for identification. Once a material has been identified, X-ray crystallography may be used to determine it's structure along with details of the inter-atomic distances and angles.

Due to the possibility of polymorphic forms of TOAc being produced as a result of recrystallisation of the material, it was decided that x-ray crystallography of selected TOAc samples would be of interest. Analysis was conducted in order to establish which of the samples exist in a single phase, and if possible to then determine their absolute structure.

Selected TOAc samples were forwarded to the Department of Chemistry, University of Aberdeen who performed the x-ray crystallographic analysis.

6.2.1 X-RAY CRYSTALLOGRAPHY RESULTS AND DISCUSSION

All of the samples were run as powder diffraction experiments and materials that produced single phase crystal powder patterns and contained crystals of a large enough size were subsequently submitted for single crystal experiments.

The data generated from single crystal analysis was used to create an image of the molecular structure of the material. The model produced was then used to generate a

theoretical powder pattern, which was compared to the actual experimental powder patterns obtained for each material.

The x-ray diffraction powder patterns obtained for the samples are contained in the following pages. A 2-theta range of 6 ° to 40 ° was used, as the relevant information was found to be contained within this range.

TOAc Material Identity	Comments
Raw material	Mixture of crystalline forms.
Recrystallised material:	
70:30 Ethanol:Water Ambient dried	Unidentified crystal structure.
70:30 Ethanol:Water Dried at 70 °C for 24 hours	Mixture of crystalline forms.
70:30 Ethanol:Water Dried at 90 °C for 24 hours	Single phase. Material structure identified. ‡
75:25 Ethanol:Water	Single phase. Material structure identified. ‡
85:15 Ethanol:Water	Single phase. Material structure identified. ‡

‡ The same molecular structure was identified, in these three samples.

Figure 6.1: Findings of the X-ray crystallographic analysis.

The theoretical powder pattern and 3 of the 6 experimental patterns (identified with ‡ in the table above) were identical in terms of peak positions, although relative and background intensities were slightly variable. This was considered to be due to variation in the quantity of sample being analysed and the size of the particles within the samples.

The theoretical powder pattern is shown below.

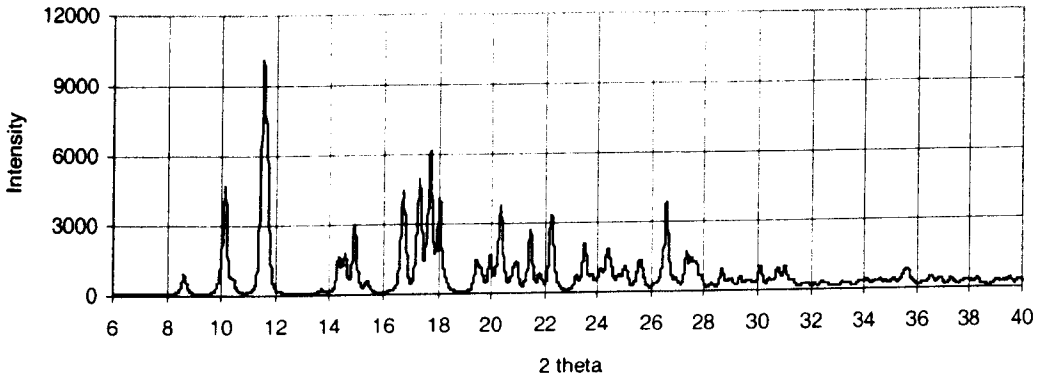

Figure 6.2: Theoretical powder pattern for recrystallised TOAc

The three materials with the same diffraction powder pattern have the same molecular structure. Single crystal analysis on these materials was carried out and the structure of the material was determined. The full 3-D view of the whole molecule is presented in figure 6.3.

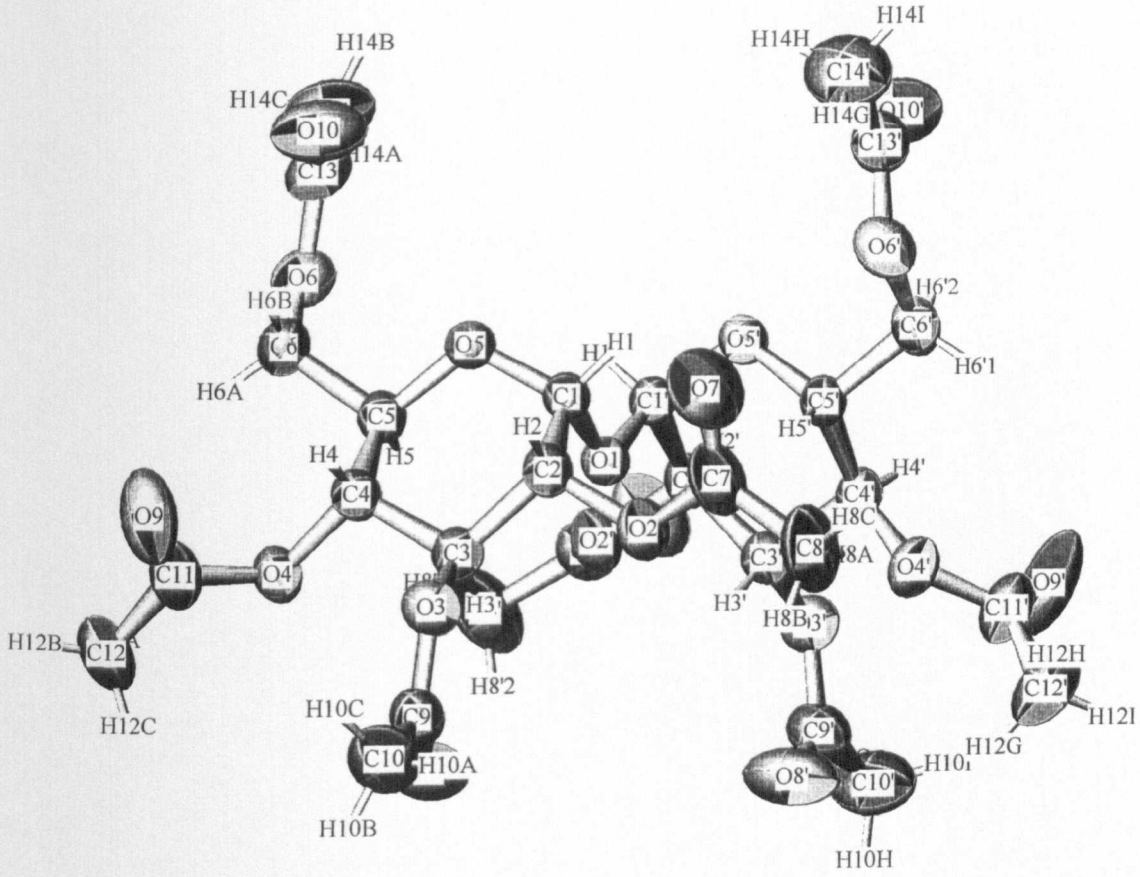

Figure 6.3: 3-D view of the whole TOAc molecule determined by single crystal analysis

The three materials with the same diffraction patterns were recrystallised from:

- 70:30 ethanol:water.
- 75:25 ethanol:water.
- 85:15 ethanol:water.

All three materials were dried at 90 °C for 24 hours.

The following are the diffraction powder patterns obtained for these materials.

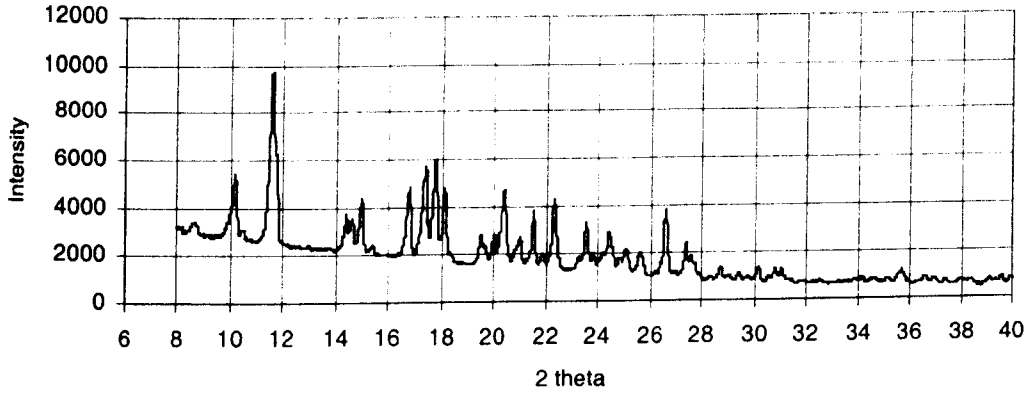

Figure 6.4: X-ray powder diffraction profile of TOAc recrystallised from 70:30 ethanol:water, dried at 90 °C for 24 hours

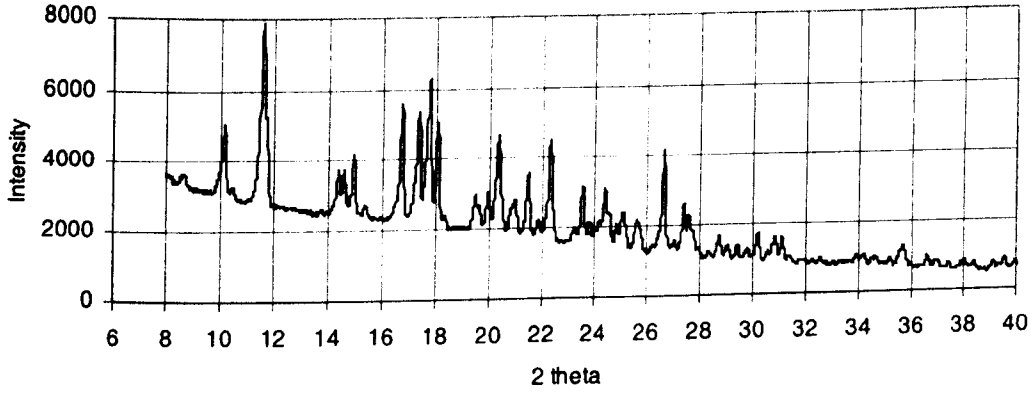

Figure 6.5: X-ray powder diffraction profile of TOAc recrystallised from 75:25 ethanol:water, dried at 90 °C for 24 hours

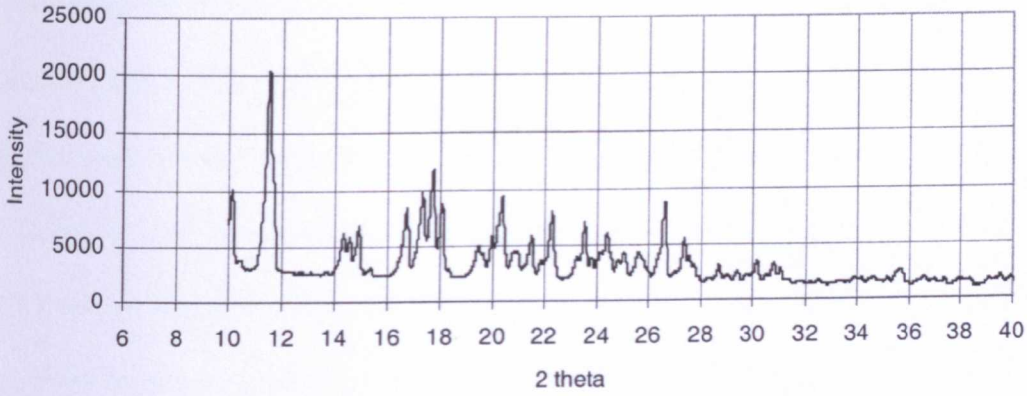

Figure 6.6: X-ray powder diffraction profile of TOAc recrystallised from 85:15 ethanol:water, dried at 90 °C for 24 hours

Figure 6.7 is an image of half of the molecule, and the point where the oxygen links to the rest of the molecule is highlighted.

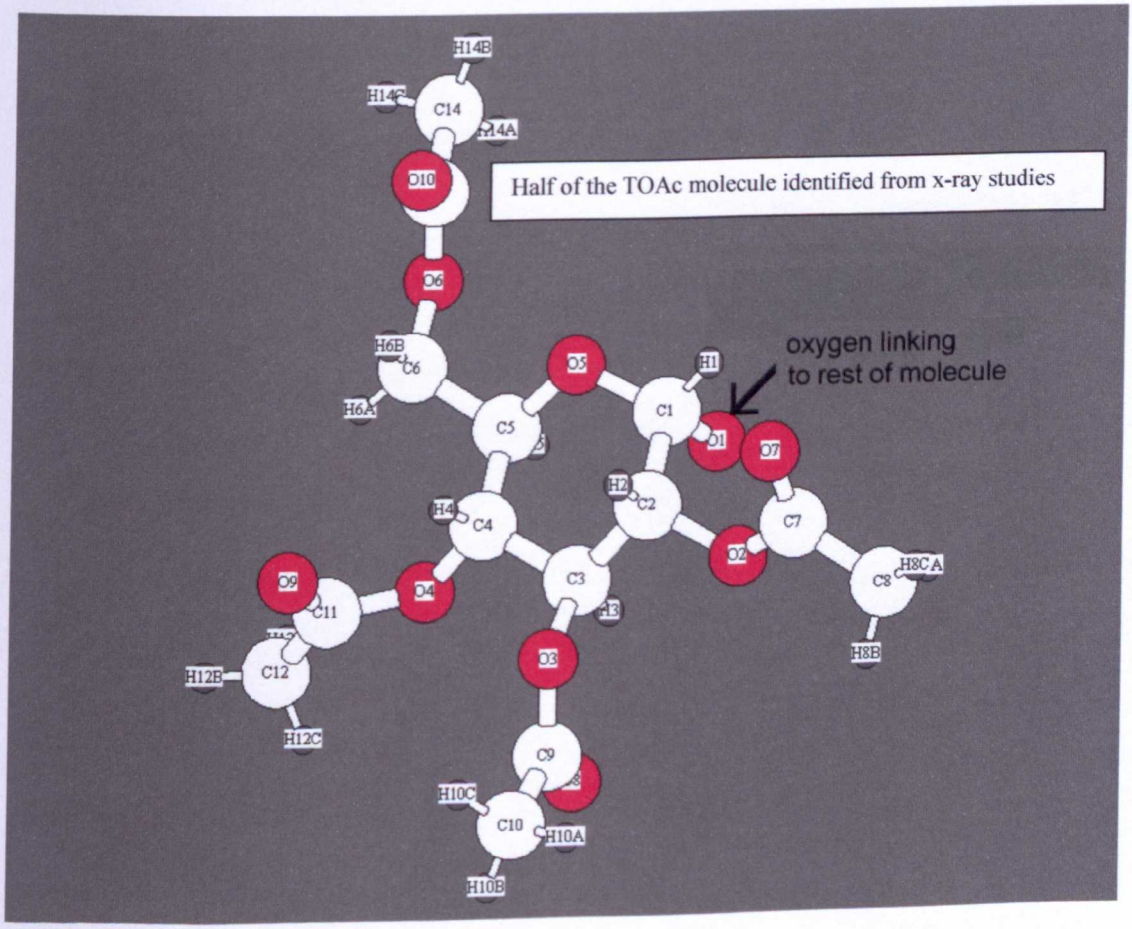

Figure 6.7: Diagram of the structure of half of the TOAc molecule identified.

The TOAc raw material was found to contain additional peaks compared to the single phase samples. The particle size of the raw material was too small to enable a single crystal experiment hence the extra peaks remain unidentified. It would appear that the raw material is a mixture of more than one phase. This implies that there is a transformation of the material occurring from a metastable crystalline form to a more stable, lower energy crystalline form and this transformation has not yet been completed. These data therefore suggests that TOAc exists in at least two crystalline forms.

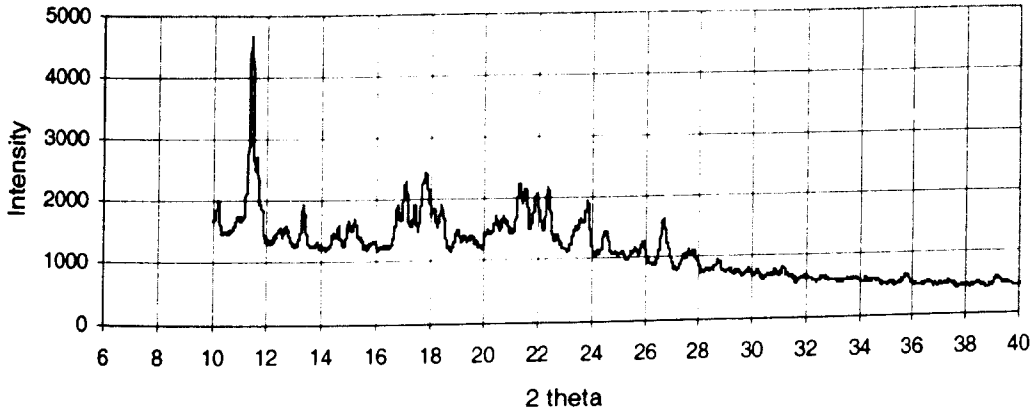

Figure 6.8 X-ray powder diffraction profile of TOAc raw material

The TOAc sample recrystallised from 70:30 ethanol:water and dried under ambient conditions generated a completely different powder pattern. The peaks obtained for this material do not correlate with the additional peaks obtained with the raw material. Unfortunately, the particle size of the material was again too small to enable single crystal analysis and so the structure of this material also remains unidentified. This data suggests that TOAc can exist in a third crystalline form.

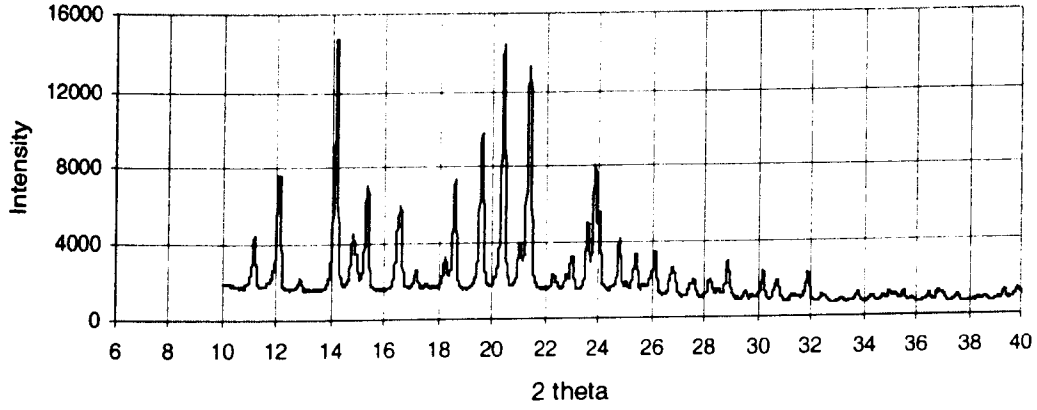

Figure 6.9: X-ray powder diffraction profile of TOAc recrystallised from 70:30 ethanol:water, dried under ambient conditions

TOAc again recrystallised from 70:30 ethanol:water but dried at 70 °C for 24 hours was also considered to be a mixture of more than one phase. This material contained all of the peaks observed in the single phase materials, but also contained some additional peaks (see figure 6.10).

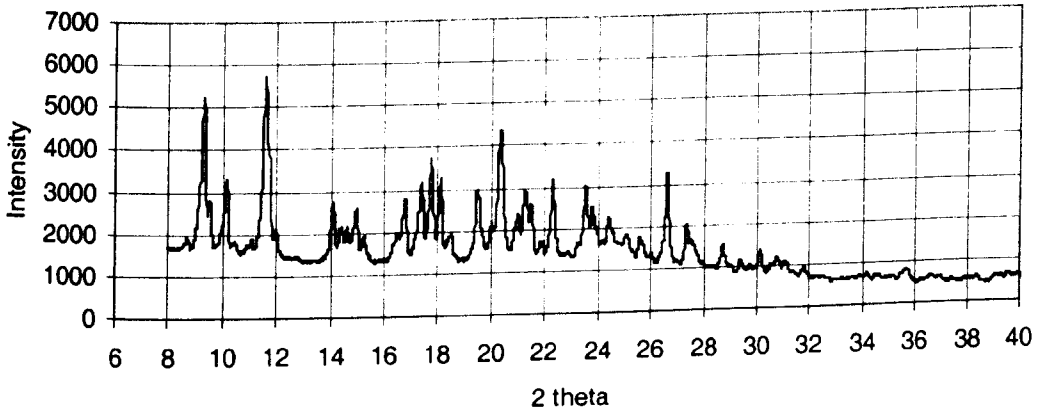

Figure 6.10: X-ray powder diffraction profile of TOAc recrystallised from 70:30 ethanol:water, dried at 70 °C for 24 hours

These additional peaks correspond to the peaks observed with the unidentified recrystallised material rather than those additional peaks observed with the raw material. This mixture of forms indicates a phase transformation is occurring that is not yet complete. Transformation of form is usually from a metastable to a stable form. It is therefore relevant to note that the polymorphic form of a material that crystallises out of solution first is often the form that is more soluble in that solvent system but less stable compared to other polymorphic modifications.

These transformations could also be related to the drying of the material following recrystallisation. The material that was dried according to the optimum conditions identified from the drying profile of TOAc generated a single phase powder pattern, the structure of which has been generated and is presented in figure 6.3. When the material dried under ambient conditions was analysed, a completely different powder pattern was observed. The material dried at 70 °C for 24 hours appears to be a mixture of these two forms. This theory is supported by the DSC profiles that were obtained for these materials.

In conclusion, these X-ray crystallography data suggest that TOAc exists in at least three different crystalline forms, only one of which it was possible to positively identify from the material available. It also appears that the form identified is the most stable, as transformations of form appear to be towards this crystalline structural arrangement.

6.3 Dynamic Vapour Sorption (DVS)

All materials are sensitive to the presence of water vapour or moisture within the atmosphere, and materials can retain water by either bulk absorption or surface adsorption.

The percentage moisture content is the simplest and most important single parameter for describing the water content of a material. However, a materials moisture content is directly dependent on the partial vapour pressure of water, commonly referred to as the relative humidity (RH), in the sample environment.

DVS is a highly precise, fully automated technique where the sample being investigated is placed on a microbalance, which is exposed to a continuous flow of air at a predetermined and constant relative humidity. As humid air passes over the sample, a zone of constant moisture concentration (relative humidity) is established around the sample. This zone allows the rapid establishment of equilibrium by maximising the mass transport of water vapour into and out of the sample.

By controlling the relative humidity that a material is exposed to, it is possible to generate a water sorption isotherm, which relates to the dependency of the equilibrium moisture content of the material and the % relative humidity. In general, the use of dynamic vapour sorption can provide both quantitative and qualitative information on a material, such as determination of amorphous content, kinetics of moisture uptake and loss, batch-to-batch variability, permeability and deliquescence in addition to an indication of the tendency of a material to form or lose hydrates. For the reasons mentioned above, it was decided to use DVS to obtain information regarding the water uptake characteristics of the samples under study in this research.

A Surface Measurement Systems DVS 2000 automated vapour sorption analyser was used to investigate the vapour sorption of water on selected lactose, trehalose and TOAc

samples. The DVS instrument was run under the control of a dedicated PC. *DVSWin* software (version 2.16) was used to set up and subsequently run the experiments. The equipment has an ultra-sensitive recording microbalance capable of measuring changes in sample mass lower than 1 part in 10 million and has good long term stability. The balance was housed within a precisely controlled constant temperature incubator that ensured high instrument baseline stability as well as accurate control of the relative humidity generation. The DVS was set to 25 °C for all of the experiments that were carried out. Mixing dry and saturated vapour gas flows in the correct proportions using mass flow controllers generated the required humidities. Humidity and temperature probes were situated below the reference and sample cups to give independent verification of the system performance. The microbalance was very sensitive to the sorption and desorption of moisture so therefore a constant dry gas purge to the balance head had to be maintained to ensure the best performance in terms of baseline stability.

Between experiments, it was important to ensure that the sample cup was clean and free from static. Any static that was present on the sample cups at the start of an experiment would have resulted in a baseline shift as the DVS moved to high relative humidity. To ensure that the pans were clean they were washed with hot water, rinsed with ethanol and then allowed to dry naturally. In the case of TOAc samples, acetone was used prior to the ethanol wash to remove all traces of the material from the sample cup. Elimination of the static was then accomplished by setting the target relative humidity (RH) to 95% with the empty sample and reference cups in place. The high RH conditions provide a conductive path to earth for the static. When the RH reaches approximately 70%, a rapid change in mass may be observed that signifies a static discharge. Once a stable baseline at the high RH was achieved, the instrument was then set to the RH that was to be used for the start of

the experiment. For TOAc samples this was 0% RH and for trehalose, the starting RH was 5%. The baseline for trehalose was set at 5% RH as if it had been set at 0%, the system would have taken a significant length of time to reach equilibrium as the trehalose contains a relatively large quantity of water.

Once a stable baseline had been established for each material at the starting RH, the balance was tared and then the sample remotely loaded into the glass sample cup. Once the sample was returned to the DVS it was allowed to settle for a while to allow the material to equilibrate to the environment. The small delay in starting the experiment also ensured that the first few data points were not affected by swinging of the sample cup. The initial weights of the samples were then recorded by the DVS before each experimental run was initiated.

6.3.1 DVS Results and Discussion

Figure 6.11 presents findings from the DVS analysis. Copies of the profiles obtained for each material can be found in appendix 6.

Material ID	Comments
LACTOSE	**Start at 0% RH**
Raw material – 325M	Quick water uptake - surface effect. Slight dip indicates recrystallisation of amorphous surface regions.
Recrystallised material:	
100% Water S=1.5 63-90 μm Batch L1 (34-18 °C)	Less water uptake than raw material. Less static, less amorphous regions, less surface energy. Less 'active sites' on the surface for water interaction.
TREHALOSE	**Start at 5% RH**
Raw material 63-90 μm	Sample takes up a lot of water. Indicates high number of amorphous regions. The sample then recrystallises (surface effect). Once recrystallised – flat plots observed. No water interaction.
Recrystallised material:	
100% Water S=1.5 63-90 μm Batch 2 (34-18 °C)	Stable material. Minimal change between sorption and desorption isotherms. No recrystallisation. Surface effect - no water into bulk. Crystalline surface – not a significant number of amorphous regions on surface.
40:60 Ethanol:Water S=1.5 63-90 μm Batch 3 (23-7 °C)	Increased uptake of water around 30%RH indicates large number of amorphous regions. No recrystallisation.
60:40 Ethanol:Water S=1.5 63-90 μm Batch 8 (34-18 °C)	Loss of static/surface charge as sample exposed to high RH (90%). No recrystallisation. Large hysterisis indicates that material is retaining water – possibly an element of anhydrous nature to the surface?
60:40 Ethanol:Water S=1.5 63-90 μm Batch 6 (23-7 °C)	Isotherm is almost identical to that for the previous material – less water taken up by sample and less water subsequently retained. Large hysterisis. No recrystallisation.
Surfaced washed material:	
Surface washed with IPA 100% Water S=1.5 63-90 μm (34-18 °C)	Similar profile to the material recrystallised from 100% water (without surface wash). Material takes up less water - confirms that uptake is only a surface effect. Stable material. No recrystallisation. Hysterisis indicates that some water is retained by the material surface.

Table continued on next page

Table continued from previous page

Material ID	Comments
TOAc	**Start at 0% RH**
Raw material 63-90 μm †	Discharge of static observed at 70%RH. The material is known to be extremely electrostatic - due to the effect of static on the equipment, conclusions about the behaviour of this material cannot accurately be drawn.
AMORPHOUS MATERIALS	**Start at 0% RH**
Spray dried material:	
TOAc (63-90 μm)	Material takes up large amount of water. No recrystallisation observed. Small hysterisis indicates that only a small amount of water retained by sample. Material appears to be stable.
Quenched from the melt:	
Powdered amorphous material: TOAc (63-90 μm)	Material takes up more water than spray dried TOAc and exhibits a larger hysterisis - more water therefore retained by this sample. No recrystallisation. Material appears to be stable.

Figure 6.11: Findings from DVS analysis.

Hysterisis in the DVS profile indicates a rearrangement of the material surface i.e. molecular movement. This occurs as the amorphous regions become crystalline and retain a proportion of the adsorbed moisture.

The recrystallised lactose appeared to contain less amorphous regions on the surface compared to the raw material as less water was adsorbed.

All of the recrystallised trehalose samples exhibited more stable surface characteristics than the trehalose raw material as only the raw material exhibited significant recrystallisation of surface amorphous regions.

The trehalose materials recrystallised from solvents containing ethanol appeared to be less stable than the material recrystallised from 100% water. This was indicated by the fact that there was very little hysterisis with the material recrystallised from 100% water and therefore little molecular movement of the surface. Although the trehalose material recrystallised from solvents containing ethanol are in comparison less stable, they only physically adsorbed approximately half the quantity of water compared to the trehalose samples recrystallised from 100% water. This indicated that trehalose recrystallised from solvents containing ethanol may exhibit a better overall long-term stability if samples were exposed to high humidity environments for any significant length of time.

Amorphous spray dried trehalose was reported to form the dihydrate during DVS experiments (Quadrant Healthcare). The spray dried particles collapse as the water is adsorbed and subsequently recrystallise. This would obviously have a significant effect on the surface characteristics of the material and so the results obtained from DVS analysis of this material would be of limited use in the context of this research.

With respect to amorphous TOAc samples, the larger amount of water uptake by the powdered amorphous material could be attributable to a larger proportion of moisture being absorbed into the bulk of the material compared to the spray dried material. Another possible theory relates to the amorphous content of the samples at the surface. If there was any significant degree of recrystallisation of the surface of the spray dried TOAc material compared to the powdered TOAc glass, one would expect less moisture to be taken up by the spray dried sample. It is also possible that the dichloromethane solvent used to produce the load solution for spray drying the TOAc could have had an effect on the water uptake characteristics of the material produced. However, the most likely reason for the

difference in the moisture uptake characteristics relates to the surface areas of the two amorphous TOAc materials. Due to the method of production, one would expect the powdered TOAc glass to have a larger surface area available for moisture adsorption compared to the spray dried TOAc material. Quantification of the surface roughness of these samples may provide support for this theory.

It had been observed in the laboratory that over time the surface of amorphous TOAc devitrified. The phenomena was observed with amorphous TOAc that had been quenched from the melt (but not powdered) and had been left in storage under ambient conditions for several months. However, it had been unclear whether the devitrification was due to bulk moisture uptake by the material or some other mechanism. The results of the DVS analysis indicate that the uptake of moisture by the amorphous TOAc samples is a surface effect only. This was due to the fact that there was no significant hysterisis observed for any of the amorphous TOAc samples tested as not much water was retained. This indicates that TOAc under high humidity conditions exhibits stability and it also indicates that humidity is not a direct cause of the devitrification of the material surface that occurs on storage.

From observations of the materials following DVS analysis, all powders remained free-flowing. All of the results indicate that any changes observed are only surface effects. No water appears to have been taken into the bulk of the samples as the percentage change in mass for all of the samples was not sufficiently high. This was also indicated by the fact that no collapse was observed for any of the samples tested.

6.4 DETERMINATION OF SURFACE ROUGHNESS

Two techniques were tested in order to determine the most appropriate method to use for quantification of the surface characteristics of the carrier materials prior to their blending and an assessment of performance.

6.4.1 ATOMIC FORCE MICROSCOPY (AFM)

The basic objective of the operation of an atomic force microscope is to measure the forces (at the atomic level) between a sharp probing tip (which is attached to a cantilever spring) and a sample surface. Unlike scanning electron microscopy, AFM does not require a current between the sample surface and the tip to operate. Images are taken by raster scanning a sample relative to the probing tip and measuring the deflection of the cantilever as a function of lateral position. Most atomic force microscopes employ an optical technique to determine the lever deflection. As the cantilever flexes, light from a laser is reflected onto a split photo-diode. By measuring the signal difference, changes in the bending of the cantilever can be measured.

Height image data obtained by AFM is three-dimensional. The usual method for displaying the data is to use a colour mapping for height. Similar colour mappings can be used for non-topographical information such as phase imaging, which works by measuring the phase difference between the oscillations of the cantilever and the detected oscillations.

Since the Cantilever obeys Hooke's Law for small displacements, the interaction force between the tip and the sample can be determined. An observed tip deflection can be

converted into an applied force (or adhesive interaction) using the following equation derived from Hooke's Law:

$$F = kD$$

where F represents the force, k represents the spring constant and D represents the cantilever deflection.

A negative sign is often used in the equation to represent that the force is always opposite to the direction of the displacement and therefore back towards the equilibrium position (restoring force). In summary, Hooke's Law states that the extension (or deflection) of a spring is directly proportional to the force acting on it, but this law only applies if the elastic limit of the spring has not been reached.

The way in which image contrast is obtained can be achieved in many ways. The three main classes of interaction are contact mode, tapping mode and non-contact mode.

Contact mode is the most common method of operation of an atomic force microscope. With this method the tip and sample remain in close contact as the scanning proceeds. As the tip is dragged over the sample, detection apparatus measures the vertical deflection of the cantilever, which indicates the local sample height. One of the drawbacks of remaining in contact with the sample is that there exist large lateral forces on the sample as the tip is dragged over the sample.

Tapping mode is the next most common mode used. When operated in air, the cantilever is oscillated at its resonant frequency (typically hundreds of kHz) and positioned above the surface so that it only taps the surface for a very small fraction of its oscillation period. This method means that contact with the surface is still made, but the very short time over which this contact occurs means that lateral forces are dramatically reduced as the tip scans over the surface compared with operating the atomic force microscope in contact mode.

Non-contact operation is another method that can be employed. For this method, the cantilever must be oscillated above the surface of the sample. However, this is a difficult mode to operate in ambient conditions as the thin layer of water contamination that exists on sample surfaces invariably forms a small capillary bridge between the tip and the sample. This can cause the tip to 'jump' to contact the surface, so imaging becomes more like that achieved in the tapping mode.

Unlike traditional microscopes, scanned-probe systems do not use lenses so the size (or more specifically the sharpness) of the probe rather than diffraction effects generally limits their resolution. One important factor that also influences resolution relates to compression. When operating an atomic force microscope in either contact or tapping mode, it should be remembered that although the force between the tip and sample may only be nN, the pressure may be MPa. This is particularly important to remember when soft materials are being analysed because it is possible for the tip-sample interaction to distort or destroy them.

It was decided to try using AFM to characterise the surfaces of two TOAc samples, in order to assess the validity of the technique for quantification of surface roughness. If successful, the technique would be used to obtain surface roughness values for all of the materials whose performance as a drug carrier was to be assessed. The AFM equipment used was located at the University of Nottingham.

The non-contact mode was not available with the equipment used, and as the sugars to be analysed were considered quite delicate, the mode with the least lateral force was used. Consequently, both samples imaged were analysed using the tapping mode in air.

In order to mount suitable samples for analysis, crystals were sprinkled onto softened wax (Tempfix) and the loose unbound crystals were blown off with a stream of nitrogen once the wax had hardened.

A Digital Instruments Multi-Mode with Nanoscope IIIa controller atomic force microscope was used to analyse both TOAc samples. The instrument had a maximum scan range of 13 μm. The depth of scanning was measured by the Z-range.

6.4.1.1 AFM Results and Discussion

Due to time constraints related to the availability of the equipment, it was not possible to generate a surface roughness value (R_a) for every area analysed. The roughness value R_a was calculated from the arithmetic average of the absolute values of all points of the profile. Selected scans considered to be of greatest interest were used to obtain values for the surface roughness of the material as determined using this analytical technique. For all of the profiles obtained, the Z-range value for the area analysed was available. The scale

bar representing colour mapping for height identified the Z-range value for the profile. This value equates to the distance from the highest peak in the area analysed to the lowest valley, and indicates the degree of movement made by the cantilever as it scanned the surface of the material. The higher the Z-range value obtained the greater the degree of surface undulation or indentation present.

The following tables contain comments on a selection of the AFM scans generated. A copy of each of the scans mentioned is included in appendix 6.

The first material tested was the orthorhombic TOAc material recrystallised from 70:30 ethanol:water, the surface washed with isopropyl alcohol following recrystallisation.

Figure 6.12 presents comments on a selection of the scans generated with this material.

Filename	Comments
CP001a	5 μm topographic view of a flat region with no large step edges. Surface appears bumpy, with some regular longitudinal striations. Z-range only 30 nm. Surface roughness value (R_a) calculated as 2.0 nm.
CP003a	5 μm topographic view of 'knobbly' features. The image is quite noisy. Z-range approximately 710 nm.
CP005a	10 μm topographic view of some step edges. Z-range 400 nm. Surface roughness value (R_a) calculated as 44.5 nm.
CP005c	Phase contrast image of CP005a. The flat areas either side of the step edges are confirmed as real flat areas, and not simply as a result of the scanner trying to move past the Z-limit (out of range) of the AFM equipment.
CP006a	Zoom in to 1.25 μm topographic view of the step edges observed in CP005a. Z-range 100 nm. Surface roughness value (R_a) calculated as 9.2 nm. The reduction in the observed R_a value is expected due to the reduction in the image size used to calculate the surface roughness.
CP009a	5 μm topographic view of a flat area between step edges. The surface here appears to have a 'honeycomb' appearance. The fine detail observed is only several nm in depth. Z-range 20 nm. Surface roughness value (R_a) calculated as 2.0 nm. Very low roughness value as could be expected from the observed AFM image. This value however is probably more influenced by the brighter 'hillocks' in the image rather than the honeycomb feature itself which appear approximately half the height of the hillocks.
CP011a	Zoom to 1μm topographic view of the honeycomb feature observed in CP009a. The scan appears to show further very fine detail too small to distinguish in the 5 μm scan. Z-range 6 nm. The honeycomb feature now appears as the vague interconnecting raised ridges. The surface appears to consist of very fine filaments, several to tens of nm in size. *Although it should be noted that at this level, tip magnification or broadening effects could come into effect.* Surface roughness value (R_a) calculated as 0.5 nm.
CP011c	Phase contrast image of CP011a highlighting the fine surface detail. The image appears to show slight differences when compared to the topographic view that could indicate amorphous regions on the surface of the material.

Figure 6.12: Comments on AFM scans of TOAc recrystallised from 70:30 ethanol:water, surface washed with isopropyl alcohol.

The second material analysed on the AFM was the acicular TOAc raw material (batch number: 033/164).

Filename	Comments
CP015a	10 μm topographic view of some large step edges. Z-range 400 nm.
CP015b	Phase contrast image of CP015a. Step edges appear sharper, highlighting the different facets of the steps.
CP019a	5 μm topographic view of a smooth flat area. Z-range 8.0 nm. The image appears noisy due to loose surface debris. Network of honeycomb features similar to that observed with sample CP009a is visible.

Figure 6.13: Comments on the AFM scans of the TOAc raw material.

A different AFM instrument was subsequently used in order to analyse the TOAc raw material over a greater scan area. The AFM used for this analysis was Digital Instruments Dimensions 3000 AFM with Nanoscope IIIa controller. This instrument has a maximum scale range of 100 μm. With this equipment the motorised stages makes it is much easier to move the sample underneath the AFM probe.

Again the samples were prepared for analysis by sprinkling a small quantity onto softened wax (Tempfix). Any unbound crystals were removed with a stream of nitrogen. Figure 6.14 presents comments on a selection of the scans obtained.

Filename	Comments
809CP00a	5 μm topographic view of a very rough area (Z-range 1.2 μm) with step edges, fragmented regions and flat planes. Roughness values are included for the entire image (R_a = 147.6 nm) and for a 500 x 500 nm area of the flat region (R_a = 4.6 nm, Z-range 92 nm) indicated by the box. *These roughness measurements highlight the difficulty in making comparable roughness measurements on samples that have a wide variation in surface structure, and when the images are on a similar scale to the features observed.*
809CP01b	10 μm topographic view of an area showing very high step edges and terracing. Z-range 1.4 μm. Surface roughness value (R_a) calculated as 223.4 nm for the whole image. A 5 x 5 μm region over the steps is also highlighted, and the surface roughness value (R_a) for this area is calculated as 223.2 nm, Z-range 933 nm.
809CP01c	As above but with surface roughness calculation on a 5 x 5 μm flat region. R_a = 29.2 nm, Z-range 864 nm. This surface roughness value has an order of magnitude difference when compared to the previous roughness calculation of an identical sized section of the same image.
809CP02a	Zoom to the 5 x 5 μm area as above. Z-range now reported as 500 nm.
809CP02c	As above with surface roughness calculations. R_a = 34.4 nm, Z-range now 262 nm for the whole image. For a flatter region of the image (343 x 347 nm) the surface roughness calculation is R_a = 4.3 nm, Z-range 33 nm.
809CP03a	Zoom to 2 μm topographic view of the flat region. Z-range 22 nm. Honeycomb feature is again highlighted, although the image is quite noisy. Longitudinal striations can also be observed with a horizontal linking element. R_a = 2.0 nm. Note larger scale raised areas at either side and the top of the image.
809CP04	Re-scan of the same area as for 809CP03a in preparation for a zoom. Note: some debris has moved. This is the likely cause of the slightly poorer quality images. R_a now calculated as 1.0 nm and Z-range 14 nm.
809CP05a	Zoom to 1 μm area of previous image. (Zoom location approximately central to 809CP04 image.) Image highlights the fine features between the ridges of the honeycomb network ridges. Surface roughness value (R_a) calculated as 0.6 nm. Z-range 15 nm.
809CP05c	Line section through the above image showing the relative heights of the honeycomb ridges and smaller scale fine filaments and nodules. Surface roughness calculation of this line analysis, R_a = 0.7 nm.

Figure 6.14: Comments on AFM scans of TOAc raw material.

The features observed with the AFM are real and are not an artifact of the AFM. Surface features observed with this equipment are only in the magnitude of nm's in depth and

these features are probably too small to be resolved by SEM as beam penetration has to be considered. The TOAc material, which is carbon and oxygen based, will not resist the electron beam of the SEM (or more accurately interact with it) to anywhere like the extent of a metal. Hence, the SEM may be imaging tens of nm below the 'real' surface. An accelerating voltage of as low as 300V for the SEM was tested with the TOAc materials and none of the surface features observed with the AFM were visible. Even with such a low accelerating voltage (which results in a drop in the image quality) the SEM may still be penetrating too far into the surface for these features to be visible. The best resolution from SEM is in the order of a few nm and this resolution worsens considerably as the accelerating voltage is lowered. Therefore, any feature observed with the AFM could be invisible to a SEM. In addition, it should also be considered that the gold sputter coating applied to the samples to allow images to be seen under the SEM may also have a masking effect on the material surface. If the gold coating applied to the sample were more than a few nm in depth, then all fine detail would be obliterated. The harsh vacuum environment created inside the SEM and/or the electron beam itself could also potentially result in a scouring away of the fine detail on the delicate sugar surface.

Heng *et al* (2000) used AFM to quantify the surface morphologies of four different lactose carriers. The conclusions of the authors were that the scanning probe microscope enabled a quantitative measure of the surface properties of the lactose carriers studied. *In vitro* deposition results using a twin impinger showed that rougher carrier surfaces generally allowed more drug particles to be emitted from the inhaler under investigation (Rotahaler®). However, they stated that although more drug was emitted with the rougher surfaced carriers, the availability of the drug to stage 2 was reduced as detachment of the drug particles from the surfaces was more hindered. The authors stated that there was an

optimum R_a value for greater delivery of drug particles to stage 2 of the twin impinger used in their research, and they concluded that lactose 325M produced the optimum performance. Lactose 325M was determined by the authors to have a surface rugosity value of 197.47 nm.

The scan size used by Heng *et al* (maximum of 8 x 8 μm) was comparable with the scan sizes used for AFM analysis of the TOAc materials in this research. However, with such a relatively small scan size the effect of any surface debris on the roughness measurements obtained has to be considered. As the inclusion of surface debris cannot be accurately controlled, any surface debris that is present on a sample may skew the surface roughness values obtained, possibly significantly compared to the surface roughness of the true sample surface. In addition, it should be noted that there is no way to determine exactly where the probe tip is located prior to scanning. This therefore allows the possibility that a scan could be made of surface debris rather than the true sample surface itself.

From personal practical experience, it appears that the range of surface roughness values it is possible to obtain with AFM for a single sample is large. The surface roughness values obtained for profile 809CP00a highlights this. For this sample, the AFM gave unreliable results with an extremely poor reproducibility. In addition, the same area was scanned for both 809CP03a and 809CP04. However, the R_a and Z-range values obtained for each of these profiles was different. For 809CP03a, R_a was 2 nm and the Z-range value was 22 nm and for 809CP04 the R_a was reported as 1 nm and the Z-range as 14 nm.
These results showed that scanning exactly the same area on successive occasions resulted in different surface roughness values. The difference in the results obtained was considered to indicate that the technique itself had an effect on the surface of the sugar

samples. Due to the fact that the probe tip made contact with the sample surface during analysis, it was possible that there was a degree of distortion or destruction of the sample surface. This would happen if the sample was delicate and therefore susceptible to the pressure or lateral forces applied during analysis by AFM.

In conclusion, I believe that AFM is not a suitable technique for reliable, reproducible quantification of the surface roughness of the sugars used in this research, as the possible variation in results that could be obtained appears to be massive.

6.4.2 LASER PROFILOMETER

Another technique typically used to determine the roughness of a surface is laser profilometry. As opposed to tactile profilers, measurement with laser profilometers is non-contact and therefore non-destructive. It uses point sensors along with highly precise stages to create profiles and three-dimensional topographies. The sample, which is placed under the sensor, is moved by the stage while the sensor transmits the height data to the measurement control unit. The technique commonly employs a principle referred to as optical triangulation. Optical triangulation uses a light source (commonly a diode laser), imaging optics and a photodetector. A diode laser is user to generate a collimated beam of light, which is then projected onto the target surface. A lens focuses the spot of reflected laser light onto the photodetector, which generates a signal that is proportional to the spot's position on the detector. Software then generates a colour three-dimensional image of the surface.

The application of this technique to analyse the surface of carrier materials was carried out as a viable alternative following the disappointing results obtained with AFM. As well as being a non-destructive method of analysing the surface of the carrier materials, another advantage of the laser profilometer over AFM was that a much larger area could be sampled in a comparatively shorter time scale. One obvious advantage of analysing a larger surface area is that it would lead to a truer representation of the surface. This technique should therefore produce a more accurate and reproducible quantification of the surface roughness of the carrier materials compared to AFM.

A UBM laser and microfocus measurement system supported by UBSoft computer software version 2.8 was used for the analysis. A Monacor video monitor was also attached and this was used to visualise the surface to be analysed to ensure suitable positioning of the laser.

A surface area of 30 μm square was analysed, with 1000 points per mm measured. A depth of field of ± 500 μm was also set (Z-range).

Parameters recorded from the laser profilometer analysis were R_a, R_q and R_{tm}. Definitions for the parameters are given below:

R_a is the arithmetic average of the absolute values of all points of the profile. It can be understood as the height of the rectangle with the same length and surface as the profile encloses with the central line. R_a is also known as CLA (centre line average) height or AA (arithmetical average).

R_q is the root mean square (RMS) of the values of all points of the profile.

R_{tm} is the mean peak to valley height and is the arithmetic average of the maximum peak to valley height of the roughness values of 5 consecutive sampling sections over the filtered profile. R_{tm} is also known as R_zDIN. Put slightly differently, this value is derived from the arithmetic average of the largest height difference in each of 25 squares, which result from splitting the surface into a 5 x 5 grid.

6.4.2.1 Laser Profilometry Results and Discussion

For each material, 26 readings were taken. From these readings, the middle 20 values were used to calculate the average roughness of the material surface. Figures 6.15, 6.34 and 6.35 contain data obtained for each parameter measured, namely R_a, R_q and R_{tm} respectively.

Material ID	R_a (μm)	SD (n=20)	%CV
LACTOSE			
Raw material – 325M	**2.70**	0.89	32.76
Recrystallised material:			
100% Water S=1.5 63-90 μm Batch L1 (34-18°C)	**2.78**	1.13	40.81
TREHALOSE			
Raw material 63-90 μm	**1.84**	0.89	48.46
Recrystallised material:			
100% Water S=1.5 63-90 μm Batch 2 (34-18°C)	**3.03**	1.56	51.58
40:60 Ethanol:Water S=1.5 63-90 μm Batch 3 (23-7°C)	**2.39**	1.95	81.25
60:40 Ethanol:Water S=1.5 63-90 μm Batch 8 (34-18°C)	**5.65**	1.72	30.43
60:40 Ethanol:Water S=1.5 63-90 μm Batch 6 (23-7°C)	**4.54**	2.20	48.50
Surfaced washed material:			
Surface washed with IPA 100% Water S=1.5 63-90 μm (34-18°C)	**2.12**	0.66	31.17

Table continued on next page

Table continued from previous page

Material ID	R_a (μm)	SD (n=20)	%CV
TOAC			
Raw material 63-90 μm †	**1.32**	0.64	48.41
Recrystallised material:			
70:30 Ethanol:Water S=1.2 63-90 μm (34-18°C)	**0.72**	0.78	109.04
70:30 Ethanol:Water S=1.5 63-90 μm (34-18°C)	**1.13**	1.23	108.91
75:25 Ethanol:Water S=1.2 63-90 μm (34-18°C)	**2.67**	0.57	21.40
85:15 Ethanol:Water S=1.2 63-90 μm (34-18°C)	**4.16**	1.62	38.89
Surface washed material:			
Surface washed with IPA 70:30 Ethanol:Water S=1.5 63-90 μm (34-18°C)	**1.91**	0.88	45.89
AMORPHOUS MATERIALS			
Spray dried material:			
Lactose 63-90 μm	**0.64**	0.84	130.87
Trehalose 63-90 μm	**0.52**	0.13	25.76
TOAc 63-90 μm	**0.78**	1.17	150.85
Quenched from the melt:			
Powdered amorphous material: TOAc 63-90 μm	**2.32**	0.51	22.11

† Sieve fraction size. Considering the morphology of the raw material, there is a high probability that particles of a larger longitudinal length than 90 μm may be present in the batch of material sieved.

Figure 6.15: Table of results (R_a) from laser profilometry analysis.

The R_a values obtained for these materials indicate that in the majority of cases, the recrystallised materials have rougher surfaces compared to the raw materials. The only exceptions were the two batches of TOAc recrystallised from 70:30 ethanol:water, along with all of the spray dried materials. With respect to spray-dried lactose and TOAc, these

materials demonstrated much higher %CV values than the other materials assessed. The smoothest surface according to the R_a values appears to be spray-dried trehalose. The low standard deviation and %CV for this material also indicate that the results obtained were highly reproducible, which implies that the material surface was relatively uniform for this material.

For the amorphous samples, the R_a values of the spray-dried materials are the lowest when considered as a group. However, the surface of the powdered amorphous TOAc was quantified as approximately three times as rough as the spray dried TOAc. This increased surface roughness will be due to the distinctly different manner in which this amorphous material was produced, namely grinding with a pestle and mortar. Within the spray-dried materials, the order of surface roughness was quantified as trehalose the smoothest followed by lactose, with TOAc as the roughest.

The maximum standard deviation value obtained in the determination of this parameter was 2.2 μm, which was obtained for a batch of trehalose recrystallised from 60:40 ethanol:water. A different batch of trehalose recrystallised from the same solvent generated the largest R_a value obtained (5.65 μm) for all of the samples analysed, which indicates that the material surface is very irregular.

With respect to the trehalose, the general trend appears to be that if all other parameters are kept constant, the R_a value increases as the solubility of the material in the solvent system decreases. It also appears that the R_a value increases if the temperature range used to recrystallise the material is increased. The results also indicate that the surface washing

of trehalose with IPA following recrystallisation gives a smoother surface than when the material is washed with the solvent from which the material was recrystallised.

With respect to TOAc, in contrast to the trehalose results the trend appears to be that the R_a value increases as the solubility of the material in the solvent system also increases. Again in contrast to the trehalose, the TOAc that was surface washed with IPA following recrystallisation appears to have a rougher surface as the R_a value has increased. The results also indicate that there is an increase in the R_a value when the TOAc is recrystallised from a higher initial supersaturation ratio.

For the lactose material, the recrystallised sample has an increased surface roughness compared to the raw material, although the increase appears to be relatively small.

The figures on the following pages are examples of the images obtained for each material during analysis with the laser profilometer.

In all cases, a profile was chosen that had generated a roughness value closest to the average value obtained for each material.

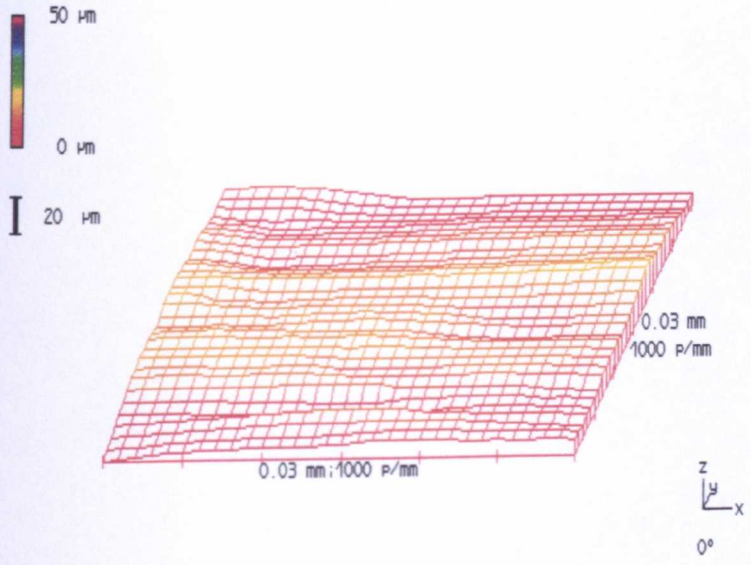

Figure 6.16: Laser profilometry image for lactose 325M raw material

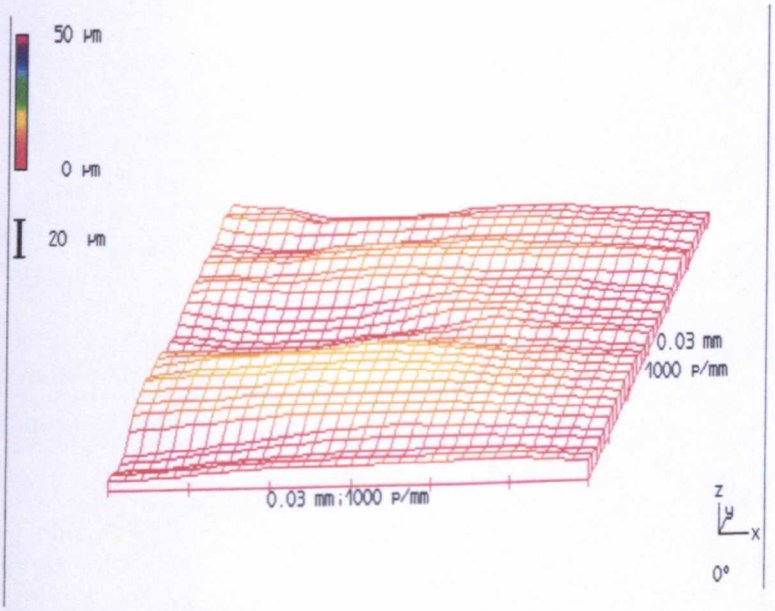

Figure 6.17: Laser profilometry image for recrystallised lactose

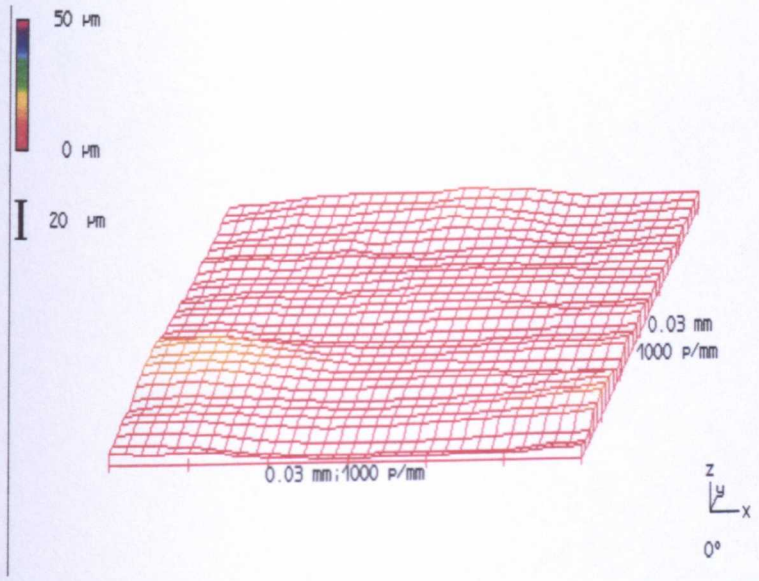

Figure 6.18: Laser profilometry image for trehalose dihydrate raw material

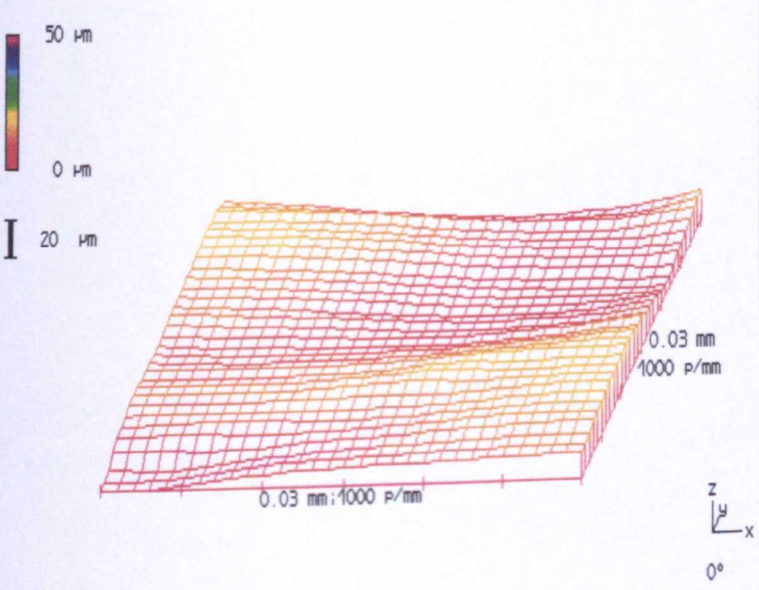

Figure 6.19: Laser profilometry image for trehalose recrystallised from 100% water

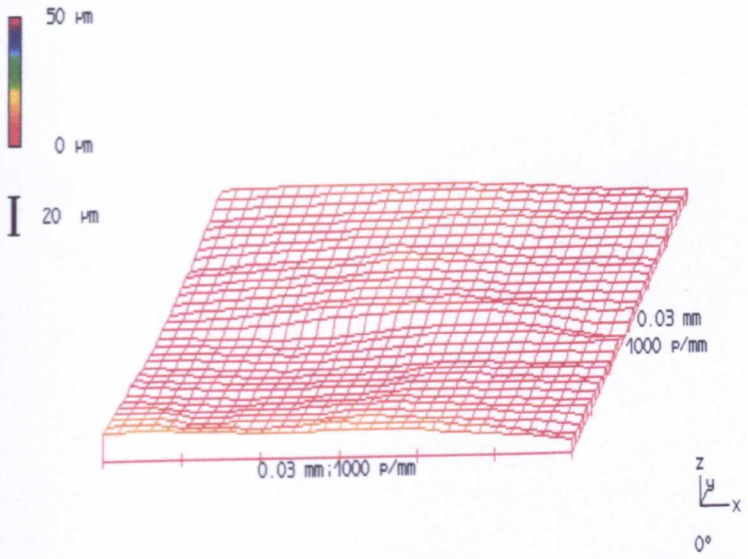

Figure 6.20: Laser profilometry image for trehalose recrystallised from 40:60 ethanol:water (23-7°C), S = 1.5

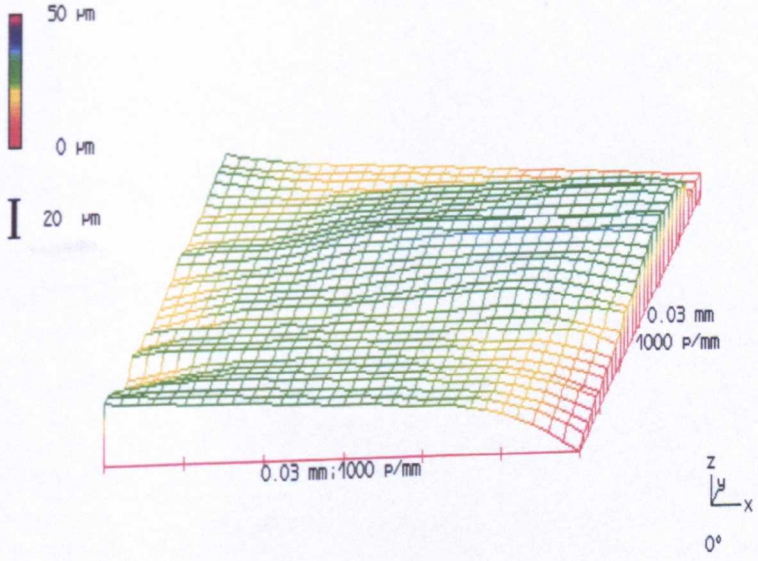

Figure 6.21: Laser profilometry image for trehalose recrystallised from 60:40 ethanol:water (23-7°C), S = 1.5

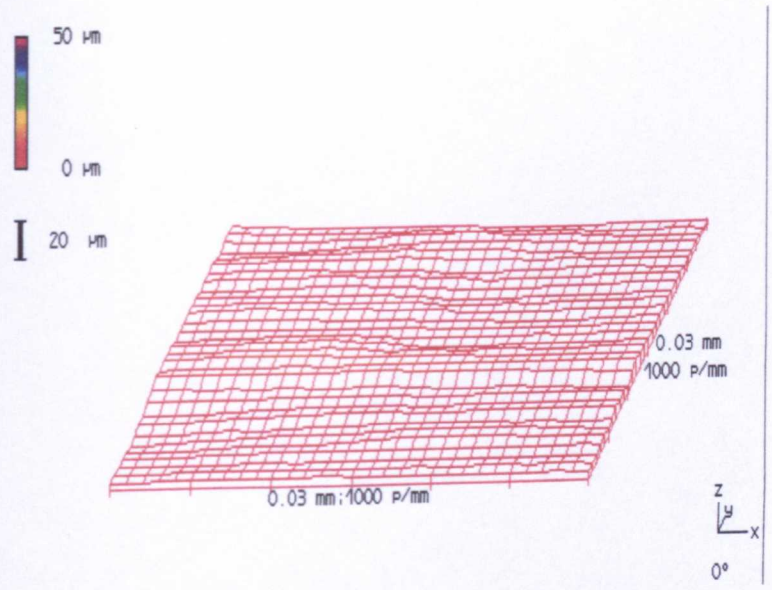

Figure 6.24: Laser profilometry image for TOAc raw material

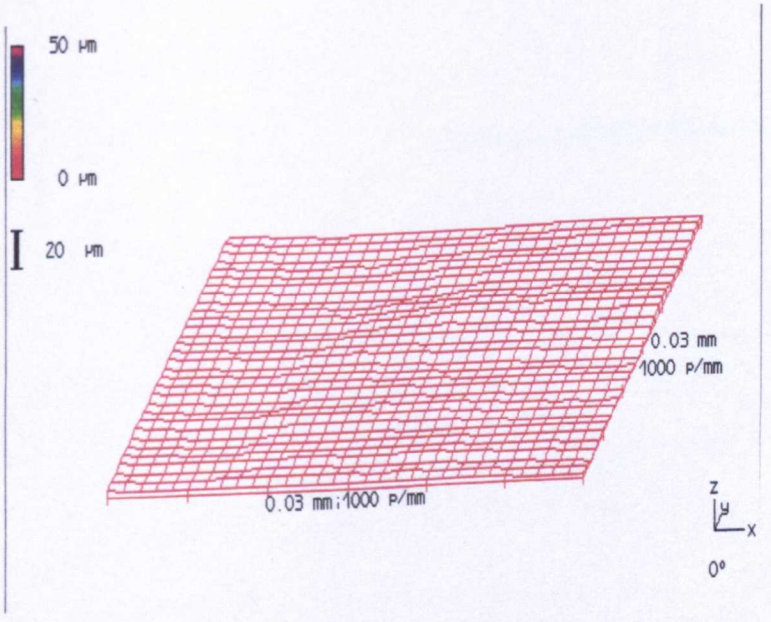

Figure 6.25: Laser profilometry image for TOAc recrystallised from 70:30 ethanol:water (34-18°C), S = 1.2

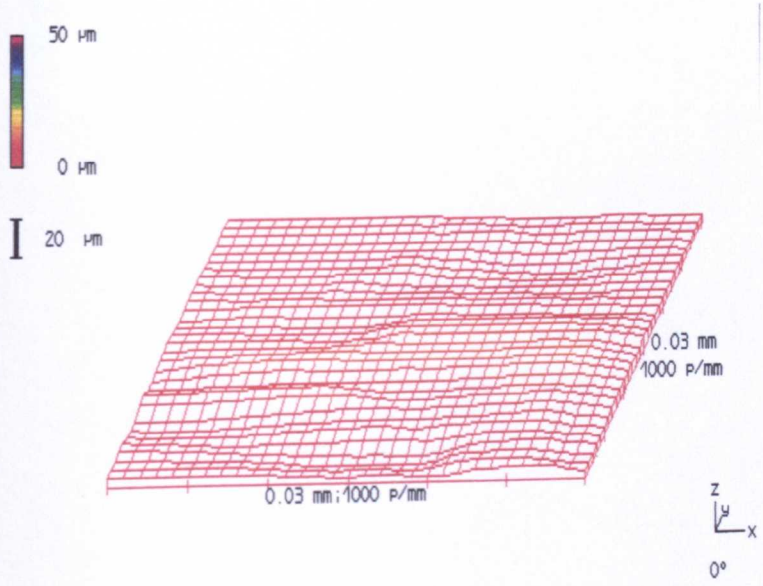

Figure 6.26: Laser profilometry image for TOAc recrystallised from 70:30 ethanol:water (34-18°C), S = 1.5

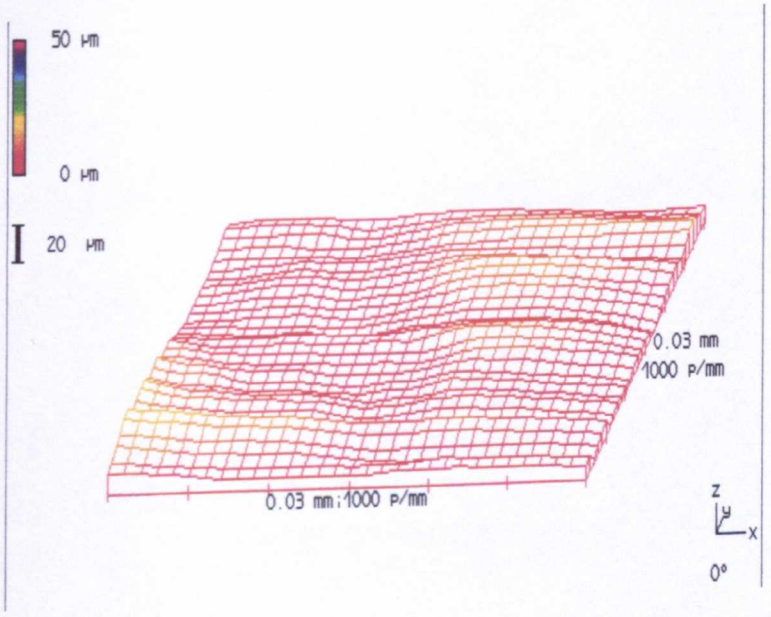

Figure 6.27: Laser profilometry image for TOAc recrystallised from 75:25 ethanol:water (34-18°C), S = 1.2

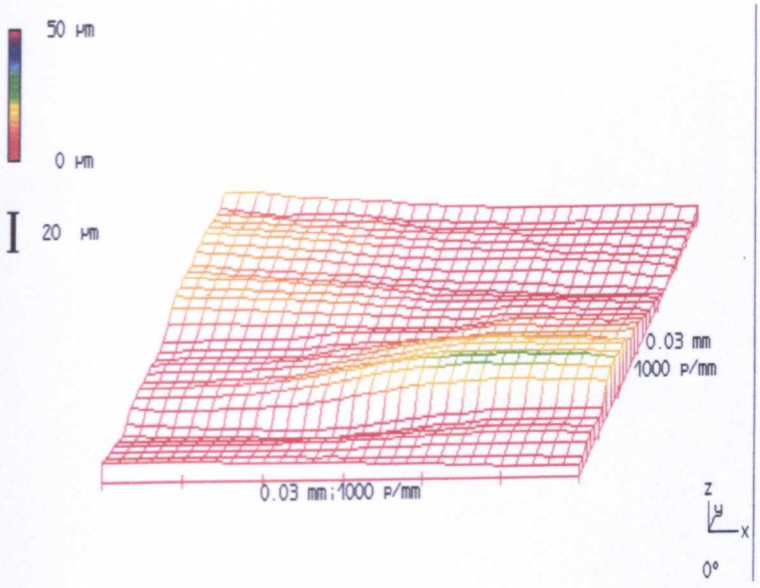

Figure 6.28: Laser profilometry image for TOAc recrystallised from 85:15 ethanol:water (34-18°C), S = 1.2

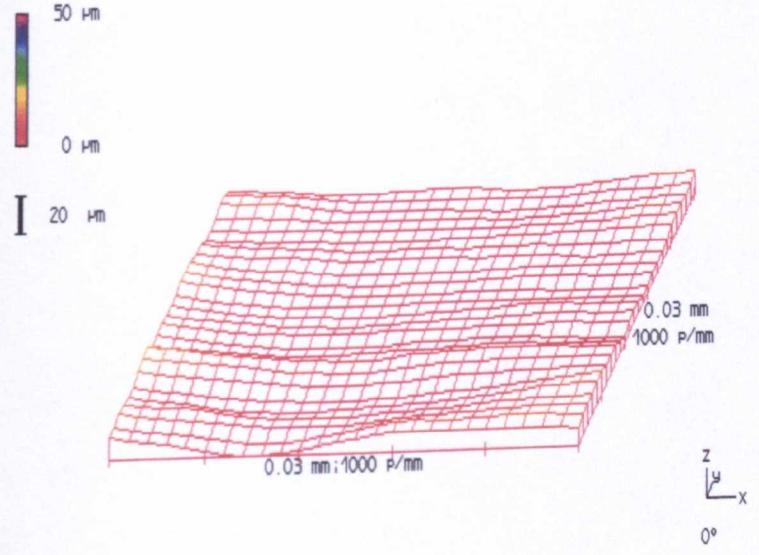

Figure 6.29: Laser profilometry image for TOAc surface washed with IPA following recrystallisation from 70:30 ethanol:water, S = 1.5

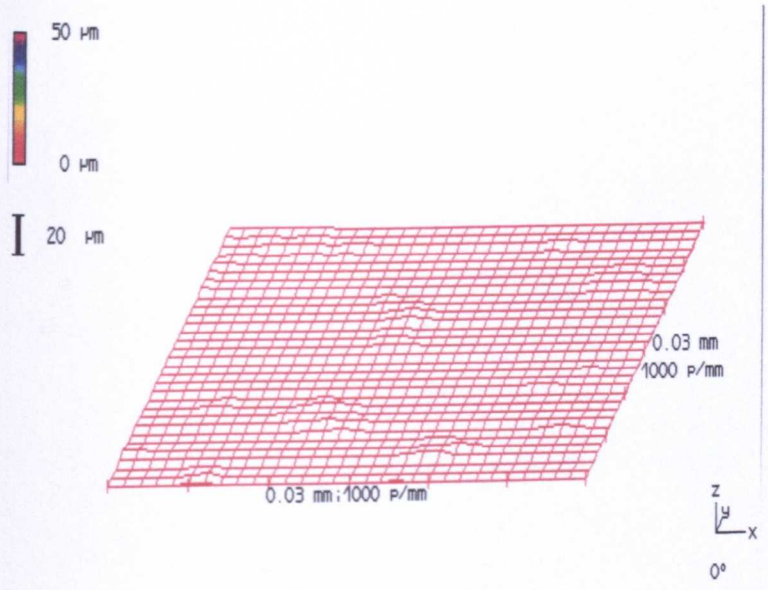

Figure 6.30: Laser profilometry image for spray-dried lactose

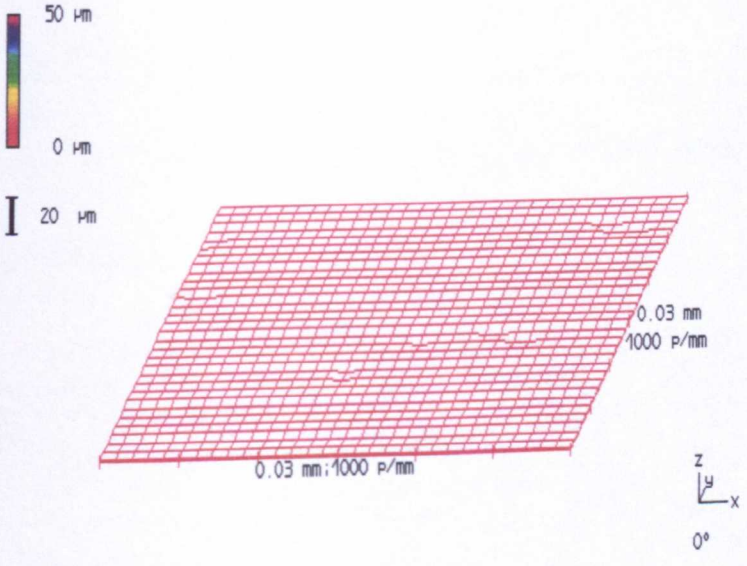

Figure 6.31: Laser profilometry image for spray-dried trehalose

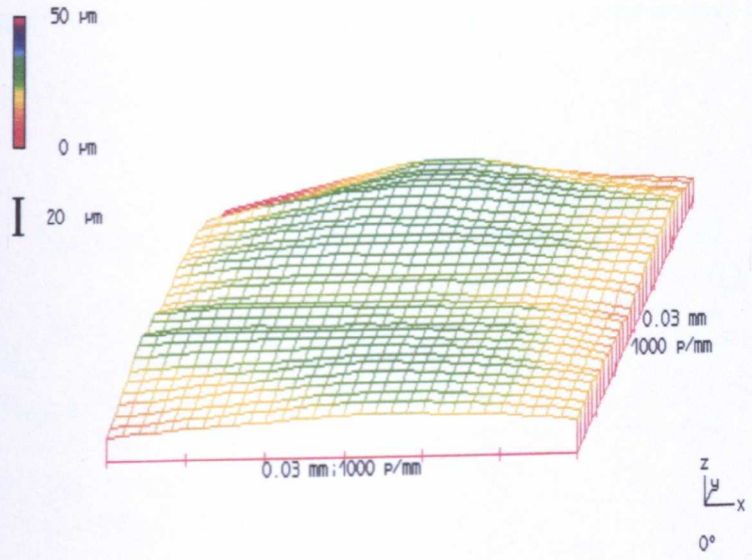

Figure 6.32: Laser profilometry image for spray-dried TOAc

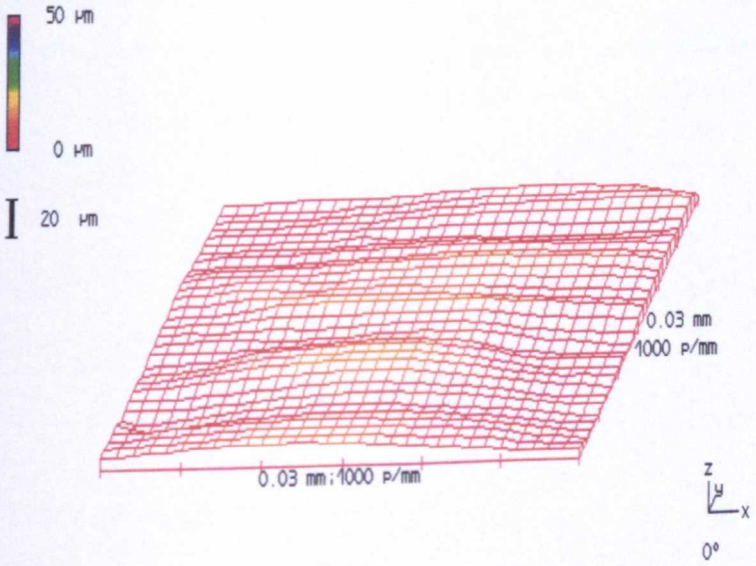

Figure 6.33: Laser profilometry image for powdered amorphous TOAc

The following table presents the data obtained using laser profilometry for determination of the parameter R_q.

Material ID	R_q (μm)	SD (n=20)	%CV
LACTOSE			
Raw material – 325M	**3.48**	1.27	36.52
Recrystallised material:			
100% Water S=1.5 63-90 μm Batch L1 (34-18°C)	**3.51**	1.39	39.55
TREHALOSE			
Raw material 63-90 μm	**2.39**	0.98	41.08
Recrystallised material:			
100% Water S=1.5 63-90 μm Batch 2 (34-18°C)	**3.94**	1.92	48.79
40:60 Ethanol:Water S=1.5 63-90 μm Batch 3 (23-7°C)	**3.13**	2.53	80.59
60:40 Ethanol:Water S=1.5 63-90 μm Batch 8 (34-18°C)	**7.40**	2.76	37.33
60:40 Ethanol:Water S=1.5 63-90 μm Batch 6 (23-7°C)	**5.70**	2.66	46.61
Surfaced washed material:			
Surface washed with IPA 100% Water S=1.5 63-90 μm (34-18°C)	**2.71**	0.76	27.97

Table continued on next page

Table continued from previous page

Material ID	R_q (μm)	SD (n=20)	%CV
TOAC			
Raw material 63-90 μm †	**1.82**	1.02	56.28
Recrystallised material:			
70:30 Ethanol:Water S=1.2 63-90 μm (34-18°C)	**0.93**	0.92	98.96
70:30 Ethanol:Water S=1.5 63-90 μm (34-18°C)	**1.56**	1.82	116.05
75:25 Ethanol:Water S=1.2 63-90 μm (34-18°C)	**3.45**	0.76	22.04
85:15 Ethanol:Water S=1.2 63-90 μm (34-18°C)	**5.21**	1.96	37.57
Surface washed material:			
Surface washed with IPA 70:30 Ethanol:Water S=1.5 63-90 μm (34-18°C)	**2.43**	1.09	44.92
AMORPHOUS MATERIALS			
Spray dried material:			
Lactose 63-90 μm	**0.80**	1.00	124.24
Trehalose 63-90 μm	**0.65**	0.16	24.90
TOAc 63-90 μm	**1.06**	1.57	147.64
Quenched from the melt:			
Powdered amorphous material: TOAc 63-90 μm	**2.90**	0.57	19.84

† Sieve fraction size. Considering the morphology of the raw material, there is a high probability that particles of a larger longitudinal length than 90 μm may be present in the batch of material sieved.

Figure 6.34: Table of results (R_q) from laser profilometry analysis.

The R_q values obtained again indicate that for the majority, the recrystallised materials have rougher surfaces compared to the raw materials. The exceptions for this parameter are again the spray dried materials along with both batches of TOAc recrystallised from

70:30 ethanol:water. Again, the %CV for the spray dried samples were the highest of those tested.

The maximum standard deviation obtained for this parameter was 2.76%, which was for a batch of trehalose recrystallised from 60:40 ethanol:water. This same batch of material generated the largest R_q value obtained (7.40 μm) from the samples analysed. According to the R_q values, the smoothest surface again appears to be spray-dried trehalose.

With respect to trehalose, the trend again appears to be that the R_q value increases as the solubility of the material in the solvent system decreases or when the temperature range used to recrystallise the material is increased. The results also show that surface washing of trehalose with IPA following recrystallisation produces a smoother surface in comparison to when the material is washed with the recrystallisation solvent.

For lactose, the recrystallised sample again appeared to have a relatively small increase in surface roughness compared to the raw material.

With respect to TOAc, the trend appears to be that the R_q value increases as the solubility of the material in the solvent system also increases. This trend is opposite to that observed for trehalose, but is the same as observed for TOAc with the R_a parameter. The sample washed with IPA also follows the trend observed with TOAc for the R_a parameter and results in an increase in the observed R_q value.

Again, the results also indicate that there is an increase in the R_q value when TOAc is recrystallised from a higher initial supersaturation ratio.

For the amorphous samples, the R_q value of the powdered TOAc again produced the highest value for the surface roughness parameter examined. Within the spray-dried materials, the order of surface roughness was quantified as being the same as for the R_a parameter with trehalose being the smoothest and TOAc the roughest.

Figure 6.35 presents the data obtained for each material using laser profilometry for the measurement of parameter R_{tm}.

Material ID	R_{tm} (μm)	SD (n=20)	%CV
LACTOSE			
Raw material – 325M	**6.36**	1.97	30.93
Recrystallised material:			
100% Water S=1.5 63-90 μm Batch L1 (34-18 °C)	**6.19**	2.57	41.52
TREHALOSE			
Raw material 63-90 μm	**4.55**	1.63	35.88
Recrystallised material:			
100% Water S=1.5 63-90 μm Batch 2 (34-18 °C)	**7.13**	3.43	48.12
40:60 Ethanol:Water S=1.5 63-90 μm Batch 3 (23-7 °C)	**5.52**	4.41	79.95
60:40 Ethanol:Water S=1.5 63-90 μm Batch 8 (34-18 °C)	**12.25**	4.84	39.53
60:40 Ethanol:Water S=1.5 63-90 μm Batch 6 (23-7 °C)	**9.68**	4.47	46.11
Surfaced washed material:			
Surface washed with IPA 100% Water S=1.5 63-90 μm (34-18 °C)	**5.04**	1.23	24.37

Table continued on next page

Table continued from previous page

Material ID	R_{tm} (μm)	SD (n=20)	%CV
TOAC			
Raw material 63-90 μm †	**3.61**	1.23	34.16
Recrystallised material:			
70:30 Ethanol:Water S=1.2 63-90 μm (34-18 °C)	**1.76**	1.64	93.56
70:30 Ethanol:Water S=1.5 63-90 μm (34-18 °C)	**2.44**	2.46	100.92
75:25 Ethanol:Water S=1.2 63-90 μm (34-18 °C)	**6.72**	1.46	21.71
85:15 Ethanol:Water S=1.2 63-90 μm (34-18 °C)	**8.15**	2.82	34.58
Surface washed material:			
Surface washed with IPA 70:30 Ethanol:Water S=1.5 63-90 μm (34-18 °C)	**4.27**	1.58	37.00
AMORPHOUS MATERIALS			
Spray dried material:			
Lactose 63-90 μm	**1.43**	1.78	124.97
Trehalose 63-90 μm	**1.09**	0.24	21.65
TOAc 63-90 μm	**1.91**	3.00	157.14
Quenched from the melt:			
Powdered amorphous material: TOAc 63-90 μm	**5.28**	1.09	20.66

† Sieve fraction size. Considering the morphology of the raw material, there is a high probability that particles of a larger longitudinal length than 90 μm may be present in the batch of material sieved.

Figure 6.35: Table of results (R_{tm}) from laser profilometry analysis.

The largest value obtained for R_{tm} was 12.25 μm which was generated by one of the trehalose batches recrystallised from 60:40 ethanol:water. This material also produced the highest standard deviation, which helps to indicate the uneven, irregular nature of the surface of this material.

For TOAc, with all of the parameters measured both of the batches recrystallised from 70:30 ethanol:water were the only samples where the recrystallised material had a lower surface roughness compared to the raw material. However, for all three parameters, the surface washing of this material with IPA increased the surface roughness to a value greater than had been observed for the raw material. It is likely that the surface washing of the TOAc with IPA introduced small asperities or cavities onto the surface that resulted in an increase in the surface roughness values obtained. In all cases, the increase in surface roughness was accompanied by an increase in the standard deviation, which indicates an increase in the irregularity of the surface.

Overall, for the parameter R_{tm} the results obtained indicate the same trends as were observed for the parameters R_a and R_q respectively.

In addition, for all of the parameter measured, the tables present the average roughness value obtained from the samples analysed. The highly variable related standard deviation and subsequent %CV determined for each sample serves to highlight the irregular nature of the samples analysed. In summary, the higher the %CV, the greater the degree of sample irregularity observed for the material under study.

A general trend appears to be that by increasing the initial supersaturation ratio and/or the temperature used to recrystallise a material it is possible to increase the surface roughness of the material obtained. In addition, the results indicate that for trehalose, when recrystallising from an ethanol:water solvent system the surface roughness of the material can be increased by using a solvent in which the material is less soluble. For TOAc, the

surface roughness increases if the solubility of the material in the ethanol:water solvent was also increased.

It should be remembered however that many physical characteristics of the materials may be significantly different if they were recrystallised from a different solvent system.

CHAPTER SEVEN

ASSESSMENT OF INHALATION PERFORMANCE

7.1 EXPERIMENTAL METHODS AND EQUIPMENT

7.1.1 PREPARATION OF BLENDS

7.1.1.1 PRE-SCREENING OF SALBUTAMOL SULPHATE

The active drug, salbutamol sulphate, was screened through a 500 μm sieve. This allowed the removal and break up of any large aggregates from the material prior to blending. Sieve sizes much smaller than this caused the material to exhibit signs of triboelectric behaviour, and hence the material would then become extremely difficult to handle.

7.1.1.2 SIEVING OF CARRIER MATERIALS

Sieving of the carrier materials was done in order to obtain the required particle size fraction. The sieves used ranged in size from 710 μm down to 45 μm, based on a $\sqrt{2}$ progression. Therefore, the full range of sieve sizes used was 710, 500, 355, 250, 180, 125, 90, 63 and 45 μm.

The particle size fraction assessed as a carrier was 63-90 μm, as this range was the closest to the particle size range of the control material, Pharmatose 325M (lactose monohydrate).

7.1.1.3 BATCH SIZE

The minimum weight of blend manufacture for each material was 1 g. This weight of blend was adequate for all sampling, testing and characterisation work that was required for individual blends.

7.1.1.4 BLENDING METHOD

Both crystalline and amorphous materials were blended using the following method.

Blends were produced using:

- the required particle size sieve fraction of carrier material
- pre-screened salbutamol sulphate.

200 µg of salbutamol base per 20 mg of blend was the required concentration. In this work salbutamol sulphate was used. This necessitated the following calculation in order to determine the quantity of salbutamol sulphate that was equivalent to 200 µg of salbutamol base.

Molecular mass of the active (g): Salbutamol: 239.3

Salbutamol sulphate: 288.35

Hence, the calculation required was: $\frac{288.35}{239.3} \times 200$

Therefore, 241 µg of salbutamol sulphate was equivalent to 200 µg of salbutamol base.

Into a small sealable glass vial, the pre-screened active material was accurately weighed. A second suitable container was used to weigh out the carrier material.

For example, if 2 g of blend was to be produced 24.1 mg of pre-screened salbutamol sulphate was weighed out. The carrier material was then weighed into a second container to adjust the total weight to 2000 mg (therefore approximately 1975.9 mg of carrier was required). This would provide 200 µg of salbutamol base per 20 mg of blend.

The 'doubling-up' method of blending was then implemented. A small quantity of carrier was added to the vial containing the active drug. The vial was then sealed, and the contents were then mixed for 1 minute using a Turbula® mixer at a setting of 62 r.p.m.

The contents of the vial was then doubled up again with carrier material, sealed and mixed for a further minute. This was repeated and the contents were mixed for 2 minutes. Following further doubling-up, the material was mixed again for 2 minutes, then for 4 minutes. The remainder of the carrier material was then added to the vial and the contents were then blended for 10 minutes. Therefore, the total mixing time for each blend was 20 minutes. The blends produced were then tested for homogeneity.

7.1.1.5 Assessment of Blend Homogeneity

The homogeneity of the blends was assessed by taking samples of the material from the top, middle and bottom. A minimum of 10 samples were taken for each blend. The samples taken were in the range of 10-20 mg, and each sample was diluted to 25 mL with wash solvent (see HPLC reagents). The samples were filtered and subsequently assayed using the HPLC method later described.

In order to pass the homogeneity test, all results had to be within 10% of the theoretical expected salbutamol base value.

If any samples failed, further mixing was carried out (recommend mixing time 5 minutes). Homogeneity testing was then repeated. This process was repeated (if required) until the blend passed the specified requirements.

Once the homogeneity of each blend was confirmed, 20 mg ± 5% was filled into size 4 hard gelatine capsules prior to assessment from the DPI.

7.1.2 Materials for Assessment from FlowCaps® DPI

The performance of the following eighteen materials was assessed from the FlowCaps® DPI.

Material ID:
LACTOSE
Raw material – 325M
Recrystallised material:
100% Water, S=1.5, 63-90 μm, Batch L1 (34-18 °C)
TREHALOSE
Raw material 63-90 μm
Recrystallised material:
100% Water, S=1.5, 63-90 μm, Batch 2 (34-18 °C)
40:60 Ethanol:Water, S=1.5, 63-90 μm, Batch 3 (23-7 °C)
60:40 Ethanol:Water, S=1.5, 63-90 μm, Batch 8 (34-18 °C)
60:40 Ethanol:Water, S=1.5, 63-90 μm, Batch 6 (23-7 °C)
Surfaced washed material:
Surface washed with IPA, originally recrystallised from 100% Water, S=1.5, 63-90 μm (34-18 °C)
TOAC
Raw material 63-90 μm †
Recrystallised material:
70:30 Ethanol:Water, S=1.2, 63-90 μm (34-18 °C)
70:30 Ethanol:Water, S=1.5, 63-90 μm (34-18 °C)
75:25 Ethanol:Water, S=1.2, 63-90 μm (34-18 °C)
85:15 Ethanol:Water, S=1.2, 63-90 μm (34-18 °C)
Surface washed material:
Surface washed with IPA, originally recrystallised from 70:30 Ethanol:Water, S=1.5, 63-90 μm (34-18 °C)
AMORPHOUS MATERIALS
Spray dried material:
Spray-dried Lactose 63-90 μm
Spray-dried Trehalose 63-90 μm
Spray-dried TOAc 63-90 μm
Quenched from the melt:
Powdered amorphous TOAc 63-90 μm

Figure 7.1: Table of materials for assessment from the DPI.

7.1.3 FLOWCAPS® DPI

A FlowCaps® DPI device (see figure 7.2) was acquired from Hovione (Portugal) and was the DPI system used to assess blend performance. The device was used at a flow rate of 50 L/min as per the manufacturer instructions in order to achieve an internal pressure drop of 4 kPa (as recommended in the 1996 USP proposal). Size 4 hard gelatine capsules were required for the formulation to be administered using the device. 20 mg of blend was used per capsule, with one capsule counting as one dose.

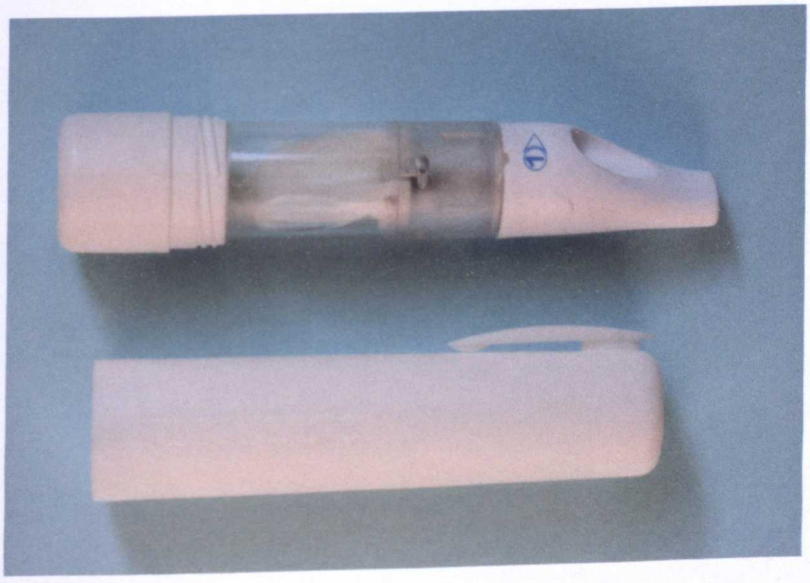

Figure 7.2: Image of the FlowCaps® DPI

7.1.3.1 INFORMATION ON FLOWCAPS®

With the FlowCaps® DPI, once the patient inhales, an area of low pressure is created inside the pierced hard gelatine capsule. Instead of moving with the airflow, the powder moves to the air admission end of the capsule, where the area of low pressure has been created. The powder is then gradually entrained towards the air exit end, carried by the

airflow out of the capsule into the mouthpiece and then out of the device. The movement of the powder inside the capsule is very turbulent.

Due to the design of the device, the capsule is visible inside the inhaler even when in the inhalation position. As the gelatine capsules used were clear, this feature was used to give assurance that the entire dose has been administered. In practice, the ability for a patient to see inside the capsules would be of particular importance with certain types of active materials, such as anti-inflammatory drugs, where an immediate effect is not induced.

7.1.4 Multi-Stage Liquid Impinger (MSLI)

A cascade impactor (also known as a MSLI) is a sampling device used to determine particle size distribution. Particles are separated and deposited on a series of stages that correspond to different aerodynamic diameters. A 5 stage MSLI was used to assess the performance of the powder blends from the FlowCaps® dry powder inhaler. An image of a MSLI is presented in figure 7.3.

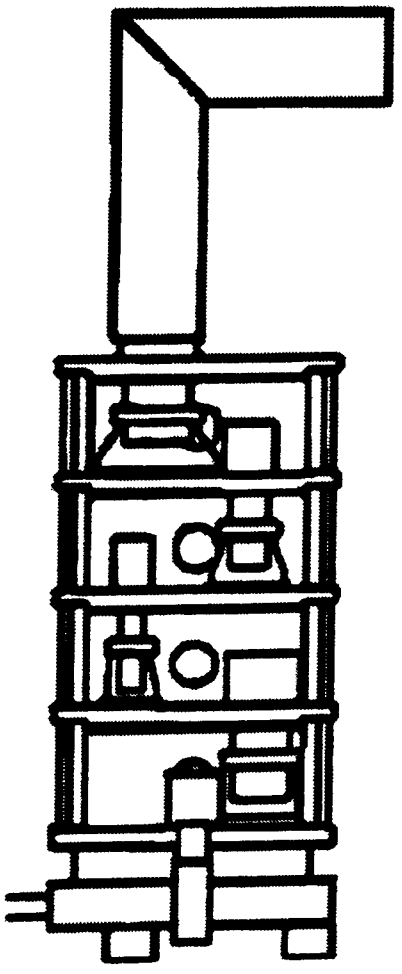

Figure 7.3: Diagram of a multi-stage liquid impinger.

7.1.4.1 Cut-Off Details for MSLI ($D_{50\%}$)

Values correct for 60 L/min (or 1 L/sec):

Stage 1	13 μm
Stage 2	6.8 μm
Stage 3	3.1 μm
Stage 4	1.7 μm

For calculation of cut-off values at other flow rates between 30 to 100 L/min:

Figure at 60 L/min (represented by x) multiplied by the inverse of the square root of the new flow rate in L/min (represented by y) divided by 60

i.e. $$x \times \frac{1}{\left(\sqrt{\frac{y}{60}}\right)}$$

$D_{50\%}$ cut-off values for flow rates of 50 L/min (as required for FlowCaps®)

Stage 1	14.24 μm
Stage 2	7.45 μm
Stage 3	3.40 μm
Stage 4	1.86 μm

N.B. For the MSLI used, the distances of the scintered glass disks from the end of the stainless steel jets were as follows:

Stage 1	9.50 mm
Stage 2	5.50 mm
Stage 3	4.00 mm
Stage 4	6.00 mm

The manufacturer of the MSLI defined these as the distances required to ensure the cut-off values calculated are correct. Stainless steel calibration blocks were manufactured and were used to ensure that these distances remained correct.

A resistance box was used to calibrate the flow rate of air through the inhaler. For FlowCaps® this should be 50 L/min, as previously specified.

A PTFE mouthpiece adapter connected the FlowCaps® inhaler to the throat of the MSLI. The adapter created an airtight seal, ensuring that the flow rate set with the resistance box was identical to that going through the device.

7.1.5 High Performance Liquid Chromatography (HPLC)

Details of the operating conditions used for analysis of the MSLI samples are given below. The conditions used were adopted from a method developed at Quadrant Healthcare. MSLI samples were filtered directly into HPLC vials prior to analysis using a sealed single use Millipore 0.25 μm filter unit.

Wash solvent:	Dilute phosphate buffer pH 4.5
Column:	Waters Nova-Pak Phenyl 150 mm x 3.9 mm
Mobile phase:	20% methanol in phosphate buffer, pH 7.4
Flow rate:	1.0 mL/min
Injection volume:	100 μL
Column temperature:	Ambient
Detection wavelength:	UV at 227 nm
Run time:	Approximately 5 minutes

The wash-out volume used for each stage was to 50 mL.

Five shots were used per MSLI run, with five MSLI runs carried out for each blend under study. Inhalations were timed to four seconds and a maximum of three inhalations were

carried out for each of the five shots per run. The additional inhalations were only used if any remaining blend was visible inside the capsule following the first four-second inhalation into the MSLI.

Salbutamol base standard solutions were prepared daily as required for each HPLC run in order to calibrate the equipment. A standard concentration of 2.0 μg/mL was produced. In addition to the standard solutions required for calibration of the HPLC, the following reagents were used.

7.1.5.1 STOCK PHOSPHATE BUFFER, PH 4.5

For each litre of solution:

Dissolve 68.05 g of potassium dihydrogen orthophosphate (HPLC Grade) in approximately 800 mL distilled water. Sonicate until dissolved and then make up to volume with distilled water. Mix well.

Shelf life of solution: 1 month

7.1.5.2 DILUTE PHOSPHATE BUFFER, PH 4.5

(Wash solvent). For each litre of solution:

Dilute 100 mL stock phosphate buffer, pH 4.5 to 1000 mL with distilled water. Check the pH of the solution. It should be between 4.00 and 4.50 without adjustment being necessary.

7.1.5.3 MOBILE PHASE; 20% METHANOL IN PHOSPHATE BUFFER, PH 7.4

For each litre of mobile phase:

Dissolve 2.13 g of disodium hydrogen orthophosphate anhydrous (AR Grade) and 2.04 g of potassium dihydrogen orthophosphate in 700 mL of distilled water. Add 200 mL of methanol and dilute to 1000 mL with distilled water. Mix well, then filter through a Whatman GF/F filter or similar and degas prior to use.

7.2 MSLI RESULTS

The performance of the materials as drug carriers from within a DPI was assessed by the % fine particle fraction (FPF) achieved by each material. The fine particle fraction was calculated from the total quantity of drug collected from stages 3, 4 and 5 (filter) of the MSLI. This was then expressed as a percentage of the total quantity of drug recovered to give the %FPF.

The following table gives details of the average % fine particle fraction obtained for each material. The average emitted weight of drug blend is also included in the table.

Material ID	Average %FPF (n=5)	SD	%CV	Average emitted weight (n=25)
LACTOSE				
Raw material – 325M	**23.58**	3.00	12.73	18.78mg
Recrystallised material:				
100% Water S=1.5 63-90 μm Batch L1 (34-18 °C)	**22.86**	2.02	8.82	18.53mg
TREHALOSE				
Raw material 63-90 μm	**14.93**	0.46	3.07	19.63mg
Recrystallised material:				
100% Water S=1.5 63-90 μm Batch 2 (34-18 °C)	**20.44**	1.26	6.16	19.88mg
40:60 Ethanol:Water S=1.5 63-90 μm Batch 3 (23-7 °C)	**21.23**	1.24	5.85	19.83mg
60:40 Ethanol:Water S=1.5 63-90 μm Batch 8 (34-18 °C)	**17.53**	0.76	4.35	19.36mg
60:40 Ethanol:Water S=1.5 63-90 μm Batch 6 (23-7 °C)	**18.41**	1.04	5.64	19.74mg
Surfaced washed material:				
Surface washed with IPA 100% Water S=1.5 63-90 μm (34-18 °C)	**22.16**	1.11	5.03	19.05mg

Table continued on next page

Table continued from previous page

Material ID	Average %FPF (n=5)	SD	%CV	Average emitted weight (n=25)
TOAc				
Raw material 63-90 μm †	**6.57**	0.89	13.57	12.58mg
Recrystallised material:				
70:30 Ethanol:Water S=1.2 63-90 μm (34-18 °C)	**18.51**	0.98	5.32	17.12mg
70:30 Ethanol:Water S=1.5 63-90 μm (34-18 °C)	**21.50**	1.14	5.30	18.74mg
75:25 Ethanol:Water S=1.2 63-90 μm (34-18 °C)	**19.67**	1.74	8.86	16.81mg
85:15 Ethanol:Water S=1.2 63-90 μm (34-18 °C)	**14.53**	1.95	13.45	16.07mg
Surface washed material:				
Surface washed with IPA 70:30 Ethanol:Water S=1.5 63-90 μm (34-18 °C)	**22.65**	1.13	5.01	19.16mg
AMORPHOUS MATERIALS				
Spray dried material:				
Lactose 63-90 μm	**3.74**	0.80	21.42	12.76mg
Trehalose 63-90 μm	**5.15**	0.77	15.00	19.69mg
TOAc 63-90 μm	**13.52**	1.81	13.40	19.75mg
Quenched from the melt:				
Powdered amorphous material: TOAc 63-90 μm	**15.59**	0.60	3.85	18.33mg

† Sieve fraction size. Considering the morphology of the raw material, there is a high probability that particles of a larger longitudinal length than 90 μm may be present in the batch of material sieved.

Figure 7.4: Summary table of the average %FPF obtained for each material.

7.3 DISCUSSION OF MSLI RESULTS

The recrystallised lactose delivered a slightly lower %FPF compared to the raw material, although the standard deviation (SD) and %CV for the recrystallised material were both lower indicating that the recrystallised lactose gave more reproducible results.

In contrast to the lactose, the recrystallised trehalose materials delivered higher %FPF values compared to the raw material, although the raw material exhibited better reproducibility as it generated lower SD and %CV values. The carrier treated with a surface wash of IPA generated the highest %FPF of the trehalose materials, delivering 48.4% more drug compared to the raw material. The material recrystallised from 100% water (S = 1.5) and not washed with IPA delivered 36.9% more drug than the raw material. The SD and %CV for the IPA washed material were lower than for the recrystallised material, indicating a better reproducibility for the IPA washed material. This indicates that for trehalose, a surface wash of the recrystallised material with IPA has a positive effect on the performance of the material as a drug carrier. With respect to the recrystallised trehalose materials as a whole, changing the solvent used and keeping all other variables constant indicates that the solvent in which the material is more soluble produces a material with a better performance as a drug carrier (trehalose recrystallised from 100% water compared to material recrystallised from 60:40 ethanol:water). However, lower SD and %CV values were obtained for the materials exhibiting the reduced %FPF, which indicates that these materials gave better reproducibility. This trend was also observed when comparing the results obtained for trehalose recrystallised from 40:60 ethanol:water with material recrystallised from 60:40 ethanol:water.

The trehalose material recrystallised from 60:40 ethanol:water over a lower temperature range (23-7 °C) indicates that the lower temperature produces a material that delivers a slightly improved %FPF although with less reproducibility on the results as a higher standard deviation was also observed. The material recrystallised from 40:60 ethanol:water was also produced using this lower temperature range, and the %FPF obtained for this material was higher than for the material recrystallised from 100% water. This result indicates that the temperature range used for the recrystallisation of trehalose has a greater influence on the carrier performance than does the solubility of the material in the solvent. It should be noted that this observation applies to the ethanol:water solvents observed, and it should be remembered that different trends may be observed with different solvent systems.

For the TOAc raw material, the %FPF obtained (6.57%) was much lower than with the other raw materials. This poor result is probably due to the acicular nature of the raw material. Recrystallisation of the material from 70:30 ethanol:water resulted in a material with an orthorhombic morphology that exhibited a significantly increased FPF (21.50%). This increased FPF means that the recrystallised material delivered 227.2% more active drug to the lower stages of the MSLI in relation to the results obtained with the TOAc raw material. The recrystallised TOAc treated with a surface wash of IPA generated a further improved FPF (22.65%). This represents a 244.7% increase in drug delivered to the respirable fraction of the MSLI compared to the raw material.

These data indicate clearly that the morphology of a material can have a significant effect on the performance of the material as a drug carrier within a dry powder inhaler. They also suggest that the processing of a material after recrystallisation can also impact on the

performance as a drug carrier, even if the overall morphology of the material remains the same.

The effect of a decrease in the initial supersaturation ratio for TOAc material recrystallised from 70:30 ethanol:water was a 3% reduction in the FPF to 18.51%. The performance of this material was still significantly better than the raw material and the SD and %CV indicate that the material performance demonstrated approximately equivalent reproducibility compared to the material recrystallised from an initial supersaturation ratio of 1.5. This result indicates that increasing the initial supersaturation ratio for TOAc has the potential to improve the performance of the material with respect to the delivery of active drug to the respirable fraction of the lungs.

With respect to the effect of changing the solvent used to recrystallise the TOAc, the results do not indicate a trend consistent with the solubility of the material in each solvent. With all other variables kept constant, the performance of the materials ranks from 75:25 ethanol:water as the highest, followed by the material recrystallised from 70:30 ethanol:water and then the material from 85:15 ethanol:water. The reproducibility of the material recrystallised from 70:30 ethanol:water was the best of the three, as was the average emitted weight. It is possible that the slight increase in the %FPF observed for the material recrystallised from 72:25 ethanol:water compared to the material recrystallised from 70:30 ethanol:water is due to the mix of morphologies contained in this material. Although mainly orthorhombic, it is possible that the small proportion of acicular crystals contained in the blend slightly enhanced the delivery performance of the material. Blends produced with small quantities of fines have been shown to increase the drug delivery performance of lactose. Lucas *et al* (1998) reported on the effects of fine particle

excipients as potential formulation performance modifiers in dry powder inhalers. They found that by the addition of low levels (typically 5% $^{w}/_{w}$) of fine particle lactose it was possible to alter the bulk properties of powders for inhalation. They concluded that mechanistically, the enhancement of performance resulted from a redistribution of drug particles from coarse carrier particles to the fine particle component in the ternary mix. In the case of TOAc, it is possible that the presence of the acicular crystals in the blend has a similar effect to the addition of fines. It could be that the acicular TOAc, having a different morphology and surface characteristics compared to the orthorhombic crystals have a positive effect on the ability of the salbutamol to deaggregate following inhalation. However, the results indicate that if the proportion of acicular crystals in the blend is too large (as with the material recrystallised from 85:15 ethanol:water) the performance is reduced, although not to the level observed with the wholly acicular raw material blend. The effect of ternary mixes (particularly where carrier particles are of different morphologies) on the performance of blends from a dry powder inhaler is certainly an area for possible future work, but is beyond the scope of this research.

In general terms, for trehalose, the more soluble the material in the solvent the better the %FPF achieved. For TOAc, this trend was reversed and the solvent with the lowest solubility profile produced the material that demonstrated the best relative performance. In the case of both trehalose and TOAc, recrystallisation of the raw material resulted in drug carrier materials that demonstrated improved performance over the raw material for all of the blends assessed. The results obtained indicate that higher supersaturation ratios, lower recrystallisation temperatures and surface washing of recrystallised material can all have positive effects on the performance of the materials as drug carriers in the dry powder inhalation system tested.

For the amorphous materials, the two TOAc blends generated significantly improved performance compared to both the trehalose and lactose blends assessed. The performance of the spray-dried lactose and trehalose materials as drug carriers was in fact surprisingly poor. This could be due in part to the relatively large size of the spray-dried particles used in this research compared to a more conventional size (approximately 5 μm) of spray-dried particles used in dry powder inhaler formulations. As amorphous materials are often more hygroscopic than crystalline materials, the particle size range of 63-90 μm for the materials used in this research also meant that the blends were more susceptible to collapse, particularly where there was significant water uptake. In comparison with the spray-dried lactose and trehalose, the amorphous TOAc materials performed well. Due to the more hydrophobic nature of TOAc, these materials would be less susceptible to water uptake, and therefore with respect to the spray-dried material, less prone to collapse. The powdered amorphous TOAc generated a slightly improved performance over the spray-dried material. This was indicative of an improved stability for the powdered material as a drug carrier compared to the spray-dried material, as the powdered material would be less susceptible to physical changes induced by environmental conditions.

CHAPTER EIGHT

DISCUSSION, CONCLUSIONS AND SUGGESTIONS FOR FUTURE WORK

8.1 GENERAL DISCUSSION

Physical characterisation of powders can often indicate that materials are identical, but the behaviour/performance of such materials can be very different. For example, it has been well established that different blends will often behave differently with respect to performance when they are tested in different dry powder inhalers. This is due to products having a greater sensitivity to material variations than analytical techniques can detect. For example, X-ray diffraction can only detect around 10% or greater of amorphous material in powders. The processing of powders and the stresses thereby induced may result in a material with a higher amorphous content than before processing of the material was carried out. Invariably, this disruption will not be uniform throughout the powder mass but rather it will be predominantly at the surface. Differences in the surface disorder of a material have been observed to have a dramatic influence on the performance of a material.

Phenomena such as batch to batch variation were associated with differences in the surface of materials by Grimsey *et al* (2002). Here, the authors observed that where a powder surface was composed of different proportions of particular crystalline faces with subsequently different molecular arrangements, differences were observed in the surface energetic parameters. With respect to blends produced for use in dry powder inhalers, a conundrum lies in the adhesion of the drug to the carrier particle. The drug particle must be adhered to the carrier strongly enough to enable a homogenous blend to be produced, but it must also remain stable during the manufacture and storage of the product. When the inhaler is in use, the adhesion of the drug must be weak enough to allow easy detachment from the carrier.

Zimon (1982) concluded that the adhesion of particles to microscopically rough surfaces was less than the adhesion to smooth or macroscopically rough surfaces. More recently, Kawashima *et al* (1998) reported on the effect of surface morphology of carrier lactose on the dry powder inhalation properties of pranlukast hydrate. The morphology of lactose carriers was observed using SEM and image analysis software was used to obtain a value for the material surface roughness. The authors concluded that particles with microscopically increased surface roughness improved the inhalation efficiency, as there was less adhesion of the drug to the carrier surface due to a reduction in the physical contact between the two particles.

In summary, Zimon and Kawashima both concluded that surface roughness could be used as a means of increasing or reducing the adhesive force between a carrier and a drug particle. It therefore follows that by alteration of the surface roughness of a carrier particle it would be possible to optimise the performance of that material as a drug carrier for use in a dry powder inhaler.

8.2 OVERALL RESULTS

Figure 8.1 presents the percent fine particle fractions obtained for each of the materials assessed alongside the three parameters (namely R_a, R_q and R_{tm}) used to measure the surface roughness.

Material ID	Average %FPF	R_a	R_q	R_{tm}
LACTOSE				
Raw material – 325M	**23.58**	**2.70**	**3.48**	**6.36**
Recrystallised material:				
100% Water S=1.5 63-90 μm Batch L1 (34-18 °C)	**22.86**	**2.78**	**3.51**	**6.19**
TREHALOSE				
Raw material 63-90 μm	**14.93**	**1.84**	**2.39**	**4.55**
Recrystallised material:				
100% Water S=1.5 63-90 μm Batch 2 (34-18 °C)	**20.44**	**3.03**	**3.94**	**7.13**
40:60 Ethanol:Water S=1.5 63-90 μm Batch 3 (23-7 °C)	**21.23**	**2.39**	**3.13**	**5.52**
60:40 Ethanol:Water S=1.5 63-90 μm Batch 8 (34-18 °C)	**17.53**	**5.65**	**7.40**	**12.25**
60:40 Ethanol:Water S=1.5 63-90 μm Batch 6 (23-7 °C)	**18.41**	**4.54**	**5.70**	**9.68**
Surfaced washed material:				
Surface washed with IPA 100% Water S=1.5 63-90 μm (34-18 °C)	**22.16**	**2.12**	**2.71**	**5.04**

Table continued on next page

Table continued from previous page

Material ID	Average %FPF	R_a	R_q	R_{tm}
TOAC				
Raw material 63-90 μm †	**6.57**	**1.32**	**1.82**	**3.61**
Recrystallised material:				
70:30 Ethanol:Water S=1.2 63-90 μm (34-18 °C)	**18.51**	**0.72**	**0.93**	**1.76**
70:30 Ethanol:Water S=1.5 63-90 μm (34-18 °C)	**21.50**	**1.13**	**1.56**	**2.44**
75:25 Ethanol:Water S=1.2 63-90 μm (34-18 °C)	**19.67**	**2.67**	**3.45**	**6.72**
85:15 Ethanol:Water S=1.2 63-90 μm (34-18 °C)	**14.53**	**4.16**	**5.21**	**8.15**
Surface washed material:				
Surface washed with IPA 70:30 Ethanol:Water S=1.5 63-90 μm (34-18 °C)	**22.65**	**1.91**	**2.43**	**4.27**
AMORPHOUS MATERIALS				
Spray dried material:				
Lactose 63-90 μm	**3.74**	**0.64**	**0.80**	**1.43**
Trehalose 63-90 μm	**5.15**	**0.52**	**0.65**	**1.09**
TOAc 63-90 μm	**13.52**	**0.78**	**1.06**	**1.91**
Quenched from the melt:				
Powdered amorphous material: TOAc 63-90 μm	**15.59**	**2.32**	**2.90**	**5.28**

† Sieve fraction size. Considering the morphology of the raw material, there is a high probability that particles of a larger longitudinal length than 90 μm may be present in the batch of material sieved.

Figure 8.1: Overall table of results for %FPF and surface roughness.

Graphical representation of the surface roughness measurements versus the average %FPF obtained for each material are presented in the following pages.

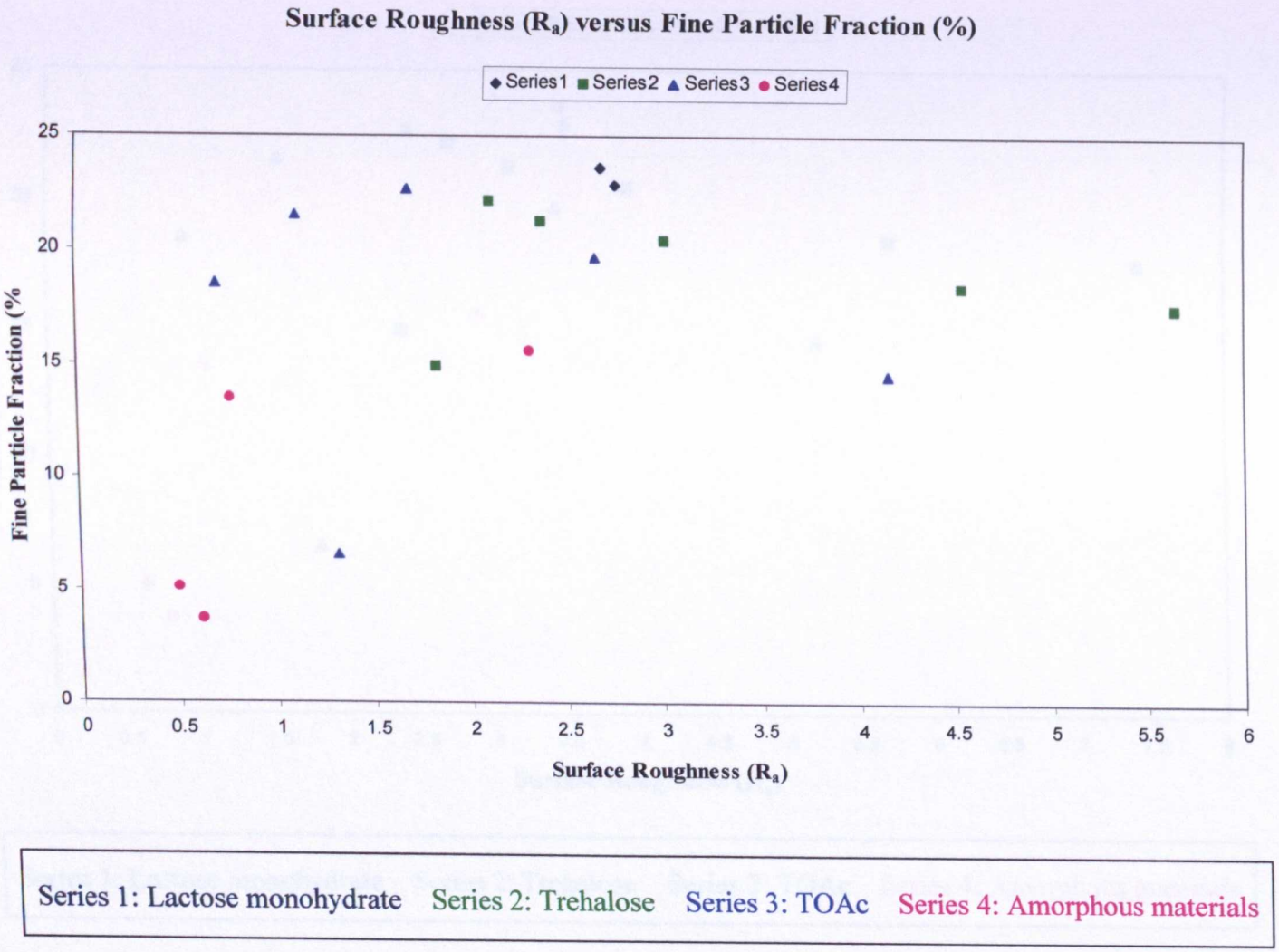

Figure 8.2 A summary graph of fine particle fraction (%) versus R_a for all of the materials assessed.

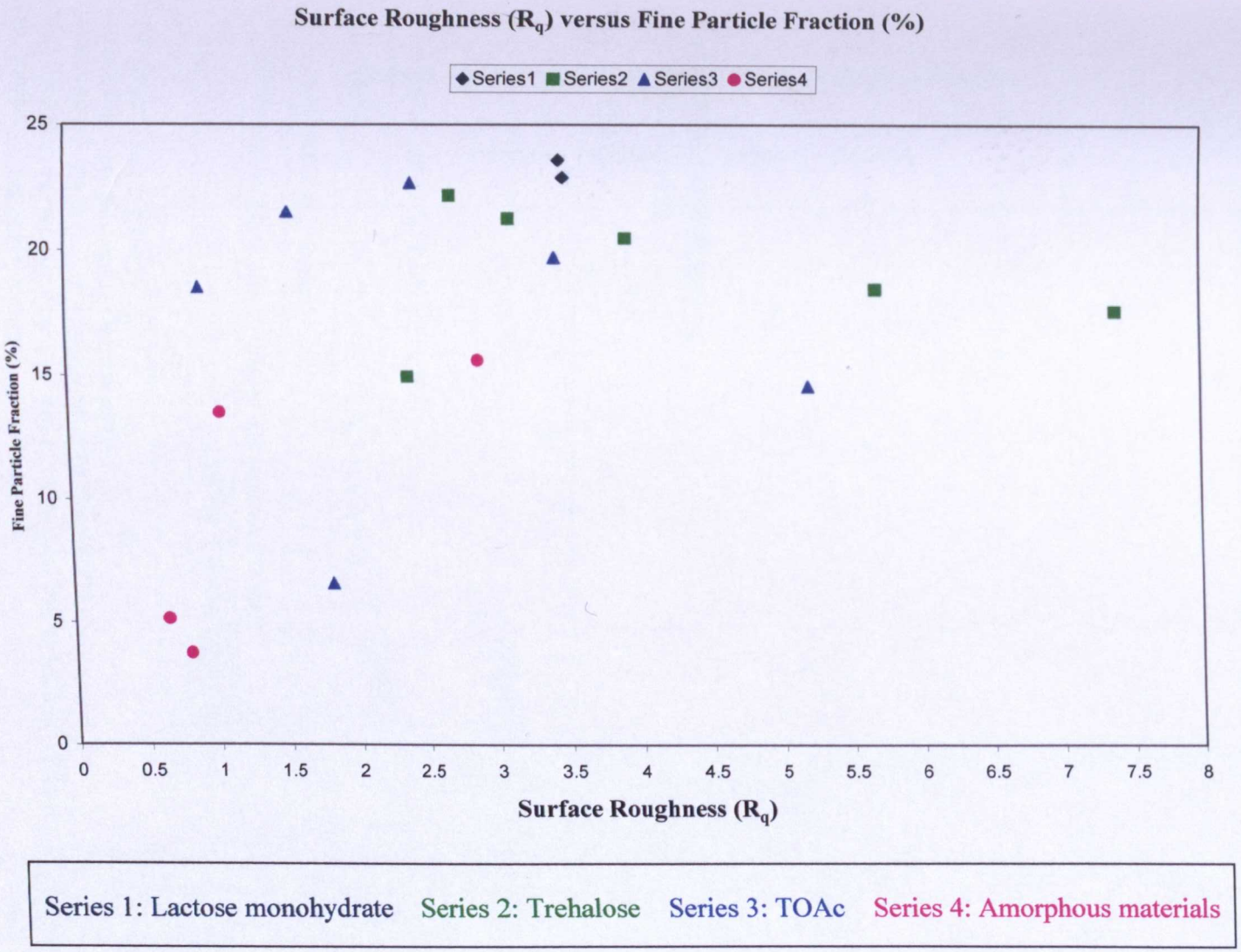

Figure 8.3: A summary graph of fine particle fraction (%) versus R_q for all of the materials assessed.

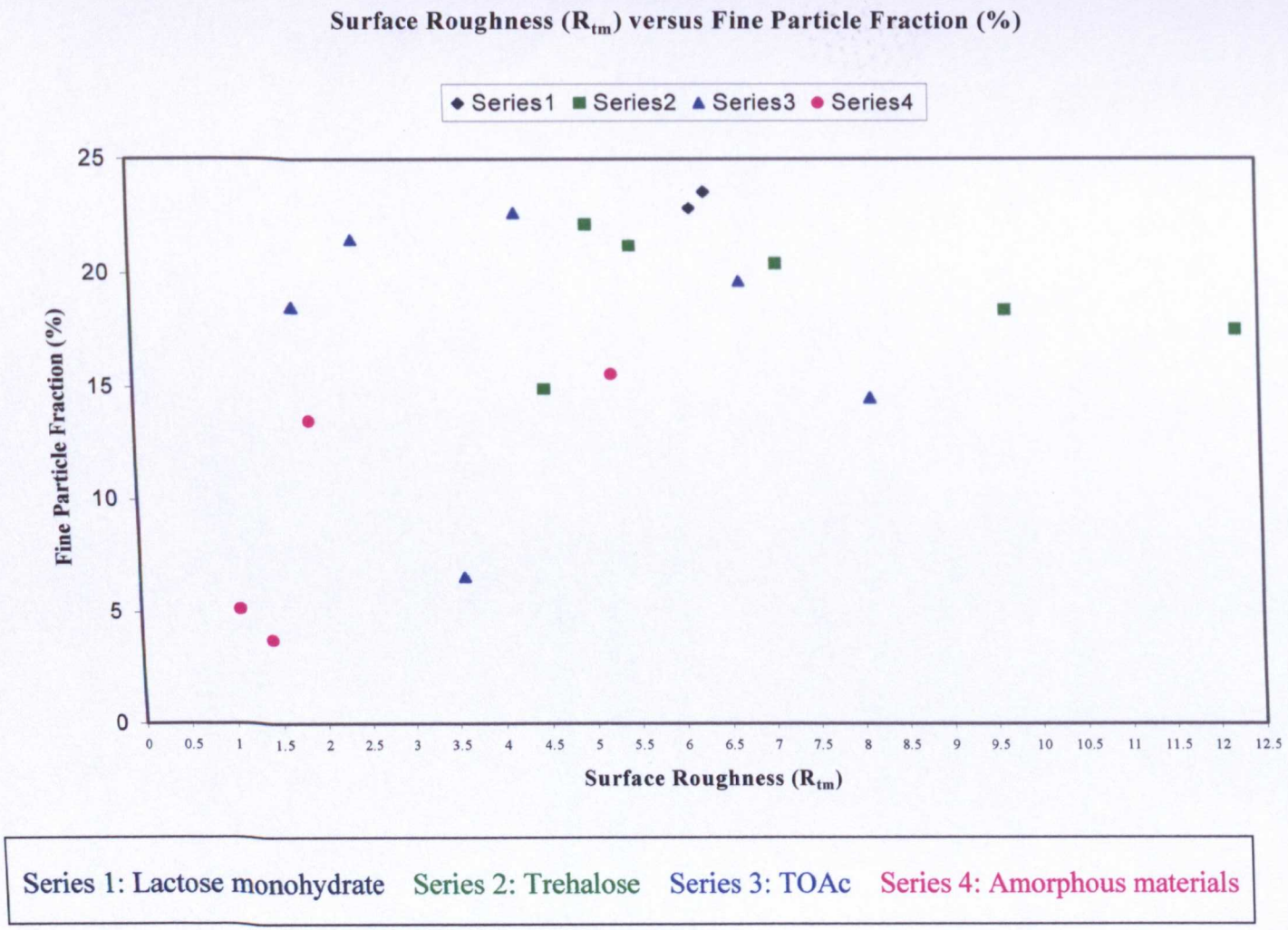

Figure 8.4: A summary graph of fine particle fraction (%) versus R_{tm} for all of the materials assessed.

8.3 OVERALL DISCUSSION

As mention in the general discussion, through alteration of the surface roughness of a carrier particle to create the optimum adhesion characteristics, an improvement in performance can be achieved. This would occur because optimum adhesion of drug to carrier results in the effective detachment of the drug from the carrier during inhalation. However, the characteristics and effect of the DPI device itself should also be considered. This is because the optimisation of a blend for use in one inhaler will invariably not produce the same degree of improvement in performance if the same blend was used in a different inhalation device. This is predominantly due to differences in the materials used to construct different inhalation devices along with their operation.

Actual surfaces may have irregularities that change the area of contact between particles and surfaces (the gap between contiguous bodies) and therefore the adhesive interaction between the two. For example, there may be relatively large distances between adherent particles if the surfaces of both bodies are rough. The magnitude of this distance has a direct effect on the specific features of molecular interaction between the neighbouring particles.

The following diagram (figure 8.5) demonstrates the influence of substrate roughness on the adhesion of drug particles.

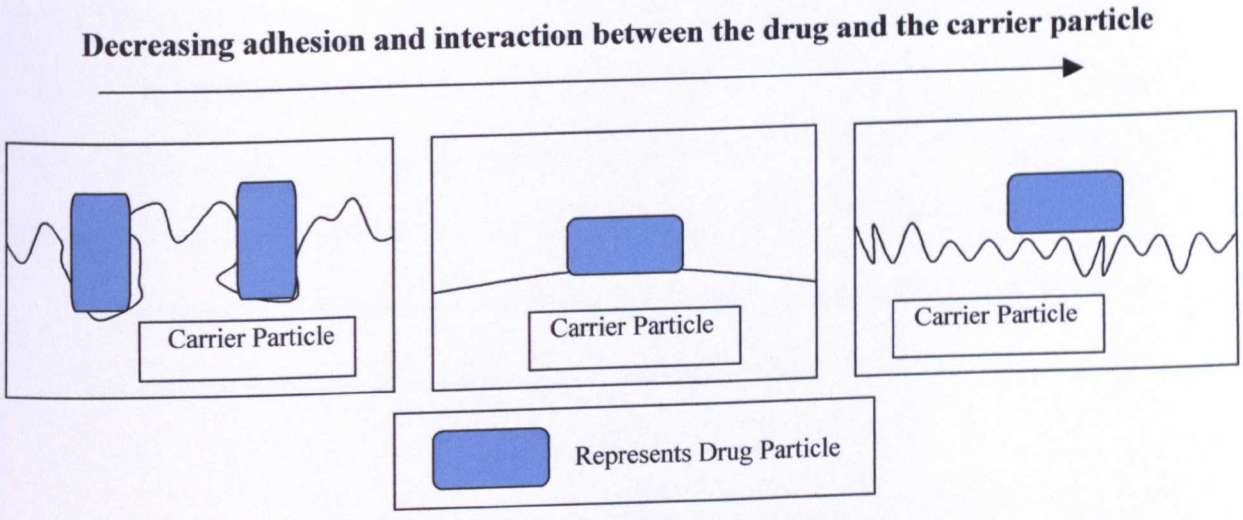

Figure 8.5: Influence of substrate roughness on drug particle adhesion.

In the first diagram, the adhesive force is greatest because of the roughness of the substrate. The size of the asperities is commensurate with the drug particle size and therefore the contact area between the two is maximised which leads to a greater force of particle adhesion. Therefore, of the three examples this drug particle requires the greatest force to detach it.

In the second diagram, the contact surfaces are ideally smooth. The adhesion of a drug particle to this type of surface is also high, as the contact between the contiguous bodies is high.

The third diagram shows a rougher surface, where the height of the asperities on the substrate is less than the drug particle size. The true contact area between the drug particle and the surface is smaller, and correspondingly the adhesion forces between the two will be less compared to an ideally smooth surface.

Surface roughness is determined by the shape and size of the asperities and is usually defined in terms of the basic dimensions of the asperities in longitudinal and transverse sections. The asperities themselves are not smooth. They will have their own micro-geometry due to defects in the crystal lattice and the emergence of dislocations. Dislocations usually form steps with a height of the order of the inter-atomic distance and this means that real surfaces all have roughness at the molecular level.

Under practical conditions, the adhesion of particles to a surface may encounter a variety of forms of surface roughness. Surface profilometry can reveal surface asperities that would result in lower adhesion but the distance between asperities has a greater influence on the adhesion characteristics of drug particles. If the asperities are closer together, the adhesion will be lower. It therefore follows that there has to be an optimum relationship between the distance between asperities (and therefore the overall surface roughness for a material) and the decreased adhesion. If the distance between the asperities became too small, then there would be an increased number of contact points between a substrate and a drug particle. This increased contact would ultimately lead to an increase in the adhesion of the drug particle to a level similar to that observed with an ideally smooth surface.

In summary, surface roughness can be used as a means of reducing or increasing the adhesive forces that exist between carrier and drug particles. This therefore directly impacts on the detachment characteristics of the drug from the carrier during inhalation and can therefore influence the drug delivery performance achieved.

Within the crystalline materials assessed in this research, the lactose control generated the highest %FPF, although approximately equivalent values were also obtained with certain

trehalose and TOAc blends. For the surface roughness parameter R_a, the recrystallised lactose was observed to have a slightly higher surface roughness value than the lactose 325M raw material, but the material's performance as a drug carrier was slightly worse than the control. When assessing the lactose using the surface roughness measurement of R_q, the difference between the surface roughness values for the two materials was less significant. With the measurement of the surface roughness parameter R_{tm} the recrystallised lactose material was actually found to have a lower surface roughness value. These data indicate that for the lactose blends assessed, there was not a significant difference in either the surface roughness of the materials assessed or their performance as drug carriers.

The comparable results obtained for the lactose blends supports the proposal that a relationship exists between the surface roughness of a material and the performance of that material as a drug carrier. This is because as a result of recrystallisation of the lactose control material, a material with a comparable surface roughness profile was obtained. This material was then found to behave in a similar manner to the lactose control with respect to drug delivery performance as the %FPF and average emitted weight obtained for both material blends were extremely close. Hence, for the lactose material assessed, the optimum performance was observed with a surface roughness value (R_a) in the region of 2.7 μm.

For the recrystallised trehalose dihydrate materials, all had higher surface roughness values for the three parameters measured compared to the raw material. In addition, each of the recrystallised trehalose dihydrate carriers also generated an improved drug delivery performance compared with the blend produced from the raw material. A trend was

observed within the results for the recrystallised trehalose dihydrate materials. As the surface roughness values increased (for all of the three parameters measured), the drug delivery performance of the materials decreased. Hence, it could be proposed that by further decreasing the surface roughness of batches of recrystallised trehalose dihydrate an improved performance could be achieved. However, all of the recrystallised trehalose dihydrate carriers assessed had surfaces that were rougher than the raw material. Therefore, it would be interesting to assess the performance as a carrier of batches of recrystallised trehalose dihydrate determined to have surfaces that were less rough than the raw material. Such an assessment would definitively establish the optimum surface roughness for recrystallised trehalose dihydrate required to obtain the optimum performance from the FlowCaps® DPI. However, from the results obtained, the material that generated the optimum performance (FPF of 22.16%) had been surface washed with IPA following recrystallisation and the surface roughness value (R_a) obtained for this material was 2.12 μm. In conclusion, the optimum performance for trehalose dihydrate from the materials assessed was achieved with a surface roughness value (R_a) in the region of 2.1 μm.

With respect to the amorphous materials, the TOAc blends performed significantly better than either the spray dried lactose or trehalose materials. The optimum performance from the amorphous materials assessed was observed with the powdered amorphous TOAc that was determined to have a surface roughness (R_a) value of 2.32 μm. This value was significantly higher than for any of the spray dried materials, and this was considered to be due to the method of manufacture for this material. As discussed earlier, the susceptibility of the spray dried materials to changes in environmental conditions probably had a detrimental effect on the performance of these materials as drug carriers.

With respect to crystalline TOAc, the raw material generated a poor drug delivery performance. It is proposed that this result was principally due to the acicular morphology of the material, as it is possible that the material experienced aerodynamic difficulties that would have hindered the detachment of the drug from the carrier. For the recrystallised TOAc samples, there was considerable improvement in the drug carrier performance compared to the raw material. An improvement in performance was even observed for the TOAc material recrystallised from 85:15 ethanol:water, which consisted of a mix of morphological forms. This material was comprised of both orthorhombic and acicular crystals, although the latter morphology was dominant. For this material, there was just over a three-fold increase in the surface roughness compared to the raw material and over a two-fold increase in the performance. The material recrystallised from 75:25 ethanol:water again comprised of a mixture of morphological forms, but for this material the orthorhombic habit was dominant. Compared to the raw material, there was a two-fold increase in the surface roughness and a three-fold improvement in the performance of the material as a drug carrier. The three purely orthorhombic batches of TOAc were recrystallised from 70:30 ethanol:water, and the performance of all three was better than the raw material. For the batches that did not undergo a surface wash with IPA following recrystallisation the results indicate that the rougher surface obtained from recrystallising the material from a higher initial supersaturation ratio had a positive effect on the performance. Both of these materials had a smoother surface compared to the raw material. The TOAc material surface washed with IPA created a surface that was rougher than the raw material, but that generated the best performance.

From the TOAc materials assessed, the overall performance of the recrystallised materials generated a slightly skewed curve that indicated the optimum performance was obtained with the IPA washed material with a surface roughness value (R_a) of 1.9 μm.

These data also indicated that an increase in the orthorhombic morphological content of TOAc blends resulted in a significant improvement in the performance of the TOAc material as a drug carrier compared to the raw material.

8.4 CONCLUSIONS

As discussed earlier, it is possible to alter the morphology of a material through manipulation of crystallisation parameters such as temperature, degree of supersaturation and choice of solvent. Variation in such parameters can alter the crystallisation route that a material follows, hence produce materials that possess different physical properties.

As was observed with TOAc, the results indicate that the morphology of a material can have a significant impact on the performance of a material as a drug carrier within a dry powder inhaler. They also suggest that the processing of a material after recrystallisation can also affect the performance as a drug carrier, even in instances where the overall morphology of the material remains the same. As one of the likely effects of post-crystallisation processing of materials would be to alter the surface characteristics of a material, it is therefore logical to derive that the surface characteristics of a material are significant in the performance of that material as a drug carrier.

The work carried out for this research was to try to establish whether a relationship exists between the surface characteristics of a material and its performance as a drug carrier.

The results obtained show that such a relationship does exist, but that the optimum relationship is determined by a number of factors. In addition to the surface characteristics,

the physiochemical properties of the carrier material and the active drug along with the characteristics of the chosen DPI device itself all contribute to the performance, and thereby the relationship.

Although limited in number, the results indicated that for lactose the optimum performance was achieved with a R_a value of 2.7 μm. For trehalose dihydrate the optimum R_a value was 2.1 μm and for TOAc it was 1.9 μm. Overall, this indicates that the surface roughness values (R_a) required to achieve the optimum performance as a drug carrier are in the range of 1.9 to 2.7 μm. In addition, for the amorphous materials the best performance was obtained with powdered amorphous TOAc. This material was determined to have a R_a value of approximately 2.3 μm, which falls within the 0.8 μm wide range identified as delivering the optimum performance with the crystalline materials. When these findings are taken in the context that R_a values were obtained for the materials assessed ranging from approximately 0.5 to 5.7 μm, the range indicating the optimum performance is shown to be relatively narrow. In addition, by looking more closely at the results it appears to be possible to compress this optimum range further.

When considering the hydrophilic nature of the lactose and trehalose carrier materials, and the more hydrophobic nature of TOAc it appears that a trend exists. In general, the optimum R_a values for the hydrophobic TOAc materials appear lower than the optimum values for hydrophilic carrier materials.

The amorphous TOAc has an increased surface roughness compared to the recrystallised TOAc generating the highest %FPF, but it should be remembered that amorphous

materials are often associated with increased solubility. The results therefore indicate an optimum surface roughness (R_a) in the range of 1.9 to 2.3 μm for hydrophobic materials and a range of 2.1 to 2.7 μm for hydrophilic materials.

In summary, through the manipulation of materials at such an early stage it is possible that the production of better pharmaceutical materials, with improved performance characteristics can be achieved. However, it is important to remember that optimising the performance of one inhaler by manipulation of the blend used in the device will not optimise the performance of the same blend in another inhaler. The performance of an inhaler is strongly dependent on the inter-relationship between the blend and the inhalation device itself. It is also important to appreciate that this process of particle manipulation translates not only to materials used in dry powder inhalation. The technique could deliver significant benefits to the performance profile of powders used in the production of pharmaceutical products for practically any application.

8.5 SUGGESTIONS FOR FUTURE WORK

The work carried out for this research suggests many possible areas of interest for future study. This includes fundamental investigations into areas such as the effect of changes in surface characteristics on the delivery from a DPI of model drugs with different physiochemical characteristics to salbutamol sulphate. This could include the assessment of drugs that are more basic or acidic, more or less hydrophilic or polar and also include less potent drug molecules that would require a higher drug loading.

Further investigation into the manipulation of factors that can affect the characteristics of recrystallised materials is also a possible area for future work. This could include an assessment of the effect of using different solvent systems for recrystallisation, different temperature ranges or a greater range of supersaturation ratios. Such work would also be useful in confirming whether the trends indicated by this research are significant in practice.

In addition, repeating the work from this research with further alternative carrier materials would also further enhance knowledge into the effect of differences in the properties of the carrier material themselves and their performance as a drug carrier. Through the investigation of a wider range of carrier materials that exhibit differing degrees of hydrophobic and hydrophilic nature, a better understanding of the impact this has on the material performance would be achieved. An investigation to assess the drug delivery performance at different relative humidities would also provide an insight into the influence of environmental conditions on the results obtained. This in combination with a range of different drugs (possessing different basic/acidic and/or hydrophobic/hydrophilic characteristics) could provide a complete picture of the relationship between surface characteristics and performance with a range of materials each possessing different physiochemical properties.

Further work into the performance of spray dried materials with a range of particle sizes, such as from below 5 μm up to the range assessed within this research could provide evidence to support the theory that the poor performance observed (in particular with the lactose and trehalose materials) was predominantly due to the relatively large particle size range used for the spray dried materials in this research. Additional investigations into

alternative methods of producing amorphous materials, such as milling or extraction could also be carried out.

Another possible area for further research involves investigation of the optimum properties required for producing controlled release characteristics for drugs delivered by inhalation, which would be useful for the systemic delivery of drugs via this route.

The performance of blends from a range of different dry powder inhalation devices could also be investigated. This would definitively establish whether a relationship exists between surface roughness and drug delivery performance that is completely independent of the type of inhalation device used. However, it is unlikely that such a relationship does exist due to the significant differences in the design and construction of different DPI devices available. Nevertheless, such research could ultimately provide useful information into the ideal characteristics and material construction desirable for a DPI device to achieve improved drug delivery performance.

Further research into the effect of post-crystallisation treatments of the recrystallised materials could be another area for investigation. This could include treatments such as the mechanical modification of material surfaces and further work into the effect of the surface treatment of materials using solvents. Preliminary work in this area, primarily carried out with the TOAc material, indicated that considerable differences in the surface appearance can be achieved.

The following SEM images are all of TOAc recrystallised from 70:30 ethanol:water. Each of the materials presented were handled differently with respect to the surface wash

applied following harvest. One of the samples was not washed at all, and the others were exposed to either single or multiple washes of a range of different solvents. The images highlight the potential impact of post-crystallisation treatments on the surface of materials, which in turn could lead to dramatic differences in their performance.

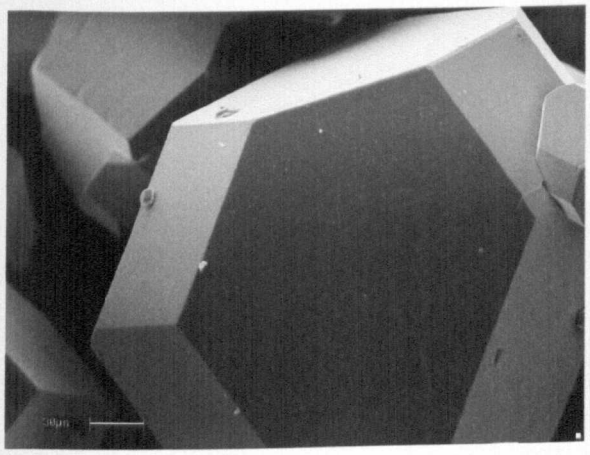

Figure 8.6: Recrystallised TOAc – surface washed with water (multiple washes).

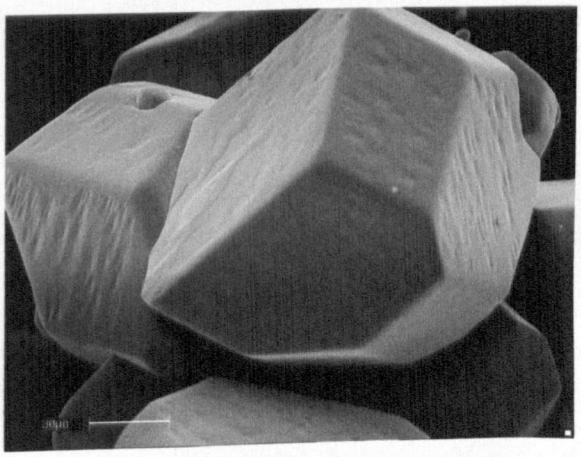

Figure 8.7: Recrystallised TOAc – surface washed with 70:30 ethanol:water (multiple washes).

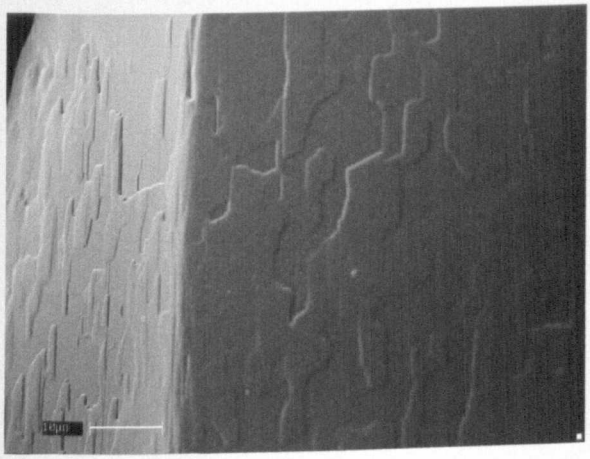

Figure 8.8: Recrystallised TOAc – surface washed with water (single wash).

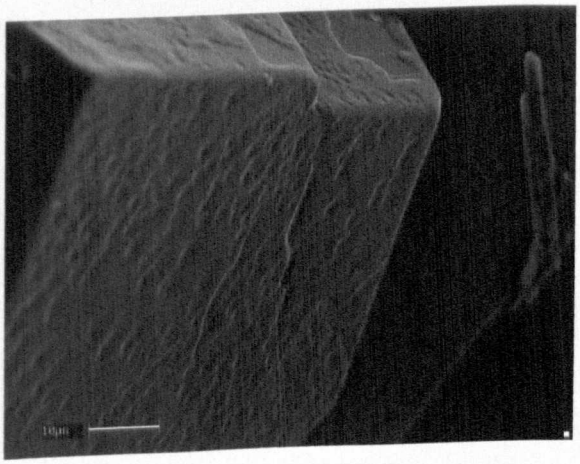

Figure 8.9: Recrystallised TOAc – surface washed with ethanol (single wash).

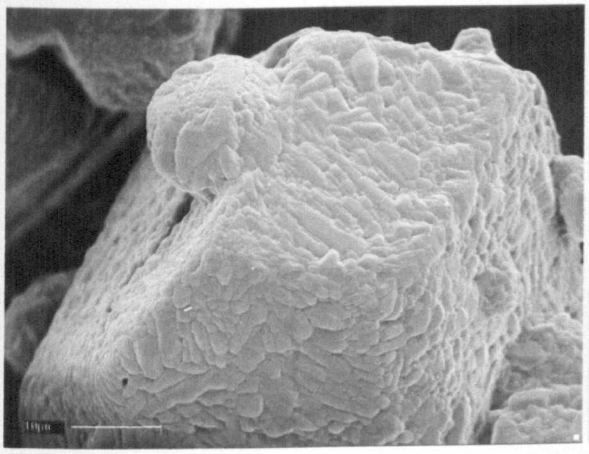

Figure 8.10: Recrystallised TOAc – surface not washed following harvest.

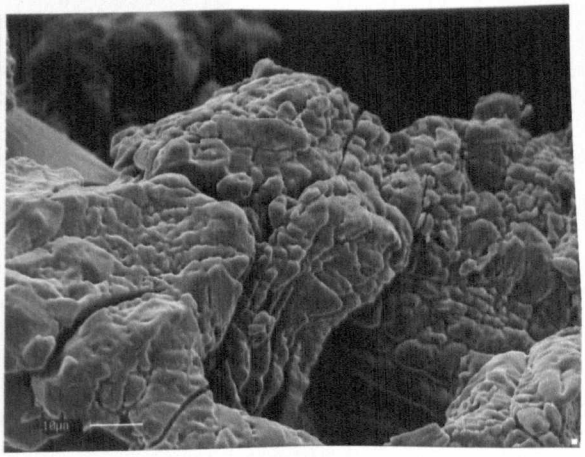

Figure 8.11: Recrystallised TOAc – surface washed with acetone (single wash).

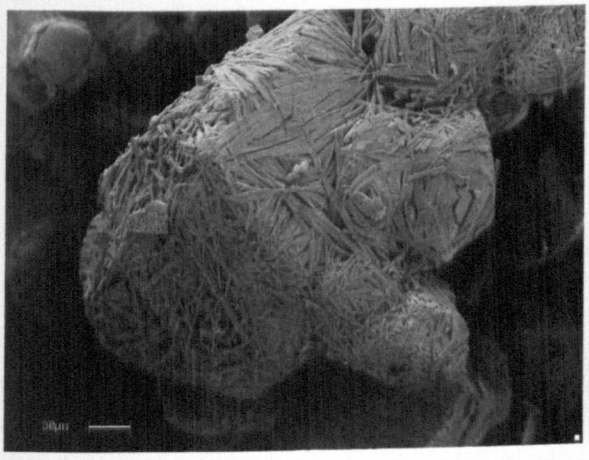

Figure 8.12: Recrystallised TOAc – surface washed with 70:30 ethanol:water followed by ethanol (single wash of each solvent).

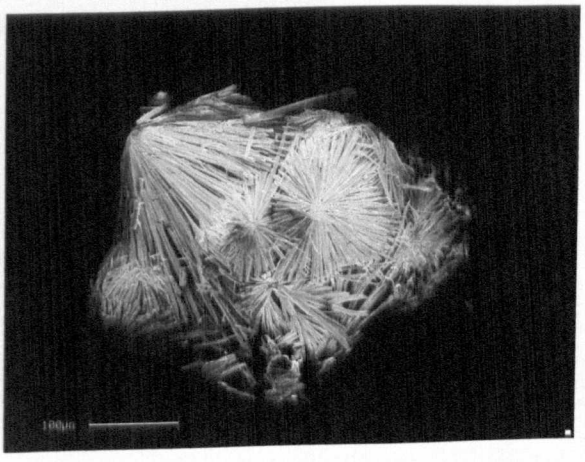

Figure 8.13: Recrystallised TOAc – surface washed with methanol (multiple washes).

Finally, the study of surface characteristics and the subsequent impact on performance of alternative dosage forms such as tablets could also be investigated. Such investigations could lead to pharmaceutical scientists in the future being able to modify and engineer materials with the intention of optimising their performance. The ultimate aim would be that this could be achieved with a high degree of both predictability and reproducibility for a wide range of pharmaceutical applications.

APPENDICES

Please Note:
Appendices are numbered according to the chapter to which they refer. Not all chapters have an appendix, so the numbering is not continuous.

The only appendices that exist for and form part of this thesis are those listed below.

APPENDIX 4:

NMR TOAc PROFILES

Proton NMR Profile of TOAc Raw Material
Proton NMR Profile of Recrystallised TOAc Material
Proton NMR Profile of Recrystallised TOAc Material plus Deuterium Oxide

Carbon NMR Profile of TOAc Raw Material
Carbon NMR Profile of Recrystallised TOAc Material

APPENDIX 6:

DVS PROFILES

Lactose monohydrate (325M) - raw material
Lactose recrystallised from 100% Water (Batch L1 (34-18 °C))
Trehalose dihydrate raw material
Trehalose dihydrate recrystallised from 100% Water (Batch 2 (34-18 °C))
Trehalose dihydrate recrystallised from 40:60 Ethanol:Water (Batch 3 (23-7 °C))
Trehalose dihydrate recrystallised from 60:40 Ethanol:Water (Batch 8 (34-18°C))
Trehalose dihydrate recrystallised from 60:40 Ethanol:Water (Batch 6 (23-7°C))
Trehalose dihydrate surface washed with IPA (recryst. from 100% Water (34-18°C))
TOAc raw material
Spray dried TOAc
TOAc quenched from the melt - powdered amorphous material

TOAc AFM PROFILES

Filename: CP001a	Filename: CP003a	Filename: CP005a	Filename: CP005c
Filename: CP006a	Filename: CP009a	Filename: CP011a	Filename: CP011c
Filename: CP015a	Filename: CP015b	Filename: CP019a	Filename: 809CP00a
Filename: 809CP01b	Filename: 809CP01c	Filename: 809CP02a	Filename: 809CP02c
Filename: 809CP03a	Filename: 809CP04	Filename: 809CP05a	Filename: 809CP05c

APPENDIX FOUR

NMR TOAc PROFILES

Proton NMR Profile of TOAc Raw Material

Proton NMR Profile of Recrystallised TOAc Material

Proton NMR Profile of Recrystallised TOAc Material plus Deuterium Oxide

Carbon NMR Profile of TOAc Raw Material

Carbon NMR Profile of Recrystallised TOAc Material

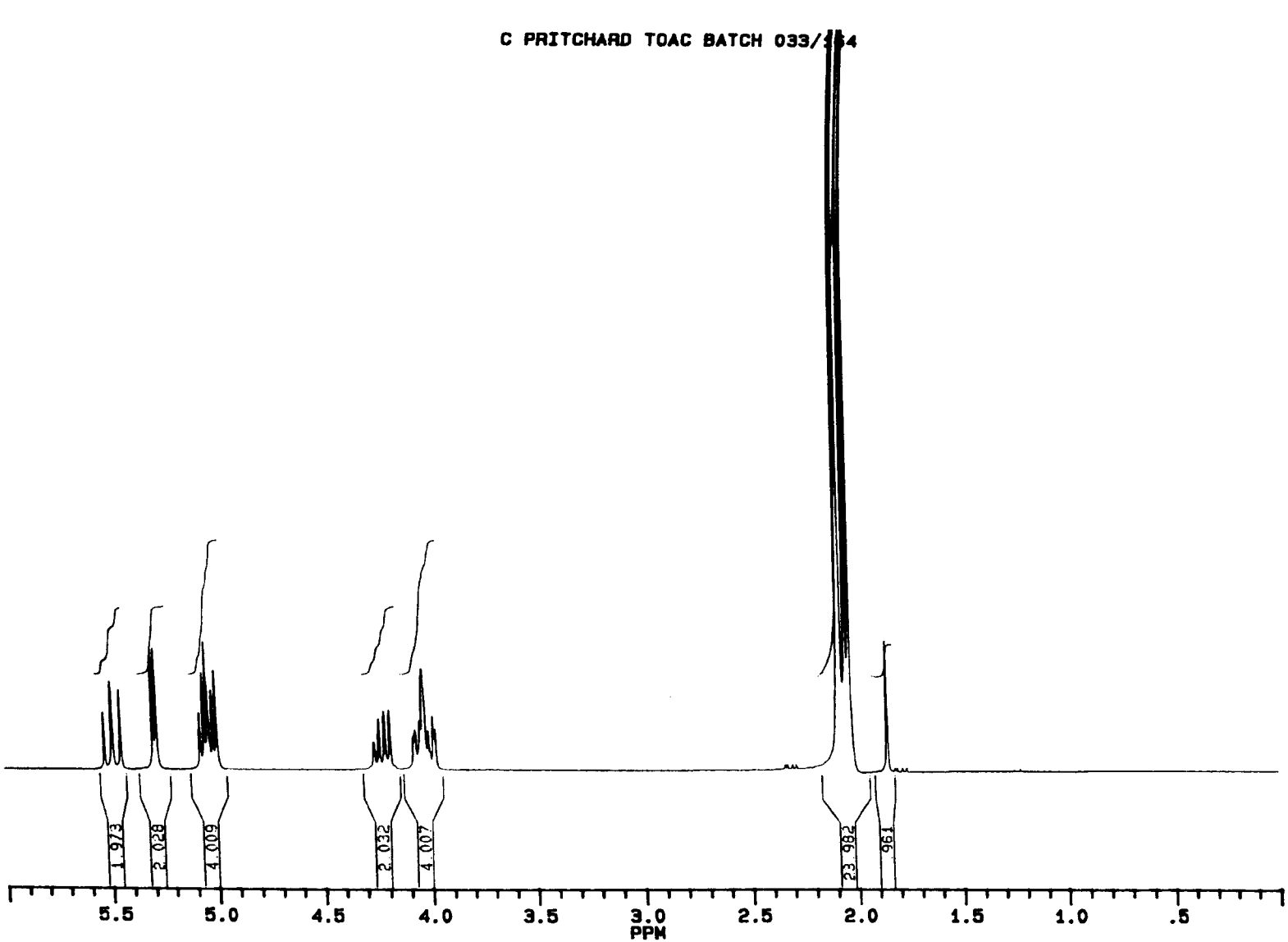

Proton NMR Profile of TOAc Raw Material

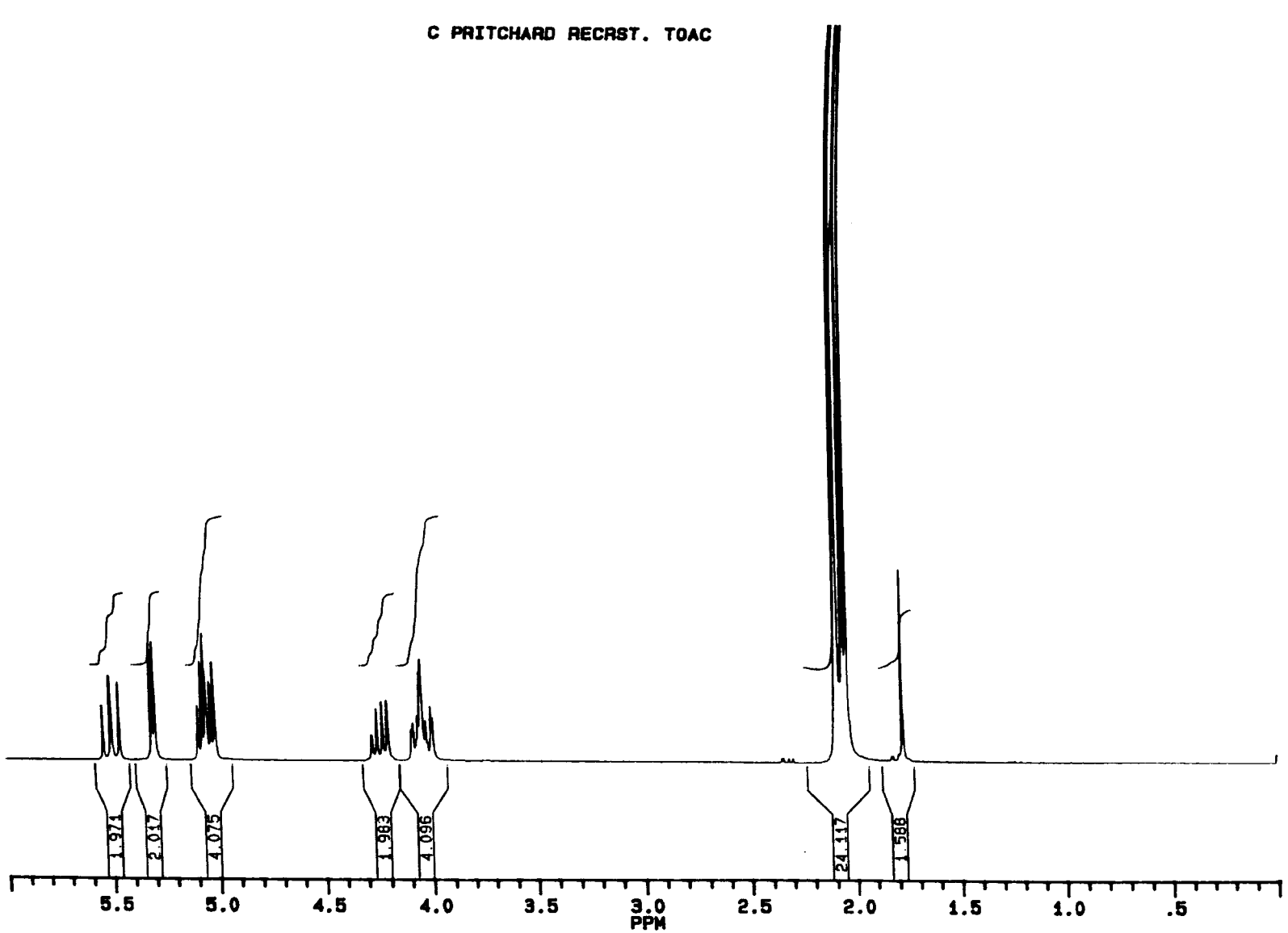

Proton NMR Profile of Recrystallised TOAc Material

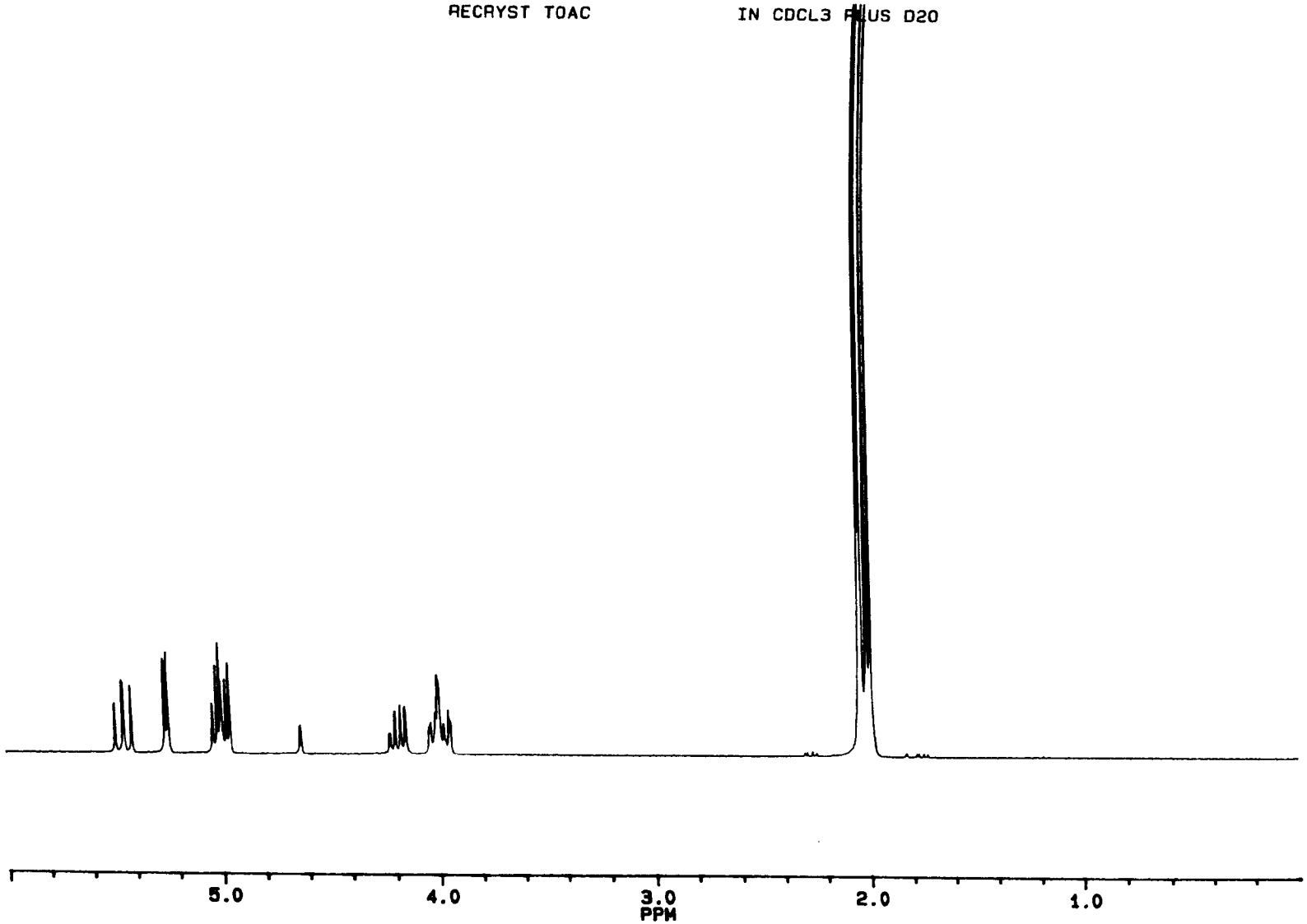

Proton NMR Profile of Recrystallised TOAc Material plus D_20

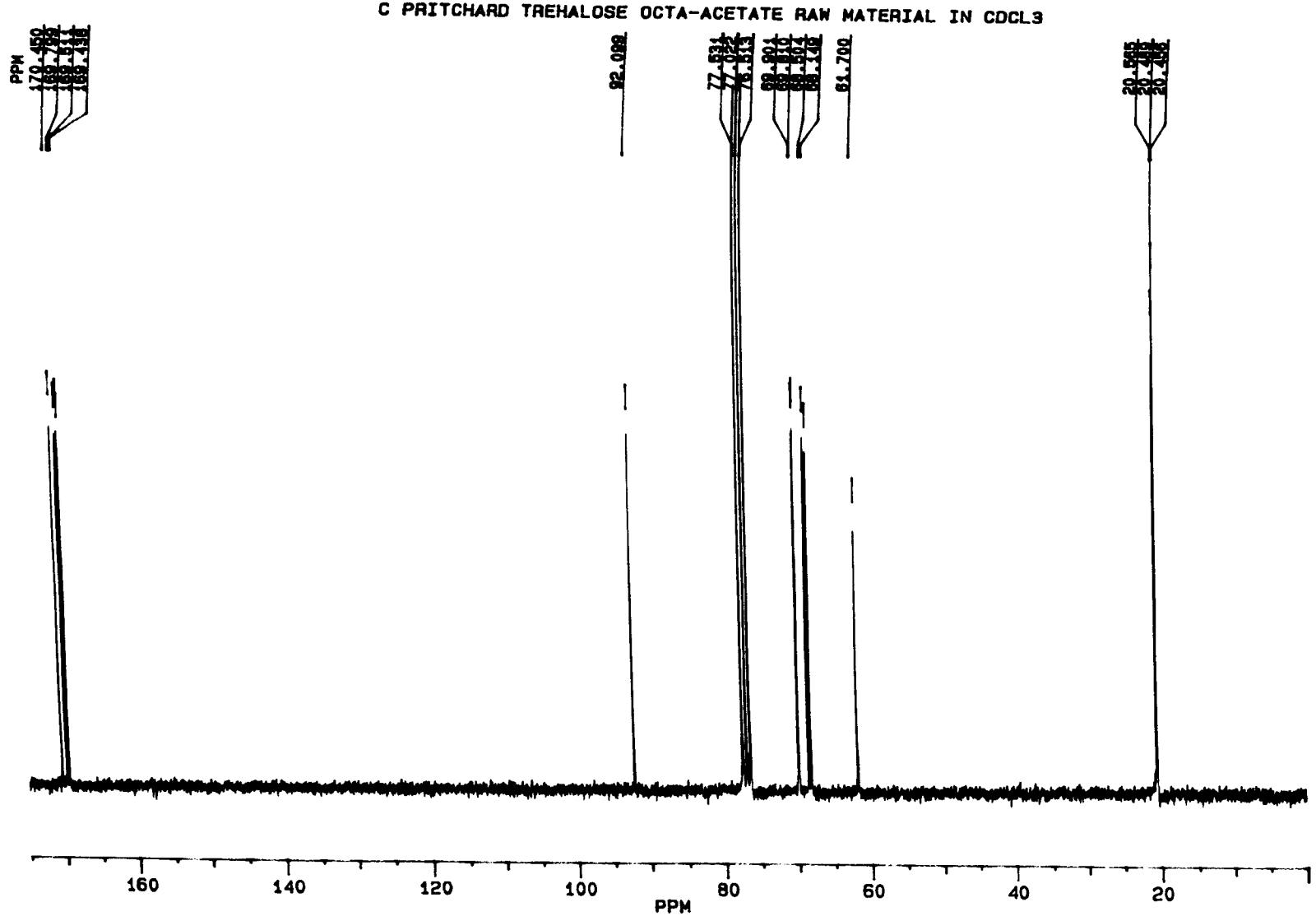

Carbon NMR Profile of TOAc Raw Material

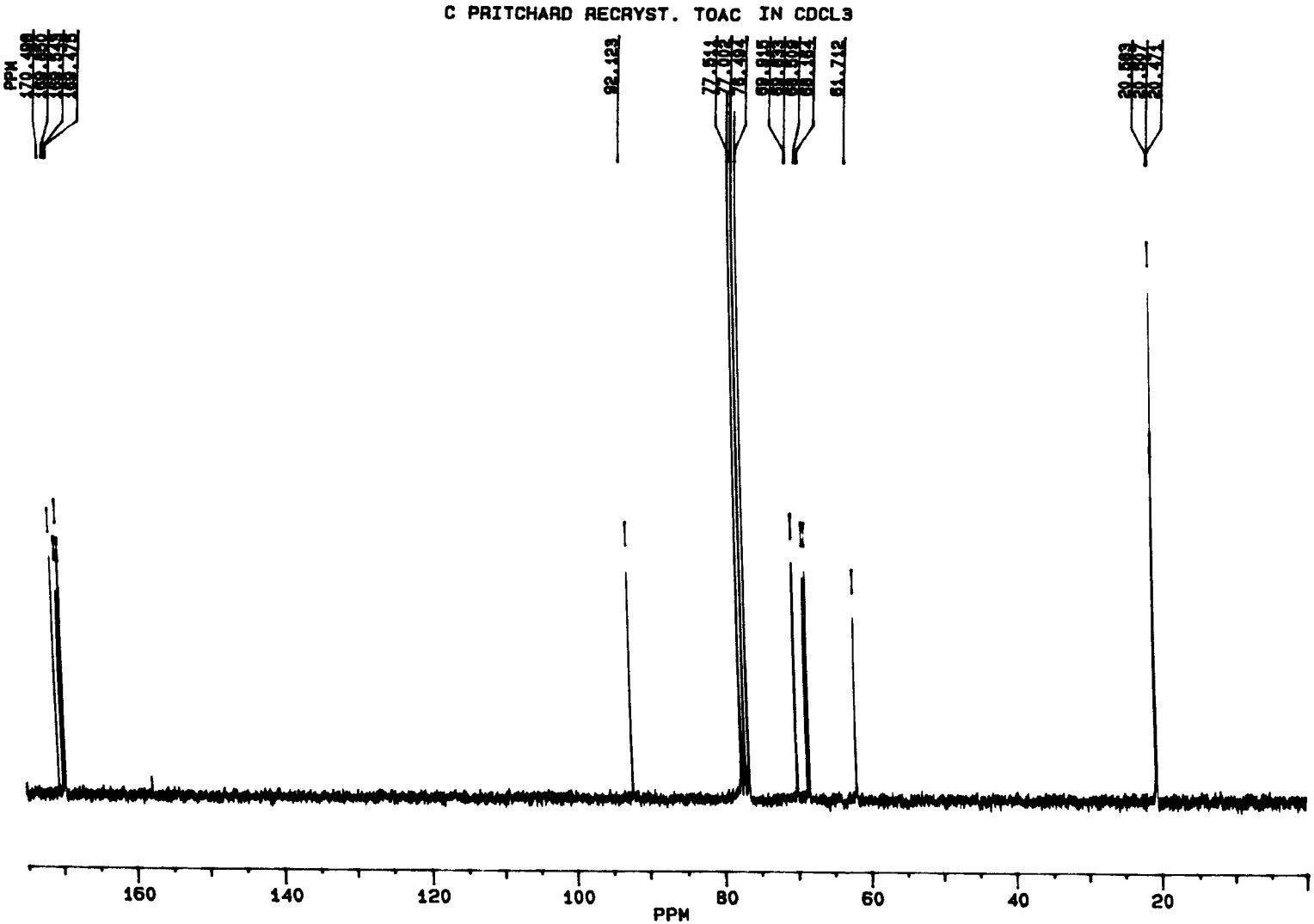

Carbon NMR Profile of Recrystallised TOAc Material

APPENDIX SIX

DVS PROFILES

Lactose monohydrate (325M) - raw material
Lactose recrystallised from 100% Water (Batch L1 (34-18 °C))

Trehalose dihydrate raw material
Trehalose dihydrate recrystallised from 100% Water (Batch 2 (34-18 °C))
Trehalose dihydrate recrystallised from 40:60 Ethanol:Water (Batch 3 (23-7 °C))
Trehalose dihydrate recrystallised from 60:40 Ethanol:Water (Batch 8 (34-18°C))
Trehalose dihydrate recrystallised from 60:40 Ethanol:Water (Batch 6 (23-7°C))
Trehalose dihydrate surface washed with IPA (recryst. from 100% Water (34-18°C))

TOAc raw material
Spray dried TOAc
TOAc quenched from the melt - powdered amorphous material

TOAc AFM PROFILES

Filename: CP001a
Filename: CP003a
Filename: CP005a
Filename: CP005c
Filename: CP006a
Filename: CP009a
Filename: CP011a
Filename: CP011c
Filename: CP015a
Filename: CP015b
Filename: CP019a
Filename: 809CP00a
Filename: 809CP01b
Filename: 809CP01c
Filename: 809CP02a
Filename: 809CP02c
Filename: 809CP03a
Filename: 809CP04
Filename: 809CP05a
Filename: 809CP05c

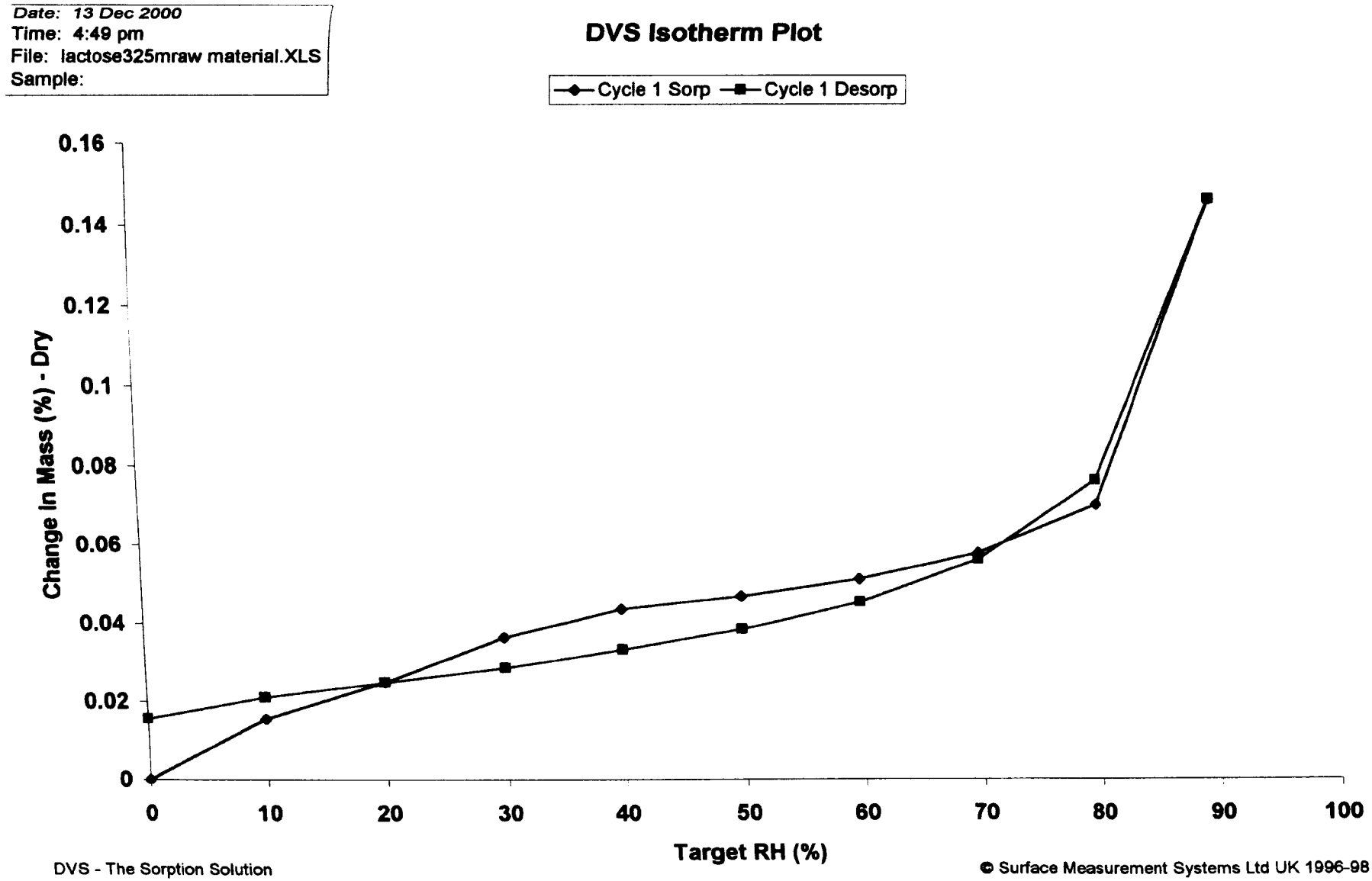

DVS Profile of Lactose (325M) Raw Material

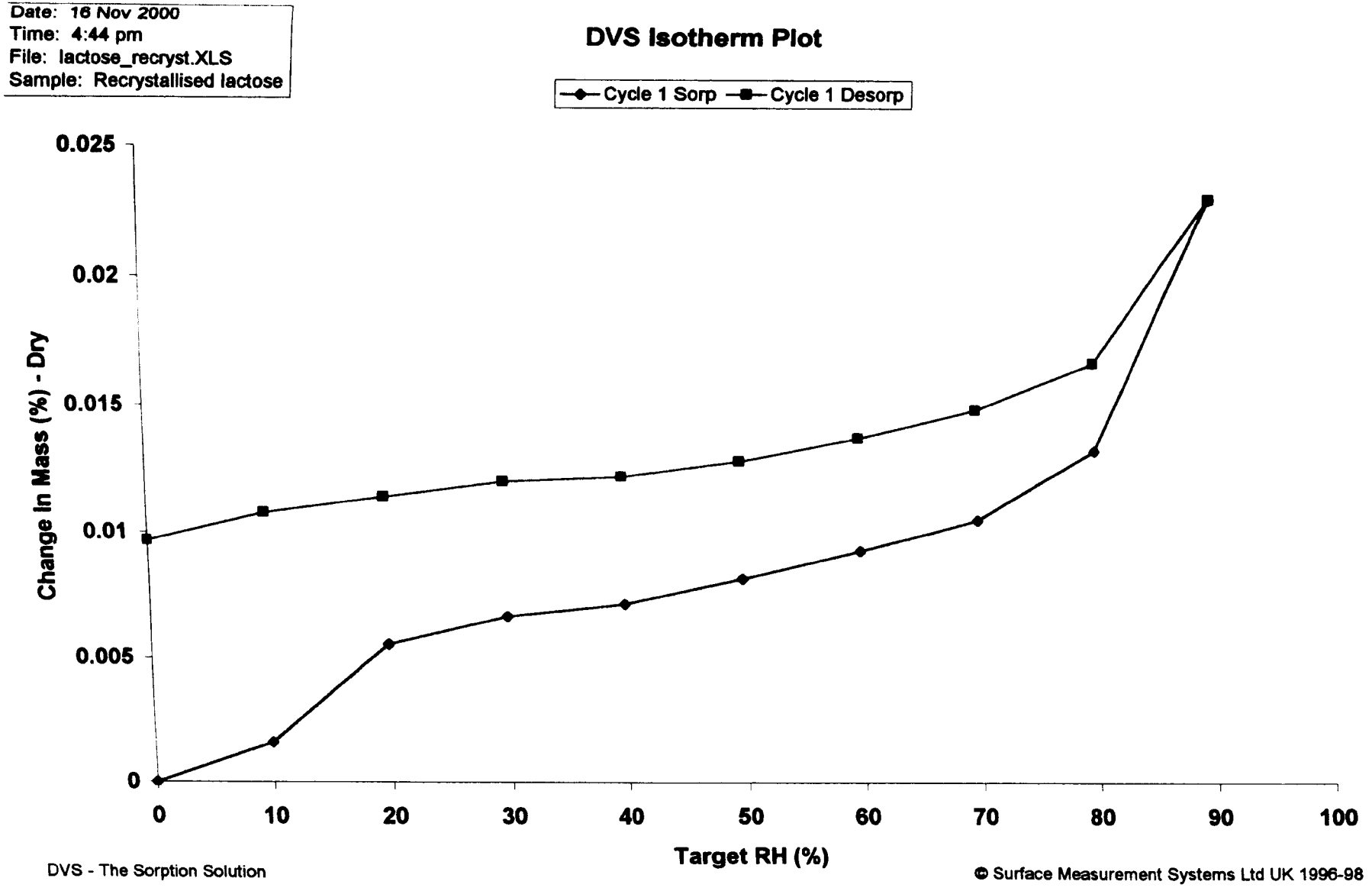

DVS Profile of Recrystallised Lactose

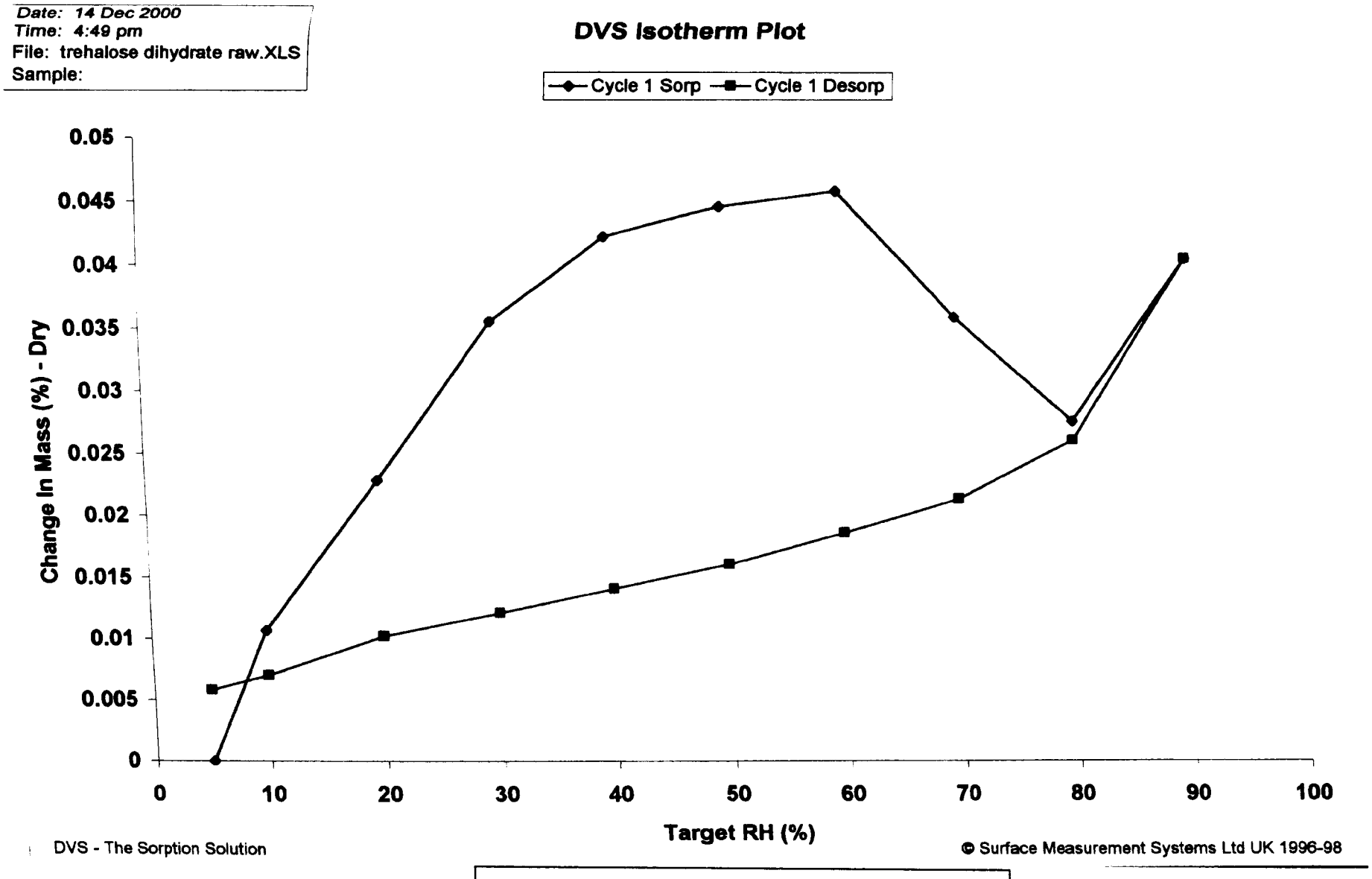

DVS Profile of Trehalose Dihydrate Raw Material

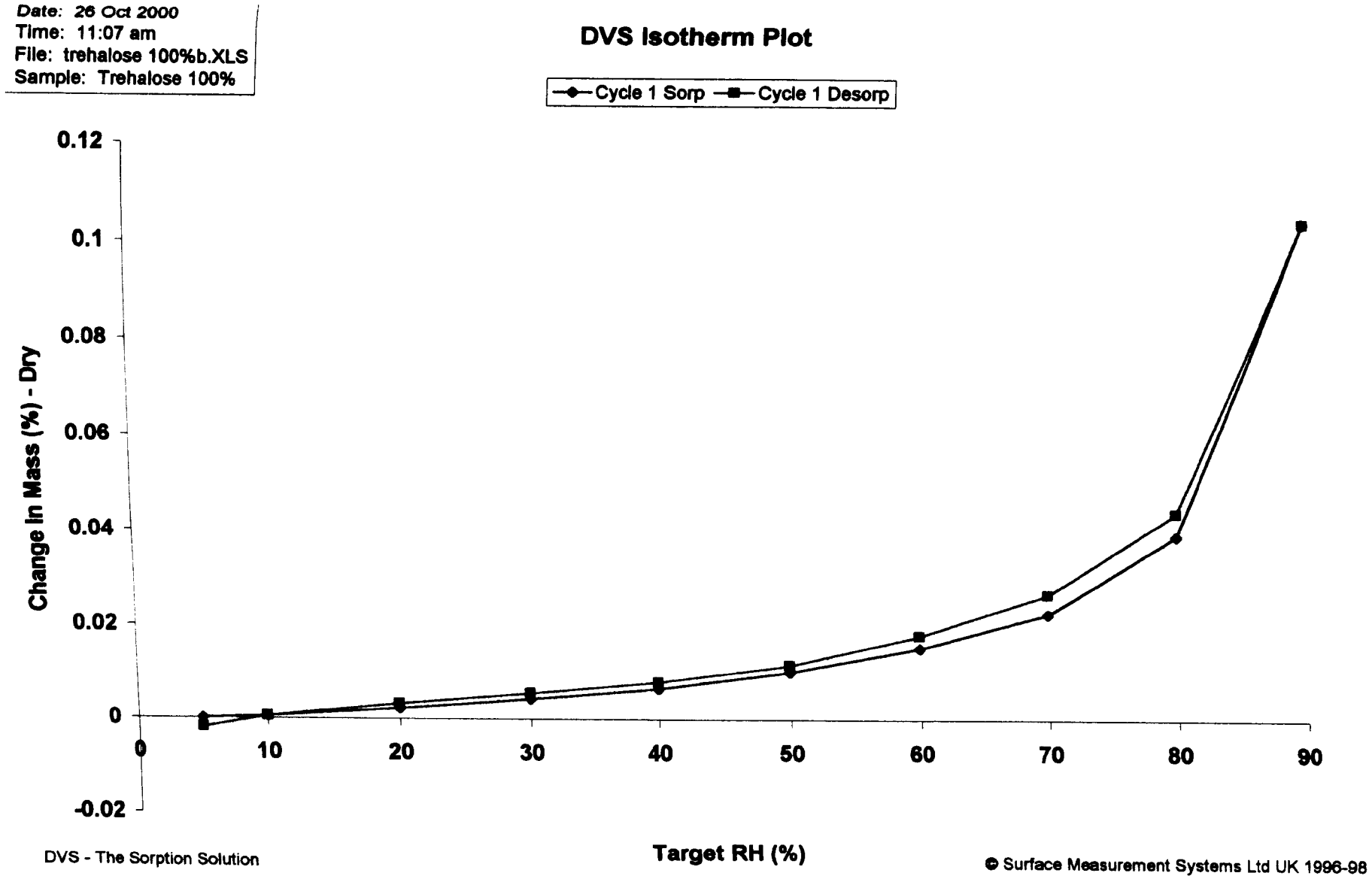

DVS Profile of Trehalose Recrystallised from 100% Water

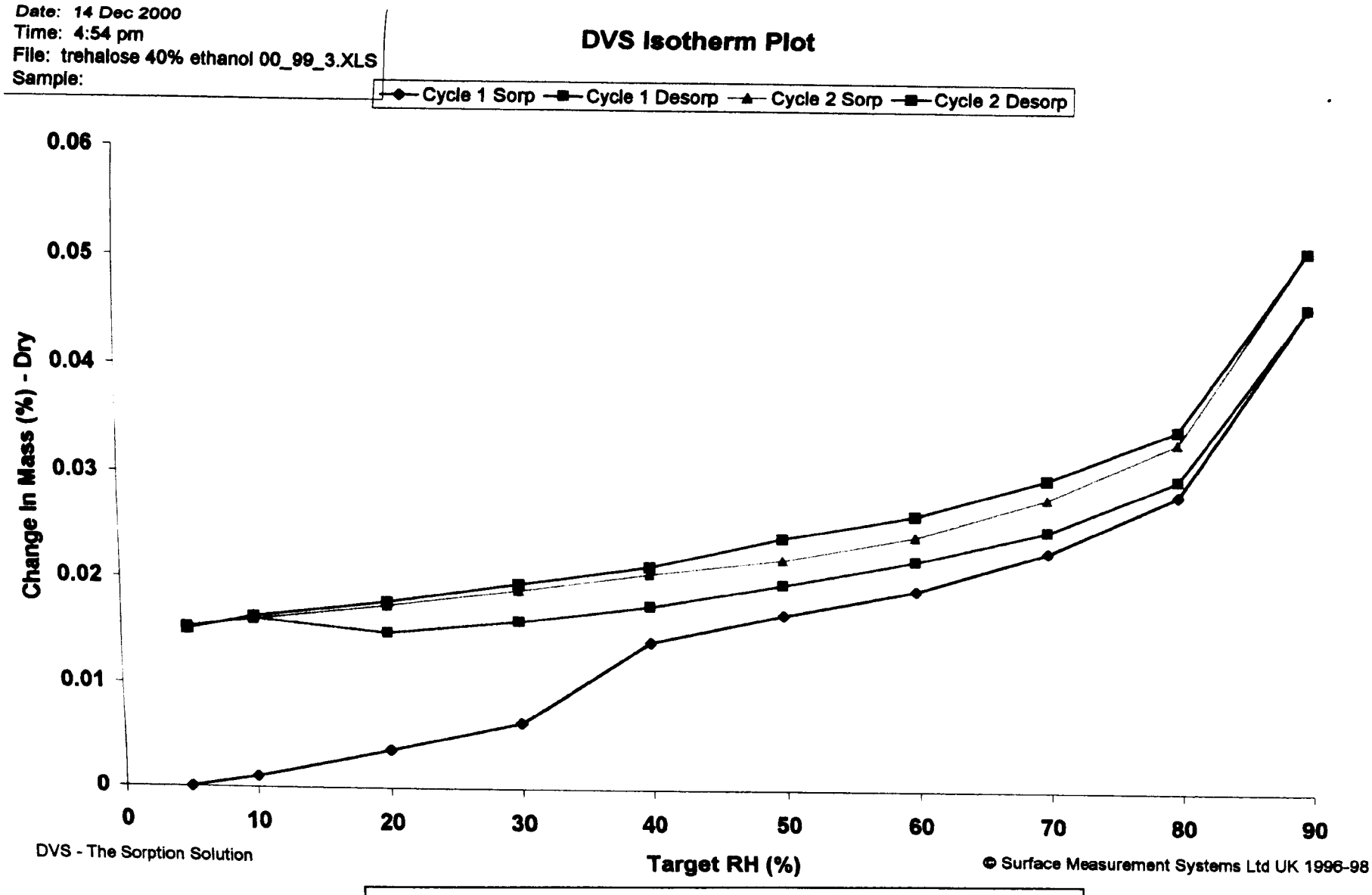

DVS Profile of Trehalose Recrystallised from 40:60 Ethanol:Water

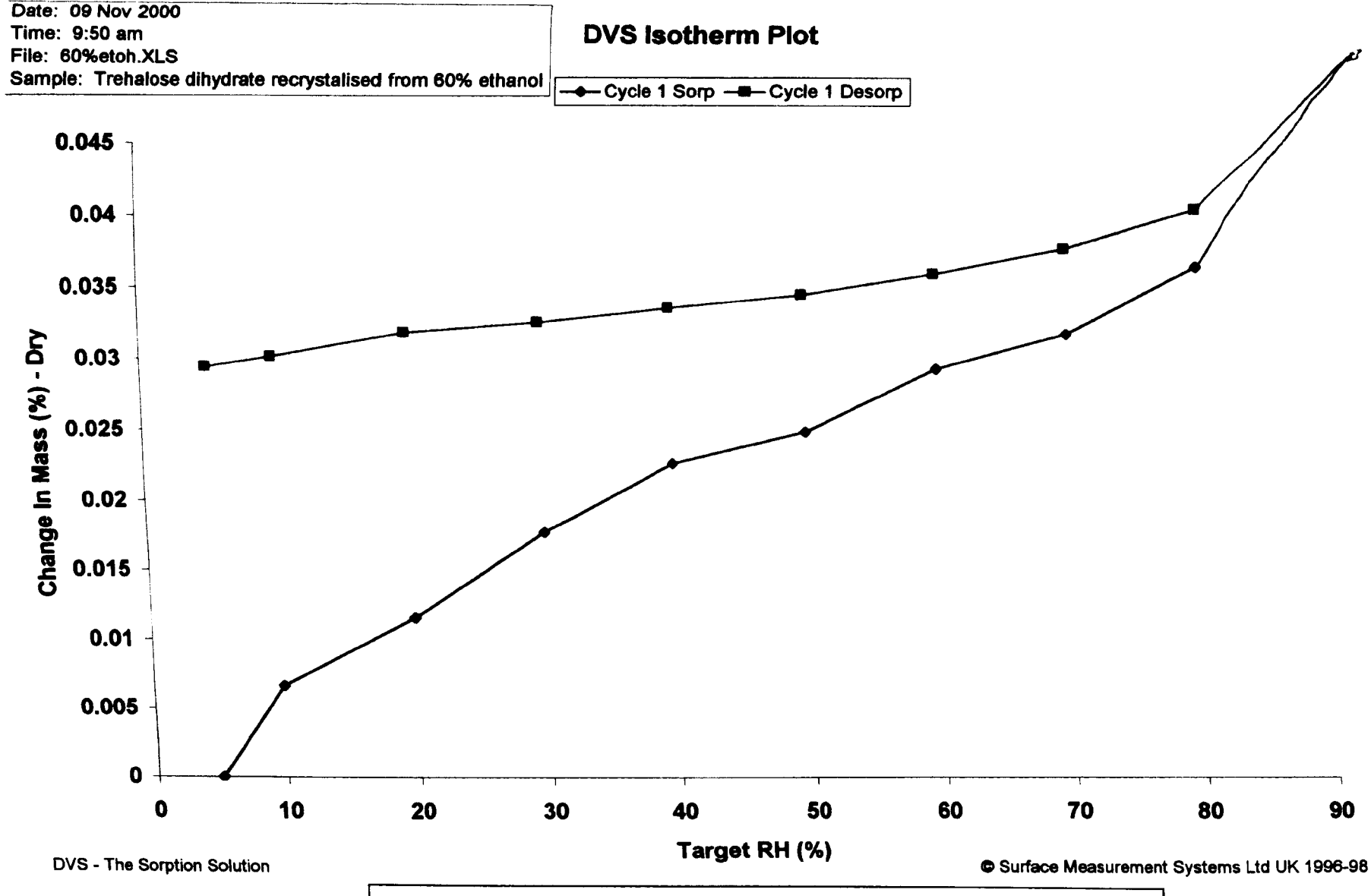

DVS Profile of Trehalose Recrystallised from 60:40 Ethanol:Water (Batch 8)

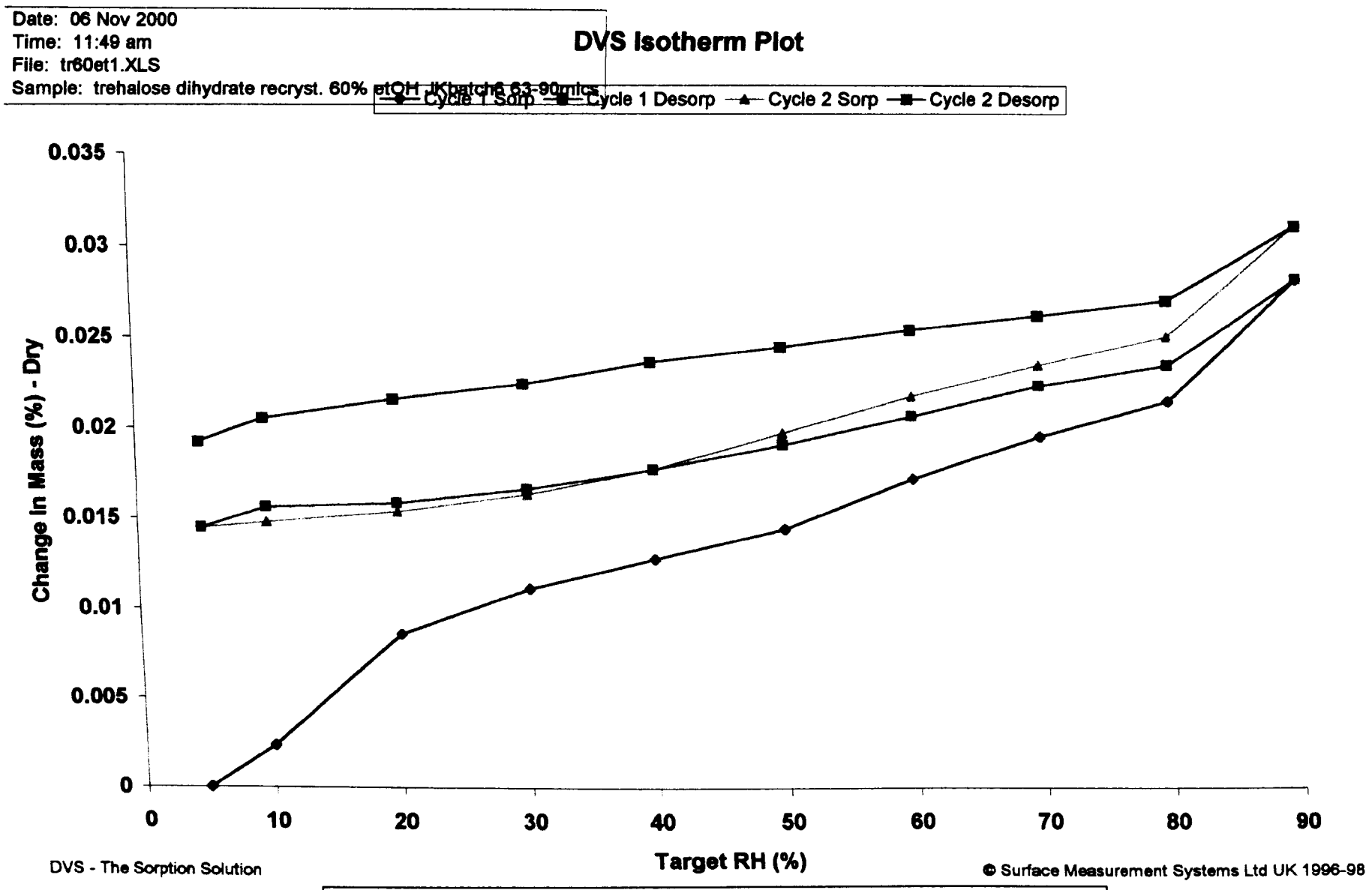

DVS Profile of Trehalose Recrystallised from 60:40 Ethanol:Water (Batch 6)

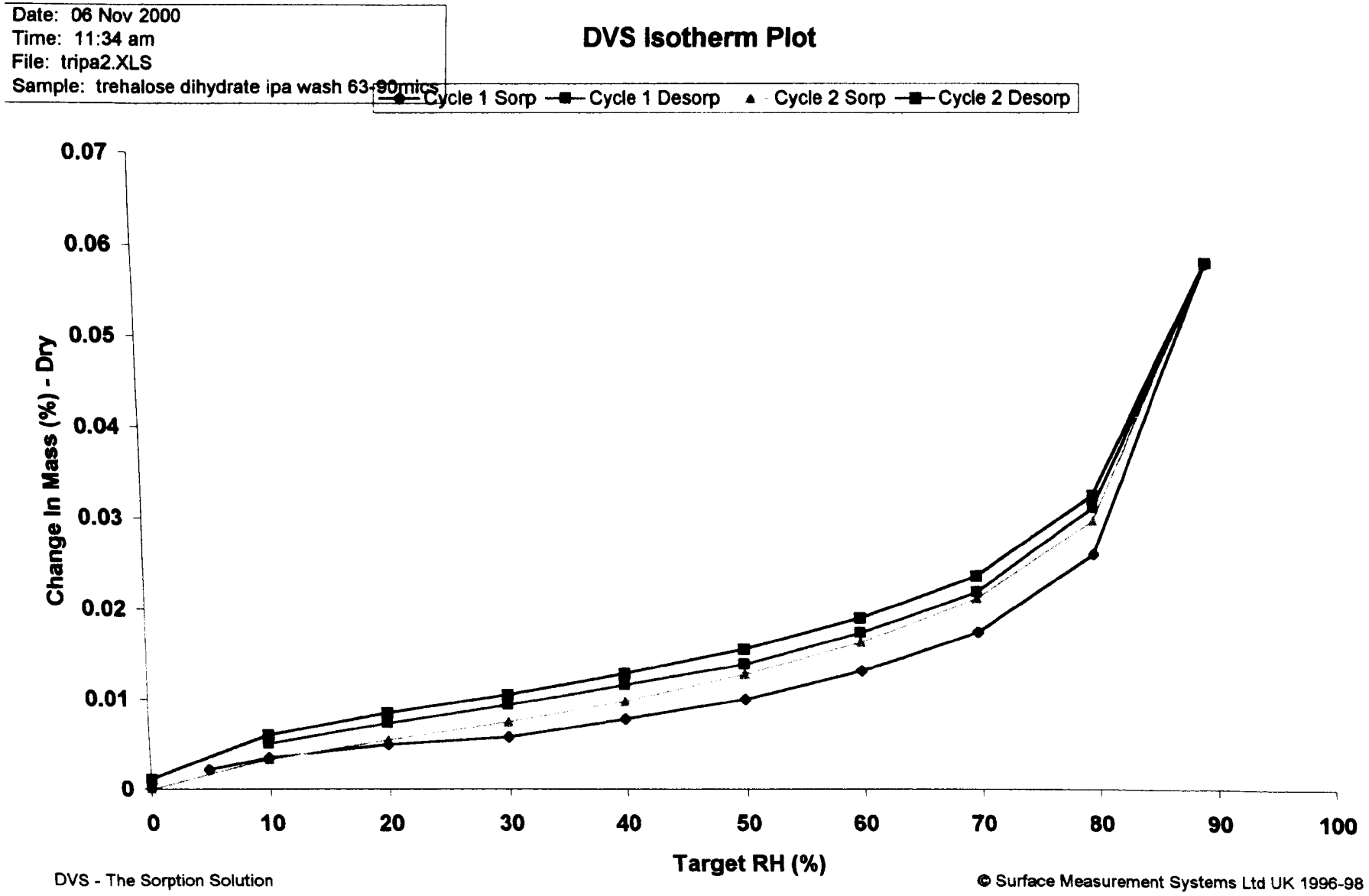

DVS Profile of Trehalose Recrystallised from 100% Water and Surface Washed with IPA

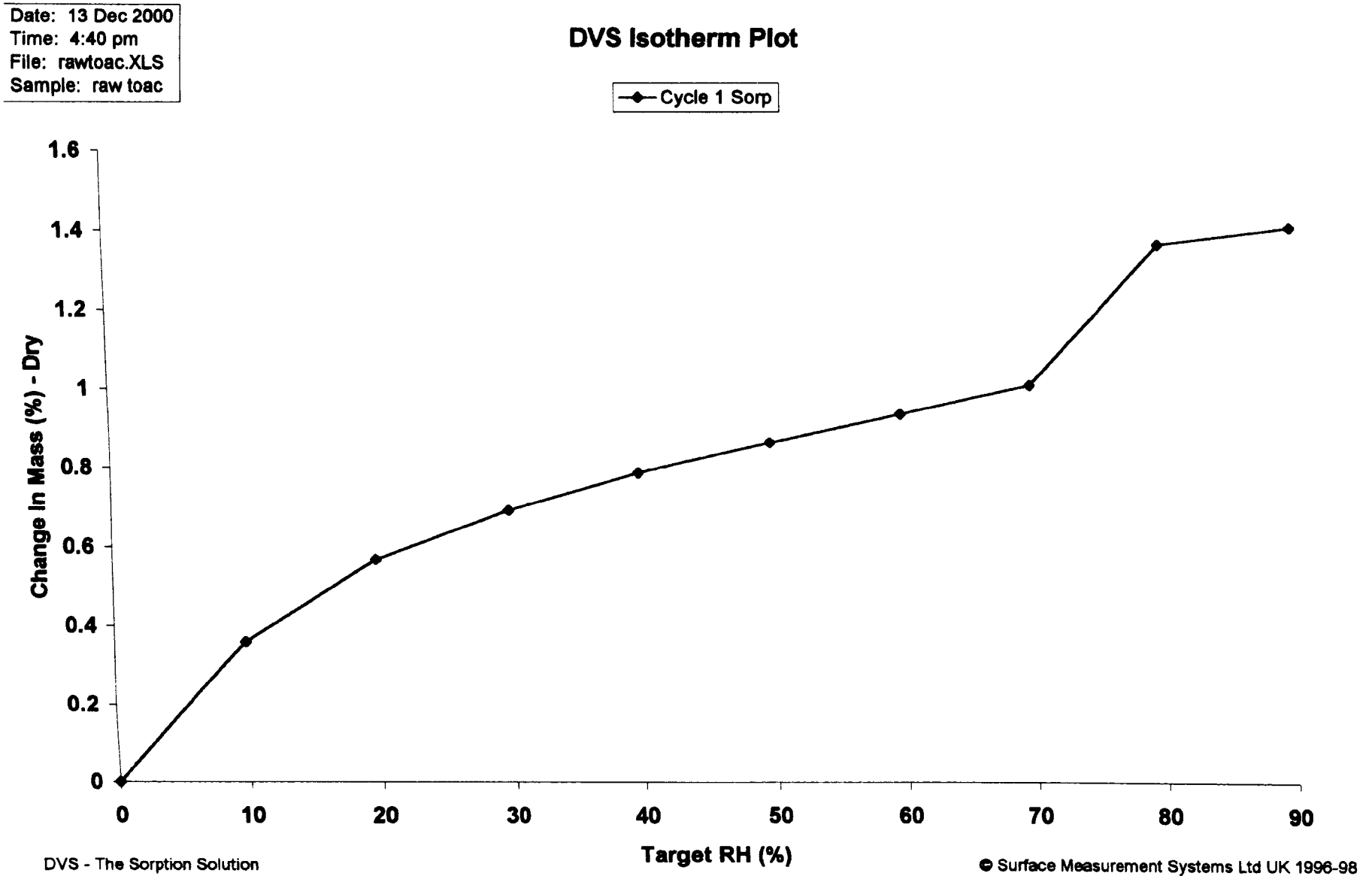

DVS Profile of TOAc Raw Material

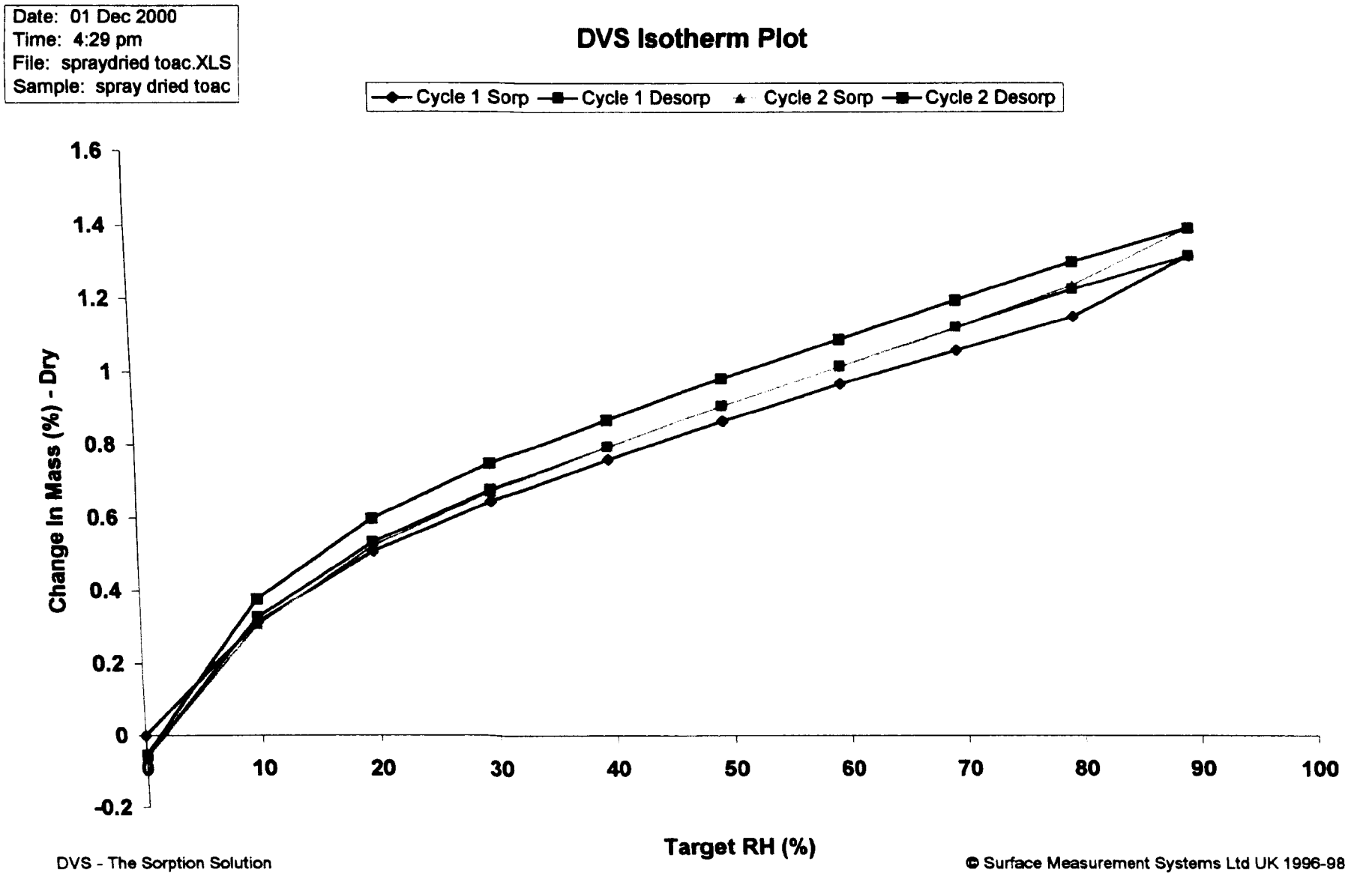

DVS Profile of Spray Dried TOAc

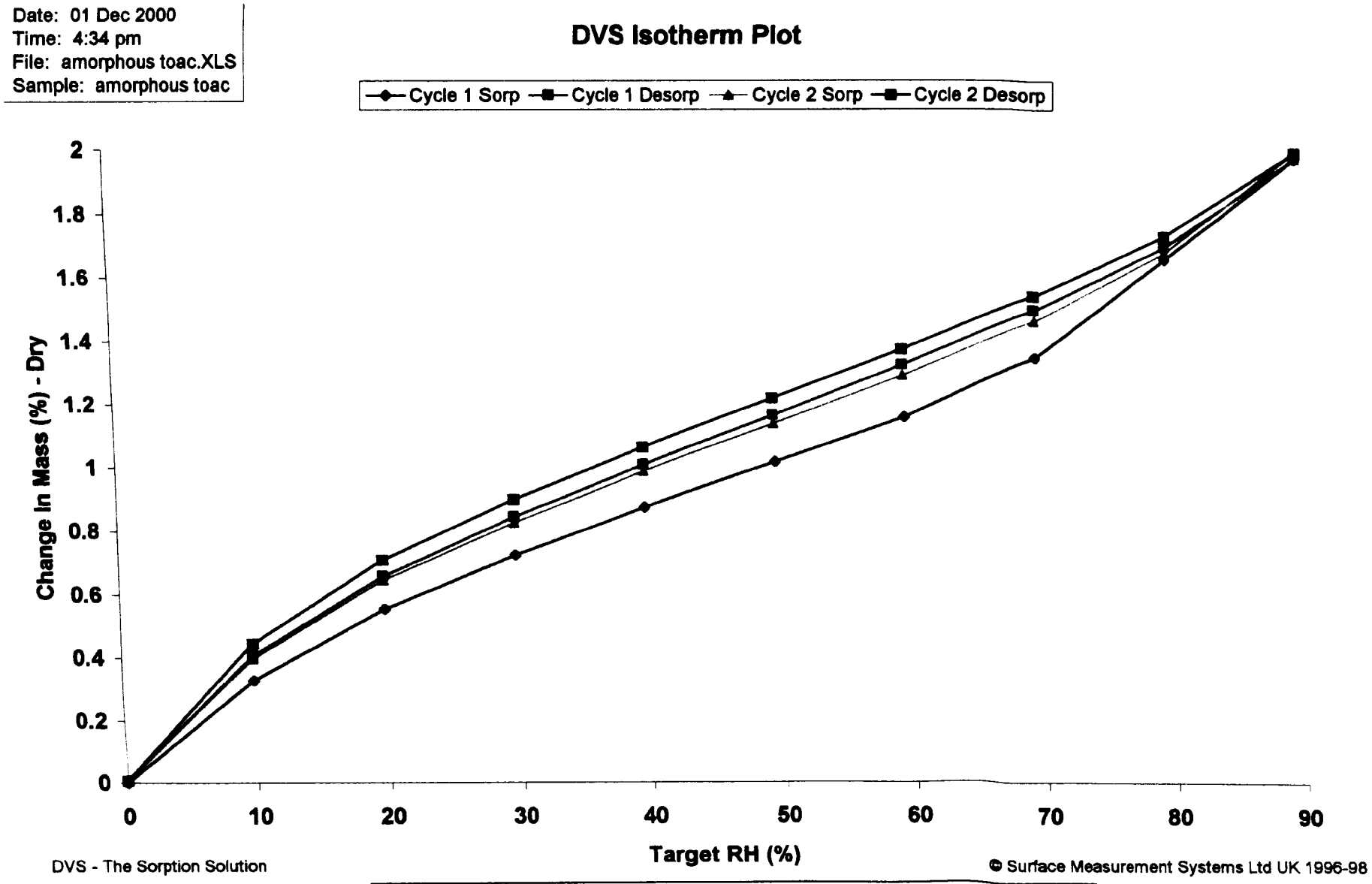

DVS Profile of Powdered Amorphous TOAc (quenched from the melt)

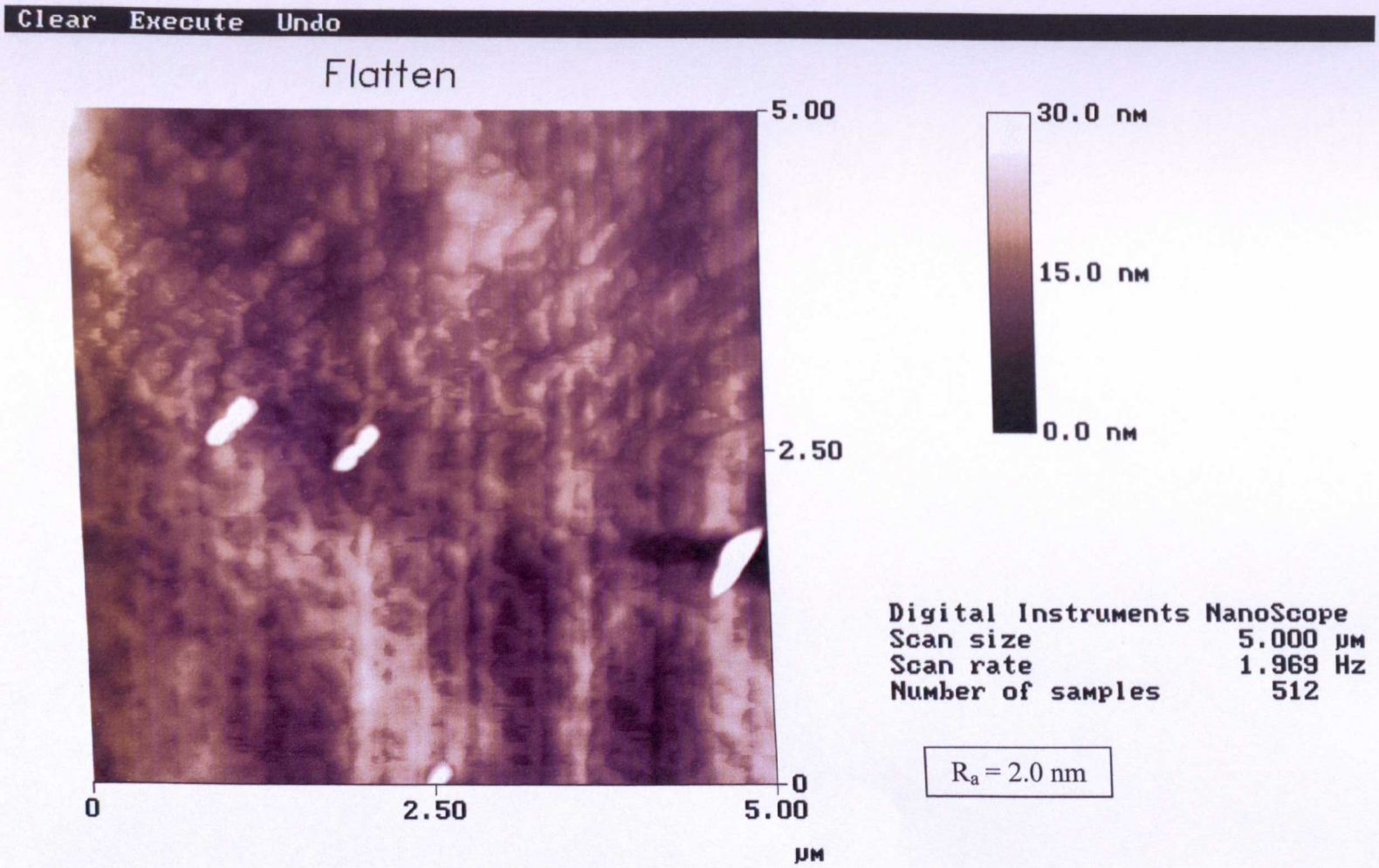

FILENAME: CP001a

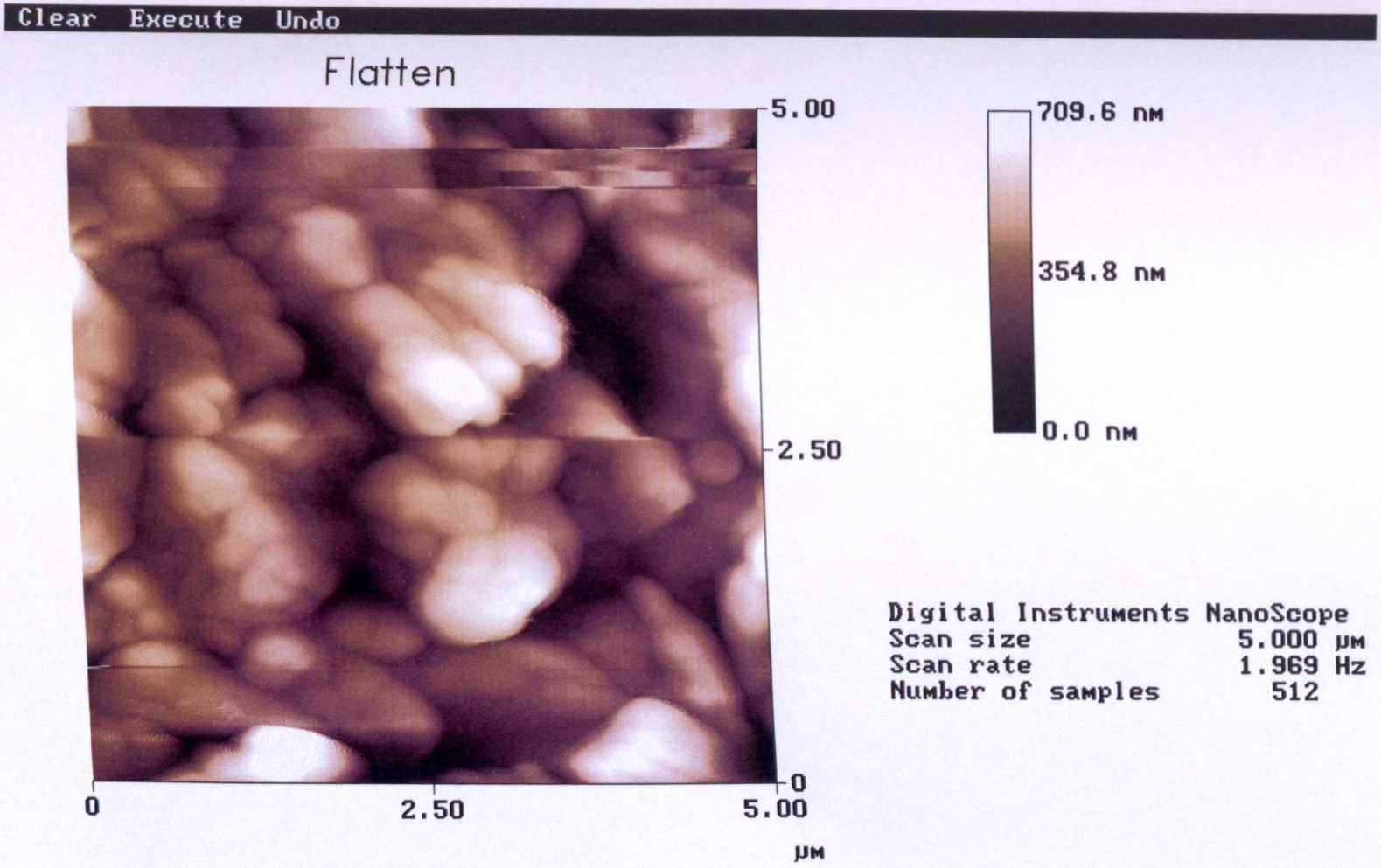

FILENAME: CP003a

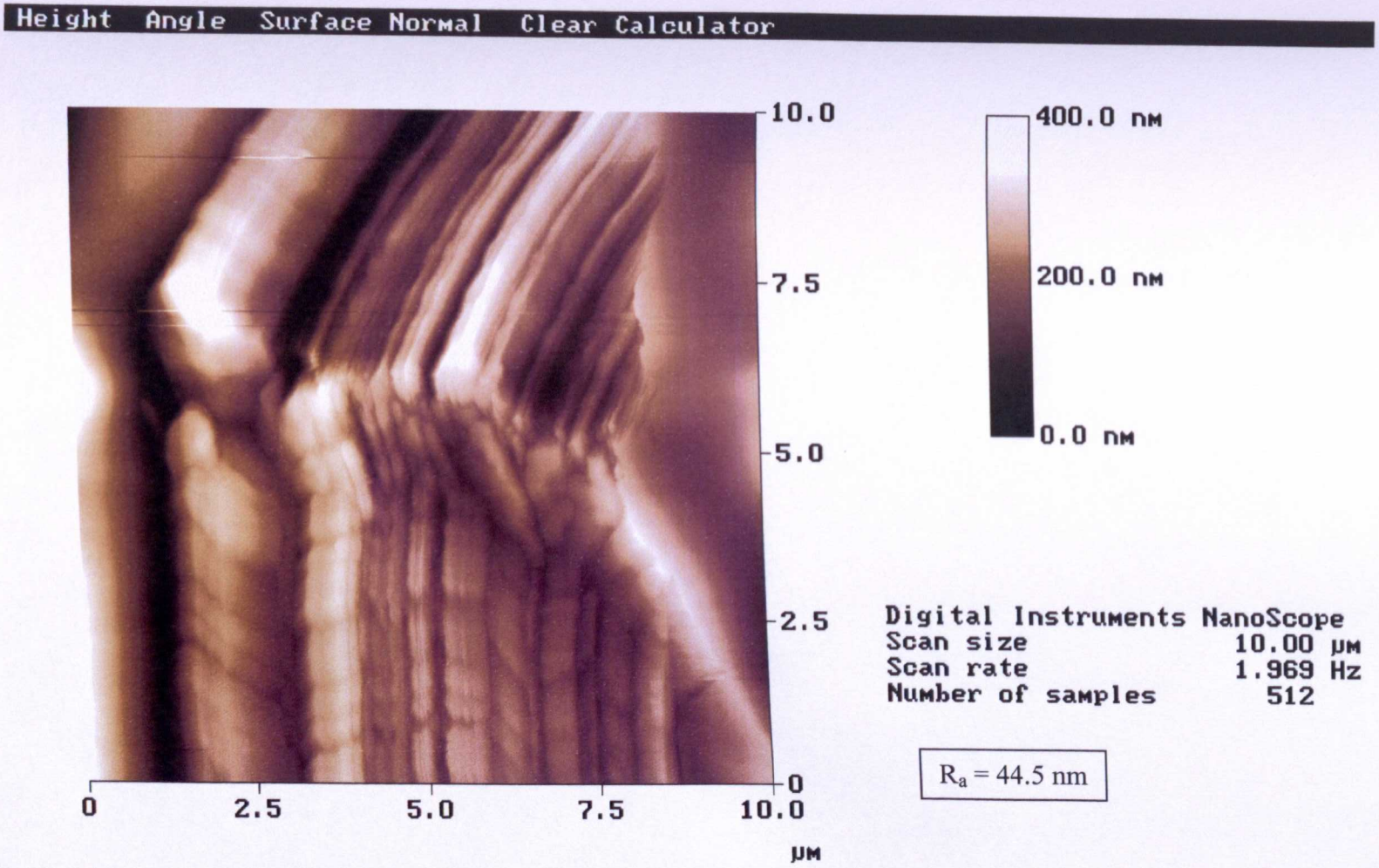

FILENAME: CP005a

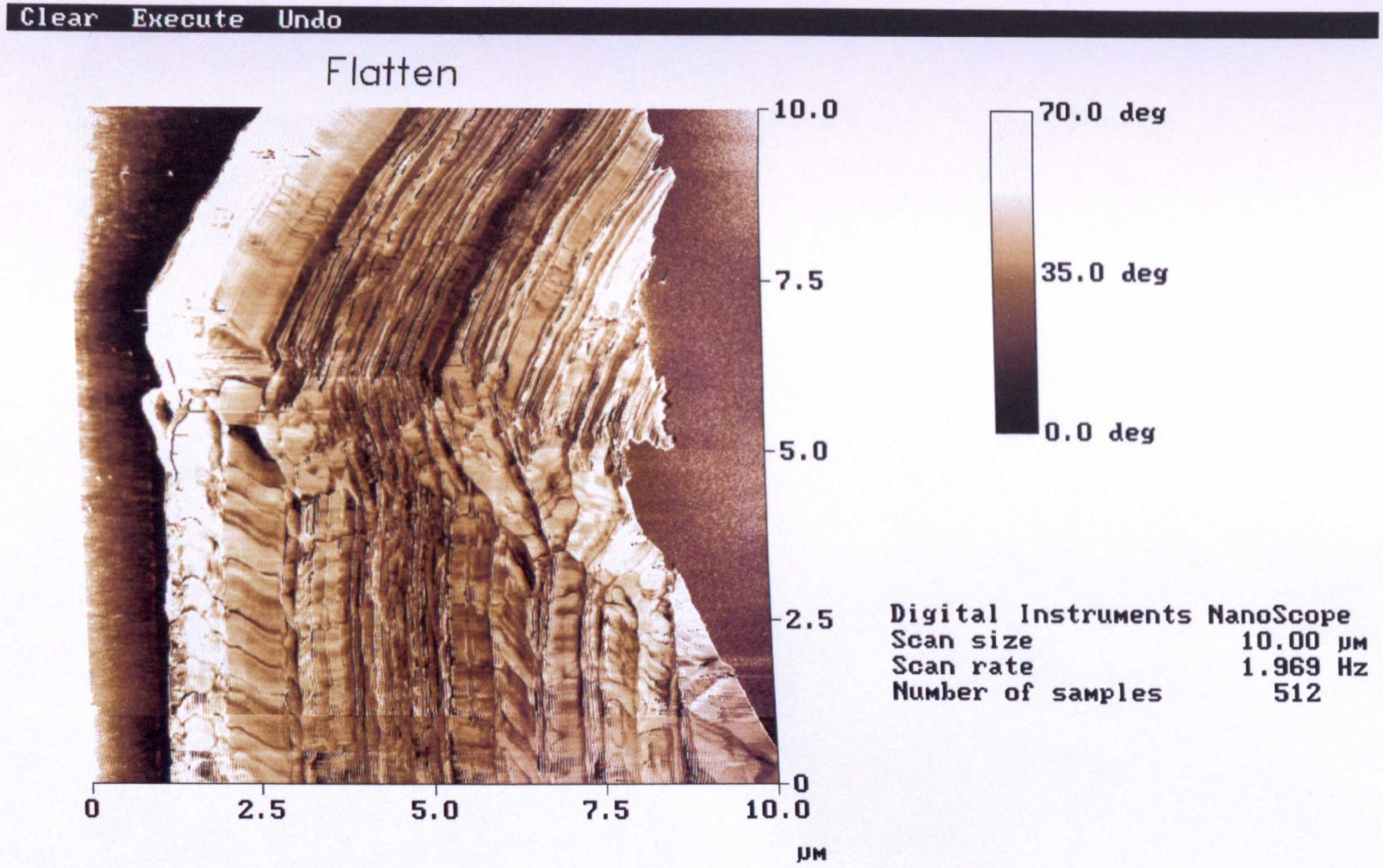

FILENAME: CP005c

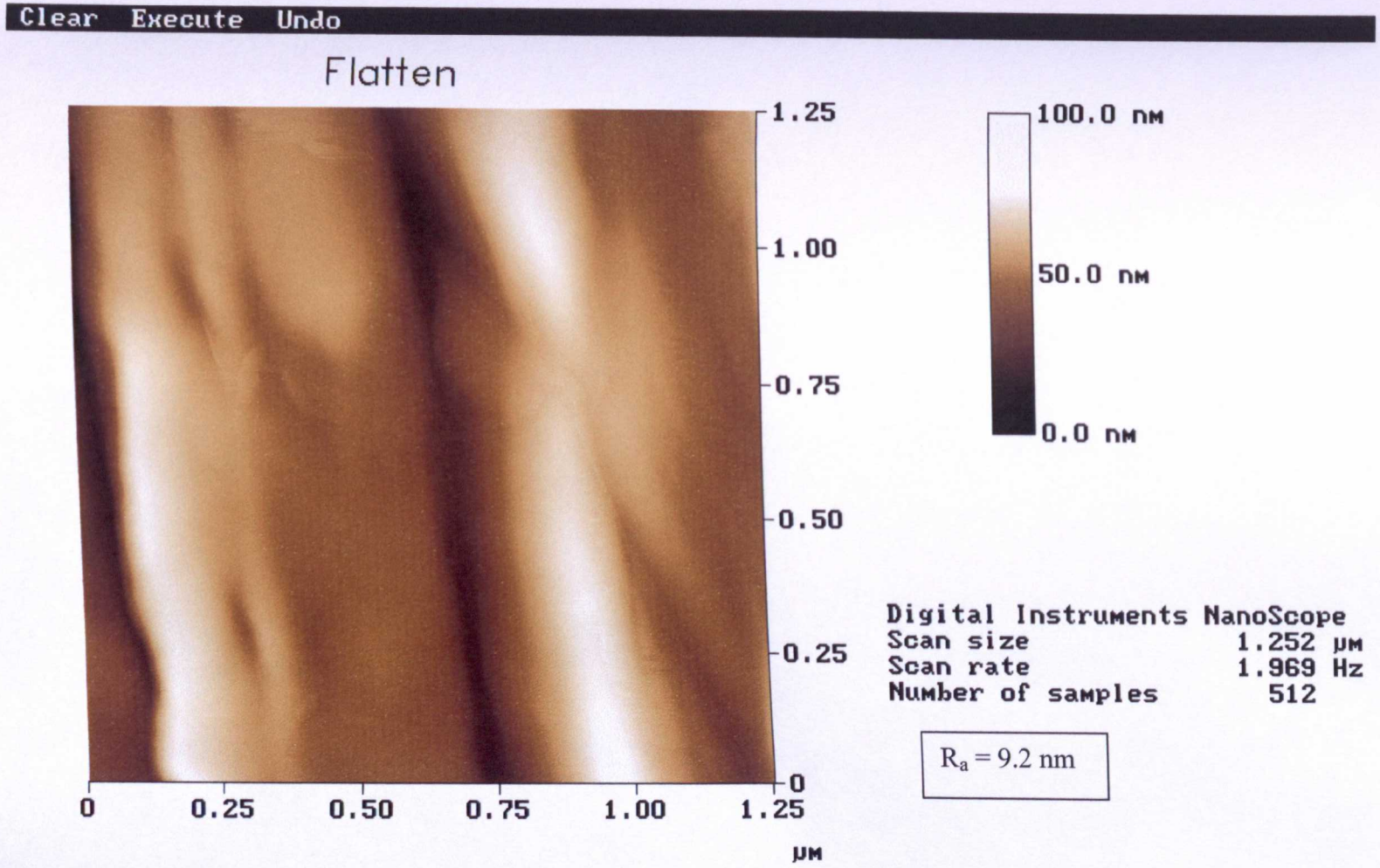

FILENAME: CP006a

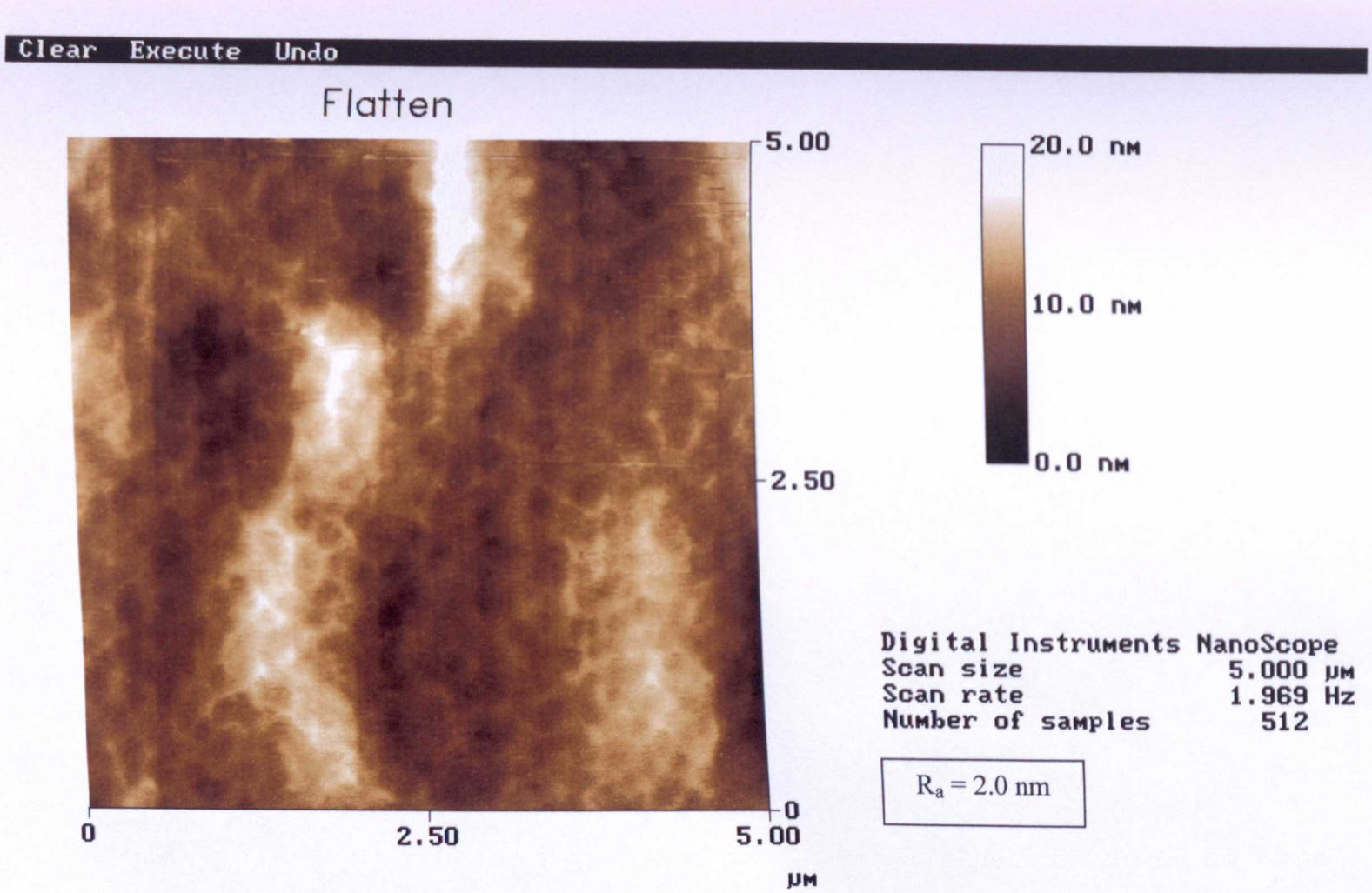

FILENAME: CP009a

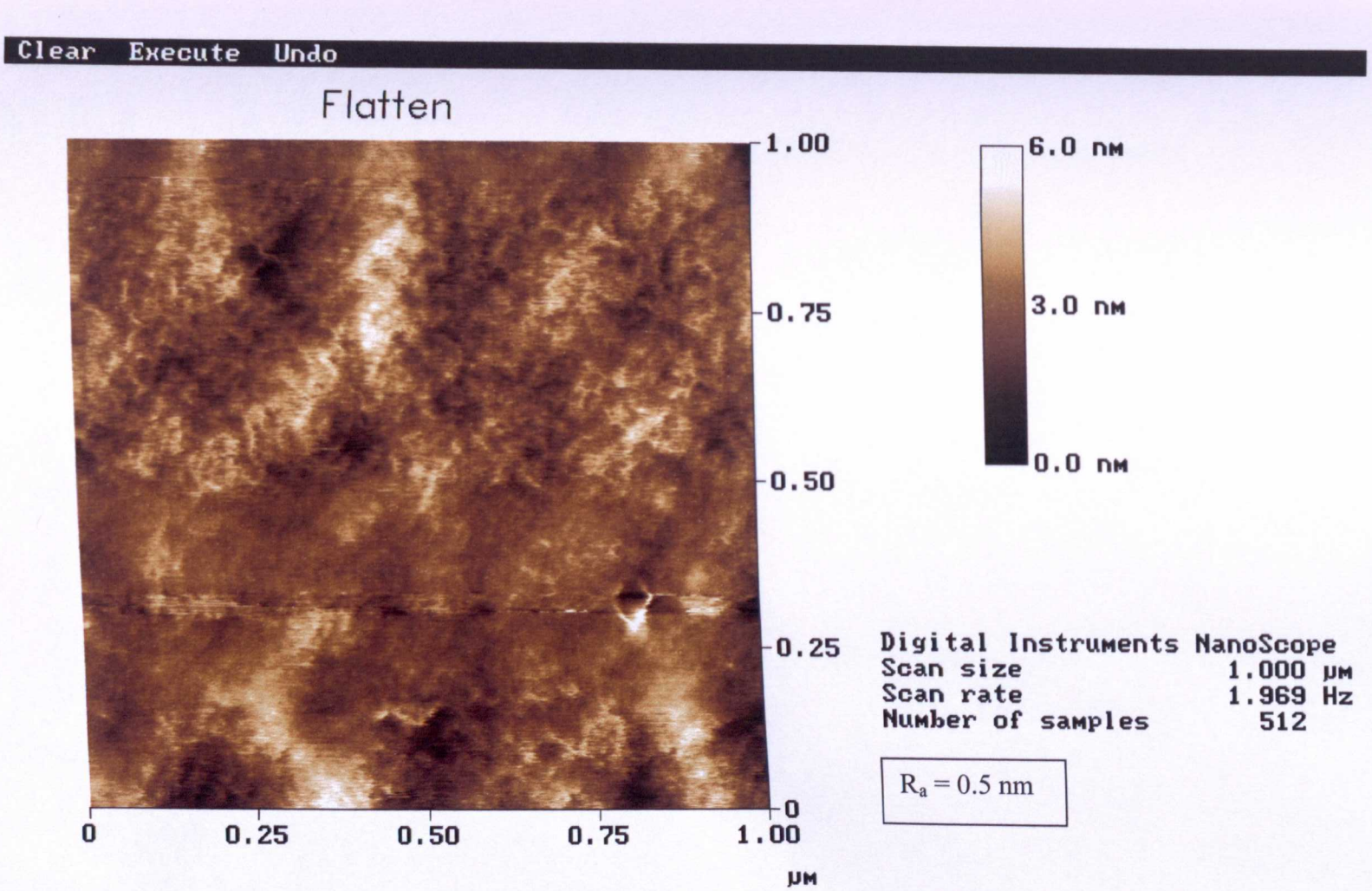

FILENAME: CP011a

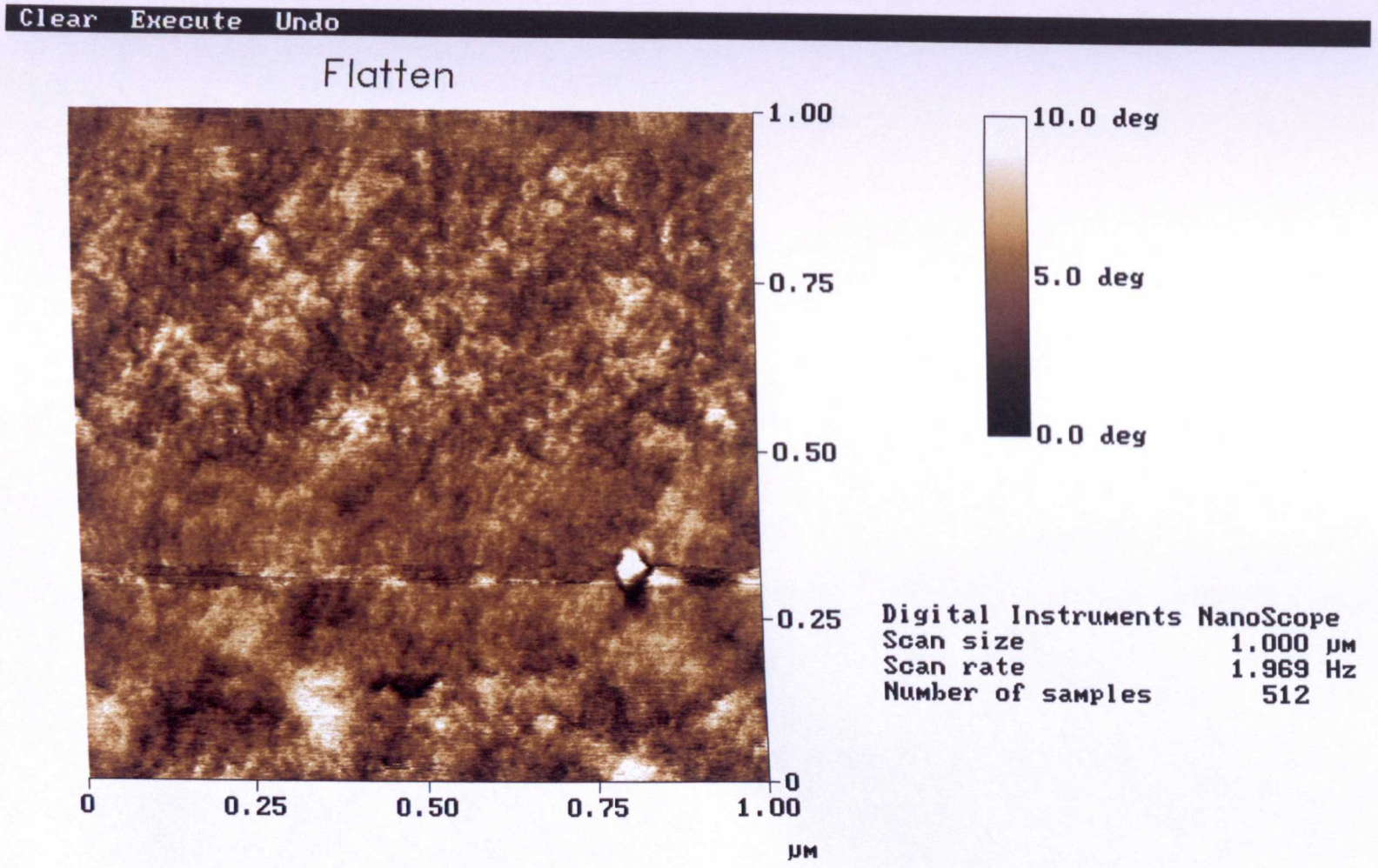

FILENAME: CP011c

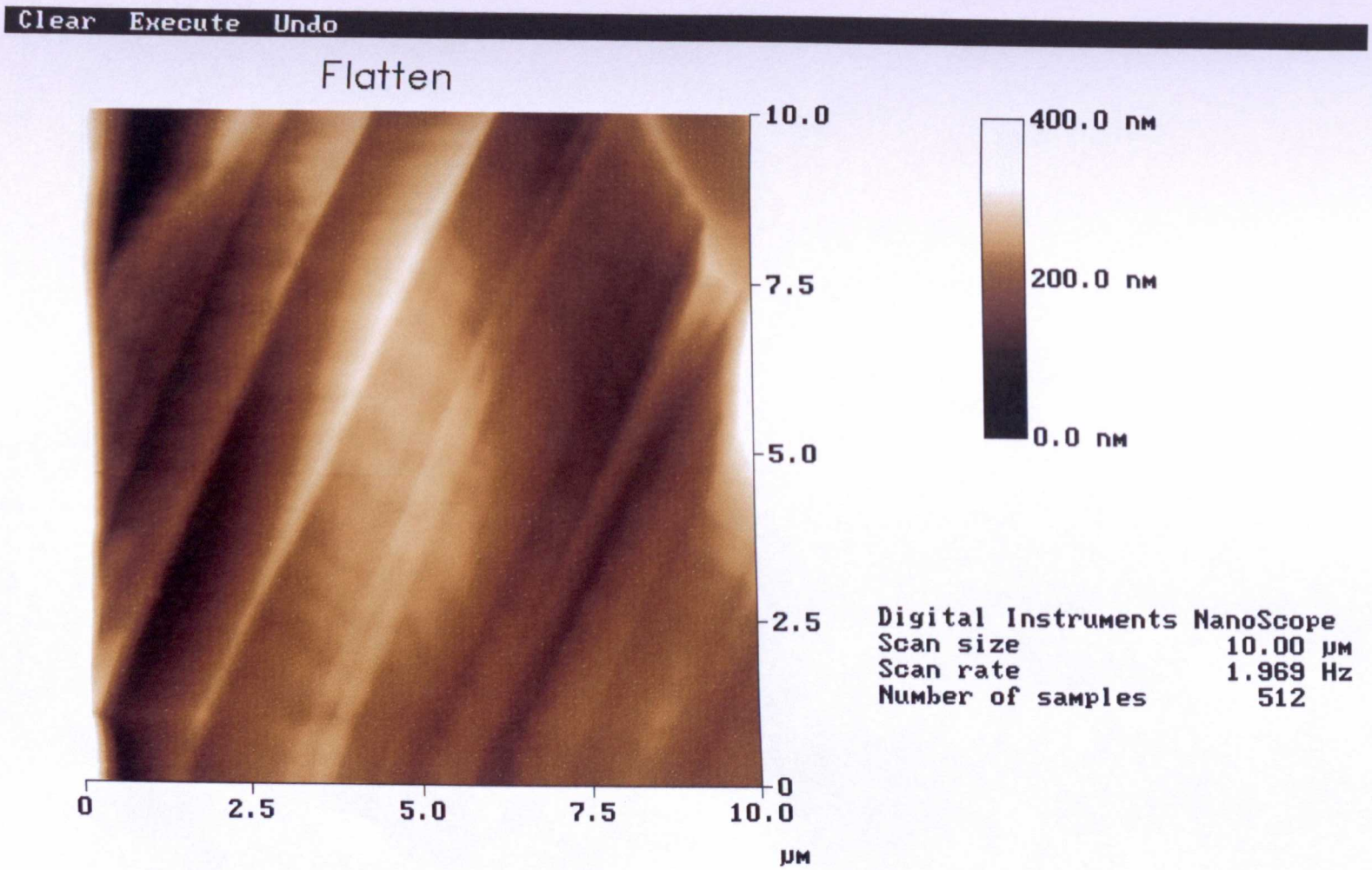

FILENAME: CP015a

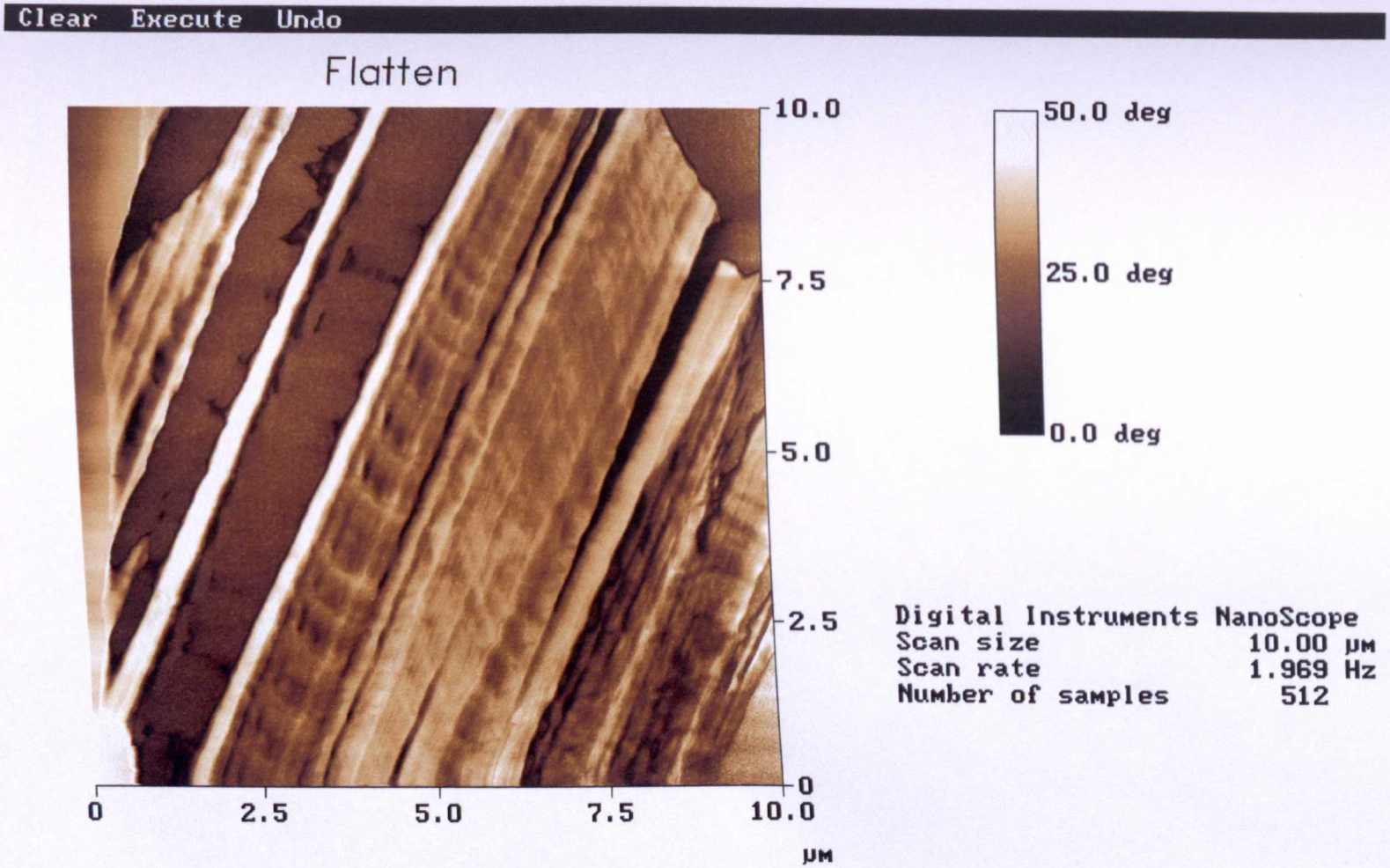

FILENAME: CP015b

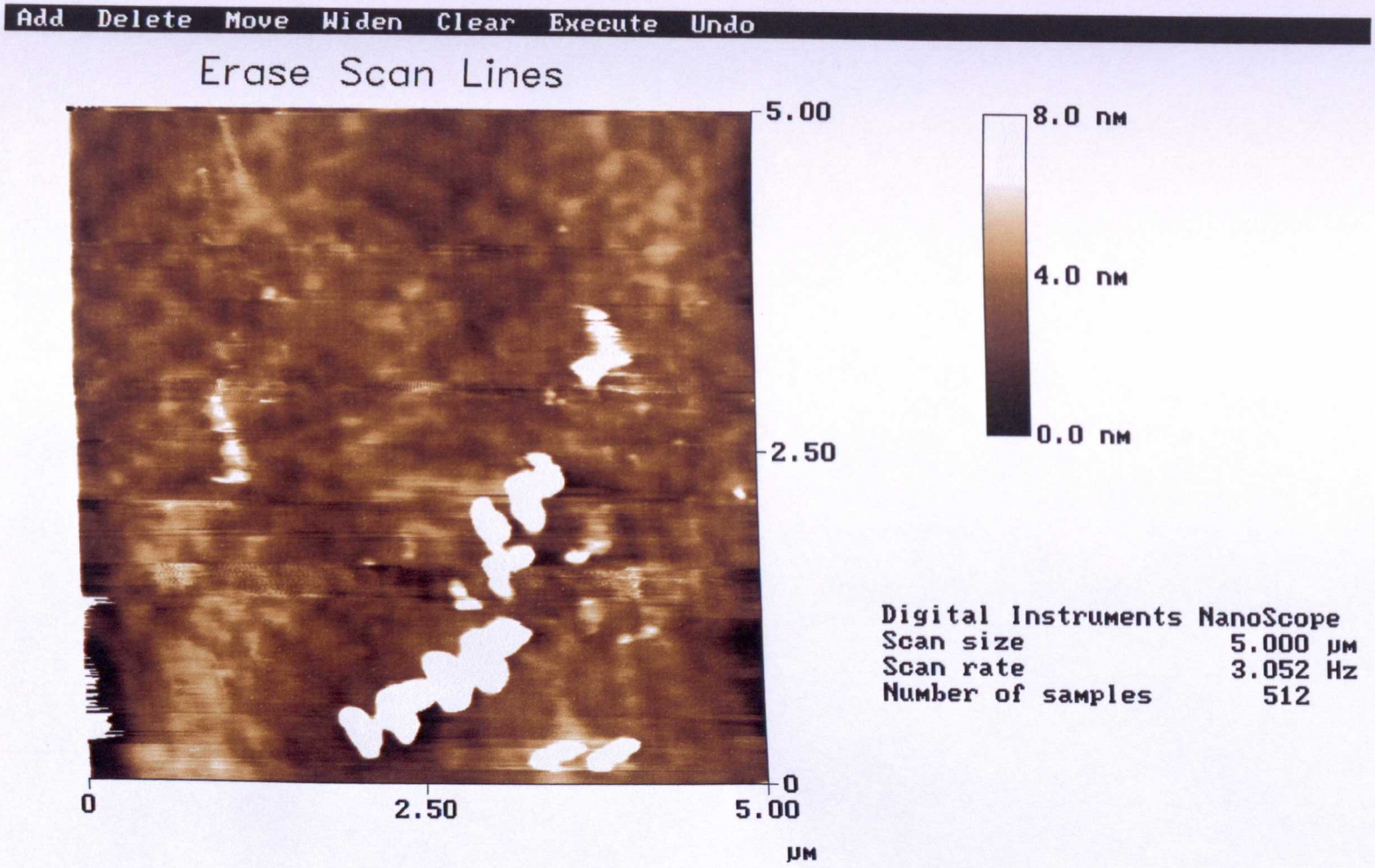

FILENAME: CP019a

Peak Surface Area Summit Zero Crossing Stopband Execute Clear

Roughness Analysis

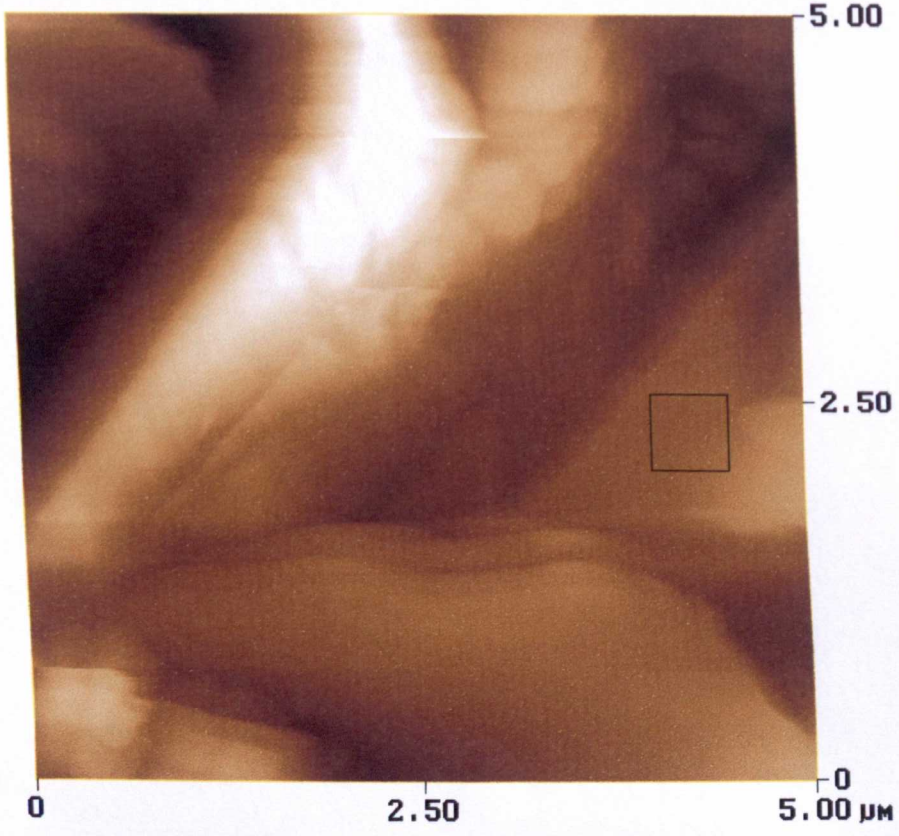

sc080900.000

Image Statistics

Img. Z range	1.219 µm
Img. Mean	-0.000003 nm
Img. Raw mean	154.86 nm
Img. Rms (Rq)	191.24 nm
Img. Ra	147.62 nm
Img. Rmax	1.219 µm
Img. Srf. area	33.022 µm²
Img. Srf. area diff	32.086 %

Box Statistics

Z range	92.448 nm
Mean	45.626 nm
Raw mean	-11.714 µm
Rms (Rq)	18.505 nm
Mean roughness (Ra)	4.566 nm
Box x dimension	499.02 nm
Box y dimension	499.02 nm

Peak off Area on Summit off Zero Cross off

FILENAME: 809CP00a

Peak Surface Area Summit Zero Crossing Stopband Execute Clear

Roughness Analysis

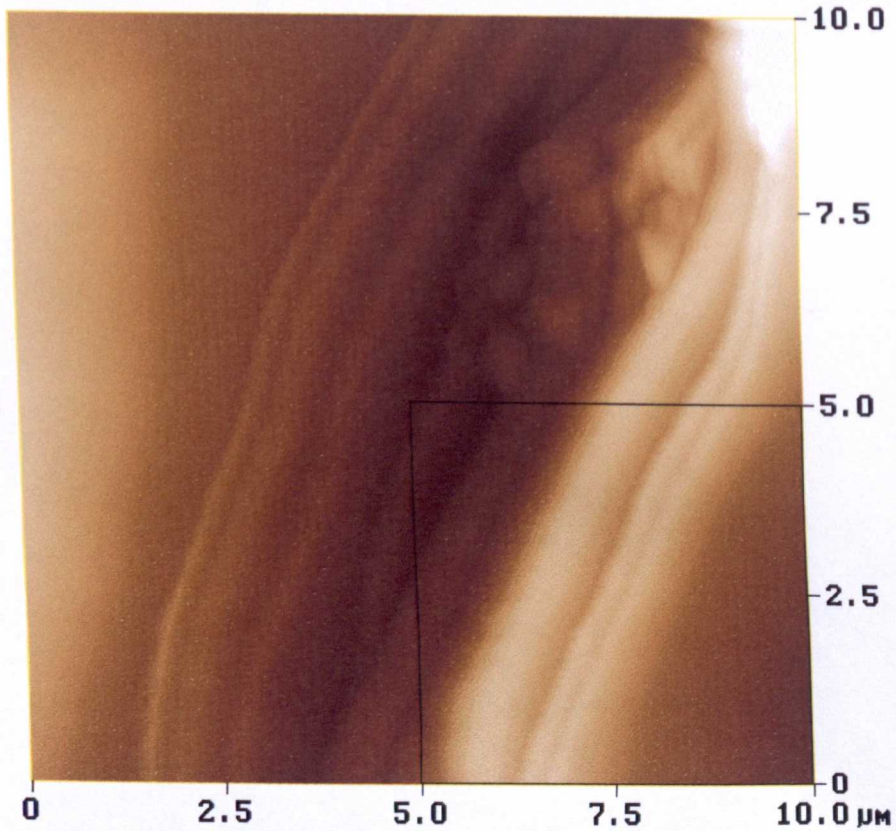

Image Statistics

Img. Z range	1.415 µm
Img. Mean	-0.014 nm
Img. Raw mean	-235.15 nm
Img. Rms (Rq)	264.09 nm
Img. Ra	223.39 nm
Img. Rmax	1.415 µm
Img. Srf. area	
Img. Srf. area diff	

Box Statistics

Z range	932.61 nm
Mean	51.131 nm
Raw mean	7.624 µm
Rms (Rq)	255.01 nm
Mean roughness (Ra)	223.16 nm
Box x dimension	5.010 µm
Box y dimension	5.010 µm

Peak off Area off Summit off Zero Cross off

FILENAME: 809CP01b

Peak Surface Area Summit Zero Crossing Stopband Execute Clear

Roughness Analysis

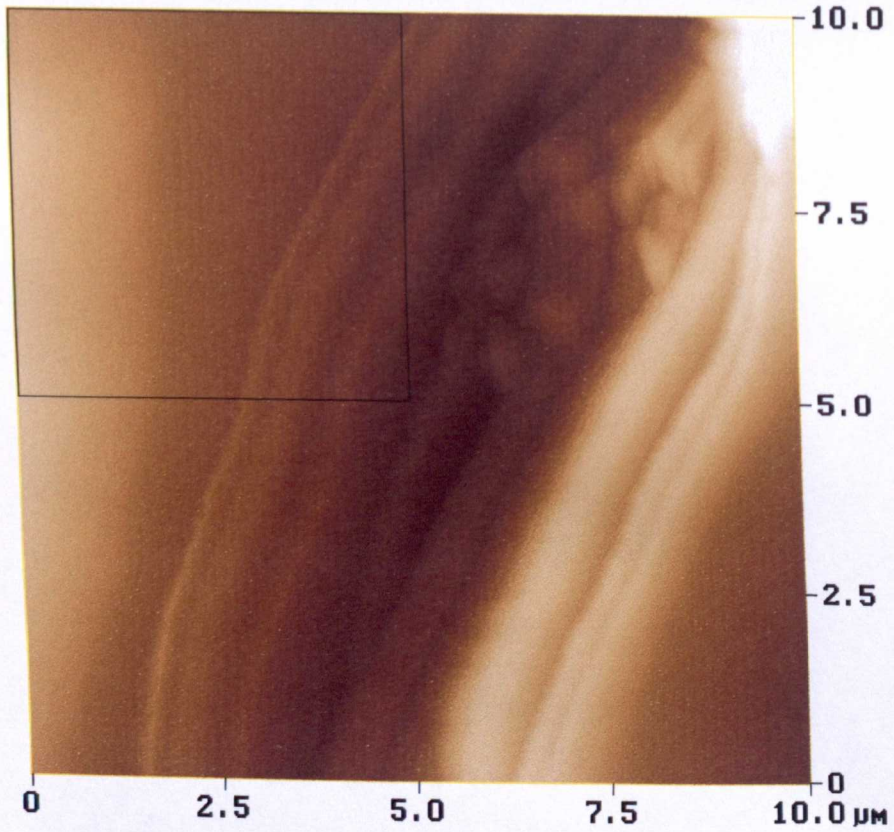

sc080900.001

Image Statistics

Img. Z range	1.415 µm
Img. Mean	-0.014 nm
Img. Raw mean	-235.15 nm
Img. Rms (Rq)	264.09 nm
Img. Ra	223.39 nm
Img. Rmax	1.415 µm
Img. Srf. area	
Img. Srf. area diff	

Box Statistics

Z range	864.31 nm
Mean	32.070 nm
Raw mean	-8.682 µm
Rms (Rq)	193.65 nm
Mean roughness (Ra)	29.193 nm
Box x dimension	5.010 µm
Box y dimension	5.010 µm

Peak off Area off Summit off Zero Cross off

FILENAME: 809CP01c

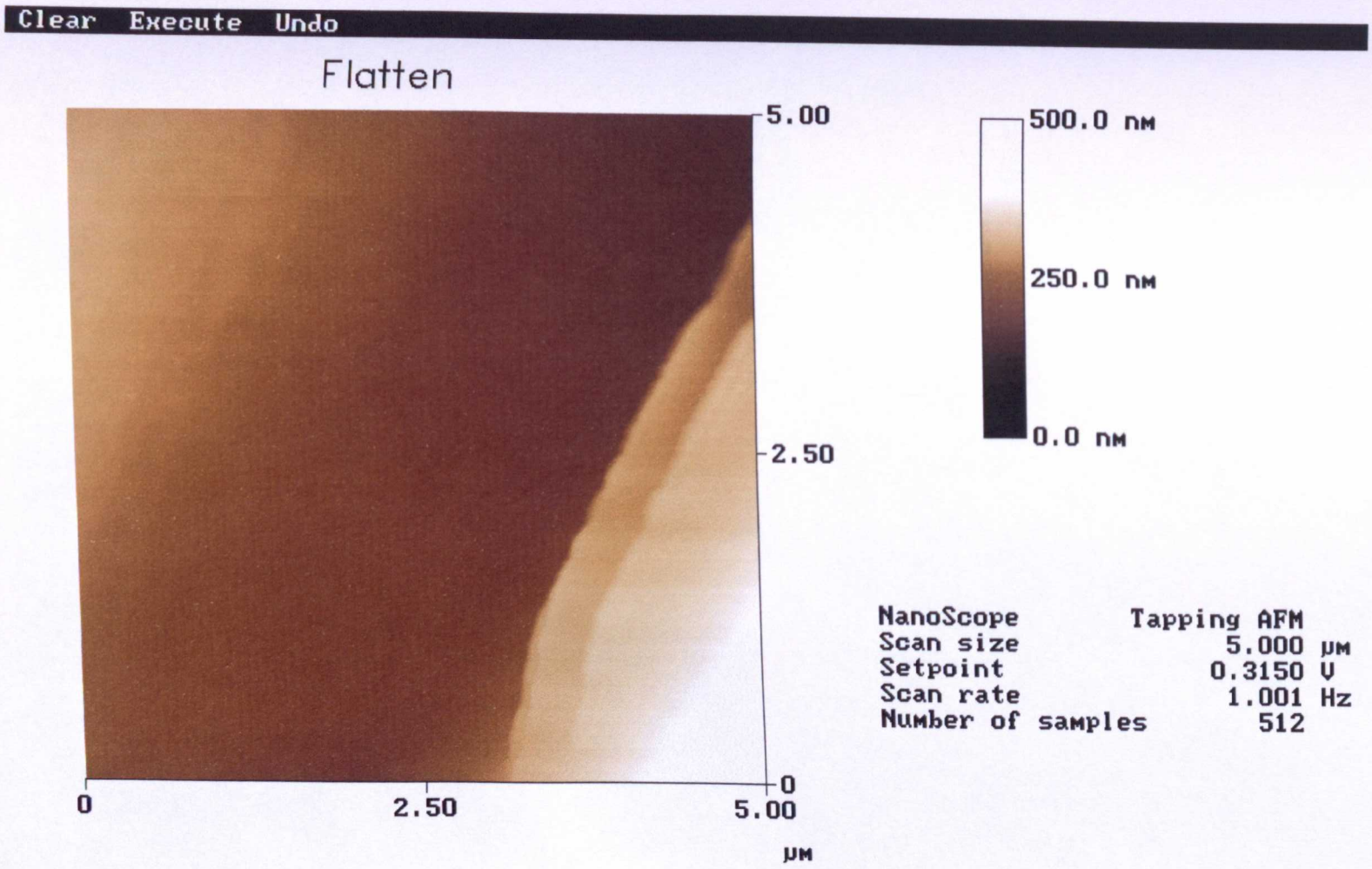

FILENAME: 809CP02a

Peak Surface Area Summit Zero Crossing Stopband Execute Clear

Roughness Analysis

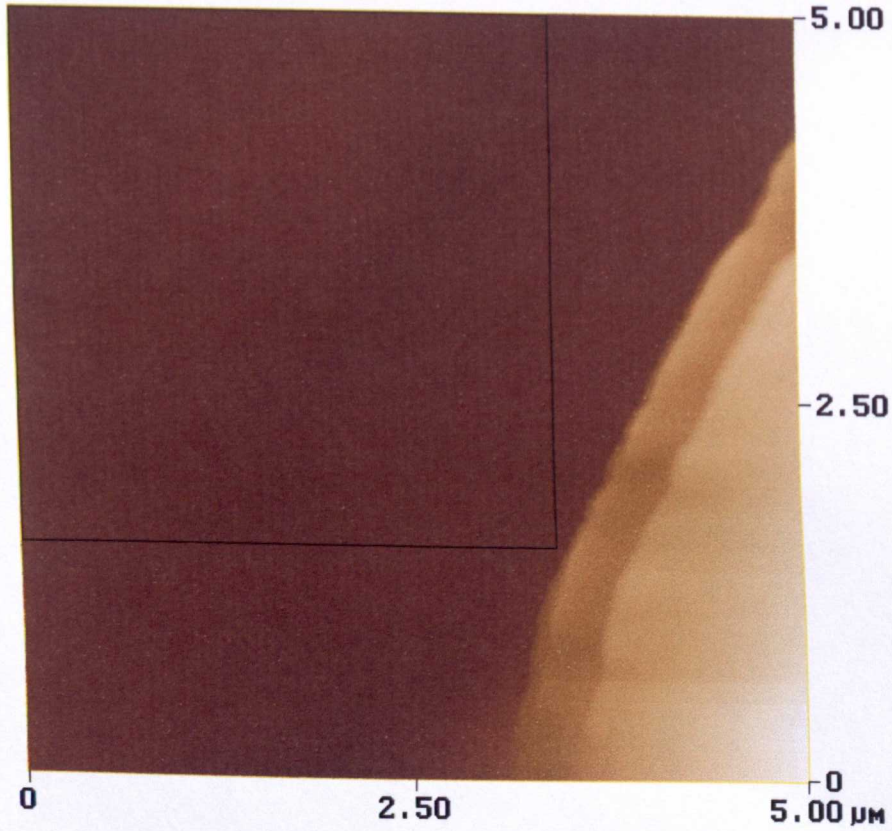

sc080900.002

Image Statistics

Img. Z range	261.82 nm
Img. Mean	0.008 nm
Img. Raw mean	-53.248 nm
Img. Rms (Rq)	55.668 nm
Img. Ra	34.415 nm
Img. Rmax	194.51 nm
Img. Srf. area	
Img. Srf. area diff	

Box Statistics

Z range	32.593 nm
Mean	-27.027 nm
Raw mean	3.585 µm
Rms (Rq)	5.376 nm
Mean roughness (Ra)	4.310 nm
Box x dimension	3.425 µm
Box y dimension	3.474 µm

Peak off Area off Summit off Zero Cross off

FILENAME: 809CP02c

Peak Surface Area Summit Zero Crossing Stopband Execute Clear

Roughness Analysis

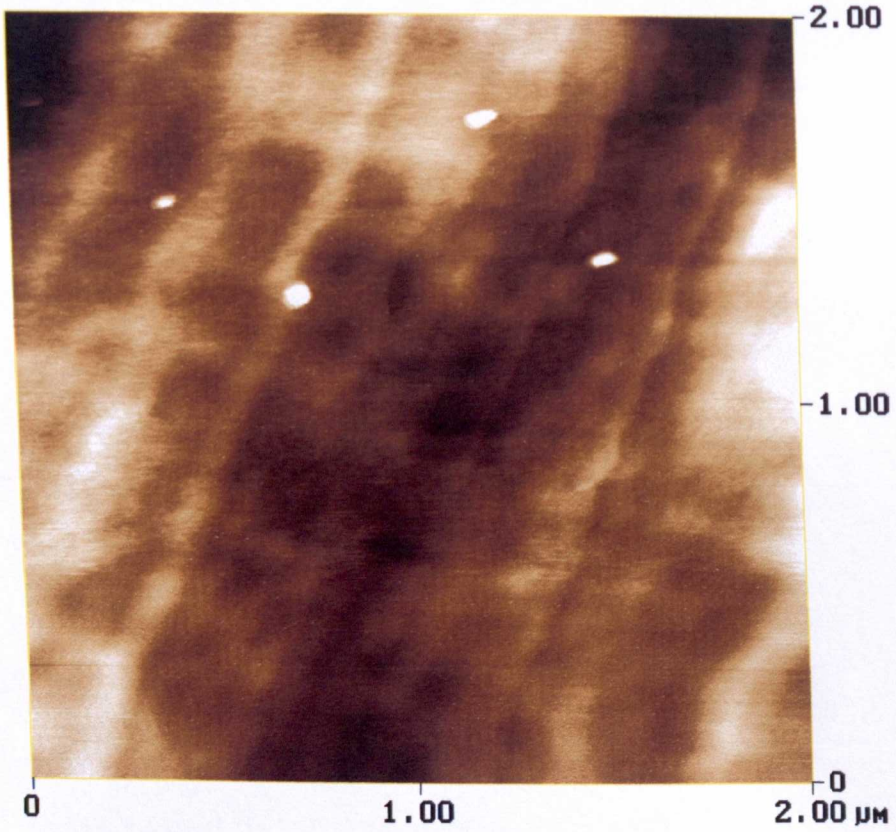

sc080900.003

Image Statistics

Img. Z range	22.079 nm
Img. Mean	-0.000000 nm
Img. Raw mean	-13.130 nm
Img. Rms (Rq)	2.453 nm
Img. Ra	1.981 nm
Img. Rmax	22.079 nm
Img. Srf. area	
Img. Srf. area diff	

Box Statistics

Z range
Mean
Raw mean
Rms (Rq)
Mean roughness (Ra)
Box x dimension
Box y dimension

Peak off Area off Summit off Zero Cross off

FILENAME: 809CP03a

Peak Surface Area Summit Zero Crossing Stopband Execute Clear

Roughness Analysis

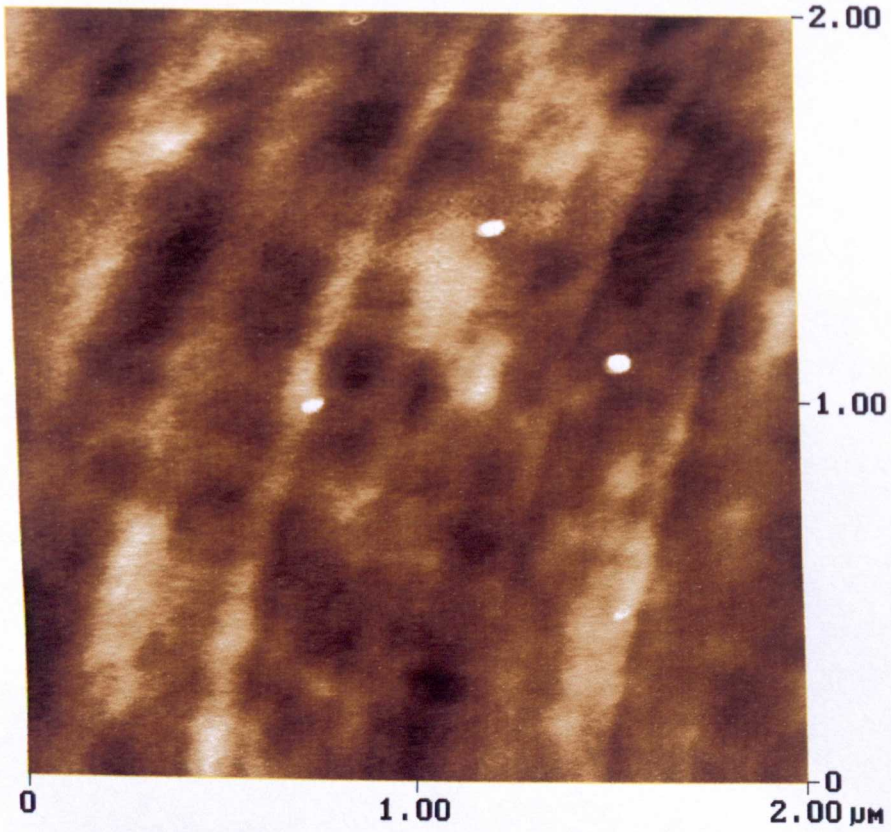

sc080900.004

Image Statistics

Img. Z range	14.138 nm
Img. Mean	0.002 nm
Img. Raw mean	-121.83 nm
Img. Rms (Rq)	1.209 nm
Img. Ra	0.956 nm
Img. Rmax	14.136 nm
Img. Srf. area	
Img. Srf. area diff	

Box Statistics

Z range
Mean
Raw mean
Rms (Rq)
Mean roughness (Ra)
Box x dimension
Box y dimension

Peak off Area off Summit off Zero Cross off

FILENAME: 809CP04

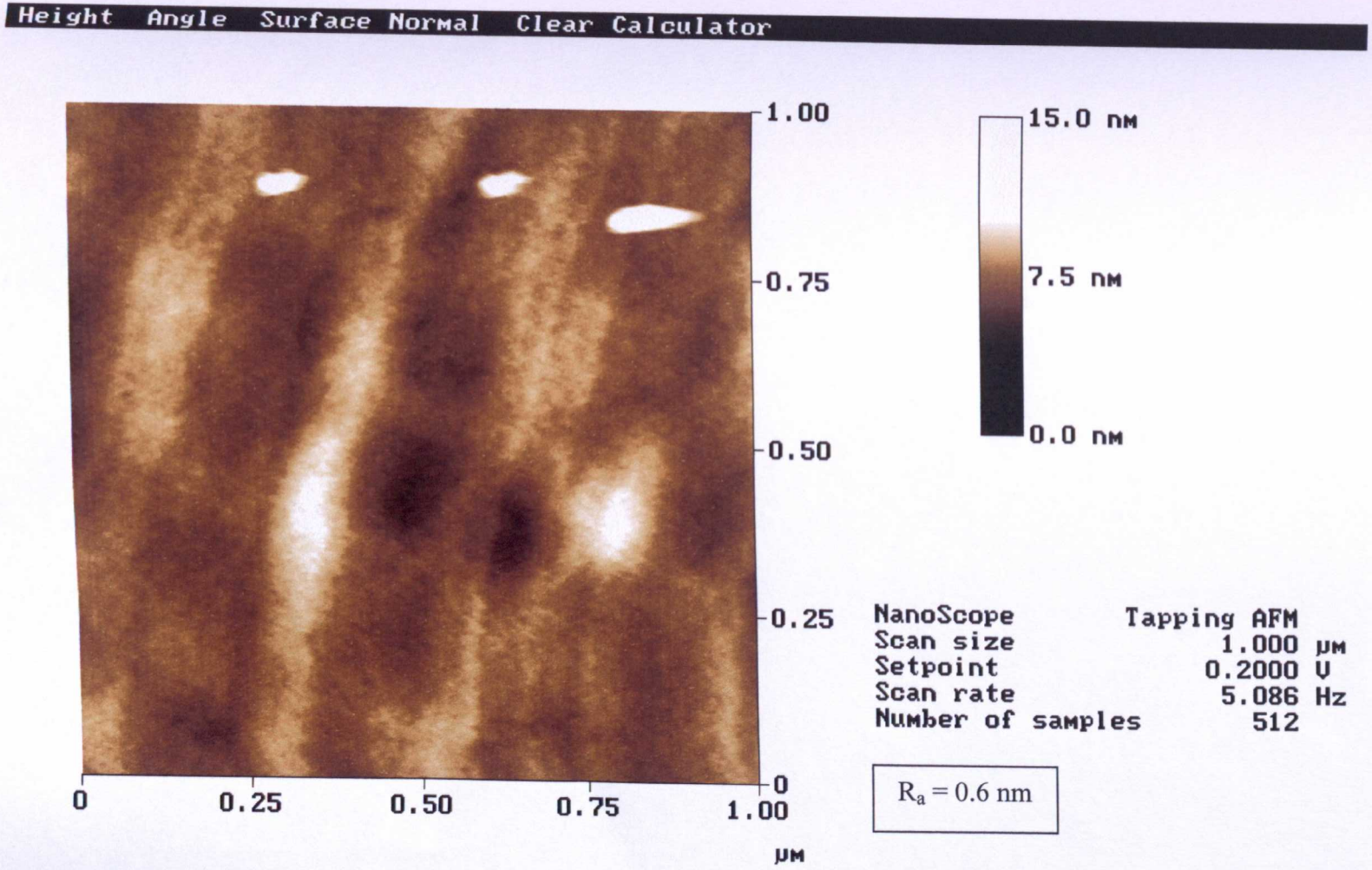

FILENAME: 809CP05a

Cursor Marker Spectrum Zoom Center Line Offset Clear

Section Analysis

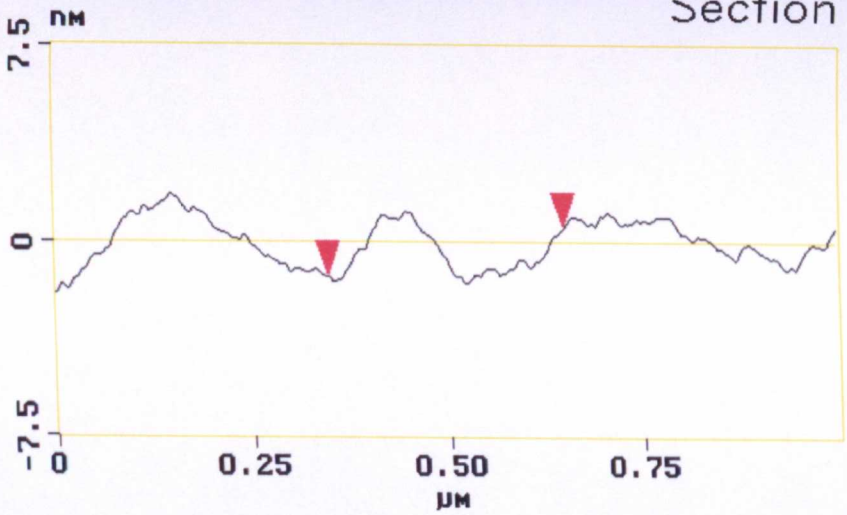

L	300.78 nm
RMS	0.848 nm
lc	DC
Ra(lc)	0.719 nm
Rmax	2.863 nm
Rz	2.600 nm
Rz Cnt	4

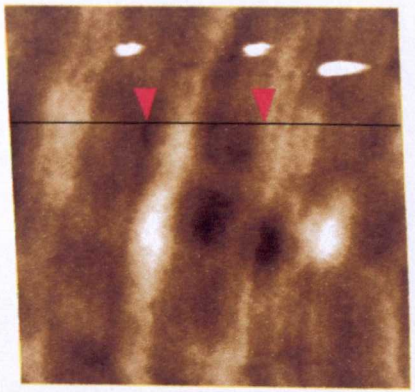

sc080900.005

Spectrum

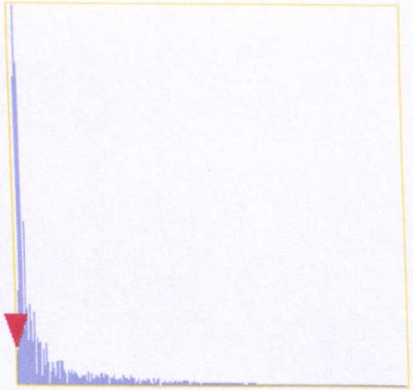

Surface distance	301.00 nm
Horiz distance(L)	300.78 nm
Vert distance	1.868 nm
Angle	0.356 deg
Surface distance	
Horiz distance	
Vert distance	
Angle	
Surface distance	
Horiz distance	
Vert distance	
Angle	
Spectral period	DC
Spectral freq	0 Hz
Spectral RMS amp	0.047 nm

Cursor: fixed Zoom: 2:1 Cen line: Off Offset: Off

FILENAME: 809CP05c

BIBLIOGRAPHY

Adler, M. & Lee, G. 1999. Stability and surface activity of lactate dehydrogenase in spray-dried trehalose. *Journal of Pharmaceutical Sciences.* **88** (2), 199-208.

Andya, J. D.; Maa, Y. F.; Constantino, H. R.; Nguyen, P. A.; Dasovich, N.; Sweeney, T. D.; Hsu, C. C. & Shire, S. J. 1999. The effect of formulation excipients on protein stability and aerosol performance of spray-dried powders of a recombinant humanized anti-IgE monoclonal antibody. *Pharmaceutical Research.* **16** (3), 350-358.

Armstrong, C. L.; Forbes, R. T.; Blair, J. & York, P. 1996. Thermal behaviour of α,α-trehalose dihydrate batches. *European Journal of Pharmaceutical Sciences.* **4** (Suppl. 1), S181.

Beckmann, W. 2003. Crystallization of pharmaceutical compounds – polymorphs, pseudo-polymorphs and particle formation. *Engineering in Life Sciences.* **3**, 113-120.

Begat, P.; Young, P. M.; Edge, S.; Kaerger, S. & Price, R. 2003. The effect of mechanical processing on surface stability of pharmaceutical powders: Visualization by atomic force microscopy. *Journal of Pharmaceutical Sciences.* **92** (3), 611-620.

Bennett, F. S.; Carter, P.A.; Rowley, G. & Dandiker, Y. 1999. Modification of electrostatic charge on inhaled carrier lactose particles by addition of fine particles. *Drug Development and Industrial Pharmacy.* **25** (1), 99-103.

Bhandari, B. R. & Howes, T. 2000. Glass transition in processing and stability of food. *Food Australia.* **52** (12), 579-582.

Buckton, G. 1995. Surface characterisation: Understanding sources of variability in the production and use of pharmaceuticals. *Journal of Pharmacy and Pharmacology.* **47**, 265-275.

Buckton, G. 1997. Characterisation of small changes in the physical properties of powders of significance for dry powder inhaler formulations. *Advanced Drug Delivery Reviews.* **26**, 17-27.

Cammenga, H. K. & Zielasko, B. 1996. Glasses of sugars and sugar substitutes. *Physical Chemistry Chemical Physics.* **100** (9), 1607-1609.

Cardew, P. T. & Davey, R. G. 1985. *Journal of Royal Society of Medicine. Proc Roy Soc, London.* **A398**, 415-428.

Cardew, P. T. & Davey, R. J. 1979. Evaluation of supersaturation in crystal growth from solution. *Journal of Crystal Growth.* **46** (4), 534-538.

Carter, P. A.; Rowley, G.; Fletcher, E.J. & Stylianopoulos, V. 1998. Measurement of electrostatic charge decay in pharmaceutical powders and polymers used in dry powder inhaler devices. *Drug Development and Industrial Pharmacy.* **24** (11), 1083-1088.

Chang, L. W.; Lim, L. T. & Heng, P. W. S. 2003. Immobilization of fine particles on lactose carrier by precision coating and its effect on the performance of dry powder formulations. *Journal of Pharmaceutical Sciences.* **92** (5), 975-984.

Chew, N. Y. K. & Chan, H-K. 1999. Influence of particle size, air flow, and inhaler device on the dispersion of mannitol powders as aerosols. *Pharmaceutical Research.* **16** (7), 1098-1103.

Chew, N. Y. K. & Chan, H-K. 2001. Use of solid corrugated particles to enhance powder aerosol performance. *Pharmaceutical Research.* **18** (11), 1570-1577.

Cline, D. & Dalby, R. 2002. Predicting the quality of powders for inhalation from surface energy and area. *Pharmaceutical Research.* **19** (9), 1274-1277.

Ding, S. P.; Fan, J.; Green, J. L.; Lu, Q.; Sanchez, E. & Angell, C. A. 1996. Vitrification of trehalose by water loss from its crystalline dihydrate. *Journal of Thermal Analysis.* **47**, 1391-1405.

El-Baseir, M.; Phipps, M. & Kellaway, I. 1997. Preparation and subsequent degradation of poly (L-lactic acid) microspheres suitable for aerosolisation: a physico-chemical study. *International Journal of Pharmaceutics.* **151**, 145-153.

Elliott, S.R. 1990. *Physics of Amorphous Materials* (2nd ed.). London, Longman Scientific & Technical.

Florence, A.T. & Attwood, D. 1988. *Physiochemical Principles of Pharmacy* (2nd ed.). 24-32. London, MacMillan Press Ltd.

Ganderton, D. 1992. The generation of respirable clouds from coarse powder aggregates. *Journal of Biopharmaceutical Sciences.* **3,** 101-105.

Ganellin, C.R. & Roberts, S.M. 1993. *Medicinal Chemistry: The role of Organic Chemistry in Drug Research* (2nd ed.). 38,242-246. London, Academic Press Ltd.

Grimsey, I. M.; Feeley, J. C. & York, P. 2002. Analysis of the Surface Energy of Pharmaceutical Powders by Inverse Gas Chromatography. *Journal of Pharmaceutical Sciences.* **91** (2), 571-583.

Gu, C-H.; Young Jr., V. & Grant, D. J. W. 2001. Polymorph screening: Influence of solvents on the rate of solvent-mediated polymorphic transformation. *Journal of Pharmaceutical Sciences.* **90** (11), 1878-1890.

Hancock, B. C. & Shamblin, S. L. 1998. Water vapour sorption by pharmaceutical sugars. *Pharmaceutical Science and Technology Today.* **1** (8), 345-351.

Hancock, B. C. & Zografi, G. 1997. Characteristics and Significance of the Amorphous State in Pharmaceutical Systems. *Journal of Pharmaceutical Science.* **86** (1), 1-12.

Hancock, B. C.; Shamblin, S. L. & Zografi, G. 1995. Molecular Mobility of Amorphous Pharmaceutical Solids Below Their Glass Transition Temperatures. *Pharmaceutical Research.* **12** (6), 799-806.

Heng, P. W. S.; Chan, L. W. & Lim, L. T. 2000. Quantification of the surface morphologies of lactose carriers and their effect on the *in Vitro* deposition of salbutamol sulphate. *Chemical and Pharmaceutical Bulletin.* **48** (3), 393-398.

Hickey, A.J. & Concessio, N.M. 1997. Descriptors of irregular particle morphology and powder properties. *Advanced Drug Delivery Reviews.* **26**, 29-40.

Hildebrand, J.H. & Scott, R.L. 1962. *Regular Solutions*. New Jersey, Prentice –Hall.

Holden, A. & Singer, P. 1964. *Crystals and Crystal Growing.* 32-36,74-77. London, Heinemann Educational Books Ltd.

Iida, K.; Leuenberger, H.; Fueg, L. M.; Muller-Walz, R. & Danjo, K. 1999. Effect of separation characteristics between salbutamol sulphate particles and model carrier excipients on dry powder for inhalation. *Journal of the Pharmaceutical Society of Japan.* **119** (10), 752-762.

Jeffrey, G.A. & Nanni, R. 1985. The crystal structure of anhydrous α,α-trehalose at -150°. *Carbohydrate Research.* **137**, 21-30.

Kawashima, Y.; Serigano, T.; Hino, T.; Yamamoto, H. & Takeuchi, H. 1998. Effect of surface morphology of carrier lactose on dry powder inhalation property of pranlukast hydrate. *International Journal of Pharmaceutics.* **172**, 179-188.

Kawashima, Y.; Serigano, T.; Hino, T.; Yamamoto, H. & Takeuchi, H. 1998. A new powder design method to improve inhalation efficiency of pranlukast hydrate dry powder aerosols by surface modification with hydroxypropylmethylcellulose phthalate nanospheres. *Pharmaceutical Research.* **15** (11), 1748-1752.

Keey, R.B. 1972. *Drying: Principles and Practice.* Oxford, Pergamon Press.

Khoshkhoo, S. & Anwar, J. 1991. Crystallisation of polymorphs: Effects of supersaturation and solvent. *Journal of Pharmacy and Pharmacology.* **43**, Suppl., 72P.

Lammert, A.M. 1997. *Physical aging, solubility and water activity of selected disaccharides.* Illinois: University of Illinois, Thesis (Ph.D.).

Lammert, A.M., Schmidt, S.J. & Day, G.A. 1998. Water activity and solubility of trehalose. *Food Chemistry.* **61** (1/2), 139-144.

Larhrib, H.; Zeng, X. M.; Martin, G. P.; Marriott, C. & Pritchard, J. 1999. The use of different grades of lactose as a carrier for aerosolised salbutamol sulphate. *International Journal of Pharmaceutics.* **191**, 1-14.

Lin, S. Y. & Chien, J. L. 2003. *In vitro* simulation of solid-solid dehydration, rehydration, and solidification of trehalose dihydrate using thermal and vibrational spectroscopic techniques. *Pharmaceutical Research.* **20** (12), 1926-1931.

Liu, Q.; Schmidt, R.K., Teo, B., Karplus, P. A. & Brady, J.W. 1997. Molecular dynamics studies of the hydration of α,α-trehalose. *J. Am. Chem. Soc.* **119**, 7851-7862.

Lucas, P.; Anderson, K. & Staniforth, J. N. 1998. Protein deposition from dry powder inhalers: fine particle multiplets as performance modifiers. *Pharmaceutical Research.* **15** (4), 562-569.

Miers, H. A. & Isaac, F. 1906. Refractive indices of crystallizing solutions. *Journal of the Chemical Society.* **89**, 413-454.

Miers, H. A. & Isaac, F. 1907. The spontaneous crystallisation of binary mixtures. *Proceedings of the Royal Society.* **A79**, 322-351.

Miller, D.P., de Pablo, J.J. & Corti, H. 1997. Thermophysical properties of trehalose and its concentrated aqueous solutions. *Pharmaceutical Research.* **14** (5), 578-590.

Mullin, J.W. 1993. *Crystallisation* (3rd ed.). London, Butterworth Heinemann Ltd.

Mullins, J.D. & Macek, T.J. 1960. *J. Am. Pharm.* **49**, 245-248.

Musante, C. J.; Schroeter, J. D.; Rosati, J. A.; Crowder, T. M.; Hickey, A. J. & Martonen, T. B. 2002. Factors affecting the deposition of inhaled porous particles. *Journal of Pharmaceutical Sciences.* **91** (7), 1590-1600.

Muster, T. H. & Prestidge, C. A. 2002. Face Specific Surface Properties of Pharmaceutical Crystals. *Journal of Pharmaceutical Sciences.* **91** (6), 1432-1444.

Olsson, B. 1995. Aerosol particle generation from dry powder inhalers: can they equal pressurised metered dose inhalers? *J. Aerosol Med.* **8** (suppl. 3), 13-18.

Park, Y.T. & Shin, J.M. 1993. Two polymorphs of structures of α,α-trehalose octaacetate monohydrate. *Bull. Korean Chem. Soc.* **14** (2), 200-206.

Philip, V. A.; Mehta, R. C.; Mazumder, M. K. & DeLuca, P. P. 1997. Effect of surface treatment on the respirable fractions of PLGA microspheres formulated for dry powder inhalers. *International Journal of Pharmaceutics.* **151**, 165-174.

Podczeck, F. 1999. The influence of particle size distribution and surface roughness of carrier particles on the in-vitro properties of dry powder inhalations. *Aerosol Science and Technology.* **31** (4), 301-321.

Quadrant Healthcare plc., TM/99/053.

Raghavan, S. L.; Ristic, R. I.; Sheen D. B. & Sherwood J. N. 2001. The bulk crystallisation of α-lactose monohydrate from aqueous solution. *Journal of Pharmaceutical Sciences.* **90** (7), 823-832.

Rees, P., Clark, T. & Moren, F. 1982. The importance of particle size in response to inhaled bronchodilators. *Eur. J. Respir. Dis.* **119**, 73-78.

Richards, A. B.; Krakowka, S.; Dexter, L. B.; Schmid, H.; Wolterbeek, A. P. M.; Waalkens-Berendsen, D. H.; Shigoyuki, A. & Kurimoto, M. 2002. Trehalose: a review of properties, history of use and human tolerance, and results of multiple safety studies. *Food and Chemical Toxicology.* **40** (7), 871-898.

Richards, J.H. 1988. Solubility and Dissolution Rate. pp63-72 In: M. E. Aulton (ed.) *Pharmaceutics: The Science of Dosage Form Design.* Edinburgh, Churchill Livingstone.

Saleki-Gerhardt, A. 1993. *The role of water in the solid state properties of crystalline and amorphous sugars.* Wisconsin, University of Wisconsin, Thesis (Ph.D.).

Sato, K. & Boistelle, R. 1983. *Journal of Colloid Interface Science.* **94** (2), 593-596.

Scheuch, G. & Stahlhofen, W. 1992. Deposition and dispersion of aerosols in the airways of the human respiratory tract: the effect of particle size. *Exp. Lung Res.* **18** (3), 343-358.

Shamblin, S. L. & Zografi, G. 1998. Enthalpy relaxation in binary amorphous mixtures containing sucrose. *Pharmaceutical Research.* **15** (12), 1828-1834.

Shekunov, B. Y. & York, P. 2000. Crystallisation processes in pharmaceutical technology and drug delivery design. *Journal of Crystal Growth.* **211**, 122-136.

Sinko, C. M.; Yee, A. F. & Amidon, G. L. 1991. Prediction of Physical Aging in Controlled-Release Coatings: The Application of the Relaxation Coupling Model to Glassy Cellulose Acetate. *Pharmaceutical Research.* **8** (6), 698-705.

Soltani, M. & Ahmadi, G. 1994. On particle adhesion and removal mechanisms in turbulent air flows. *J. Adhesion Sci. Technol.* **8**, 763-785.

Srichana, T.; Martin, G. P. & Marriott, C. 1998. On the relationship between drug and carrier deposition from dry powder inhalers in vitro. *International Journal of Pharmaceutics.* **167**, 13-23.

Stuart, B. O. 1984. Deposition and clearance of inhaled particles. *Environ. Health Perspect.* **55**, 369-390.

Sussich, F.; Princivalle, F. & Cesàro, A. 1999. The interplay of the rate of water removal in the dehydration of α,α-trehalose. *Carbohydrate Research.* **322**, 113-199.

Swaminathan, V. & Kildsig, D. 2000. The effect of particle morphology on the physical stability of pharmaceutical powder mixtures: The effect of surface roughness of the carrier on the stability of ordered mixtures. *Drug Development and Industrial Pharmacy.* **26** (4), 365-373.

Swarbrink, J. & Boylan, J.C. 1995. *Encyclopaedia of Pharmaceutical Technology: Volume 12.* 305-306,322-324. London, Marcel Dekker.

Taylor, L. S. & York, P. 1998. Characterisation of the phase transitions of trehalose dihydrate on heating and subsequent dehydration. *Journal of Pharmaceutical Sciences.* **87** (3), 347-355.

Taylor, L. S. & York, P. 1998. Effect of particle size and temperature on the dehydration kinetics of trehalose dihydrate. *International Journal of Pharmaceutics.* **167**, 215-221.

Taylor, L. S.; Williams, A. C. & York, P. 1998. Particle size dependent molecular rearrangements during the dehydration of trehalose dihydrate *in situ* FT-Raman spectroscopy. *Pharmaceutical Research.* **15** (8), 1207-1214.

Thorsson, L. 1995. Influence of inhaler systems on systemic availability, with focus on inhaled corticosteroids. *J Aerosol Med.* **8** (suppl. 3), S29-S36.

Tiller, W.A. 1991. *The Science of Crystallisation – Microscopic Interfacial Phenomena.* Cambridge, Cambridge University Press.

Vanbever, R.; Mintzes, J. D.; Wang, J.; Nice, J.; Chen, D.; Batycky, R.; Langer, R. & Edwards, D. A. 1999. Formulation and physical characterisation of large porous particles for inhalation. *Pharmaceutical Research.* **16** (11), 1735-1742.

Wade, A. & Weller, P. J. (eds.) 1994. *Handbook of Pharmaceutical Excipients* (2nd ed.). London, The Pharmaceutical Press.

Wells, J. I. 1988. *Pharmaceutical Preformulation: The Physiochemical Properties of Drug Substances.* London, Ellis Horwood Ltd.

Wilson, R. 1997. pp9-42 In J. C. Vickerman (ed.) *Surface Analysis.* Chichester, John Wiley & Sons.

Young, J. P. & Shin, J. M. 1993. Two Polymorphs of Structures of α,α-Trehalose Octaacetate Monohydrate. *Bull. Korean Chem. Soc.* **14**, 200-206.

Yu, L.; Reutzel, S. M. & Stephenson, G. A. 1998. Physical characterization of polymorphic drugs: an integrated characterization strategy. *Pharmaceutical Science and Technology Today.* **1** (3), 118-127.

Zallen, R. 1983. *The Physics of Amorphous Solids.* New York, John Wiley & Sons.

Zeng, X. M.; Martin, G. P.; Marriott, C. & Pritchard, J. 2000. The influence of carrier morphology on drug delivery by dry powder inhalers. *International Journal of Pharmaceutics.* **200**, 93-106.

Zeng, X. M.; Martin, G. P.; Marriott, C. & Pritchard, J. 2000. The influence of crystallisation conditions on the morphology of lactose intended for use as a carrier for dry powder aerosols. *The Journal of Pharmacy and Pharmacology.* **52** (6), 633-643.

Zeng, X. M.; Martin, G. P.; Marriott, C. & Pritchard, J. 2001. Lactose as a carrier in dry powder formulations: The influence of surface characteristics on drug delivery. *Journal of Pharmaceutical Sciences.* **90** (9), 1424-1434.

Zimon, A.D. 1982. *Adhesion of Dust and Powders* (2nd ed.). New York, Consultants Bureau.

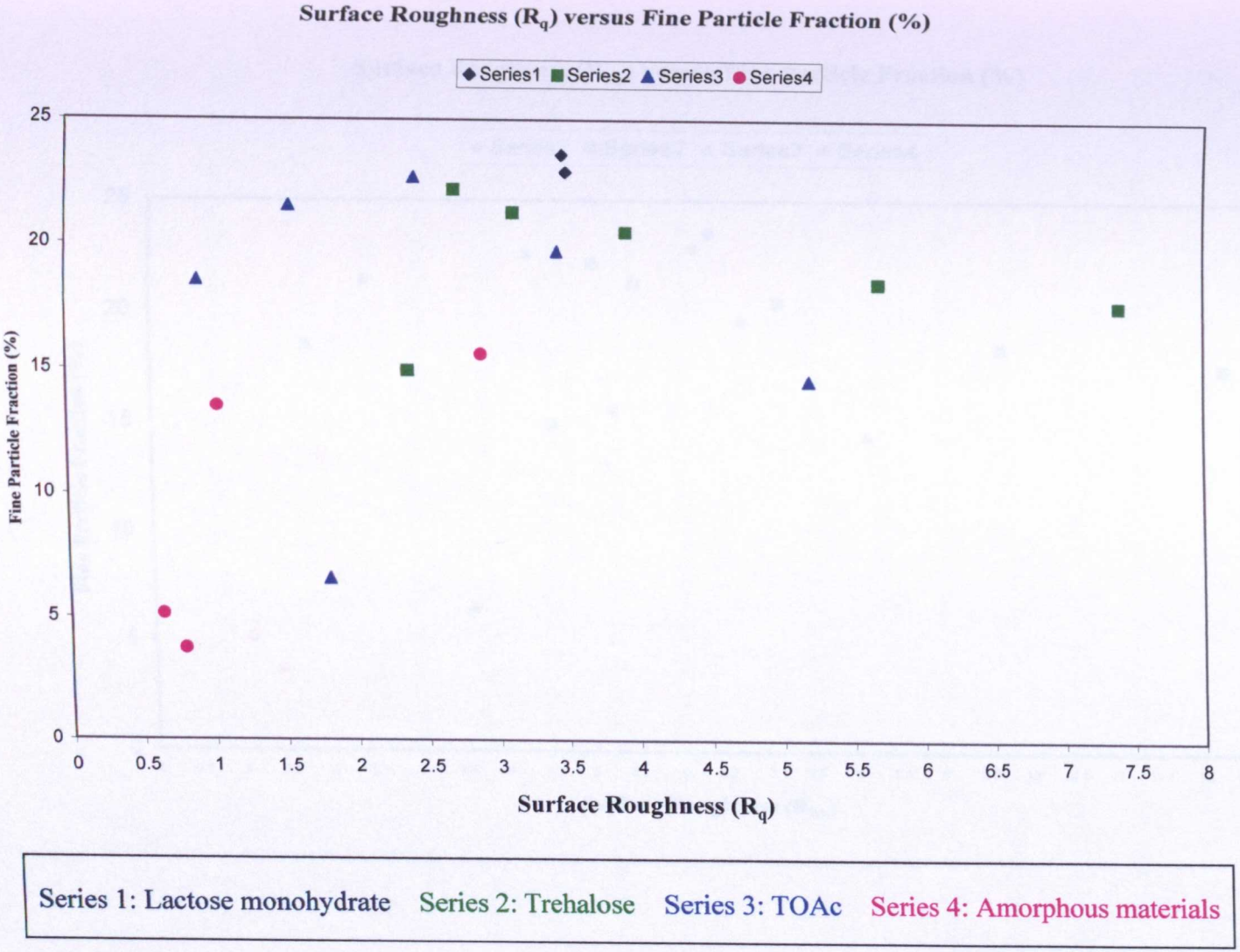

Figure 8.3: A summary graph of fine particle fraction (%) versus R_q for all of the materials assessed.